Max-Planck-Institut
für Meteorologie

MAX-PLANCK-GESELLSCHAFT

International Max Planck Research School
on Earth System Modelling

On the relationship between the Tropical Easterly Jet over West Africa and Sahel rainfall across various time scales

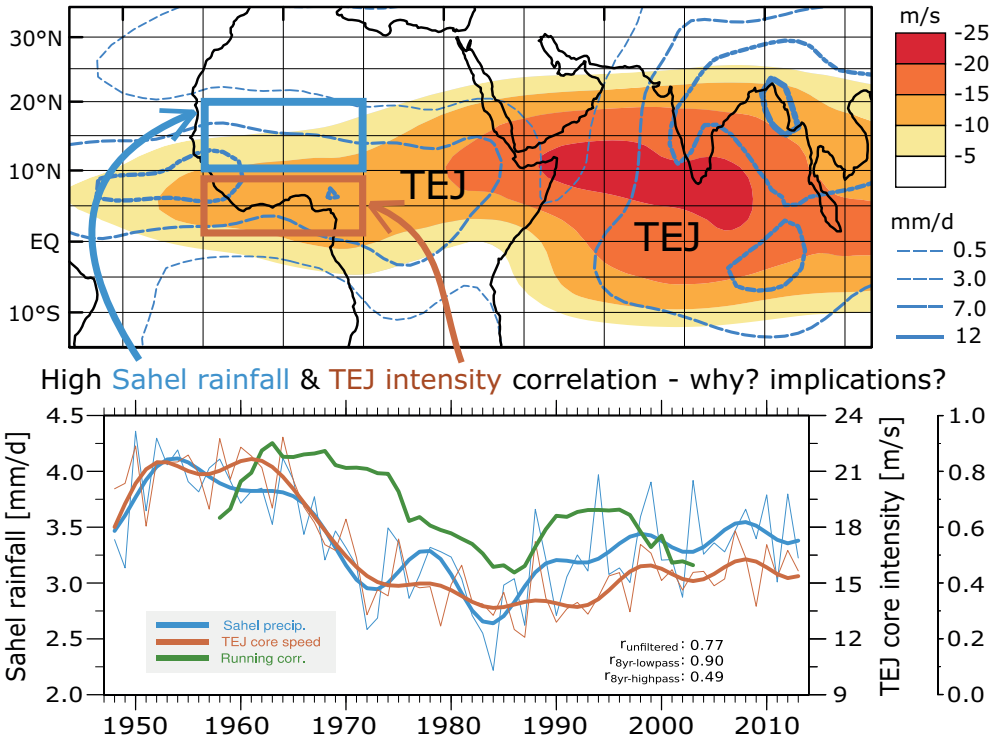

Alexander Lemburg

Hamburg 2020

Berichte zur Erdsystemforschung
Reports on Earth System Science

226
2020

Hinweis

Die Berichte zur Erdsystemforschung werden vom Max-Planck-Institut für Meteorologie in Hamburg in unregelmäßiger Abfolge herausgegeben.

Sie enthalten wissenschaftliche und technische Beiträge, inklusive Dissertationen.

Die Beiträge geben nicht notwendigerweise die Auffassung des Instituts wieder.

Die "Berichte zur Erdsystemforschung" führen die vorherigen Reihen "Reports" und "Examensarbeiten" weiter.

Notice

The Reports on Earth System Science are published by the Max Planck Institute for Meteorology in Hamburg. They appear in irregular intervals.

They contain scientific and technical contributions, including Ph. D. theses.

The Reports do not necessarily reflect the opinion of the Institute.

The "Reports on Earth System Science" continue the former "Reports" and "Examensarbeiten" of the Max Planck Institute.

Anschrift / Address

Max-Planck-Institut für Meteorologie
Bundesstrasse 53
20146 Hamburg
Deutschland

Tel./Phone: +49 (0)40 4 11 73 - 0
Fax: +49 (0)40 4 11 73 - 298

name.surname@mpimet.mpg.de
www.mpimet.mpg.de

Layout

Bettina Diallo and Norbert P. Noreiks
Communication

Copyright

On the relationship between the Tropical Easterly Jet over West Africa and Sahel rainfall across various time scales

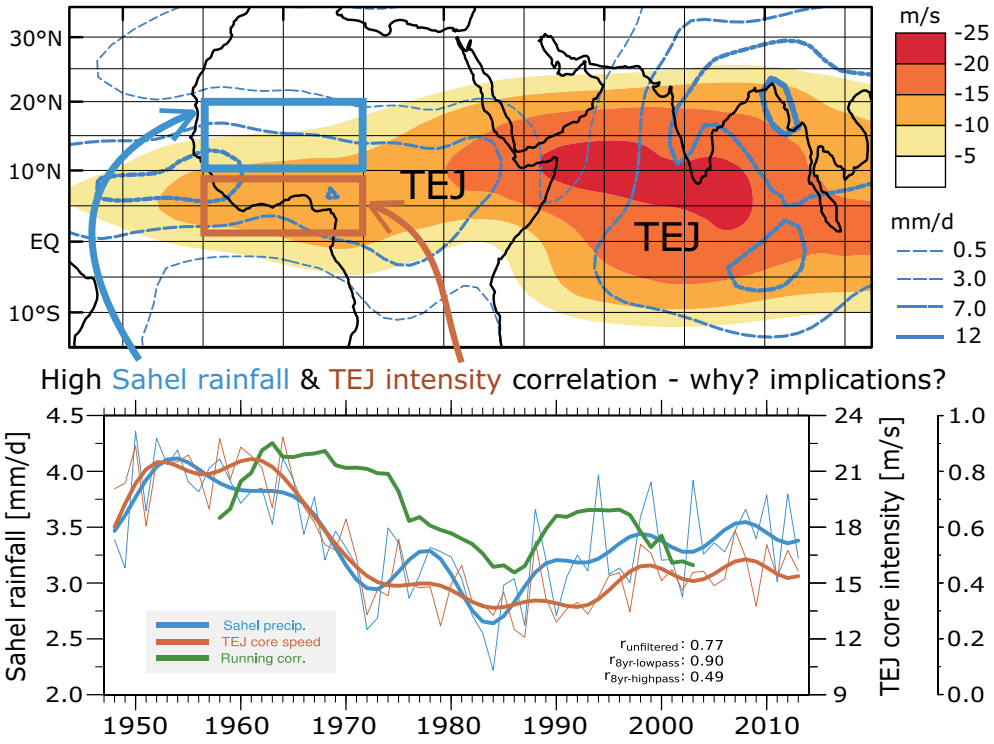

Alexander Lemburg

Hamburg 2020

Alexander Lemburg
aus Lübeck, Deutschland

Max-Planck-Institut für Meteorologie
The International Max Planck Research School on Earth System Modelling
(IMPRS-ESM)
Bundesstrasse 53
20146 Hamburg

Universität Hamburg
Geowissenschaften
Meteorologisches Institut
Bundesstr. 55
20146 Hamburg

Tag der Disputation: 20. Januar 2020

Folgende Gutachter empfehlen die Annahme der Dissertation:
Dr. Jürgen Bader
Prof. Dr. Martin Claußen

Vorsitzender des Promotionsausschusses:
Prof. Dr. Dirk Gajewski

Dekan der MIN-Fakultät:
Prof. Dr. Heinrich Graener

Berichte zur Erdsystemforschung / Max-Planck-Institut für Meteorologie 226
Reports on Earth System Science / Max Planck Institute for Meteorology 2020

ISSN 1614-1199

Abstract

The upper-tropospheric Tropical Easterly Jet over West Africa (WA-TEJ) is an integral part of the West African Monsoon (WAM) circulation and is strongly correlated with Sahel rainfall changes on interannual to multi-decadal time scales. This thesis aims to understand the underlying mechanisms and implications of this statistical relation and explores whether the WA-TEJ might play an active role for Sahel rainfall as proposed by previous studies.

In the first scientific chapter, temporally high-resolved observations and reanalyses are used to clarify whether the WA-TEJ fosters convection over the Sahel via its influence on the upper-level divergence, as suggested by former studies. I conduct an analysis of nearly 300 Sahelian mesoscale convective systems and find that neither their initiation nor their degree of organization is significantly associated with WA-TEJ anomalies or jet-induced upper-level divergence. On synoptic time scales, WA-TEJ anomalies also significantly lag anomalies in convective activity by one or two days, indicating that convection anomalies are more likely to drive changes in the WA-TEJ than vice versa. In synopsis, the results of the first chapter suggest that the WA-TEJ does not play an active role for Sahel rainfall, at least not via its effect on upper-level divergence.

WAM rainfall anomalies can significantly affect the WA-TEJ intensity, but does the local forcing of the WA-TEJ by WAM rainfall-related latent heating really explain the observed WA-TEJ – rainfall covariability on interrannual to decadal time scales? The second scientific chapter tackles this question by investigating the main tropical drivers of WA-TEJ variability. For this purpose, PUMA, an AGCM based on dry dynamics, is driven by summer mean 3D diabatic heating fields of the period of 1979-2017. The heating fields are split up into a local African and remote rest of world part. Simulations are conducted in which the year-to-year variability of the diabatic heating is either restricted to the local or remote regions. It is found that the interannual to decadal variability of WA-TEJ intensity is dominated by the influence of the remote forcing, especially by the effect of ENSO. The solely local forcing-induced WA-TEJ variability, while highly correlated with Sahel rainfall, is too weak to stand out against the remote influences. Ultimately, the variability of the remote diabatic heating – in particular over the tropical Pacific – can likely be viewed as an important driver of the observed Sahel rainfall–WA-TEJ relationship as it not only dominates the WA-TEJ variability, but also tends to induce same-sign changes in Sahel rainfall.

The objective of the third scientific chapter is to explore whether the TEJ – Sahel rainfall covariability may fundamentally change in a different climate. As a suitable case study, I select the mid-Holocene, a climatic period when the WAM was substantially stronger and its variability was less affected by teleconnections. Compared to a pre-industrial control climate, the state-of-the-art Earth system model MPI-ESM simulates for the mid-Holocene a weaker covariability between WAM rainfall and WA-TEJ intensity on interannual to decadal time scales. To better understand this, the tropical drivers of the mid-Holocene WA-TEJ variability are investigated via PUMA experiments, using the same methods as in chapter two. In contrast to today, both the local forcing through WAM rainfall anomalies and the remote diabatic forcing play an equal role for the WA-TEJ variability during the mid-Holocene. This difference to the present-day

state appears to be primarily caused by the diminished importance of the remote diabatic forcing, whose amplitude is attenuated mainly due to the reduced interannual variability of SSTs in the tropical Pacific. I propose that the diminished importance of the remote diabatic forcing also mainly explains the reduced TEJ–rainfall covariability.

Zusammenfassung

Der obertroposphärische tropische Oststrahlstrom über Westafrika (Tropical Easterly Jet über West Africa, WA-TEJ), ein integraler Bestandteil der westafrikanischen Monsunzirkulation (WAM), ist stark mit Schwankungen des Sahelniederschlags auf interannuallen bis multidekadischen Zeitskalen korreliert. Diese Arbeit ergründet die ursächlichen Mechanismen sowie die Implikationen dieses statistischen Zusammenhangs und untersucht zudem, ob der WA-TEJ eine aktive Rolle für die Niederschlagsentwicklung in der Sahelzone spielt, wie in früheren Studien vorgeschlagen.

In dem ersten wissenschaftlichen Kapitel dieser Arbeit werden zeitlich hochaufgelöste Beobachtungen und Reanalysen analysiert, um zu klären, ob der WA-TEJ die Konvektion über der Sahelzone durch seine Auswirkungen auf die obertroposphärische Divergenz unterstützt, wie in früheren Studien vorgeschlagen. Eine Analyse von 300 mesoskaligen konvektiven Systemen in der Sahel-Region zeigt, dass weder ihre Auslösung noch ihr Organisationsgrad mit signifikanten WA-TEJ-Anomalien oder TEJ-induzierten Divergenzen in der oberen Troposphäre verbunden sind. Auf der synoptischen Zeitskala hinken WA-TEJ-Anomalien signifikant Anomalien der konvektiven Aktivität um ein bis zwei Tage hinterher, was darauf hindeutet, dass Konvektionsanomalien eher Veränderungen im WA-TEJ bewirken als umgekehrt. Die Ergebnisse des ersten Kapitels deuten somit darauf hin, dass der WA-TEJ keine aktive Rolle für die Sahelniederschläge spielt, zumindest nicht über seine Auswirkungen auf die obertroposphärische Divergenz.

WAM-Niederschlagsanomalien können die Intensität des WA-TEJ signifikant beeinflussen, aber erklärt der lokale Antrieb des WA-TEJ durch die mit dem WAM-Niederschlag verbundene latente Erwärmung wirklich die beobachtete Kovariabilität zwischen WA-TEJ-Intensität und Sahelniederschlag auf interannualen bis dekadischen Zeitskalen? Mein zweites wissenschaftliches Kapitel befasst sich mit dieser Frage, indem es die wichtigsten tropischen Treiber der WA-TEJ-Variabilität untersucht. Dazu wird PUMA, ein atmosphärisches Zirkulationsmodell basierend auf trockener Dynamik, durch über die jeweilige Sommersaison gemittelte, dreidimensionalen Felder der diabatischen Heizung angetrieben über den Zeitraum 1979-2017. Die Felder des diabatischen Antriebs werden in einen lokalen afrikanischen und einen entfernten „Rest der Welt“-Teil aufgeteilt. Es werden Simulationen durchgeführt, bei denen sich die Jahr-zu-Jahr-Variabilität der diabatische Heizung entweder auf die lokale oder abgelegene Regionen beschränkt. Ich zeige, dass die interannuelle bis dekadische Variabilität der WA-TEJ-Intensität durch den Einfluss des entfernten diabatischen Antriebs dominiert wird, insbesondere durch die Wirkung von ENSO. Die WA-TEJ-Variabilität, die ausschließlich auf die lokale diabatische Heizung zurückzuführen ist, ist zwar stark mit dem Sahelniederschlag korreliert aber schwach im Vergleich zur Wirkung der Ferneinflüsse. Letztendlich kann der entfernte diabatische Antrieb als ein wichtiger Treiber für die beobachtete Sahelniederschlag–WA-TEJ-Beziehung angesehen werden, da er nicht nur die WA-TEJ-Variabilität dominiert, sondern auch oft Sahelniederschlagsanomalien mit gleichem Vorzeichen induziert.

Ziel des dritten wissenschaftlichen Kapitels ist es, herauzufinden, ob sich die Kovariabilität zwischen TEJ und Sahelniederschlag in einem anderen Klima grundlegend

ändert. Als Fallstudie wähle ich das mittlere Holozän, eine Epoche, in der der WAM-Niederschlag viel intensiver war und seine Variabilität weniger durch Telekonnektionen beeinflusst wurde. Im Vergleich zu einem vorindustriellen Kontrollklima simuliert das komplexe Erdsystemmodell MPI-ESM für das mittlere Holozän eine schwächere Kovariabilität zwischen WAM-Niederschlag und WA-TEJ-Intensität auf interannuellen bis dekadischen Zeitskalen. Um dies besser zu verstehen, werden die tropischen Treiber der WA-TEJ-Variabilität im mittleren Holozän mittels PUMA-Experimenten mit der selben Methodik wie im zweiten Kapitel untersucht. Im Gegensatz zum heutigen Klima bestimmen nun der lokale und der entfernte diabatische Antrieb gleichermaßen die WA-TEJ-Variabilität. Dieses unterschiedliche Verhalten im Vergleich zum gegenwärtigen Klima scheint in erster Linie auf die abnehmende Bedeutung des entfernten diabatischen Antriebs zurückzuführen zu sein, dessen Amplitude vor allem durch die geringere interannuelle Variabilität der Meeresberflächentemperaturen im tropischen Pazifik abgeschwächt wird. Die Ergebnisse deuten darauf hin, dass die verminderte Bedeutung des entfernten diabatischen Antriebs auch die verringerte Kovariabilität zwischen WA-TEJ und Sahelniederschlag während des mittleren Holozäns erklärt.

Teilveröffentlichungen dieser Dissertation

Pre-Published Work Related to this Dissertation

Lemburg, A., Bader, J., Claussen, M. (2019). Sahel Rainfall–Tropical Easterly Jet Relationship on Synoptic to Intraseasonal Time Scales. Monthly Weather Review, 147(5), 1733-1752. – see chapter 2

Lemburg, A. and Bader, J. (2020). Role of remote versus local diabatic heating for the interannual to decadal variability of the Tropical Easterly Jet over West Africa. In preparation. – see chapter 3

Formal remarks about the use of "we" and "I" in this thesis

This cumulative thesis features three studies that were conducted under the supervision and guidance of Dr. Jürgen Bader and Prof. Dr. Martin Claußen. The conducted research further depends on the contributions of many other people regarding data and technical solutions. Chapters 2-4, containing these three separate studies in form of classic research papers, are therefore written in first person plural. The contributions to each of the papers are highlighted at the title page of each of those chapters.

Nonetheless, this PhD thesis can mainly be viewed as a solitary work as many of the research ideas were developed by the doctoral candidate. Furthermore, nearly all work in terms of experiment design and execution as well as data analysis and the manuscript writing was conducted by the doctoral candidate. Therefore chapter 1, the unifying essay which presents an overview over all conducted studies, is written in the first person singular.

Contents

Acronyms

AEJ	African Easterly Jet
AEW	African Easterly Wave
AMC	Angular Momentum Conserving (circulation)
CAPE	Convective Available Potential Energy
CIN	Convective Inhibition
CMT	Convective Momentum Transport
ENSO	El Niño Southern Oscillation
ITF	Intertropical Discontinuity
ITF	Intertropical Front
ITCZ	Intertropical Convergence Zone
JJAS	June, July, August, September
LFC	Level of Free Convection
MCS	Mesoscale Convective Complex
MCS	Mesoscale Convective System
MJO	Madden Julian Oscillation
MPI-ESM	Max Planck Institute Earth System Model
OLR	Outgoing Longwave Radiation
PUMA	Portable University Model of the Atmosphere
QBZD	Quasi Biweekly Zonal Dipole
STJ	Subtropical (westerly) Jet
SST	Sea Surface Temperature
TEJ	Tropical Easterly Jet
WAM	West African Monsoon
WA-TEJ	West African branch of the Tropical Easterly Jet

"When Kepler found his long-cherished belief did not agree with the most precise observation, he accepted the uncomfortable fact. He preferred the hard truth to his dearest illusions, that is the heart of science."

Carl Sagan (1934 – 1996)

1 Unifying essay

1.1 Motivation and brief thesis outline

The West African Monsoon (WAM) is of utmost importance for millions of people in sub-Saharan Africa. First and foremost, food security and water resources, but also the functioning of many economic and societal sectors depend decisively on the strength of this seasonal large-scale circulation system (Haile, 2005; Dilley et al., 2005). In accordance with the likely Arabic origin of the word ($mausim \mathrel{\widehat{=}} season$), the term *monsoon* designates a marked seasonal reversal of the prevailing near-surface winds (Webster, 1981). With the shift in low-level winds from northeasterly to southwesterly, moist air from the oceanic regions can be carried far northward allowing substantial rainfall to occur in the Sahel – a region that is very arid the rest of the year. In July and August, the WAM circulation reaches its maximum northward extent. Widespread precipitation of more than 3 mm per day can then be observed as far north as 16°N on average. WAM and in particular Sahel rainfall not only varies substantially from year to year but may also be subject to decadal trends that may be more extreme than anywhere else in the world (Nicholson, 2013). During the 1950s and the first half of the 1960s, the Sahel region experienced persistent above-average rainfall which allowed an expansion of agriculture areas to feed the growing population (Glantz, 1995; Nicholson et al., 2018). Roughly 20 years later, a massive drought (which has already begun quite abruptly in 1968) reached its maximum severity in the years 1983 and 1984 (Nicholson, 1985, 2013). In these two years, spatially-averaged Sahel rainfall fell short of the long-term average by about 50% which led to devastating widespread crop failures and water scarcity.

The extreme variability of monsoon rainfall in this vulnerable region motivates to further our understanding of the crucial mechanisms that govern the WAM circulation and its variability. Many studies in recent decades have demonstrated the sensitivity of Sahel rainfall to sea surface temperature anomalies (SST) either in the regional setting or in remote areas of the world (Folland et al., 1986; Rowell et al., 1995; Giannini et al., 2003; Bader and Latif, 2003; Rodríguez-Fonseca et al., 2015). Moreover, the Sahel region numbers among the hot spot regions in which land atmosphere feedbacks play an important role (Koster et al., 2004). Much research therefore also concentrated

on whether natural or man-made changes in the land surface may explain trends in Sahel rainfall (Xue and Shukla, 1993; Nicholson, 2000; Taylor et al., 2002). In addition to the impact of SST anomalies and land surface changes, the role of mid- and upper-tropospheric atmospheric dynamics has also been investigated. The mid-tropospheric African Easterly Jet (AEJ) and the related African Easterly Waves (AEWs), which form at the southern boundary of this jet, have been subject to numerous studies (Carlson, 1969; Burpee, 1972; Kiladis et al., 2006; Mekonnen et al., 2006). Much less attention has been directed to the role of the Tropical Easterly Jet (TEJ). The TEJ designates a band of strong easterly winds observed in the summer upper troposphere at about 12-14 km altitude. Over the Indian monsoon region the TEJ is most developed but it extends westwards to Africa until it decays over the tropical Atlantic. Observations, reanalysis data and model simulations have shown that wet years in the Sahel are generally characterized by a stronger TEJ whereas drought years exhibit a weaker TEJ intensity (Grist and Nicholson, 2001; Sylla et al., 2010). The causes of this strong statistical relationship and the question of cause and effect have not yet been sufficiently studied. It is therefore also an open question whether the TEJ plays a more active or passive role for Sahel rainfall.

This thesis therefore aims at understanding the mechanisms explaining the observed statistical relationship between rainfall and the intensity of the Tropical Easterly Jet (TEJ) over the West African monsoon region. An emphasis is put on the question whether the TEJ might significantly affect Sahel rainfall through its possibly substantial control on the upper-level divergence. Over the course of my PhD work, this overarching research goal led to three studies. The first study elucidates the TEJ – Sahel rainfall relationship on synoptic to intraseasonal time scales and investigates whether the TEJ significantly affects convection over the Sahel via inducing anomalous upper-level divergence. In the second study, it is explored what mainly drives the interannual to decadal TEJ variability in order to understand the observed high TEJ intensity – Sahel rainfall correlation. The third study addresses the stationarity of the observed TEJ – Sahel rainfall relationship by asking whether it may change under the different conditions that prevailed during the mid-Holocene. This unifying essay aims to bring together the essence of these three studies.

In the following introducing sections I would first like to provide the reader with a basic understanding of monsoons in general, followed by a more specific description of the West African monsoon circulation. The subsequent section discusses the mechanisms that lead to the formation of the TEJ and gives an overview over its climatological mean state as well as its variability over various time scales. I will then introduce the current state of the research with respect to the observed relationship between the TEJ and WAM rainfall. By highlighting the gaps in our current understanding I will make clear what makes this study novel. For readers who are experts in the field of the WAM circulation, I would advise to take the short cut to page 16. This is the page where I finally formulate four research questions which form the base frame of this dissertation. Thereafter, I summarize and discuss the main findings of my PhD studies and provide an outlook for possible future research.

1.2 Monsoons – A theoretical perspective

The phenomenon of a marked seasonal wind shift in some tropical regions was already taken into account on the nautical charts of Halley (1686). He proposed that the monsoon winds are driven by the differential heating between land and ocean. This is a theoretical concept which should be recognized as true until very recently – but more about that later. A recreational meteorologist with a confusingly similar last name, George Hadley, has devoted much of his life to the understanding of the steady winds observed in the lower latitudes. Hadley suggested that the southwesterly directions of the monsoon winds in the Northern hemisphere are a result of the deflection of cross-equatorial winds by Coriolis forces resulting from Earth's rotation (Hadley, 1735). Nowadays, the term monsoon is not only used to describe the observed seasonal wind shift, it further denotes the associated very complex atmospheric circulation system. In this section, I will provide a brief insight into our theoretical concepts about monsoons according to the most recent literature. It is important to get one thing straight: Our picture of monsoons has changed fundamentally within the last years. Thereafter, the subsequent section will focus more specifically on the West African monsoon and describe its basic dynamical features as well as the rainfall climatology and variability over various temporal and spatial scales.

The mechanisms driving the monsoon circulations as well as the factors governing their northward extent and intensity have been studied extensively in the past decades. We are now beginning to get a more advanced understanding of the physical mechanisms that explain the onset and maintenance of this regional overturning circulation phenomenon. The necessary external forcing without which we would observe no monsoon circulations on earth is, without a doubt, the seasonal cycle of incoming solar radiation. An important observation to make, however, is that the northward migration of monsoonal rainbelts is somewhat faster and less linear than the solar forcing itself (Lau and Yang, 1996; Sultan and Janicot, 2000). This observation suggests the existence and importance of dynamical feedbacks.

Until not long ago, monsoons were generally thought of as giant sea breeze circulations on seasonal time scales (Gadgil, 2018). At least the onset of monsoon circulations was mainly attributed to the thermal contrast between land and oceans that emerges in summer due to the low thermal inertia of the land. The sea breeze-like circulation would advect moist air inland where it would eventually be forced to ascend as a consequence of near-surface convergence. The associated latent heat release in the mid troposphere would then maintain and further intensify the initial circulation, leading to a sustained and deep overturning circulation. However, to compare monsoons with sea breezes – which are shallow overturning circulations occurring on diurnal time scales – would be an oversimplification. Recent studies also raise serious doubts about the validity of the sea breeze theory when it comes to explaining even the onset of the monsoon circulation.

In a more modern view, monsoon circulations may be considered regional cross-equatorial Hadley cells. In fact, the averaged mass streamfunctions of the three most intense northern-hemispheric summer monsoons project considerably onto the familiar zonal-mean picture of a strong cross-equatorial Hadley cell during solstice (Zhai

and Boos, 2015). Therefore, the most recent theoretical concepts about monsoon dynamics are founded on the mainly theoretical work of Schneider and Lindzen (1977), Held and Hou (1980), Lindzen and Hou (1988) and Plumb and Hou (1992), to name a few. These seminal papers furthered our understanding of the physical processes governing and constraining the extent and intensity of the global Hadley circulation. In succession to the work of Schneider and Lindzen (1977), who developed a model of an axisymmetric Hadley cell, Held and Hou (1980) successfully predicted the latitudinal extent of the annual mean global Hadley circulation. The Held-Hou model describes the Hadley cell as an axisymmetric circulation in a stably stratified rotating Boussinesq fluid under zonally-uniform differential heating. If the flow is sufficiently inviscid, a nearly angular momentum conserving (AMC) circulation establishes whose intensity and extent is governed by the conservation of angular momentum and the maintenance of thermal wind balance. The necessary condition for a shift to a stable AMC regime is that the absolute vorticity in the upper troposphere becomes close to zero. With the help of an AGCM based on dry dynamics, Plumb and Hou (1992) explored how the tropical overturning circulation responds to off-equatorial forcing. They found a nonlinear behaviour: When a critical heating threshold is reached, a state in which only weak overturning exists suddenly shifts towards an intense AMC meridional circulation. This behaviour can be explained as follows: When the thermal forcing reaches the critical level, the resulting meridional temperature gradient is then able to maintain a geostrophically balanced upper-level flow strong enough to reduce the absolute vorticity in the upper troposphere to zero.

Using the theoretical framework described above, recent studies marked a turning point for our understanding of the essential mechanisms that generate monsoons. In their landmark study, Bordoni and Schneider (2008) showed that realistic monsoon circulations can exist on an aqua planet in the absence of any topography or land-sea contrasts. The only prerequisites for monsoons to develop are a seasonal variation in insolation and a shallow-layer ocean mimicking a homogeneous surface with a heat capacity much lower than an actual ocean. This reaffirms the conceptual picture that monsoons should be understood as regional cross-equatorial Hadley circulations and not as giant sea breeze circulations. A recent study by Geen et al. (2018) seems to confirm this hypothesis. In their study, Bordoni and Schneider (2008) have also examined what drives the rapid onset of the monsoon, the so-called monsoon jump. They found that at a certain threshold value of the maximum heating latitude a rapid regime shift occurs: from an equinox-like eddy-dominated tropical overturning circulation with two weak Hadley cells to a regime with only one strong cross-equatorial cell which is nearly angular momentum conserving. In the former regime, extratropical eddies and associated momentum flux divergence at the poleward edges of the Hadley cells put a constraint on the intensity and latitudinal extent of the Hadley cells. In the latter case, the cross-equatorial Hadley cell is only constrained by the energy budget. Upper-level easterlies that begin to establish in the summer hemisphere shield the overturning circulation from any eddy activity. This allows the monsoon circulation to gain further strength as long as it is not energy-limited. At the same time, a low-level countergradient flux of cool and dry air shifts the latitude of maximum moist static energy farther northwards. The resulting increase in near-surface baroclinicity and the north-

ward shift of the zone of maximum deep convection leads, in turn, to a further intensification and northward extent of the upper-level easterlies. A positive feedback loop comes into existence.

Whereas the presence of land masses, orography and the differential heating between land and ocean might not be fundamental to explain the existence of monsoons, it is important to note, however, that real world monsoon circulations are nonetheless strongly affected by them (Meehl, 1992; Sato and Kimura, 2007). The complex configuration of topography and ocean basins with different SSTs exerts strong control on rainfall patterns which introduces strong zonal asymmetries in the large-scale distribution and intensity of equatorial and off-equatorial diabatic heating. The role of such zonal asymmetries appears to be much more important than previously assumed. Chen (2003) found a clear spatial quadrature relationship between the upper-level planetary-scale divergent circulation and the monsoon anticyclones. He suggested that the monsoon circulations are mainly driven by east-west differential heating and dynamically maintained by a Sverdrup balance. The latter term designates a dynamical balance in which the generation of vorticity through stretching is counteracted by the horizontal advection of planetary vorticity.

In summary, monsoons can be considered complex regional cross-equatorial overturning circulations which react to a variety of both local and remote forcings while being at the same time constrained by the planetary-scale transports and gradients of energy and momentum.

1.3 The West African monsoon circulation

During April and May, incipient upwelling of cold water in the Gulf of Guinea pushes the centre of convective activity from the open ocean towards the West African coast line (Okumura and Xie, 2004; Hagos and Cook, 2009; Thorncroft et al., 2011). Until the beginning of June, substantial precipitation is mainly restricted to the coastal regions around the 5°N latitude. Only few deep convective systems would reach farther north than 10°N at this point in time. At the same time, the Saharan region is more and more characterized by a thermally driven shallow low pressure system, called the Saharan heat low (SHL; Sultan et al., 2003; Lavaysse et al., 2009). As a consequence of the SHL development, the surface pressure gradient between the Sahara and the coastal region intensifies. Southwesterly winds begin to penetrate far inland where they meet consistent dry northeasterlies emanating from Northeast Africa. The location at which both low-level winds converge is referred to as the Intertropical Front (ITF), Intertropical Discontinuity (ITD) or Intertropical Convergence Zone (ITCZ). All three terms are not perfectly accurate and some scholars suggested that the term ITCZ should be avoided in this context (Hayward and Oguntoyinbo, 1987; Ramage, 1995). I will still use the term, as in Nicholson (2013), because it accurately describes the zone of maximal near-surface convergence. Important to note, however: over West Africa, the ITCZ(/ITD) only marks the pronounced discontinuity between two fundamentally different air masses but is not associated with significant monsoonal rainfall.

Between mid-June and the beginning of July, deep convection rapidly ceases over the coastal regions and moves northward rapidly some 5-7°N in about two weeks (Ramel

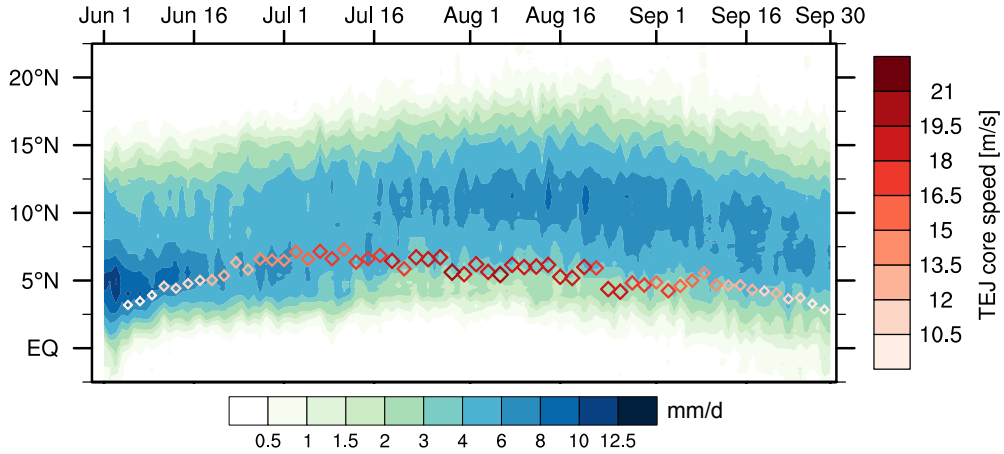

Figure 1.1: Time - latitude Hovmoeller plot depicting the climatological seasonal march of precipitation over the western Sahel and the TEJ core latitude and intensity. Precipitation is represented by daily climatological mean values (1980-2004) of the NOAA NCEP CPC FEWS Africa daily data set (Xie and Arkin, 1996; Herman et al., 1997) zonally averaged between 15°W and 15°E. The intensity and latitude of the TEJ core (depicted by reddish circles) is derived by first finding the daily jet core maximum for each longitudinal strip on the basis of daily ERA-Interim (Dee et al., 2011) output of zonal wind at 200 hPa. Thereafter, the jet core latitude and velocity values are zonally averaged between 15°W and 15°E and a daily climatology is calculated for the years 1980-2004.

et al., 2006; Hagos and Cook, 2007). Figure 1.1 visualizes this behaviour as a rapid northward shift of the darker blue shades in a Hovmoeller plot based on observed daily rainfall climatology. The fast and non-linear migration of precipitation towards the north, called monsoon jump, may be favoured by the involvement of the rather complex dynamical feedbacks which were briefly discussed in the previous section. From now on, the Sahel region is characterized by the frequent passage of large and organized convective systems (Mathon et al., 2002; Lebel et al., 2003; Lebel and Ali, 2009). Depending on the size, they are called mesoscale convective systems (MCSs) or mesoscale convective complexes (MCCs). Henceforth, I will always refer to the large organized systems as MCSs for simplicity. MCSs generally move from east to west as they are mainly steered by the mid-tropospheric easterlies. Sahelian MCSs are characterized by a high level of organization, resulting in exceptionally large system sizes and high longevity. MCSs with cloud shield radii $\geq$ 100 km and life times $\geq$ 9 hours explain more than 80% of the total MCS-associated integrated cloud cover (Mathon and Laurent, 2001). During its life time, one MCS can therefore cover not only hundreds but thousands of kilometres. Integrated over the time of a whole monsoon season, all individual MCSs will leave a trace of maximum precipitation in a region often referred to as monsoonal rainbelt. On the climatological time scale, this rainbelt is situated between 8°N and 16°N (Nicholson, 2008).

The main features of the WAM circulation in its mature stage are illustrated in figure 1.2 which depicts a vertical cross section averaged from 15°W to 15°E. The rainbelt (marked by the thick blue line on the x-axis) is associated with a deep cross-equatorial overturning circulation which is mainly driven by the release of latent heat. It is again important to point out the clear spatial separation between the rainbelt and the ITCZ, which is typical for the WAM. The zone of maximum rainfall is significantly south of

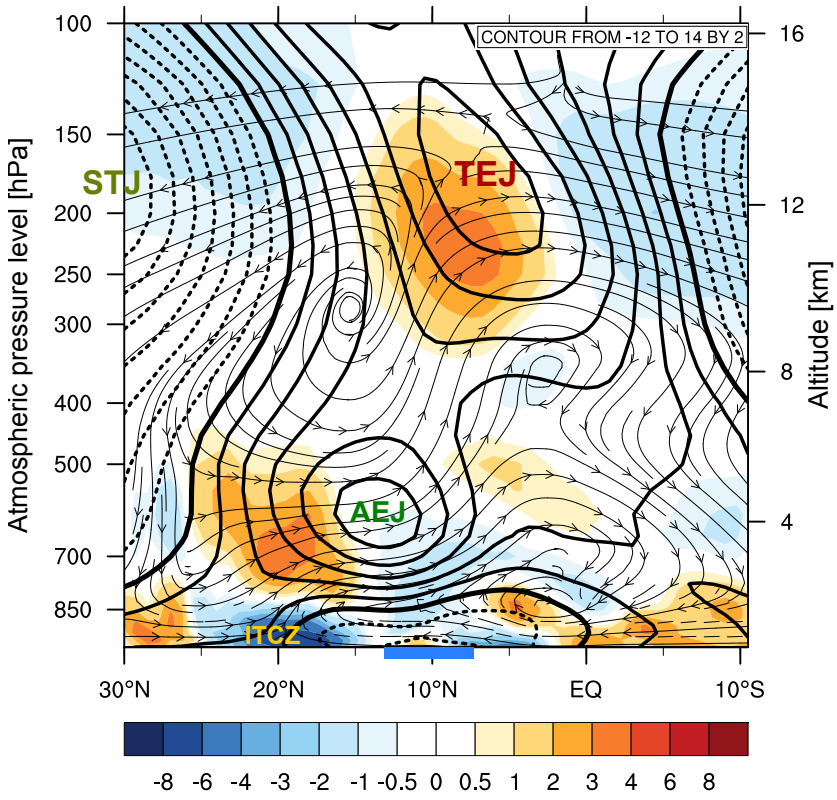

Figure 1.2: The WAM circulation depicted by a regional latitude - height cross section for West Africa with zonal mean values (based on 1979-2017 climatological mean values from ERA-Interim) averaged over 15°W to 15°E. The divergence is shown by means of coloured shadings, the zonal wind is depicted with contours (easterlies as solid lines) and the meridional-vertical circulation is represented by streamlines (vertical velocity is multiplied by 100 to make the overturning circulation visible).

the latitude where the surface convergence is maximal on average. ITCZ and WAM rainbelt are not only spatially separated by at least 400 km (Issa Lélé and Lamb, 2010), the timings of ITCZ shifts and the local onset of the rainy season in the Sahel are also nearly uncorrelated (Sultan et al., 2003).

The monsoonal rainbelt appears to be precisely bordered by the African Easterly Jet (AEJ) to the north and the Tropical Easterly Jet (TEJ) to the south (see Fig. 1.2 and 1.3). This remarkable observation is specific for the WAM and led to the suggestion that the position and intensity of the jets exert a control on the northward extent and width of the rainbelt. The AEJ, an easterly mid-tropospheric jet at 600–700 hPa, is a characteristic feature of the WAM circulation. It is maintained by the low- to mid-tropospheric thermal gradient which arises from a combination of differential sensible heating, mainly (but not only) due to marked north-south gradients in soil moisture, and unique geophysical and orographic features (Burpee, 1972; Cook, 1999; Thorncroft and Blackburn, 1999; Wu et al., 2009). A mix of baroclinic and barotropic instability along the AEJ gives rise to wave disturbances. These so-called African Easterly Waves (AEWs) are characterized by periods of 2–7 days and wavelengths between 2000 and 5000 km (Carlson, 1969; Burpee, 1972; Reed et al., 1977; Kiladis et al., 2006; Mekonnen et al., 2006). AEWs modulate and organize convection over the Sahel: over 60% of organized squall lines in summer are associated with AEWs (Fink and Reiner, 2003). They are further known

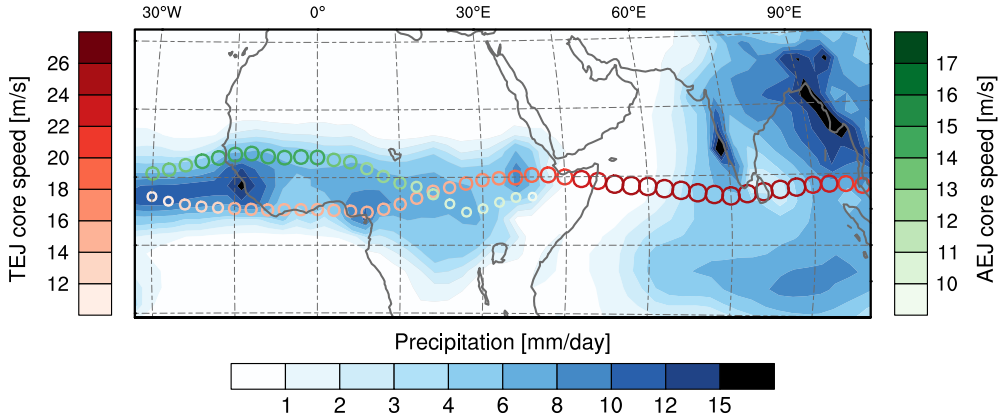

Figure 1.3: 1979-2017 JJAS mean rainfall (based on CRU TS3.22, Harris et al., 2014) and TEJ climatology. The climatological position and intensity of the TEJ (depicted by reddish circles) is derived by finding the daily jet core maximum for each longitudinal strip on the basis of daily ERA-Interim output of the zonal wind at 200 hPa. The same method is applied for zonal wind at 600 hPa to find the climatological position and intensity of the AEJ which is depicted by greenish circles.

to be a necessary precursor for tropical cyclones in the Atlantic (Landsea, 1993; Thorncroft and Hodges, 2001). The TEJ, an upper-tropospheric jet generally found south of the monsoon rainbelt, will be discussed in detail in the next section.

WAM precipitation exhibits intraseasonal variability that can be separated into three time scales: 2–8 day (synoptic-scale variability), 10–25 day, and 30–90 day variability. Synoptic-scale variability dominates on regional scales at the order of ∼1000 km and is mainly associated with the aforementioned AEWs which tend to foster and organize deep convection. At larger spatial scales (≫1000 km), synoptic-scale variability is more and more filtered out and rainfall variability is increasingly confined to time scales longer than 10 days. There are two dominant modes of variability on the 10–25 day time scale: the so-called Sahel mode which designates an envelope of enhanced convective activity travelling through the Sahel region from southeast to northwest. Large-scale atmospheric dynamics associated with equatorial Rossby waves and soil-moisture related land surface-atmosphere interactions are possible mechanisms for this mode (Sultan et al., 2003; Janicot et al., 2010). A second mode only affects the southernmost parts of the Sahel region: the quasi-biweekly zonal dipole mode (QBZD; Mounier et al. 2008) is associated with a quasi-stationary zonal dipole of convection and a corresponding Walker-type circulation between the Guinean coast and the western part of the equatorial Atlantic which changes sign about every 7 days. On the lower frequency band (periods between 30–90 days), WAM rainfall variability is mainly caused by the Madden-Julian Oscillation (MJO).

Summer mean Sahel precipitation varies strongly on interannual to multi-decadal time scales. On these time scales, SST anomalies in various basins have been identified as the most important drivers (Folland et al., 1986; Rowell et al., 1995; Janicot et al., 1996; Giannini et al., 2003; Bader and Latif, 2003). Changes in the land surface are thought to exert an amplifying effect but cannot solely explain the strong decadal trends (Taylor et al., 2002; Giannini et al., 2003). Important to note is the non-stationary nature of the observed correlations between SST anomalies and Sahel rainfall. Whereas the interannual WAM rainfall variability during the wet 1950s and 1960s was nearly exclu-

sively linked to SST anomalies in the Atlantic, WAM rainfall is nowadays much more affected by the El Niño Southern Oscillation (ENSO) via an atmospheric teleconnection mechanism (Janicot et al., 1996, 2001; Losada et al., 2012). Decadal trends of Sahel rainfall have been associated with global warming-related SST increases in the tropical oceans (Bader and Latif, 2003; Lu and Delworth, 2005) and combinations of multidecadal modes of SST variability such as the Atlantic Multidecadal Oscillation or the Interdecadal Pacific Oscillation (Zhang and Delworth, 2006; Mohino et al., 2011; Villamayor and Mohino, 2015). The recent recovery of Sahel rainfall may be explained also by extratropical SST forcings, in particular by the pronounced warming of the eastern Mediterranean Sea (Park et al., 2016).

1.4 The TEJ – Generation, climatology and variability

Upper-level easterlies generally span the entire globe in the tropical latitudes during boreal summer. Within a zonal-mean perspective, Yang et al. (2013) have shown that this observation can be mainly explained by the advection of absolute angular momentum by the cross-equatorial Hadley circulation. The TEJ stands out, however, as it represents a jet-like intensification of easterlies that only covers a limited area between the Maritime Continent and West Africa.

Examining radiosonde measurements, Rao (1952) first noticed that a limited band of intense easterlies exist in the upper troposphere over the Asian monsoon region. Six years later, Koteswaram (1958) provided the first in-depth description of what he called the "easterly jet stream in the tropics". The commonly used name changed into a more handy term shortly after: Tropical Easterly Jet (TEJ). Koteswaram (1958) and Flohn (1964) both described the TEJ as being exceptionally persistent in position and intensity with only minor fluctuations across subseasonal time scales. They further noted that the TEJ can be considered a nearly geostrophic flow that is maintained by the thermal contrast between the subtropical and equatorial region which develops in early summer over parts of the Northern hemisphere. In other words, the intensity and vertical extent of the TEJ can be deduced from the thermal wind relation.

In earlier studies (e.g., Flohn, 1964), the aforementioned thermal contrast and consequently the TEJ was often assumed to be driven by the massive surplus sensitive heating of the strongly elevated Tibetan plateau. However, newer studies found that the orography or orography-related differences in sensible heating play a minor role whereas the distribution and intensity of latent heating is a much more important forcing for the TEJ (Rao and Srinivasan, 2016). The latent heating is provided by the deep convection inside the active monsoon region. Within the context of tropical diabatic heating, the presence of the TEJ can be successfully explained by the analytical Gill model (Gill, 1980) which is based on previous theoretical work by Matsuno (1966). The Gill model comprises a set of shallow water equations linearised about a state of rest. Its analytical solution predicts the existence of the TEJ as a stationary Rossby wave response to an imposed mixed equatorial and off-equatorial heating. Although heavily simplified and based on linear dynamics, the model is able to represent the TEJ's basic shape, its core latitude, width and longitudinal extent in good approximation. In this context, the TEJ can also be considered closely linked to the Indian monsoon circulation

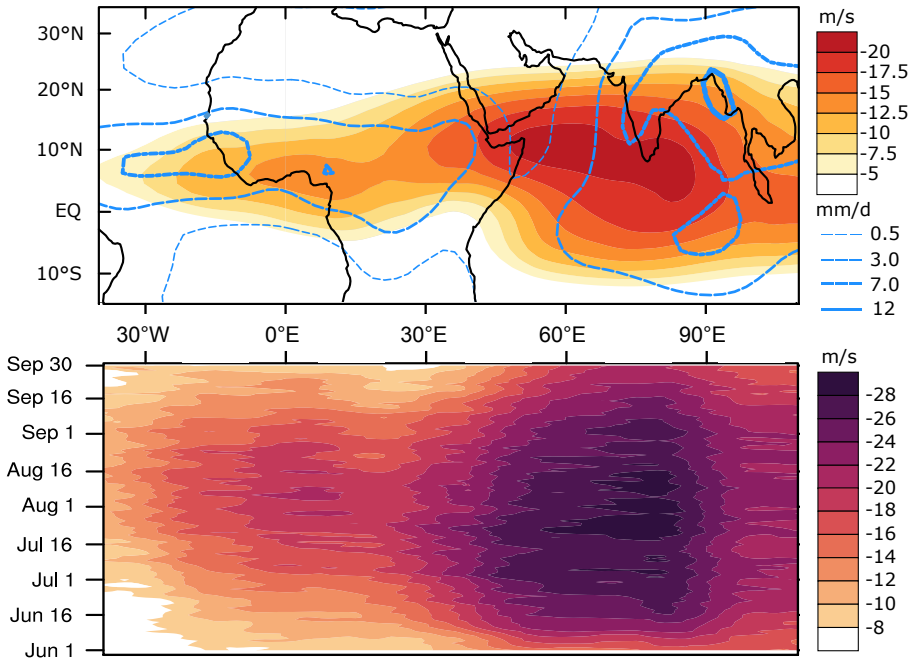

Figure 1.4: TEJ and rainfall summer mean climatology and climatological seasonal evolution of the TEJ core. Top) Lon-lat plot depicting the 1979-2017 climatological JJAS mean zonal wind at 200 hPa (based on ERA-Interim). Contours show rainfall based on CRU TS3.22. Bottom) Lon-time plot of the climatological seasonal evolution of the intensity of the TEJ core. The intensity and latitude of the TEJ core is derived by first finding the daily jet core maximum for each longitudinal strip on the basis of daily ERA-Interim output of zonal wind at 200 hPa.

whose abundant rainfall provides a substantial source off-equatorial heating. The TEJ can then be understood as the equatorward outflow of the Tibetan anticyclone which turns into a marked easterly current due to the conservation of angular momentum.

It would however be a fallacy to view the TEJ exclusively as part of the respective regional monsoon and to conceptually decouple it from the planetary-scale divergent tropical circulation. Although the rotational part of the wind field holds at least 90% of the mean kinetic energy (irrespective of the consideration of eddy or zonal mean energy), it is nevertheless the divergent circulation that is very important as it feeds the energy into the rotational part (Chen, 1980; Lambert, 1989). This conversion occurs efficiently in a standing low-wave-number mode (Chen, 1980). In this context, the upper-level divergence and the advection of planetary vorticity with the divergent wind is the vorticity source which maintains the planetary-scale stationary monsoon eddies. Thus, the intensity of the TEJ is further strongly dependent on the intensity and spatial distribution of the planetary-scale centres of upper-level divergence and is therefore directly linked to the variability of the Hadley and Walker circulations.

Using modern-day reanalysis data products as ERA-Interim (Dee et al., 2011), a climatological description of the TEJ is much easier to conduct than in the first pioneering studies: The TEJ extends from the Maritime Continent over the Indian Ocean towards West Africa, until it begins to decay over the Atlantic (measured by the extent of the summer mean 10 m s^{-1} isotach at 200 hPa). It is most developed over the Indian monsoon system where it reaches a climatological summer maximum of slightly more

than 20 m s^{-1} (Fig. 1.4). The core latitude of the TEJ is generally found between 5 and 15°N in its climatological mean state, being more northwards over the Indian system and closer to the equator over West Africa. However, substantial easterlies are also observed south of the equator as the 10 m s^{-1} isotach extends from 10°S to 25°N. Similar to the core latitude, the climatological altitude of the jet core also varies from east to west. Over the Indian monsoon system, highest wind speeds are generally observed between 100 and 150 hPa ($\sim$ 14-16 km altitude), whereas maximum winds over most of Africa are found around 200 hPa (12 km).

The TEJ depicts a seasonal evolution which is generally in close connection with the seasonal march of monsoonal rainfall (see figure 1.1 and 1.4). Over the Indian monsoon system, a coherent structure and sustained wind speeds over 10 m s^{-1} begin to develop on average at the beginning of June. Over West Africa, the TEJ develops on average about two weeks later. In most cases, the formation of a persistent coherent TEJ coincides with the rapid jump of the monsoonal rainbelt from the coastal area towards the north. In August, the TEJ is generally most developed over both the Indian and the West African monsoon region. Maximum daily mean wind speeds at 200 hPa height can then surpass 35 m s^{-1} over the Indian Ocean and come close to 30 m s^{-1} over the West African coast.

An important observation is the temporary presence of a second TEJ maximum over the coast of West Africa. Whereas the climatological summer mean TEJ appears rather zonally homogeneous over Africa with a general deceleration trend towards the west, the picture might be different on shorter time scales. Over the course of days or weeks, the TEJ may display a regional maximum that is well separated from the climatological TEJ maximum over the Indian Ocean by weaker wind speeds over Central Africa. Koteswaram (1958) was the first to notice and referred to it as a more or less independent West African branch of the TEJ. In years with above-average rainfall, this second maximum tends to be clearly visible even in monthly means. As of yet, it is not clear, whether this regional intensification of the TEJ over West Africa purely portrays the time-integrated upper-level circulation response to the positive heating anomaly of a wetter than normal monsoon season or whether other mechanisms are involved.

Although being described as exceptionally persistent, the TEJ nonetheless exhibits some variability over a wide range of time scales – from the subdaily up to the multidecadal time scale. With the help of Doppler radar measurements, substantial subdaily to daily variability of the TEJ has been observed and associated with the advective motion of embedded jet cores, activity of fast waves and an effect of convection (Ratnam et al., 2011). Moreover, Sathiyamoorthy et al. (2007) reported a significant variability of the TEJ over the Indian monsoon system on time scales between 32 and 64 days. They linked it to meridional displacements of the TEJ core that follow some 14 days after shifts of the Indian monsoon rainbelt (, which tend to occur on similar time scales). For the West African branch of the TEJ, subseasonal modes of variability have not been systematically studied yet.

The summer mean intensity and position of the TEJ also varies from year to year. Figure 1.5 depicts the local variability of the JJAS (June, July, August, September) mean TEJ intensity over the last seven decades as provided by radiosonde measurements over Abidjan (Ivory Coast) and a number of reanalysis data sets. As evident from the fig-

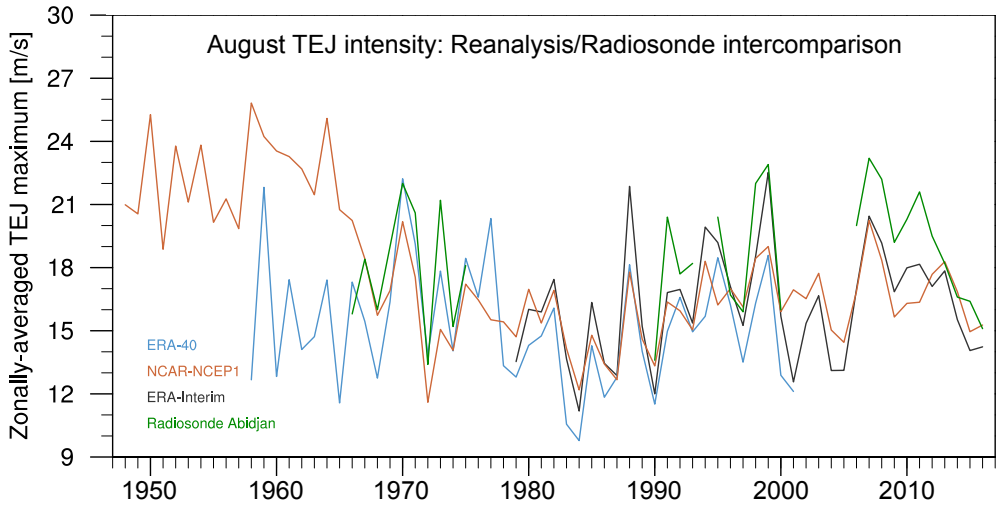

Figure 1.5: Time series from 1948 - 2013 depicting either the radiosonde-derived TEJ intensity at Abidjan (Ivory Coast) or the values derived from three reanalyses at the grid point closest to Abidjan, respectively.

ure, the JJAS mean velocity of the TEJ in one particular year may surpass that of another year by more than 50% in some regions over West Africa. This interannual variability of the TEJ may be attributed to both the effects of more local or remote forcings. Anomalies in WAM rainfall and related changes in the diabatic heating and momentum fluxes constitute a local forcing as illustrated in Lafore et al. (2010, their Fig. 1). Remotely induced TEJ variability can be associated with large-scale anomalies in tropical SSTs. For instance, ENSO-related surplus diabatic heating strongly modulates the divergent Walker circulation and regional Hadley circulations, which can substantially affect the TEJ intensity. Over India, the TEJ is generally weakened during a developing El Niño event, whereas it is intensified in the course of a La Niña event (Chen and van Loon, 1987; Pattanaik and Satyan, 2000; Nithya et al., 2017). It is important to note that the local forcing of TEJ variability – changes in local monsoon rainfall – may also be caused by changes in the remote forcing in the first place – a disentanglement of observed TEJ anomalies into locally- and remotely-driven parts is therefore hard to conduct without the help of dedicated numerical experiments. In addition to the tropical diabatic heating, the mid-latitude circulation may also substantially effect the interannual variability of the TEJ (Tanaka, 1982).

On decadal to multi-decadal time scales, the TEJ shows a long-term weakening trend over the Indian monsoon region. The relatively stronger warming of the equatorial upper troposphere over the Indian Ocean compared to the warming over subtropical regions, reduces the thermal contrast and thereby weakens the TEJ as a result of the thermal wind relationship (Joseph and Sabin, 2008; Abish et al., 2013). Trends in TEJ intensity over West Africa fundamentally differ from those observed over the Indian region. During the last 40 years, the seasonal mean TEJ intensity remained nearly constant. For the wet period of the 1950s and 1960s the NCAR-NCEP reanalysis shows a much stronger TEJ (Fig. 1.5), but the robustness of the reanalysis output is questionable as it not well constrained due to the nonavailability of satellite-derived data (Stickler and Brönnimann, 2011).

1.5 Relationship between the TEJ and Sahel rainfall

In the previous section, I emphasized that the TEJ and rainfall in the tropics are intrinsically linked since the latent heat release by tropical deep convection is one of the main drivers of the TEJ. In this section, in which I review the current state of literature regarding the observed TEJ – Sahel rainfall relationship, I will therefore focus on the possible **active** role of the TEJ on rainfall over West Africa.

Shortly after its detection via radiosonde measurements, the variability of the TEJ has been put in relation to monsoon rainfall variability – first for the Indian monsoon system. Early observational studies by Kobayashi (1974) and Kanamitsu and Krishnamurti (1978) reported a correlation between monsoonal rainfall over India and the regional TEJ velocity. Later on, multiple studies followed for the relationship between rainfall and the TEJ intensity over Africa. Hulme and Tosdevin (1989) noted that rainfall in the eastern Sahel region may be affected by the TEJ on synoptic to interannual time scales. In particular the interannual variability of precipitation over Sudan appears to be highly correlated with the year-to-year changes of the TEJ. Grist and Nicholson (2001) and Sylla et al. (2010) used observations and numerical model experiments to show that rainfall over the Sahel region and the TEJ velocity are strongly correlated on interannual to decadal time scales. Figure 1.6 shows that not only decadal trends (thicker lines) are very similar, but even on a year-to-year basis, Sahel rainfall changes often coincide with same-sign anomalies in TEJ intensity. Nicholson (2009) even suggested that "the link between the TEJ and rainfall is a causal one with the strong TEJ enhancing rainfall by enhancing upper-level divergence". But does the Tropical Easterly Jet really play an active role for precipitation?

As mentioned in the section before, the main climatological features of the TEJ (intensity, position, extent) can be interpreted as the planetary-scale stationary wave response to the global distribution of tropical diabatic heating; or in other words: tropical precipitation drives the large-scale tropical circulation including the TEJ and not vice versa. Kiladis and Weickmann (1997) investigated the lead-lag relationship between convection and the large-scale circulation at 200 hPa on time scales between 6 and 30 days. According to them, this statement holds mainly true in regions of upper-level easterlies on such time scales.

Nonetheless, it would probably be mistaken to consider the TEJ an exclusively passive phenomenon in relation to rainfall. On shorter, synoptic to intraseasonal time scales, the TEJ exhibits spatially inhomogeneous fluctuations in its zonal velocity. Spatially coherent regional maxima with a width of some hundreds of kilometres may appear from time to time. These regional maxima bear resemblance to jet streaks on mid-latitude jets which are known to modulate the upper-level divergence and thereby aid cyclogenesis or foster widespread deep convection. Redelsperger et al. (2002) observed a spatio-temporal connection between regional TEJ maxima and organized convection and noted that the spatial configuration exhibits similarities with that typically observed at mid-latitude jet streaks. He called attention, however, to the uncertainty of this relationship in terms of cause and effect. By examining a number of selected synoptic cases, Besson and Lemaître (2014) highlighted that upper-level divergence in the entrance region of regional TEJ maxima might play an important role for the initi-

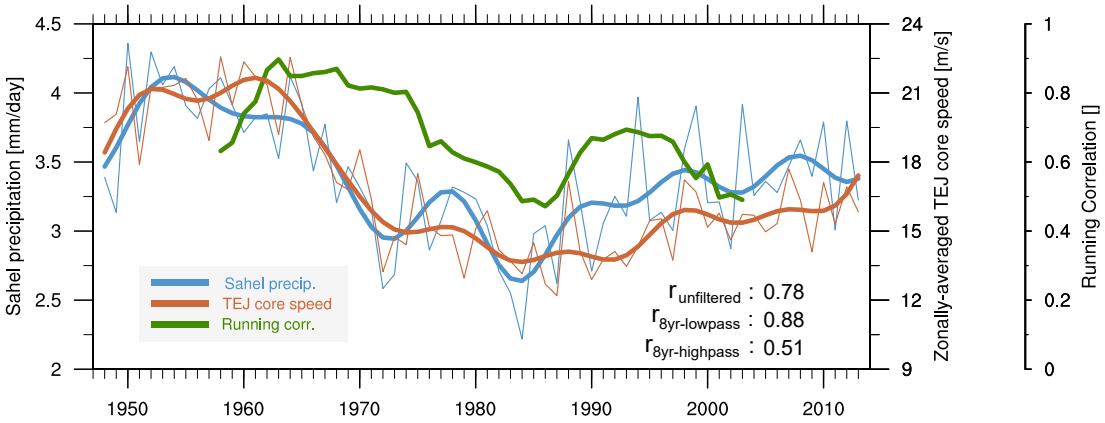

Figure 1.6: Time series from 1948 - 2013 of JJAS mean Sahel precipitation (from CRU TS3.22 data spatially averaged over 10°W to 10°E and 10°N to 20°N) and JJAS mean West-African TEJ intensity (for a representative TEJ intensity measure that is insensitive to latitude changes, the average JJAS TEJ core speed is calculated from daily NCAR-NCEP reanalysis fields of 200 hPa zonal wind data as follows: Within a domain between 15°W to 15°E and 5°S to 25°N, the daily maximum of easterly 200 hPa zonal wind speed is found for each longitudinal strip of grid points. The found maximum speeds of each longitude are then averaged over the whole domain to obtain an average speed of the TEJ core). Thin, light lines depict the unfiltered yearly means. Thick lines show the 10-year low pass filtered time series. The green line depicts the 21-year running correlation. This figure is directly taken from Lemburg et al. (2019, see chapter 2).

ation and particularly organization of mesoscale convective systems (MCSs). Druyan (1998) also suggested that the sustained anomalous upper-level divergence in the right entrance of regional TEJ maxima over West Africa may promote convective activity in certain parts of the Sahel.

As shown in figure 1.7a, the TEJ can in fact exhibit a jet streak-like intensification over the coastal region of West-Africa on synoptic time scales. According to quasi-geostrophic theory, jet streaks are associated with substantial ageostrophic flows in their entrance and exit regions. Depending on the Rossby number (Ro), which characterizes the applicability of the quasi-geostrophic approximation, theory predicts different patterns of anomalous convergence and divergence in the proximity of the jet streak: For $Ro \ll 1$, a symmetric four cell divergence-convergence pattern exists, with anomalous upper-level divergence at the anticyclonic-shear side (poleward in case of an easterly jet) entry as well as at the cyclonic-shear side (equatorward) exit of a jet stream (e.g., Uccellini and Johnson, 1979, see figure 1.7b). If Ro surpasses 0.5, the four cell pattern transforms to a simpler two-cell pattern, with divergence in the entrance and convergence at the exit of a jet streak (Van Tuyl and Young, 1982). This may be the most likely state observed at the TEJ over West Africa, given that its typical mean position ($\sim 6°$N) typically yields $Ro \approx 0.7$ (see calculation Besson and Lemaître, 2014). Substantial divergence can therefore only be expected at jet entrance regions.

However, it is important to stress the fundamental differences to quasi-geostrophic dynamics at mid-latitude jet streaks. Because of the smallness of the Coriolis parameter and the resulting weak temperature gradients, synoptic-scale forced dry ascent throughout the troposphere is generally assumed to be weak (Charney, 1963; Raymond et al., 2015). As a consequence, jet streaks at the TEJ cannot feature any deep transverse circulation with large-scale lifting along sloped isentropes, as observed at

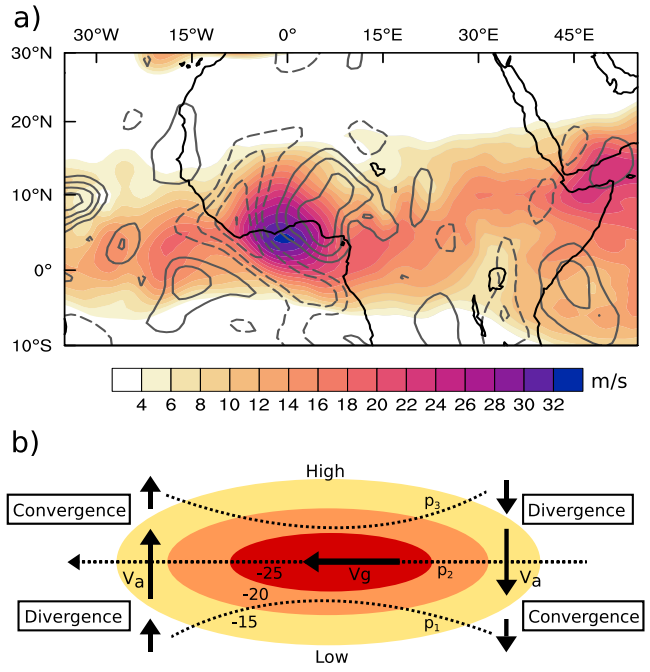

Figure 1.7: Divergence pattern possibly associated with regional TEJ maxima. **a)** 12-hour averaged 200 hPa zonal wind field from ERA-Interim on August 28th 2009. Contours show anomalous divergence (solid) and convergence (dashed) with an interval of $5 \cdot 10^{-6}\,\mathrm{s}^{-1}$. **b)** Sketch of the idealized situation at a straight easterly jet streak with the typical upper-level divergence at the right entry/left exit. Dashed lines depict isobars and the contours show isotaches. This figure is directly taken from Lemburg et al. (2019, see chapter 2).

their mid-latitude counterparts (e.g., Uccellini and Johnson, 1979). However, Besson and Lemaître (2014) described TEJ streak-induced ascending motions reaching down as far as 4 km above ground level. Thereby, TEJ-induced divergence may pre-condition the atmosphere by decreasing its static stability, making convection more likely to occur. In line with this, Couvreux et al. (2012) have shown with idealized LES simulations that prescribed anomalies in large-scale mid-tropospheric ascent of only $2\,\mathrm{cm\,s}^{-1}$ can be a deciding factor for the initiation of convection in the semi-arid Sahel region. Jet streak-related divergence may further benefit the organization and in particular the persistence of MCSs by aiding the upper-level outflow (Besson and Lemaître, 2014).

From a more climatological point of view, Flohn (1964) already utilized the jet streak concept to explain the differences in the northward extent between the Indian monsoon system and the WAM. He suggested that West Africa is influenced by a thermally indirect jet exit circulation which induces large-scale subsidence north of the TEJ and thereby sharply limits the northward spread of WAM rainfall. Over the Indian subcontinent in the TEJ entrance region, the opposite transverse circulation favours rainfall reaching much further north. Interestingly, Koteswaram (1958) drew a similar conceptual picture, but already included the West African branch of the TEJ. He argued that precipitation in certain parts of the Sahel may be promoted by the favourable upper-level dynamics within the right entrance of this second branch. It should be noted again, however, that it is hard to disentangle cause and effect, particularly on longer time scales, on which the second TEJ maximum might be mainly considered a response rather than a possibly active phenomenon. I therefore want to point out that the first

part of my PhD research, which I will outline in the next section, concentrates on the role of synoptic-scale jet maxima over West Africa as shown in figure 1.7a.

The TEJ may also exert a secondary order effect on rainfall via its summer mean background state. As mentioned in the prior theoretical section about monsoons, the upper-level easterlies play an important role in shielding the monsoon circulation from the effect of extratropical eddies (Bordoni and Schneider, 2008). The background mean flow in the equatorial upper troposphere may further affect the activity of AEWs (Yang et al., 2018). A stronger and wider TEJ is associated with favourable equatorial Rossby wave propagation characteristics which promotes AEW activity – and thereby possibly rainfall.

1.6 Novelty and objectives of this study

As highlighted in the previous section, it is still unclear whether the TEJ over West Africa plays an active role for Sahel rainfall. A plausible explanation for the observed high covariability between rainfall and TEJ intensity on interannual to multi-decadal time scales is also still missing. This is followed immediately by the next important question: Is the TEJ – Sahel rainfall relationship stationary or does it fundamentally change under different climatic conditions? In this thesis, I aim to shed light on these unanswered issues by framing them into four specific research questions. This section provides an outline of my research questions and sets forth the rationale and novelty of the research related to them.

First I want to explore whether the TEJ over West Africa exerts any significant effect on Sahel rainfall. To tackle this problem, I will first conduct an in-depth statistical investigation of the TEJ – Sahel rainfall relationship on much shorter, synoptic to intraseasonal time scales. Such a study has been missing so far, since most investigations on the TEJ – Sahel rainfall relationship focused on longer time scales. The subseasonal variability of the West African TEJ has generally been studied little and it is not clear whether it is linked to any of the more extensively studied modes of synoptic to intraseasonal rainfall variability. The first part of my thesis therefore aims to close this gap by asking:

RQ1: Is the strong TEJ – Sahel rainfall relationship observed at interannual and decadal time scales also present at much shorter, synoptic to intraseasonal time scales?

In a closely related follow-up part, I will focus on the question whether the TEJ may affect mesoscale convective systems – and thereby possibly Sahel rainfall – through modulations of the upper-level divergence in the proximity of embedded jet maxima.

Besson and Lemaître (2014) and Redelsperger et al. (2002) identified a notable dynamical setup between TEJ streaks and convection and suggested that TEJ streaks may aid the development of mesoscale convective systems. It has to be kept in mind that synoptic-scale balanced ascent is generally thought to be weak in the tropics due to the smallness of the Coriolis parameter and the associated weak temperature gradients (Charney, 1963; Raymond et al., 2015). In other words, the high Rossby numbers that

characterize the tropics may call into question the applicability of a quasi-geostrophic frame work within the context of jet streaks on the TEJ. However, the latitude of the TEJ and the resulting Rossby numbers may lie within a range where the application of quasi-geostrophic concepts may still be justified to some extent. I therefore substantially extend the work of Besson and Lemaître (2014) and provide a more complete statistical investigation of the upper-level winds and their divergence before the initiation of Sahelian MCSs. I will further test whether any significant anomalies in MCS lifetime, size or intensity are associated with TEJ-induced divergence. In contrast to Besson and Lemaître (2014), my analysis is not limited to a few individual MCS events, but involves roughly 300 MCS initiation cases in the period 2007-2015 which allows to assess statistical robustness. A further novelty of my study is the inclusion of the Eumetsat divergence data set (EUMETSAT, 2005). Derived from atmospheric motion vectors of satellite-tracked water vapour features, this data set provides a very reliable measure of the large-scale upper-tropospheric divergence. My second research question can be summarized as follows:

RQ2: Does the TEJ over West Africa substantially affect convection over the Sahel via a previously proposed effect of upper-level divergence induced by regional TEJ maxima?

After answering the first two research questions, I will shift the focus towards explaining the observed, substantial covariability between Sahel rainfall and TEJ intensity on interannual to decadal time scales. Existing literature (e.g., Mathon et al., 2002; Lafore et al., 2010) and also the research related to RQ1 and RQ2 show that the TEJ over West Africa can be substantially accelerated by strong convection over the Sahel. Integrated over a whole monsoon, the effect of anomalous convective activity on the TEJ could be significant as high-frequent noise of the upper-level wind is filtered out. But does this effect really explain the high covariability between the TEJ intensity and Sahel rainfall observed on interannual to multi-decadal time scales? To answer this question, one has to understand both what drives the variability of WAM rainfall and that of the TEJ over West Africa. As already outlined in section 1.3, the interannual to multi-dedadal variability of precipitation and its relation to more local (e.g., land surface changes, SST in the Gulf of Guinea) or remote forcings (e.g., SST anomalies in the Indian Ocean) has been studied extensively and will not be further explored in this thesis. What drives the interannual to decadal variability of the TEJ over West Africa, however, is unclear. One the one hand side, there is the previously mentioned local diabatic forcing by WAM convection: a regional TEJ intensification can be understood as the upper-level Gill-type response to an anomalous off-equatorial heating or, in other words, simply as the balanced equatorward outflow of widespread convection over the Sahel. One the other hand side, previous studies have also noted that the TEJ (over India and also West Africa) is influenced by the variability of the remote diabatic heating via the induced changes in the planetary-scale divergent tropical circulation (e.g., Chen and van Loon, 1987; Preethi et al., 2015; Nithya et al., 2017). To the best of my knowledge, no study has yet attempted to disentangle and quantify the role of remote versus local diabatic heating which motivates the third research question of my thesis:

RQ3: What are the dominant tropical drivers of the interannual to decadal variability of the West African TEJ? Is the local diabatic forcing associated with WAM rainfall variability important or does the remote diabatic forcing play a substantial role?

Answering this question will greatly help to understand the observed strong TEJ – Sahel rainfall covariability on interannual to decadal time scales. This study will further be valuable in the context of the studies of Bordoni and Schneider (2008) and Yang et al. (2018) who implied that the mean "background" state of the TEJ (width and intensity of easterlies) may modulate WAM rainfall. A further novelty of this study is the attribution of TEJ intensity anomalies to precipitation changes in certain regions of the globe with the help of additional experiments. Thereby I aim to identify the key regions whose diabatic heating variability exerts substantial influence on the West African TEJ. What is the pure effect of ENSO, what is the role of Indian rainfall and how strongly does a much wetter than normal WAM season affect the TEJ?

In the last part of my PhD study, I will utilize my previously gained knowledge about the TEJ – WAM rainfall relationship in today's climate and investigate whether this relationship changes under different climatic conditions. A very-well suited example is the mid-Holocene, a climatic period in which the WAM was much more intense and extended farther northwards than today (Street-Perrott and Perrott, 1993; Claussen and Gayler, 1997; Jolly et al., 1998). Evidence from climate proxies and model results suggest that the WAM was less affected by teleconnections as a consequence of attenuated tropical SST variability (Otto-Bliesner, 1999; Koutavas et al., 2006; Zhao et al., 2007). Moreover, Collins et al. (2017) suggested that the TEJ might have played a role in explaining the rapid end of the African humid period. This food for thought motivates me to investigate whether the spatial configuration and temporal relationship between the TEJ and WAM rainfall are similar to today or fundamentally different under mid-Holocene conditions. How are rainfall and TEJ intensity correlated on interannual to (multi-)decadal time scales? Is the remote diabatic heating still such a dominant driver of the West African TEJ variability? Besides the study of Collins et al. (2017) I am not aware of any study that has yet investigated the TEJ – WAM rainfall relationship under mid-Holocene conditions. I therefore conclude my PhD research with the following question:

RQ4: Does the TEJ – Sahel rainfall relationship change under different climatic conditions as they were present during the mid-Holocene?

In summary, this thesis aims to extend our current understanding of the relationship between the TEJ and rainfall over West Africa – an "understanding" which is so far mainly based on statistical relationships found on interannual to decadal time scales. To my best knowledge, this is the first comprehensive study that explores extensively the variability of the West African TEJ over a wide range of time scales and relates it to changes in rainfall. A special emphasis is placed on the question of whether the TEJ may play an active role for Sahel rainfall by promoting convection via its influence on the upper-level divergence.

1.7 Summary and discussion of results

In this section, I summarize and discuss the main findings of my PhD thesis, providing answers to the four research questions I posed in the previous section. Research question 1 and 2 are answered in detail in the attached paper (chapter 2) entitled "Sahel rainfall – Tropical Easterly Jet relationship on synoptic to intraseasonal time scales" which has been published in the "Monthly Weather Review". The third research question is examined in-depth in the second attached paper (chapter 3) with the title "Role of remote versus local diabatic forcing for the interannual to decadal variability of the Tropical Easterly Jet over West Africa", which is currently prepared for submission. The research related to research question 4 is also attached in form of a research article but represents ongoing work (chapter 4). Therefore, some of the results with regard to research question 4 are preliminary and the scope of this work might be extended upon in the future.

1.7.1 Sahel rainfall – TEJ relationship on subseasonal time scales

Multiple studies highlighted the high correlation between the summer mean intensity of the TEJ over West Africa and summer mean Sahel rainfall (Grist and Nicholson, 2001; Sylla et al., 2010). Years with higher than normal Sahel precipitation are on average accompanied by a regionally enhanced TEJ south of the main rain band. If one assumes a direct interaction between the TEJ and Sahel rainfall, it should be observable also on much shorter time scales - even in the presence of a much higher noise level in the upper-level wind field. However, so far there has been no in-depth investigation of this relationship for much shorter synoptic to intraseasonal time scales. In this study I therefore quantify the covariability and the lead-lag relationship between the TEJ over West Africa and convection over the Sahel over a range of synoptic to intraseasonal time scales. For this, spectral analysis, lead-lag correlations and regression analysis are applied to a 32-year-long record of observed daily outgoing longwave radiation (NOAA-OLR, Lee, 2014) and daily output from multiple reanalyses: ERA-Interim, NCAR-NCEP and JRA-55 (Kobayashi et al., 2015). OLR is chosen as a suitable proxy for convective activity. My main findings can be summarized as follows:

- The statistical relationship between the West African TEJ intensity and convective activity over the Sahel is substantially weaker on synoptic to intraseasonal time scales (correlations below 0.3) than on interannual to decadal time scales (correlations between 0.5 and 0.9)
- On synoptic time scales (2-8 days), periods of anomalous convective activity significantly lead changes in the regional TEJ intensity by one or two days which suggests that convection anomalies are more likely to cause changes in the regional TEJ than vice versa

The main results are well supported by figure 1.8. It shows the results of a lead-lag correlation analysis applied to a 32-year-long data set of daily OLR and corresponding daily ERA-Interim output of 200 hPa zonal wind. With the help of bandpass-filtering, the lead-lag relationship between the TEJ intensity and convective activity over the Sahel is determined for three time scales: synoptic (2–8 days), submonthly (10–25 days)

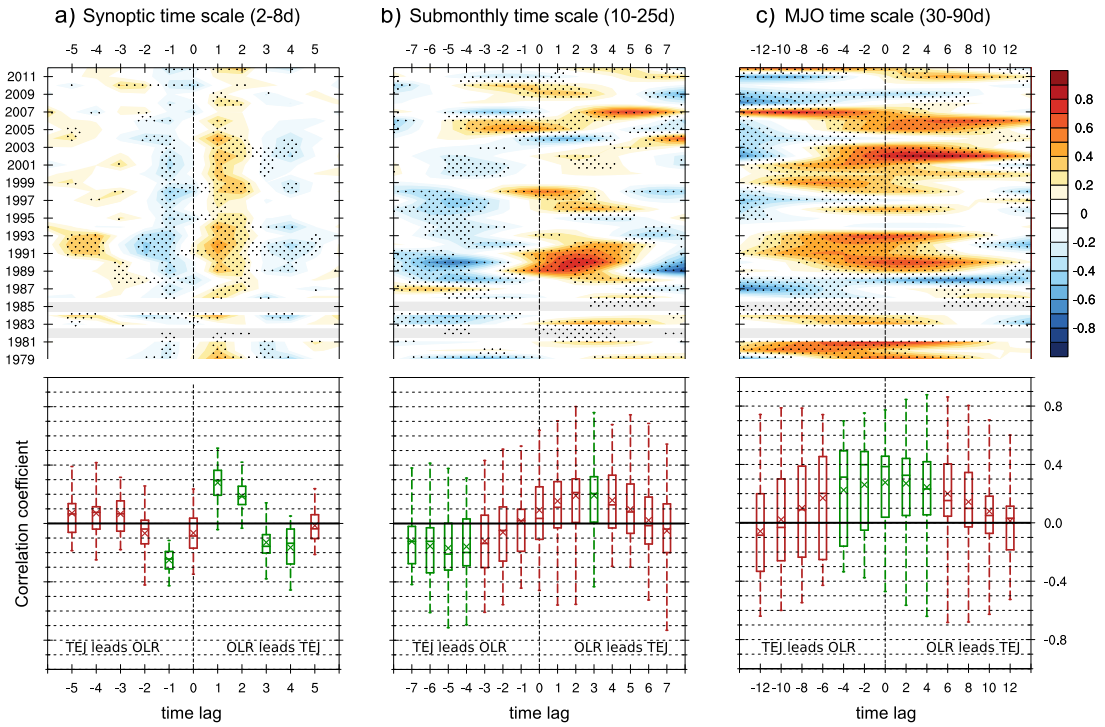

Figure 1.8: Relationship between regional TEJ intensity and convective activity in the Sahel over a range of synoptic to intraseasonal time scales. Top: Lead-lag correlations between OLR and 200 hPa zonal wind throughout 32 years. A positive correlation coefficient means that increased convection (negative OLR anomaly) goes along with increased TEJ speed (negative zonal wind anomaly) or vice versa. Positive correlations observed at positive time lags indicate that phases of an intensified TEJ lag phases of stronger convective activity. The correlations are calculated separately for each year from daily bandpass-filtered JJAS data of regionally averaged OLR (15°W to 15°E and 8°N to 16°N OLR and 200 hPa zonal wind (averaged from 15°W to 15°E and 2°N to 10°N). Stippling indicates statistical significance at the 5% level determined by a bootstrapping test with 5000 iterations. Bottom: Box and Whisker plot for the corresponding minima, maxima, the 25%, 50% and 75% quartiles and the average (crosses) of the correlation coefficients. Positive lag means that changes in OLR lead changes in 200 hPa zonal wind. The green color of the boxes denote time lags for that the average correlation is statistically significant at the 5% level (determined by a bootstrapping test with 5000 iterations). This figure is directly taken from Lemburg et al. (2019, see chapter 2).

and MJO time scale (30–90 days). Lead-lag correlations are calculated for each monsoon season individually (see top half of Fig. 1.8) and averaged afterwards (see bottom half). A positive correlation coefficient means that increased convection (negative OLR anomaly) goes along with increased TEJ speed (negative zonal wind anomaly) or vice versa. Positive correlations observed at positive time lags indicate that phases of an intensified TEJ lag phases of stronger convective activity. For synoptic time scales (2-8 days), a clear and significant relationship is identified: OLR anomalies consistently lead TEJ anomalies by one or two days (Fig. 1.8a), meaning that an intensified TEJ is mainly observed after a period of increased convective activity and not vice versa. On time scales between 10 and 90 days, the lead-lag relationship is less clear due to the lack of clear, well-separated peaks in the correlogram. The main result, the significant lead-lag relationship on synoptic time scales, is consistent among all three analysed reanalyses (not shown).

The finding that the statistical connection between the TEJ intensity and convective activity over the Sahel is much weaker on shorter time scales is certainly not un-

expected. High-frequent noise in the upper-level wind is not filtered out, as it is the case when correlations are calculated for seasonal averages over longer multi-year time scales. By means of lead-lag correlation analysis, I have shown, however, that a clear and significant lead-lag relationship exists particularly on synoptic time scales: Easterlies tend to be weakened before a burst of increased convection and only increase thereafter. This result suggests that increased convection is in most cases not promoted in the entrance region of regional TEJ maxima. It further provides a strong hint that the balanced outflow of widespread deep convection might accelerate the TEJ. The found lead-lag relationship generally agrees with the findings of Kiladis and Weickmann (1997) who investigated the spatio-temporal relationship between the upper-level flow and convective activity, but on a global scale using other data sets and a different time filtering (6-30 days). They demonstrated that in regions of upper-level easterlies, the convection generally drives the upper-level circulation and not the other way around.

1.7.2 The effect of TEJ-induced upper-level divergence on MCSs

The research related to RQ1 addresses the intensity fluctuations of the zonal component of the TEJ and their relationship to Sahel rainfall. For a better understanding of the role of the TEJ, one also has to consider the upper-level divergence associated with the ageostrophic components of the TEJ. In this follow-up study I therefore revisit the possible effect of TEJ-induced upper-level divergence on convection over the Sahel. Nicholson (2009) and Besson and Lemaître (2014) stressed a possible important role of the TEJ in modulating the upper-level divergence field. Besson and Lemaître (2014) observed regional jet streak-like maxima at the TEJ and compared them to their much more-studied counterparts found at the mid-latitude jets. They argued that upper-level divergence in the entrance regions of such jets could be favourable for the development of well-organized and persistent MCSs. The limiting factor of this study is that it is based on a rather small number of case studies, which calls into question the robustness of their results. My study overcomes this drawback by including a sufficiently large number of MCS cases.

An objective MCS tracking algorithm developed by Huang et al. (2018) is applied to the 3-hourly Gridsat-B1 brightness temperature data set (Knapp and Wilkins, 2017). I search for long-lived (>= 9 hours) and large (>= 100 km radius) Sahelian-type MCSs which are responsible for the lion's share of Sahel rainfall (Mathon and Laurent, 2001) and are the convective systems most likely to interact with large-scale dynamics (Fink and Reiner, 2003). To rule out that the upper-level flow is too heavily modulated by preceding or adjacent MCS, it is checked that each tracked MCS represents a more or less isolated system that is temporally and spatially well separated from other systems. The tracking algorithm is applied for 9 monsoon seasons (JJAS) between 2007–2015 (limited to the availability period of the Eumetsat divergence data set). The Eumetsat divergence data set is based on satellite-derived atmospheric motion vectors and thereby represents a good estimate of the large-scale upper-tropospheric divergence (EUMETSAT, 2005). I focus on MCSs that are initiated in a Sahel region between 10°W to 10°E and 10°N to 15°N. Of all MCSs generated in this area over the span of 9 years, I create a temporal and spatial composite such that all developing MCSs are now centred at the origin of a MCS genesis relative coordinate system. Due to this large composite,

my analysis is thereby not limited to a few individual MCS events as in Besson and Lemaître (2014), but involves an ensemble of 289 MCS initiation cases. This enables a robust investigation of the average synoptic conditions before, during and after initiation of MCSs and allows further to assess the range of conditions under which MCSs form. The analysis of the atmospheric state before and during MCS initiation is based on the aforementioned Eumetsat divergence product and the reanalyses ERA-Interim (Dee et al., 2011), JRA-55 (Kobayashi et al., 2015) and MERRA-2 (Gelaro et al., 2017). The most important results of this study can be summed up as follows:

- In the clear majority of cases, MCS initiation is not associated with TEJ streaks or any other significant anomalies of the upper-tropospheric wind field
- TEJ streak-related upper-level divergence and/or anomalous TEJ intensity are not significantly correlated with size, lifetime, intensity or movement speed of MCSs

The first main finding is illustrated by figure 1.9. It shows anomalies in OLR and atmospheric conditions associated with the initiation of 289 MCSs in form of a composite mean depicted on a MCS initiation-centred relative lon-lat grid. The first row shows the composite-averaged situation 3 hours before 289 large Sahelian MCSs form. At this time, the composite mean shows an insignificant westerly wind anomaly of up to $1\,\mathrm{m\,s^{-1}}$ slightly southwest and a weak, but significant southerly anomaly of $0.5\,\mathrm{m\,s^{-1}}$ to the east of the future MCS genesis region. Consistent with the composite-averaged anomalous wind field as diagnosed from ERA-Interim reanalysis, the Eumetsat divergence product shows a weak but significant convergence anomaly in the upper troposphere right above the MCS genesis area. This anomalous convergence is observed over 24 hours before MCS formation – in both, the Eumetsat and ERA-Interim data set. An ensemble-wide evaluation of absolute Eumetsat-based divergence values shows that only 21% of all 289 MCSs are initiated under large-scale upper-level divergence exceeding the climatological summer mean of that area. Substantial divergence larger than $5 \cdot 10^{-6}\,\mathrm{s^{-1}}$ is only registered in 15% of all cases, and values above $10^{-5}\,\mathrm{s^{-1}}$ exist in only 2% of all cases.

The second main finding is supported by figure 1.10. Here I present, in the form of scatter plots, the relationship between several MCS key parameters and pre-existing large-scale divergence at 200 hPa. This analysis is motivated by the high intra-composite variability of upper-level wind anomalies among the 289 MCS initiation cases. All scatter plots strongly resemble random distributions with no apparent clusters. No significant correlations are found between any MCS-related parameter (lifetime, size, intensity, movement speed) and pre-existing anomalous divergence. It is further tested whether any significant relationship exists when one filters out the noise of the anomalous divergence field by only considering substantial deviations from the median. According to this method (see figure caption for details), substantially above-median MCS lifetime, size, intensity or movement speed are not significantly associated with pre-existing anomalous divergence at the TEJ level. Thus, I conclude that the TEJ plays no major role for MCS organization, at least not by modulating the upper-level divergence field.

Although my findings draw a rather robust picture, I cannot rule out that individual cases exist in which a distinct TEJ streak could foster MCS development. Thus,

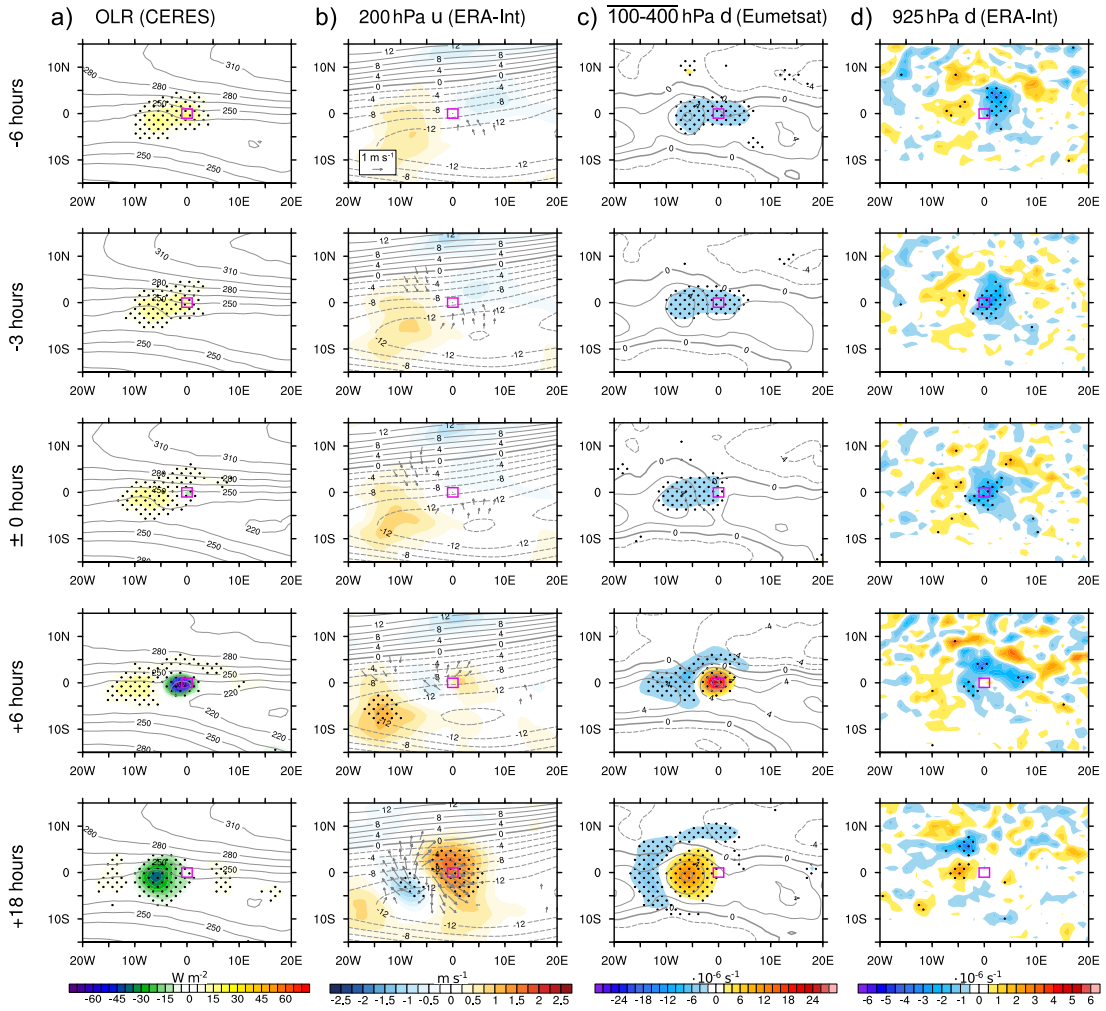

Figure 1.9: MCS initiation centred relative latitude-longitude maps of composite mean anomalies (average over 289 MCS initiation cases in the Sahel-Sudanian region) of OLR (CERES), 200 hPa zonal wind u (shaded) and significant 200 hPa wind vectors (both ERA-Interim), upper-tropospheric $\overline{100–400\,\text{hPa}}$ divergence d (Eumetsat), and 925 hPa divergence d (ERA-Interim). Anomalies are calculated against the time of day reference state obtained by 12-day low-pass filtering (shown with contour lines). Rows designate different time lag/lead relative to the time of MCS genesis. The small magenta box is a visual aid depicting the MCS genesis area. Dots indicate statistical significance at the 5% level tested by bootstrapping with 5000 iterations. This figure is directly taken from Lemburg et al. (2019, see chapter 2).

my results do not necessarily stand in contrast to the findings of Besson and Lemaître (2014). Because of the much larger sample size, however, it becomes evident that both the initiation and the degree of organization of MCSs are not significantly associated with jet streaks on the TEJ, or more generally, any kind of anomalous upper-level divergence. Only after an MCS has already formed, the upper-level wind field is modulated by its anticyclonic divergent outflow in a way that the zonal wind field resembles a classic jet streak configuration. My results therefore raise doubts on the applicability of a jet-streak based conceptual framework at very low latitudes and generally question the relevance of forced synoptic-scale ascent for promoting tropical convection. Thus, my findings are consistent with previous theoretical work which stressed that balanced dry ascent is generally weak in the tropics and should play no major role for convection (e.g., Charney, 1963; Raymond et al., 2015).

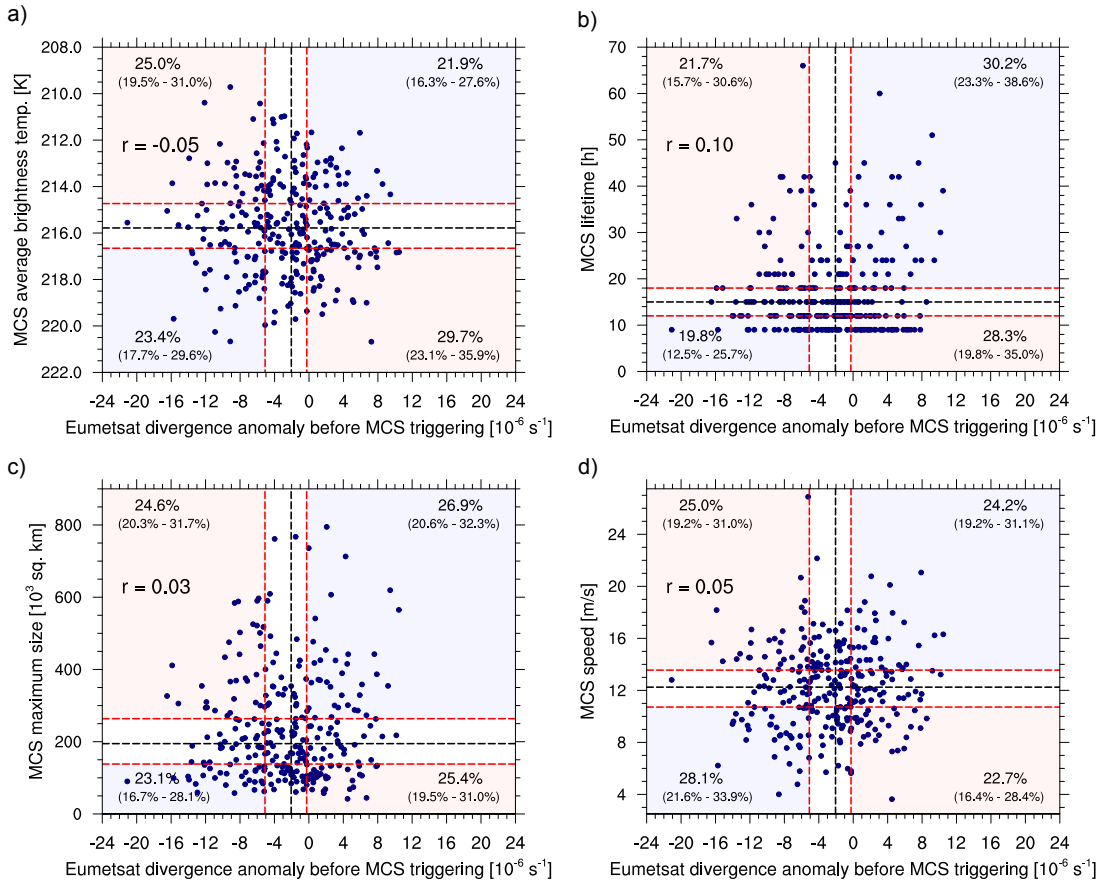

Figure 1.10: Relationship between pre-existing large-scale divergence and several MCS parameters characterizing its degree of organization for the ensemble of 289 MCSs in the Sahel-Sudanian region. Scatter plots showing the a) MCS intensity (average brightness temperature), b) MCS lifetime, c) MCS maximal size and d) MCS travel speed as a function of anomalous large-scale divergence 6 hours prior to MCS genesis. The horizontal black line shows the median value of the respective MCS quantity, the black vertical line represents the median for the preceding divergence anomaly. Red lines depict the respective tertiles for the MCS quantity and preceding divergence. The percentage values express the relative frequency of MCS for each of the four outer quadrants which are bounded by the horizontal and vertical red lines (and marked by the light shading). The percentages in parentheses denote the 5% and 95% confidence bound determined by a bootstrapping routine with 5000 iterations. If 25% is not within this span, we assume that above/below median MCS parameter values are significantly more/less often observed in the respective quadrant. This figure is directly taken from Lemburg et al. (2019, see chapter 2).

In summary, the results of the first part of this dissertation (research questions 1 and 2) question the previously proposed hypothesis that the TEJ might play a role for Sahel rainfall via its effect on the upper-level divergence. The conducted statistical analyses demonstrate that the regional TEJ intensity over West Africa and convection over the Sahel are only weakly correlated on synoptic to intraseasonal time scales. More importantly, anomalous convective activity seems to induce changes in the regional TEJ and not vice versa – hinting at a rather passive role for the TEJ. This result is supported by the in-depth statistical analysis of nearly 300 MCSs and the contemporaneous synoptic conditions in the upper troposphere. Neither their initiation nor their degree of organization is significantly associated with TEJ-induced upper-level divergence or anomalous TEJ intensity.

Of course, some questions with regard to RQ1 and RQ2 remain open due to the limitations of this study. All analyses are confined to the satellite era (after 1979) because only from there on is the atmospheric state well-enough constrained resulting in generally high agreement among different reanalysis models. Therefore, the wet WAM phase during the 1950s and 1960s has not been covered. If the NCAR-NCEP reanalysis can be trusted before the satellite era, this period was characterized by a West African TEJ that was likely both more intense and more closely related to Sahel rainfall. One can therefore conceive that the TEJ over West Africa might have played a more active role for Sahel rainfall in that period. Another possible limitation is the use of OLR as a proxy for rainfall and the rather low temporal (3 hours) and spatial resolution (1°) of the OLR and reanalysis data sets. Because the TEJ and possible embedded streaks are mainly synoptic-scale features, there is nonetheless grounds for confidence that they are reasonably well represented by the rather coarse-resolution reanalyses. Therefore, the study's main purpose, the analysis of the upper-tropospheric flow prior to the formation of MCSs, should not be limited too severely by the low resolution. The last and possible the most important limiting factor is the focus on TEJ-induced upper-level divergence. It cannot be ruled out that the TEJ over West Africa may affect Sahel rainfall via other mechanisms.

1.7.3 Role of remote vs. local diabatic forcing for TEJ variability

What is the explanation of the high correlation between the summer mean TEJ intensity over West Africa and Sahel rainfall? To find an answer, I will focus on a directly related question: What is the dominant tropical diabatic forcing that drives the interannual to decadal variability of the TEJ over West Africa? Is it the local diabatic forcing variability associated with anomalous WAM rainfall or do anomalies of the remote diabatic heating play a substantial role?

To tackle this research question, I first analyse observational and reanalysis data of the last 40 years. Linear correlation and regression analysis is used to discover the relationships between the West African TEJ intensity, observed rainfall and SST anomaly patterns. It becomes evident that in particular the interannual variability of the TEJ over West Africa is not only strongly correlated with changes in WAM rainfall, but also with remote changes in rainfall over India, the Maritime Continent and the Pacific (Fig. 1.11a,b). Moreover, TEJ intensity and WAM rainfall are both strongly linked to remote SST anomalies. However, some differences show up on the correlation maps shown in figure 1.11c/d: The variability of the TEJ over West Africa appears to be substantially more linked to remote tropical anomalies (particularly in the Pacific) whereas WAM rainfall is slightly more influenced by extratropical SST changes. For a better understanding, a suite of dedicated numerical experiments is carried out.

PUMA, an AGCM based on dry dynamics and very simple physics (Fraedrich et al., 1998), is driven with 3D JJAS mean diabatic heating patterns of the years 1979-2017. An additional nudging towards a previously-tuned zonally-uniform relaxation temperature (Newtonian cooling) is applied in a way that it enforces a quite realistic global circulation (including mid-latitude jets, baroclinic eddies) while simultaneously allowing an as free as possible response to diabatic forcing anomalies. The model is run in T63 resolution (≈ 200 km) with 31 vertical levels. For each experiment, the period of

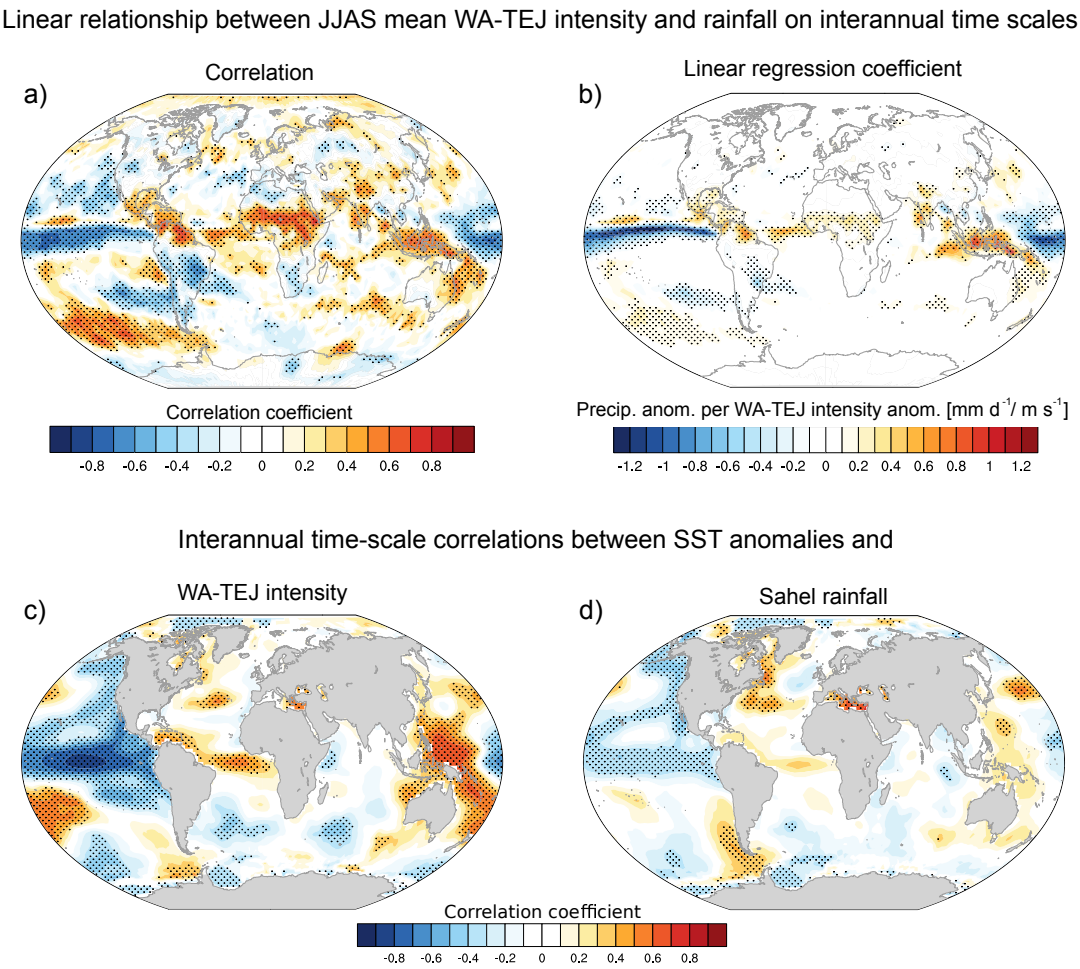

Figure 1.11: a) Linear point-wise relationships between the West African TEJ intensity and global observed precipitation. The left column depicts the Pearson correlation coefficient between 8-year high-pass filtered values of an West African TEJ intensity index (derived from ERA-Interim) and also 8-year high-pass filtered global observed precipitation (GPCP). The right column depicts the linear regression coefficient determined via least-squares method. b) Linear point-wise correlations between observed SST anomalies and West African TEJ intensity left column) and Sahel rainfall (right column). The West African TEJ intensity is derived from ERA-Interim by first finding the daily jet core maximum for each longitudinal strip on the basis of daily ERA-Interim (Dee et al., 2011) output of zonal wind at 200 hPa. Thereafter, the jet core latitude and velocity values are zonally averaged between 15°W and 15°E and temporally averaged over each respective monsoon season (JJAS). Sahel rainfall is represented by a field mean in a box over 15°W to 15°E and 10°N to 20°N. This figure is compiled from two figures in Lemburg and Bader (2020, see chapter 3).

1979-2017 is simulated in form of 39 individual time slice experiments meaning that for each monsoon season, the PUMA model is run for 11 simulated years. This technique guarantees robust estimates of the quasi-equilibrium response to the respective diabatic forcing. The key quantity for this study is the JJAS mean TEJ intensity over West Africa which is calculated as follows: using daily output, the TEJ core maximum is found for each longitudinal strip and then averaged in space over the longitudes 15°W to 15°E and in time over the last 10 simulated years (first year disregarded as spin-up).

Three main experiments are designed: In the control experiment, the so-called total forcing simulation (PUMA-TF), the interannual to decadal variability of the TEJ is simulated as realistically as possible by letting the total global summer mean diabatic

heating field vary from year to year. In the other two experiments, we disentangle the respective contributions from the local WAM-related forcing and the remote forcing. For this, the diabatic heating field is split up geographically into an African and rest of globe part. In the local forcing experiment (PUMA-LF), the diabatic heating is only allowed to vary over Africa but is kept constant at climatological values everywhere else. Vice versa, the remote forcing experiments (PUMA-RF) feature realistic year-to-year diabatic heating variability over most of the globe but fixed climatological heating over Africa. Due to the limitations in the temporal availability of robust reanalysis data from which we derive diabatic heating patterns (1979-2017), I focus particularly on the interannual (but do not explicitly exclude the decadal) variability of the TEJ intensity. With additional simulations, I further aim to understand the isolated effects of substantial diabatic heating anomalies in those regions which show high correlations between West African TEJ intensity and observed rainfall. The main results of this study can be summarized as follows:

- Remote diabatic heating variability is the dominant forcing that explains most of the simulated TEJ variability and induces TEJ anomalies with amplitudes close to typically observed ones
- The local forcing through WAM rainfall changes alone only explains one third of the West African TEJ variability within the PUMA model space and only induces TEJ anomalies one third as strong as observed ones
- By far the most dominant forcing for interannual TEJ variability is ENSO: La Niña related changes in the tropical diabatic heating significantly increase the intensity of the TEJ over West Africa whereas typical El Niño type anomalies weaken the TEJ by about 20%

The first two main results are both encapsulated in figure 1.12. It depicts the variability of the JJAS mean West African TEJ intensity as simulated by the dedicated PUMA experiment suite (solid, coloured lines) and compares it to the ERA-Interim-observed variability (black, dashed line). The green line represents the PUMA-TF simulation which is driven with the unaltered diabatic heating fields in which the total global year-to-year variability is retained and not restricted to either the local African or remote regions. The correlation between PUMA-TF and ERA-Interim amounts to 0.81 which means that the PUMA model is able to explain two thirds of the observed TEJ variability over West Africa.

Shifting the focus to the blue and red lines, which depict the local (PUMA-LF) and remote forcing (PUMA-RF) simulations, respectively, one obtains a remarkably clear result with regard to the role of local vs. remote forcing: The interannual to decadal variability of the West African TEJ is dominated by the effect of remote diabatic heating variations. Measured within the PUMA model space, i.e., with respect to the total forcing PUMA-TF simulation, PUMA-RF displays a very high correlation of 0.95 which translates to an explained variance of 91% (95% confidence interval 84%-95%). The local forcing associated with WAM rainfall variability plays a comparatively minor, albeit also statistically significant role. The simulation in which the remote forcing is held constant, PUMA-LF (blue line), displays a substantially lower correlation of 0.59 to PUMA-TF which translates to an explained variance of 35% (95% confidence interval:

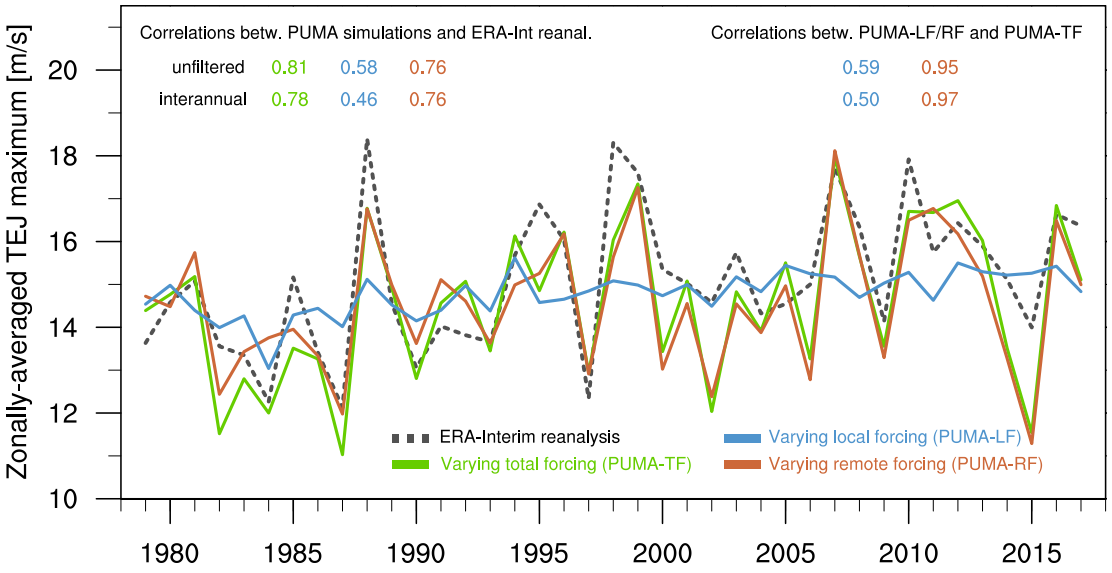

Figure 1.12: The conducted PUMA simulations suggest that the remote forcing is the dominant driver of the interannual to decadal variability of the West African TEJ intensity. The dashed black line depicts the TEJ intensity as given by the ERA-Interim reanalysis. The blue lines show the simulated TEJ intensity of the **PUMA-LF** (local forcing) simulations in which the year-to-year variability of the JJAS mean diabatic heating fields is restricted to the African region, meaning that outside of Africa, the diabatic heating is kept constant to climatological values. The red lines depict the simulated TEJ intensity of the **PUMA-RF** (remote forcing) simulations in which the diabatic heating is kept constant over Africa but is allowed to vary in the rest of the globe. The green line shows the results of simulations driven with the **PUMA-TF** (total forcing), in which the total (local and remote) variability of the diabatic heating is retained. All simulations were run with the same PUMA model setup with a tuned zonally-uniform relaxation temperature field in order to enforce a realistic extratropical circulation, and a simple, subjectively tuned vertical diffusion scheme that mimics the convective momentum transport. All depicted correlations coefficients (Pearson's r) are significant at the 5% level tested via bootstrapping with 5000 iterations. This figure is directly taken from Lemburg and Bader (2020, see chapter 3).

11-59%). A multivariate regression analysis is not performed because the local forcing is substantially forced by the remote diabatic heating and is therefore not an independent predictor. This is why the explained variances do not add up to 100%. Why does the local forcing play a minor role in comparison to the remote forcing? The PUMA simulations indicate that although the solely local forcing-induced West African TEJ anomalies are strongly correlated to Sahel rainfall, they are too weak, however, to be on par with the much stronger anomalies caused by the remote forcing (the standard deviation of the TEJ intensity is three times smaller in PUMA-LF compared to PUMA-RF).

ENSO clearly represents the dominant forcing on the interannual time scale (see pronounced TEJ intensity peaks/dips in La Niña years 1988, 1998 and 2007 and El Niño years 1982, 1987 and 1997). However, even if all years with strong ENSO events are removed from the time series, significant correlation between simulated TEJ variability in the remote forcing-driven experiments and observed TEJ variability still exists although the explained variability with respect to ERA-Interim drops from from 58% to 33%. Measured within the PUMA model space, the remote forcing remains the dominant one, though.

By means of additional experiments, I identify the key regions for which observed

changes in the diabatic heating exert the largest effect on the West African TEJ. In general agreement with the linear relationships presented in figure 1.11, SST anomalies and associated anomalous heating in the tropical Pacific display the most substantial effect on the upper-level easterlies over West Africa. El Niño, for instance, represents a very strong heating over the central and eastern Pacific which is nearly symmetric about the equator. The atmospheric response to such an anomalous heating is very similar to the familiar Matsuno-Gill-type pattern (see Gill, 1980). A stationary Kelvin wave response is excited to the east of the heating which induces anomalous upper-level westerlies over a wide longitudinal range including West Africa. Thereby, the core speed of the TEJ can be substantially diminished by about $3\,\mathrm{m\,s^{-1}}$ on average. These results, which highlight the substantial effects of ENSO, are in good agreement with the findings of Chen and van Loon (1987) and Nithya et al. (2017). Changes in the Indian monsoon rainfall, however, show no significant influence on the intensity of the West African TEJ as long as the rainfall and associated diabatic heating anomalies are constrained to the observed variability.

The conducted study is limited mainly by two factors. First, the fact that the PUMA simulation with the total forcing is only able to explain two thirds of the observed TEJ variability over the last 39 years. One possible cause is the use of the described time slice setup instead of a transient run in order to isolate the steady-state response to a diabatic forcing. Averaging over the 10-year integration time eliminates the atmospheric noise due to transient disturbances which is why differences to the real-world observed state are therefore expectable, particularly in years where the anomalous diabatic forcing is weak. Further explanations are the simplified physics of the model and any systematic errors of the model input fields (relaxation temperature, diabatic heating fields). The second drawback is the fact that only the TEJ variability of the last 39 years is investigated because reliable forcing data is only available from the begin of the satellite era in 1979 to today. As mentioned earlier, Sahel rainfall was substantially stronger in the 1950s and 1960s. Therefore it cannot be ruled out that the contribution of the local forcing was more important during this wet period.

Despite its limitations, the results of this study provide valuable insight into the observed TEJ – Sahel rainfall relationship although the interpretation is not straightforward. The PUMA simulations show that the local forcing-induced TEJ variability is very strongly correlated to Sahel rainfall. As evident from figure 1.12, the induced anomalies are, however, much weaker than the anomalies caused by the remote forcing. Moreover, in the real world the mean TEJ intensity of a particular monsoon season might be affected by atmospheric noise associated with transient disturbances. Therefore, only the remote forcing induces substantial variability that may stand out against a background noise level. How this affects the Sahel rainfall – TEJ relationship depends on whether the remote forcing induces simultaneous same-sign changes in Sahel rainfall. In the recent decades, same-sign changes occur, for instance, in years with a pronounced La Niña where the anomalous remote diabatic heating not only intensifies the TEJ over West Africa but also promotes increased Sahel rainfall (e.g., Janicot et al. 1996; Rowell 2001). The SST-related variability of the remote diabatic heating over the tropical Pacific may therefore be viewed as important driver of the observed Sahel rainfall – TEJ relationship over the recent four decades.

1.7.4 The TEJ – WAM rainfall relation during the mid-Holocene

During the mid-Holocene, the WAM was much more intense and extended much farther to the north. Moreover, WAM rainfall variability was likely less affected by teleconnections as particularly tropical Pacific SST variability was weaker than today according to proxy data and coupled model simulations (Otto-Bliesner, 1999; Koutavas et al., 2006; Zhao et al., 2007). These pronounced differences to the present state motivate an analysis of the WAM rainfall – TEJ relationship under mid-Holocene conditions.

I analyse existing fully-coupled climate simulations conducted with MPI-ESM 1.2 (Giorgetta et al., 2013): a mid-Holocene control run with orbital parameters and greenhouse gas levels at the level of 8000 year BP in which the atmosphere is coupled to a sufficiently spun-up ocean (see for details Brovkin et al., 2019). As a control experiment, I use a fully-coupled pre-industrial control simulation with modern-day orbital parameters and greenhouse gases prescribed to pre-industrial levels. Both simulations are rerun for 60 years with daily output frequency and additional temperature tendency output from which diabatic heating can be diagnosed. The mid-Holocene TEJ intensity – WAM rainfall relationship on interannual to decadal time scales and its contrast to the present-day is characterized by means of time series and the application of standard correlation analysis. To assess a possibly changing importance of teleconnections, I further produce correlation maps of both TEJ intensity and WAM rainfall with respect to simulated global SST anomalies. As in the previous section related to RQ3, I ask again what are the important tropical drivers of the TEJ variability on interannual to decadal time scales: Is the remote diabatic heating as important as in today's climate or does the local forcing associated with WAM rainfall become more important during the mid-Holocene? To answer this question I conduct simulations with PUMA in which the diabatic heating is this time taken directly from the MPI-ESM model output. The direct contributions from either the local or the remote diabatic forcing on the TEJ variability are separated using the same technique as in Lemburg and Bader (2020, in prep.; see section 3.2 of this thesis). All results I summarize here have been recently created in the course of ongoing work and should therefore be considered preliminary:

- The covariability between the summer mean TEJ intensity over West Africa and Sahel rainfall is simulated to be substantially weaker under mid-Holocene conditions than today
- The "centre of action" in the spatio-temporal TEJ – rainfall relationship over West Africa moves substantially to the northeast (correlations are close to zero when evaluating western Sahel rainfall; significant correlations around 0.6, which are closer to today's observed values, only occur in relation to eastern Sahel rainfall)
- The interannual to decadal variability of the West African TEJ is no longer dominated by the remote diabatic forcing, but is explained to equal parts by the local forcing associated with WAM rainfall anomalies and the remote forcing

The first two main results are supported by figure 1.13 which depicts the interannual to multi-decadal relationship between the West African TEJ intensity and Sahel rainfall for the simulated mid-Holocene climate (Fig. 1.13a,b) and the pre-industrial control climate (Fig. 1.13c). In stark contrast to today, the relationship between the TEJ over

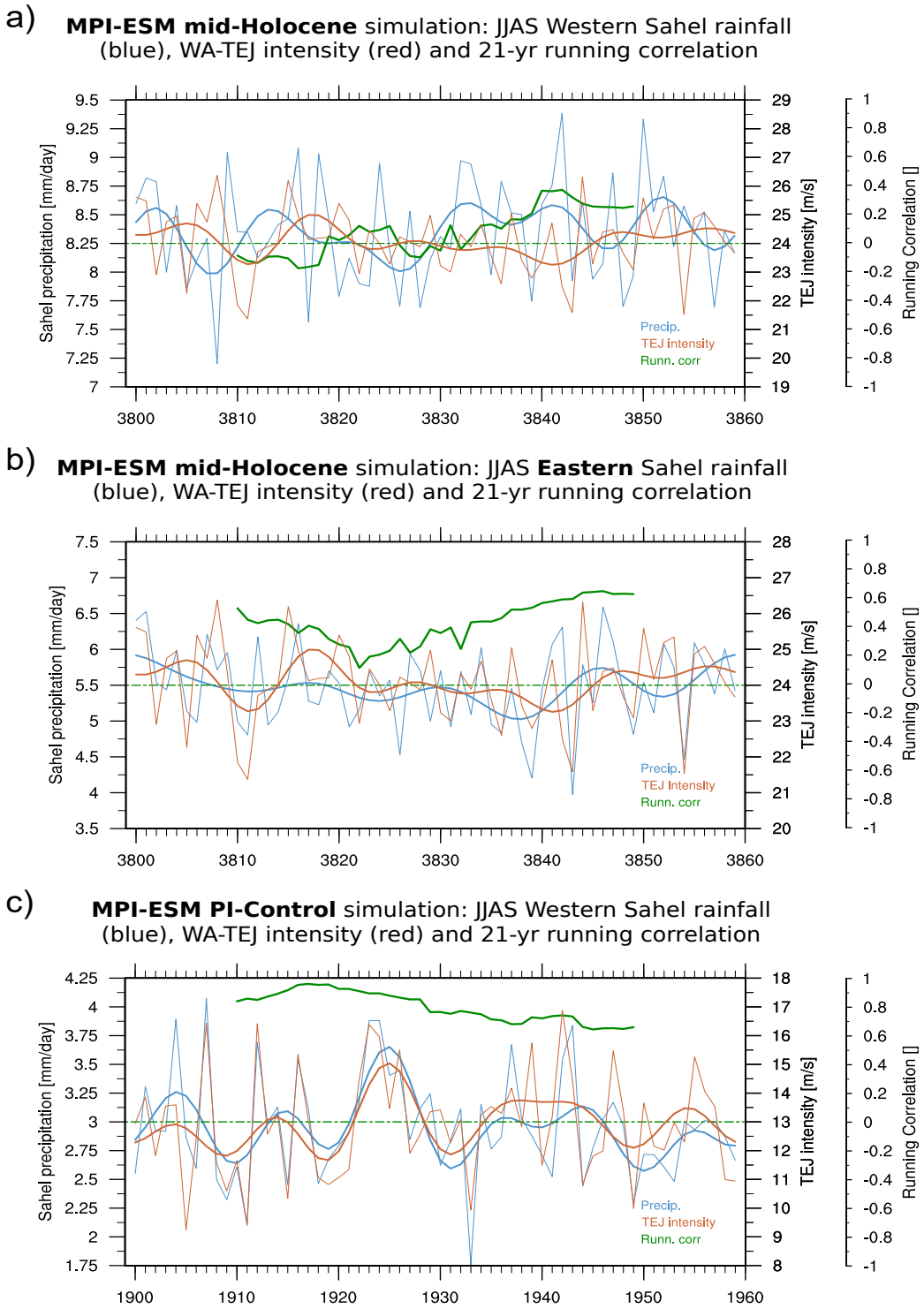

Figure 1.13: 60-year-long time series of simulated JJAS mean Sahel precipitation and West African TEJ intensity, and running correlation between both quantities for the mid-Holocene (a,b) and the pre-industrial control climate (c). The difference between a) and b) is the region over which Sahel rainfall is averaged: for a) the western Sahel, rainfall is averaged over 15°W to 15°E and 10°N to 20°N whereas for b) the eastern Sahel, rainfall is averaged over 0°E to 30°E and 12°N to 25°N. For a representative TEJ intensity measure that is insensitive to latitude changes, the average JJAS TEJ core speed was calculated from daily output of 200 hPa zonal wind data as follows: Within a domain between 15°W to 15°E, the daily maximum of easterly 200 hPa zonal wind speed is found for each longitudinal strip of grid points. The found maximum speeds of each longitude are then averaged over the whole domain to obtain an average speed of the TEJ core. Thin, light lines depict the unfiltered yearly means. Thick lines show the 10-year low pass filtered time series. The green lines depict the 21-year running correlations.

West Africa and rainfall over the Sahel is simulated to be considerably lower under mid-Holocene conditions. Particularly in the western Sahel, the correlations between regionally-averaged rainfall and TEJ intensity are insignificant (Fig. 1.13a). The "centre of action", the region where WAM rainfall and West African TEJ intensity are substantially correlated, moves northeastward in the simulated mid-Holocene WAM. Shifting the averaging box to the eastern Sahel and extending it slightly further northwards, the correlation rises and becomes statistically significant again (r=0.54, Fig. 1.13b). However, the mid-Holocene TEJ – rainfall relationship remains substantially below what is simulated for the pre-industrial climate (r=0.77, in range with observations of the present-day climate of the last four decades).

The last-listed striking result, the fundamentally changing role of the remote diabatic forcing, is illustrated by figure 1.14. In the simulated mid-Holocene climate, the interannnual to decadal variability of the TEJ is driven in equal parts by the local and the remote diabatic forcing which marks a strong contrast to the present-day climate for which the remote forcing is clearly dominant. Expressed within the model space, i.e., with respect to the PUMA total forcing simulation, 44% of the TEJ variability over the 60 simulated mid-Holocene years is captured when the variability of the diabatic heating is restricted to the African continent (local forcing experiment, blue bar on the very left in Fig. 1.14). Only 33% of the TEJ variability can be solely explained by the variability of the remote diabatic forcing (remote forcing experiment, red bar). By means of statistical tests, no forcing can be considered dominant during the mid-Holocene, though (see wide confidence interval depicted as error bars). For the pre-industrial control experiment, the obtained results are consistent with the main findings related to RQ3 where I used reanalyses and observations of the last decades as input for PUMA (depicted as a reference on the very right in Fig. 1.14). The interannual to decadal variability of the TEJ over West Africa is explained to a large extent by the variability of the remote diabatic heating (88% explained variance). Only 24% of the TEJ variability is reproduced in the local forcing experiment which isolates the sole effect of anomalous diabatic heating associated with WAM rainfall anomalies.

The presented results may be compromised by the comparatively low capability of my model setup in reproducing the TEJ variability during the mid-Holocene. The total forcing simulation, driven with simultaneously varying local and remote forcing, only explains 46% of the MPIESM-simulated TEJ variability (in contrast to 60% which is the case for the present-day climate, see the green numbers above the bars in Fig. 1.14). Possible causes of this drop in explainable TEJ variability may involve an increased importance of extratropical influences and/or an overall reduced signal-to-noise ratio. Nevertheless, the following can be said with certainty: With regard to the role of the tropical diabatic heating (even if its importance for TEJ variability is generally diminished) the remote forcing loses its role as clearly dominant forcing as both the remote and the local forcing become equally important under mid-Holocene conditions.

What is the cause for such a fundamental shift, from a remote forcing-dominated to a much more local forcing-driven TEJ variability? A likely explanation is the simulated attenuation of the Pacific SST variability which is in accordance with previous studies (Otto-Bliesner, 1999; Zhao et al., 2007). In line with the reduced SST variability, the variability of tropical precipitation and the associated predominantly condensational

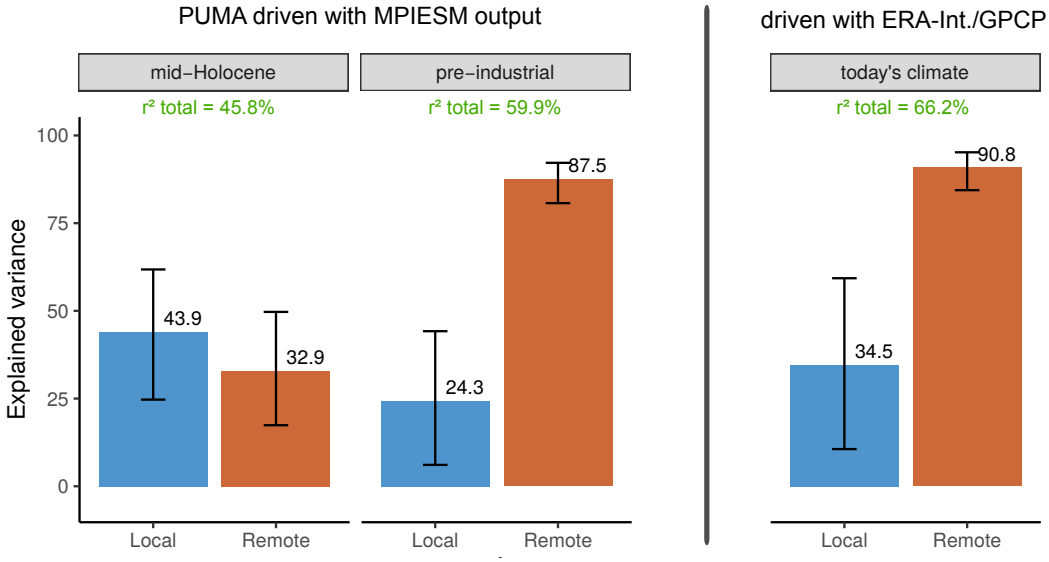

Figure 1.14: The role of the remote vs. local forcing for explaining the West African TEJ variability during the mid-Holocene compared to today's climate. The four bar plots on the left show, for either the simulated mid-Holocene or pre-industrial climate, the respective interannual to decadal variability of the TEJ that is explained by either the local or remote diabatic forcing. The explained variance is calculated with respect to the so-called total forcing PUMA simulations (PUMA-TF) in which the total global year-to-year variability of the diabatic heating is retained. The diabatic heating fields are taken from the previously-conducted mid-Holocene and pre-industrial control simulations with the complex model MPI-ESM. Error bars show the 95% confidence interval as determined by a bootstrapping procedure with 5000 iterations. The green numbers printed above the bars denote the explained variance of the respective PUMA-TF simulation with respect to the interannual to decadal TEJ variability that is directly calculated from the MPI-ESM simulations. As a reference, the two separated bar plots on the right show the related results from chapter 3 where the role of remote vs. local forcing was evaluated for the last 40 years based on ERA-Interim and GPCP rainfall-related diabatic heating fields.

heating also diminishes. Furthermore the rainfall anomaly patterns and amplitudes associated with dominant modes of SST variability change, especially over the Pacific, which alters the characteristics of the induced atmospheric response. Thereby, the remote influence on the West African TEJ, which is communicated mainly by a standing Kelvin wave, becomes much less pronounced. In addition to the attenuated importance of the remote forcing, one could argue that the increased magnitude of the local forcing due to the much higher precipitation plays a role in explaining the switch in the dominant drivers of TEJ variability. However, although the climatological precipitation rises by a factor of 2 to 3 over the Sahel, the more important year-to-year variability and the associated anomalous heating remains comparable to the present-day climate. It therefore seems likely that the diminished tropical SST variability is the main reason why the TEJ variability in the mid-Holocene is not dominated by the variability of the remote diabatic heating as is the case in today's climate.

The reduced importance of the remote diabatic heating is likely also the explanation why the Sahel rainfall – TEJ intensity relationship is simulated to be weaker in the mid-Holocene compared to today. As outlined in the discussion to RQ3, in the present-day state (over the last four decades) the variability of the diabatic heating over the Pacific marks a substantial forcing which often induces substantial in-phase changes in both Sahel rainfall and TEJ intensity. In the mid-Holocene, the attenuation of the remote

forcing leads to an overall decrease of the signal-to-noise ratio. The relationship between WAM rainfall and TEJ intensity may apparently be closer due to the increased importance of the local forcing. The TEJ anomalies induced by the local forcing, however, are likely too weak to stand out against the atmospheric noise level.

1.8 Overarching conclusions

Summer mean Sahel rainfall and the intensity of the TEJ over West Africa are strongly correlated on interannual to (multi-)decadal time scales. A number of studies hypothesized that the TEJ might play an important role for Sahel rainfall via its control on upper-level divergence (Druyan, 1998; Redelsperger et al., 2002; Nicholson, 2009; Besson and Lemaître, 2014). In my thesis, I therefore comprehensively investigated the relationship between the TEJ and Sahel rainfall over a wide range of time scales. A particular emphasis was put onto the question whether the TEJ might significantly affect rainfall through the modulation of the upper-level divergence. In addition, I explored the underlying mechanisms which explain the observed high TEJ – rainfall covariability on longer time scales by investigating the dominant drivers of the TEJ variability. As a last question, I asked whether the TEJ – Sahel rainfall relationship observed today might had been fundamentally different in the altered climate state that prevailed during the mid-Holocene. At the end of this unifying essay, I briefly summarize the most important findings as answers to the four posed research questions:

RQ1: Is the strong TEJ – Sahel rainfall relationship observed at interannual and decadal time scales also present at much shorter, synoptic to intraseasonal time scales?

The covariability between the intensity of the West African TEJ and convection over the Sahel is substantially weaker on synoptic to intraseasonal than on longer, interannual to (multi-)decadal time scales. More importantly, phases of anomalous convective activity significantly lead changes in the regional TEJ intensity by one or two days, suggesting that convection anomalies are more likely to cause changes in the regional TEJ than vice versa. These results are obtained by an in-depth statistical analysis involving lead-lag correlations and spatio-temporal regression analysis applied to daily data of multiple reanalyses.

RQ2: Does the TEJ over West Africa substantially affect convection over the Sahel via a previously proposed effect of upper-level divergence induced by regional TEJ maxima?

Neither the initiation nor the degree of organization of MCSs over the Sahel is associated with significant West African TEJ anomalies or anomalous jet-induced upper-level divergence. This finding is based on the results of a composite analysis of the reanalysis-derived anomalous atmospheric fields and observed upper-level divergence anomalies in association with the initiation of nearly 300 MCSs. In combination, the results related to RQ1 and RQ2 strongly suggest that the TEJ cannot be considered an active player with regard to Sahel rainfall, at least not via its influence on the upper-level divergence field as suggested before. It has to be stressed, however, that a possible effect of the TEJ on Sahel rainfall via other mechanisms cannot be ruled out and should

be subject to future studies.

RQ3: What are the dominant tropical drivers of the interannual to decadal variability of the West African TEJ? Is the local diabatic forcing associated with WAM rainfall variability important or does the remote diabatic forcing play a substantial role?

The interannual to decadal variability of the TEJ intensity over West Africa is governed to large extent by the variability of the remote diabatic heating. This conclusion, valid for the recent four decades, is based on a suite of experiments conducted with the PUMA model which is able to explain two thirds of the ERA-Interim-"observed" TEJ variability when driven with summer mean diabatic heating fields of the period 1979-2017. The interpretation of this finding with regard to the observed Sahel rainfall – TEJ intensity relationship is not straightforward. While the solely local forcing-induced TEJ anomalies are strongly correlated to Sahel rainfall, they are too weak, though, to stand out against the much stronger anomalies caused by the remote forcing. However, particularly the strong diabatic forcing anomalies in connection with ENSO – the dominant mode of tropical SST variability – generally tend to force same-sign changes in both Sahel rainfall and TEJ intensity. The remote diabatic forcing associated with tropical Pacific SST variability may therefore be viewed as one of the most important drivers of today's observed Sahel rainfall – TEJ relationship, at least on interannual time scales.

RQ4: Does the TEJ – Sahel rainfall relationship change under different climatic conditions as they were present during the mid-Holocene?

Under mid-Holocene conditions, the simulated spatio-temporal TEJ – Sahel rainfall covariability on interannual to decadal time scales decreases substantially compared to the present-day climate. The summer mean intensity of the TEJ is not significantly correlated to western Sahel rainfall and an nearly as strong relationship as today exists only to rainfall in the more eastern parts of the Sahel. Probably the most important reason for this simulated decline in covariability is the diminished role of the remote forcing which has substantially less influence on both rainfall and the TEJ intensity over West Africa compared to today.

In synopsis, my PhD work is a prime example that a thorough investigation of an observed correlation is always valuable, if not necessary. The connection between the TEJ and Sahel rainfall is not straightforward and one has to be careful when drawing implications from a mere statistical analysis. The high observed correlation does not necessarily reflect a strong causal link but is more of an indicator for the influence of a third variable, namely the remote diabatic heating, that induces substantial in-phase changes in both Sahel rainfall and West-African TEJ intensity. During the mid-Holocene, for instance, one would a priori expect a closer connection between Sahel rainfall and the West-African branch of the TEJ as both are much pronounced compared to the present-day state. However, the opposite is the case. The attenuated tropical SST variability weakens the role of the remote forcing as an important driver of both WAM rainfall and the West-African TEJ intensity which may explain the weaker simulated Sahel rainfall – TEJ relationship.

1.9 Outlook

Of course, some puzzle pieces are still missing to complete our understanding of the TEJ – Sahel rainfall relationship. The first missing piece I want to stress concerns the research related to RQ1 and RQ2. By means of in-depth statistical analyses I demonstrate that the TEJ over West Africa does not seem to have any substantial influence on convection over the Sahel, at least not via inducing anomalous upper-level divergence. However, the TEJ could still affect Sahel rainfall via other mechanisms than through the modulation of the upper-level divergence field. What I have not addressed in my studies is the possible interaction between the TEJ and AEWs. Smith (2008) provided an analysis of the dynamics of the AEJ and TEJ presenting a theoretical framework which highlighted the complex interaction between TEJ, AEJ, AEW and Sahel rainfall. In his conclusions, he expresses that the TEJ "can no longer be thought of a passive system with regard to AEW development", but that "a more comprehensive study of its dynamical impacts is necessary". The role of observed planetary-scale waves at the TEJ and their possible interaction with AEWs and synoptic-scale convection was also stressed in Nicholson et al. (2007) and Mekonnen and Thorncroft (2016).

A further important question is whether not only subseasonal fluctuations but rather the background mean state of the TEJ influences Sahel rainfall. In their idealized model study, Bordoni and Schneider (2008) stressed the importance of upper-level easterlies which shield the regional monsoon circulation from the disruptive influences of extratropical eddies. In addition, Yang et al. (2018) showed that AEW activity is influenced by the mean flow characteristics of the equatorial upper troposphere. A stronger and wider TEJ is associated with favourable equatorial Rossby wave propagation characteristics which promotes AEW activity. As I have shown in my study with regard to RQ3, the seasonal background state of the TEJ – its width and intensity – is mainly influenced by remote influences. This leaves the door open for a more "subtle", indirect effect of the TEJ on Sahel rainfall. Due to the rather long chain of interactions specified in Yang et al. (2018), one may only expect a more secondary-order effect, particularly with regard to the more direct effects that are exerted for instance by ENSO (increase of static stability due to upper-tropospheric warming). Further research on this subject can nevertheless be valuable.

My research related to RQ3 shows that the interannual to decadal variability of the TEJ over West Africa is mainly explained by the variability of the remote diabatic heating, in particular over the Pacific. By taking into account the literature that stresses a robust connection between Sahel rainfall and SST anomalies in the tropical Pacific, I propose that the remote diabatic heating is likely also the most important common forcing that explains the high observed covariability between summer mean Sahel rainfall and TEJ intensity. In the near future, this hypothesis should be tested with the help of more complex models that can simulate both the response of the TEJ and Sahel rainfall to a given forcing. The disadvantage of using a complex model would be the missing possibility to disentangle the contributions of the local and remote forcing on the modulation of the TEJ intensity. However, taking the results of my conducted PUMA experiments in consideration, one can argue that the interannual deviations of the summer mean TEJ intensity over West Africa are to large extent directly attributable to the

sole effect of the remote diabatic heating. I therefore envision to conduct a series of SST sensitivity experiments with imposed ENSO-type anomalies to check whether the TEJ – Sahel rainfall covariability is indeed higher when a strong anomalous diabatic heating over the Pacific exists.

Another possible extension of my research related to RQ3 concerns the role of extratropical influences on the TEJ. As Tanaka (1982) noted, the TEJ might be substantially affected by the interannual variability of the extratropical circulation. At least over the Asian monsoon, the effect might be comparable to the effect of ENSO. So far, no studies have attempted to assess the role of the extratropical circulation for the TEJ variability over West Africa. Therefore, a future study could be designed such that the influences of the mid-latitude dynamics on the TEJ over West Africa can be explored. Within a suited numerical model, a prescribed (fixed or transient) diabatic forcing may be imposed for all tropical regions, whereas the extratropical regions may be nudged towards the transient observed climate state. Such a model setup would allow to disentangle the effects of tropical and extratropical forcing. In this context, it would also be valuable to conduct an in-depth analysis of the momentum budget of the TEJ, either applied to model results or multiple reanalyses.

The last part of my PhD study explores the TEJ – rainfall relationship during the mid-Holocene, as an appropriate example for a different but not fundamentally altered climate state. Further study could investigate how the relationship evolves in future climate scenarios. Recent studies have suggested that Sahel rainfall will be increasingly affected by extratropical forcing (Park et al., 2016). Will this also be true for the TEJ? Or could TEJ and Sahel rainfall variability decouple from each other? To answer these questions, one has to investigate how the important drivers of TEJ variability evolve in contrast to the ones of Sahel rainfall. With regard to the TEJ, an emphasis has to be put onto the question of whether the respective roles of local and remote diabatic heating may change in a future climate. As I demonstrate in my last study with regard to RQ4, the importance of the diabatic heating variability was likely diminished during the mid-Holocene, mainly due to changes in the characteristics of tropical Pacific SST variability. It is therefore of particular interest to investigate how tropical SST variability and in particular ENSO change under global warming and whether an influence as substantial as today on the West African TEJ will still exist in the future. Moreover, one has to understand how the climatological TEJ or more generally the mean state of the upper-tropospheric circulation of the tropics reacts to the projected changes of the upper-tropospheric temperature gradients and static stability. For instance, it was already suggested that the recent decrease in TEJ intensity over the Indian monsoon system is attributable to a global warming-related weakening of upper-level temperature gradients (Joseph and Sabin, 2008; Abish et al., 2013). Of course, the future development of the TEJ – Sahel rainfall relationship also depends strongly on the projected rainfall changes over West Africa. A first brief look into existing CMIP5 RCP8.5 scenarios reveals a pronounced divergence in Sahel rainfall projections among different models, with MIROC showing a clear wetting trend whereas GFDL simulates a drying over West Africa. In these models, also the strength of the TEJ – Sahel rainfall relationship differs strongly and the multi-decadal trends of this relationship oppose each other (MIROC-ESM shows a drop in the correlations between TEJ intensity and Sahel

rainfall and divergent trends in those quantities over the last 30 years of the simulations). The evolution of the TEJ – Sahel rainfall relationship is therefore uncertain at this point, and should be subject to future study.

Bibliography

Abish, B., P. Joseph, and O. M. Johannessen (2013). Weakening trend of the tropical easterly jet stream of the boreal summer monsoon season 1950–2009. *Journal of Climate 26*(23), 9408–9414.

Bader, J. and M. Latif (2003). The impact of decadal-scale Indian Ocean sea surface temperature anomalies on Sahelian rainfall and the North Atlantic Oscillation. *Geophysical Research Letters 30*(22).

Besson, L. and Y. Lemaître (2014). Mesoscale convective systems in relation to African and tropical easterly jets. *Monthly Weather Review 142*(9), 3224–3242.

Bordoni, S. and T. Schneider (2008). Monsoons as eddy-mediated regime transitions of the tropical overturning circulation. *Nature Geoscience 1*(8), 515.

Brovkin, V., S. Lorenz, T. Raddatz, T. Ilyina, M. Heinze, I. Stemmler, M. Toohey, and M. Claussen (2019). What was the source of the atmospheric CO2 increase during Holocene? *Biogeosciences 16*, 2543–2555.

Burpee, R. W. (1972). The origin and structure of easterly waves in the lower troposphere of North Africa. *Journal of the Atmospheric Sciences 29*(1), 77–90.

Carlson, T. N. (1969). Synoptic histories of three African disturbances that developed into Atlantic hurricanes. *Monthly Weather Review 97*(3), 256–276.

Charney, J. G. (1963). A note on large-scale motions in the tropics. *Journal of the Atmospheric Sciences 20*(6), 607–609.

Chen, T.-C. (1980). On the energy exchange between the divergent and rotational components of atmospheric flow over the tropics and subtropics at 200 mb during two northern. *Monthly Weather Review 108*(7), 896–912.

Chen, T.-C. (2003). Maintenance of summer monsoon circulations: A planetary-scale perspective. *Journal of climate 16*(12), 2022–2037.

Chen, T.-C. and H. van Loon (1987). Interannual variation of the tropical easterly jet. *Monthly Weather Review 115*(8), 1739–1759.

Claussen, M. and V. Gayler (1997). The greening of the Sahara during the mid-Holocene: results of an interactive atmosphere-biome model. *Global Ecology and Biogeography Letters*, 369–377.

Collins, J. A., M. Prange, T. Caley, L. Gimeno, B. Beckmann, S. Mulitza, C. Skonieczny, D. Roche, and E. Schefuß (2017). Rapid termination of the African humid period triggered by northern high-latitude cooling. *Nature Communications 8*(1), 1372.

Cook, K. H. (1999). Generation of the African easterly jet and its role in determining West African precipitation. *Journal of climate 12*(5), 1165–1184.

Couvreux, F., C. Rio, F. Guichard, M. Lothon, G. Canut, D. Bouniol, and A. Gounou (2012). Initiation of daytime local convection in a semi-arid region analysed with high-resolution simulations and AMMA observations. *Quarterly Journal of the Royal Meteorological Society 138*(662), 56–71.

Dee, D., S. Uppala, A. Simmons, P. Berrisford, P. Poli, S. Kobayashi, U. Andrae, M. Balmaseda, G. Balsamo, P. Bauer, et al. (2011). The ERA-Interim reanalysis: Configuration and performance of the data assimilation system. *Quarterly Journal of the royal meteorological society 137*(656), 553–597.

Dilley, M., R. S. Chen, U. Deichmann, A. L. Lerner-Lam, and M. Arnold (2005). *Natural disaster hotspots: a global risk analysis*. The World Bank.

Druyan, L. (1998). The role of synoptic systems in the interannual variability of Sahel rainfall. *Meteorology and Atmospheric Physics 65*(1-2), 55–75.

EUMETSAT (2005). Upper level Divergence Product Algorithm Description. Technical report, EUM/MET/REP/05/0163.

Fink, A. H. and A. Reiner (2003). Spatiotemporal variability of the relation between African easterly waves and West African squall lines in 1998 and 1999. *Journal of Geophysical Research: Atmospheres 108*(D11).

Flohn, H. (1964). *Investigations on the tropical easterly jet*. Dümmlers Vlg.

Folland, C., T. Palmer, and D. Parker (1986). Sahel rainfall and worldwide sea temperatures, 1901–85. *Nature 320*(6063), 602–607.

Fraedrich, K., E. Kirk, and F. Lunkeit (1998). Portable university model of the atmosphere. *DKRZ Rep 16*.

Gadgil, S. (2018). The monsoon system: Land–sea breeze or the ITCZ? *Journal of Earth System Science 127*(1), 1.

Geen, R., F. Lambert, and G. Vallis (2018). Regime change behavior during Asian monsoon onset. *Journal of Climate 31*(8), 3327–3348.

Gelaro, R., W. McCarty, M. J. Suárez, R. Todling, A. Molod, L. Takacs, C. Randles, A. Darmenov, M. G. Bosilovich, R. Reichle, et al. (2017). The Modern-Era Retrospective Analysis for Research and Applications, Version 2 (MERRA-2). *Journal of Climate* (2017).

Giannini, A., R. Saravanan, and P. Chang (2003). Oceanic forcing of Sahel rainfall on interannual to interdecadal time scales. *Science 302*(5647), 1027–1030.

Gill, A. (1980). Some simple solutions for heat-induced tropical circulation. *Quarterly Journal of the Royal Meteorological Society 106*(449), 447–462.

Giorgetta, M. A., J. Jungclaus, C. H. Reick, S. Legutke, J. Bader, M. Böttinger, V. Brovkin, T. Crueger, M. Esch, K. Fieg, et al. (2013). Climate and carbon cycle changes from 1850 to 2100 in MPI-ESM simulations for the Coupled Model Intercomparison Project phase 5. *Journal of Advances in Modeling Earth Systems 5*(3), 572–597.

Glantz, M. (1995). Drought follows the plow: Cultivating marginal areas. *Ribot, J.; magalhães, A.; Panagides, S.: Climate Change, Climate Variability and Social Vulnerability in the Semi-Arid Tropics. Cambridge University Press, Cambridge*.

Grist, J. P. and S. E. Nicholson (2001). A study of the dynamic factors influencing the rainfall variability in the West African Sahel. *Journal of climate 14*(7), 1337–1359.

Hadley, G. (1735). VI. Concerning the cause of the general trade-winds. *Philosophical Transactions of the Royal Society of London 39*(437), 58–62.

Hagos, S. M. and K. H. Cook (2007). Dynamics of the West African monsoon jump. *Journal of Climate 20*(21), 5264–5284.

Hagos, S. M. and K. H. Cook (2009). Development of a coupled regional model and its application to the study of interactions between the West African monsoon and the eastern tropical Atlantic Ocean. *Journal of Climate 22*(10), 2591–2604.

Haile, M. (2005). Weather patterns, food security and humanitarian response in sub-Saharan Africa. *Philosophical Transactions of the Royal Society B: Biological Sciences 360*(1463), 2169–2182.

Halley, E. (1686). *An historical account of the trade winds and monsoons, etc.*, Volume 16.

Harris, I., P. Jones, T. Osborn, and D. Lister (2014). CRU TS3. 22: Climatic Research Unit (CRU) Time-Series (TS) Version 3.22 of High Resolution Gridded Data of Month-by-month Variation in Climate (Jan. 1901-Dec. 2013). *NCAS British Atmospheric Data Centre, 24th September 2016*.

Hayward, D. F. and J. S. Oguntoyinbo (1987). *Climatology of West Africa*. Rowman & Littlefield.

Held, I. M. and A. Y. Hou (1980). Nonlinear axially symmetric circulations in a nearly inviscid atmosphere. *Journal of the Atmospheric Sciences 37*(3), 515–533.

Herman, A., V. B. Kumar, P. A. Arkin, and J. V. Kousky (1997). Objectively determined 10-day African rainfall estimates created for famine early warning systems. *International Journal of Remote Sensing 18*(10), 2147–2159.

Huang, X., C. Hu, X. Huang, Y. Chu, Y.-h. Tseng, G. J. Zhang, and Y. Lin (2018). A long-term tropical mesoscale convective systems dataset based on a novel objective automatic tracking algorithm. *Climate Dynamics*, 1–15.

Hulme, M. and N. Tosdevin (1989). The tropical easterly jet and Sudan rainfall: a review. *Theoretical and applied climatology 39*(4), 179–187.

Issa Lélé, M. and P. J. Lamb (2010). Variability of the intertropical front (ITF) and rainfall over the West African Sudan–Sahel zone. *Journal of Climate 23*(14), 3984–4004.

Janicot, S., V. Moron, and B. Fontaine (1996). Sahel droughts and ENSO dynamics. *Geophysical Research Letters 23*(5), 515–518.

Janicot, S., F. Mounier, S. Gervois, B. Sultan, and G. N. Kiladis (2010). The dynamics of the West African monsoon. Part V: The detection and role of the dominant modes of convectively coupled equatorial Rossby waves. *Journal of Climate 23*(14), 4005–4024.

Janicot, S., S. Trzaska, and I. Poccard (2001). Summer Sahel-ENSO teleconnection and decadal time scale SST variations. *Climate Dynamics 18*(3-4), 303–320.

Jolly, D., I. C. Prentice, R. Bonnefille, A. Ballouche, M. Bengo, P. Brenac, G. Buchet, D. Burney, J.-P. Cazet, R. Cheddadi, et al. (1998). Biome reconstruction from pollen and plant macrofossil data for Africa and the Arabian peninsula at 0 and 6000 years. *Journal of Biogeography 25*(6), 1007–1027.

Joseph, P. V. and T. Sabin (2008). Trends in SST and reanalysis 850 and 200 hPa wind data of Asian summer monsoon season during the recent six decades. In *Proceedings of 3rd WCRP international conference on reanalysis—Tokyo, Japan*.

Kanamitsu, M. and T. Krishnamurti (1978). Northern summer tropical circulations during drought and normal rainfall months. *Monthly Weather Review 106*(3), 331–347.

Kiladis, G. N., C. D. Thorncroft, and N. M. Hall (2006). Three-dimensional structure and dynamics of African easterly waves. Part I: Observations. *Journal of the Atmospheric Sciences 63*(9), 2212–2230.

Kiladis, G. N. and K. M. Weickmann (1997). Horizontal structure and seasonality of large-scale circulations associated with submonthly tropical convection. *Monthly weather review 125*(9), 1997–2013.

Knapp, K. R. and S. Wilkins (in prep., 2017). Gridded Satellite (GridSat) GOES and CONUS data. *Earth systems Science Data*.

Kobayashi, N. (1974). Interannual variations of tropical easterly jet stream and rainfall in South Asia. *Geophys. Mag 37*, 123–134.

Kobayashi, S., Y. Ota, Y. Harada, A. Ebita, M. Moriya, H. Onoda, K. Onogi, H. Kamahori, C. Kobayashi, H. Endo, et al. (2015). The JRA-55 reanalysis: General specifications and basic characteristics. *Journal of the Meteorological Society of Japan. Ser. II 93*(1), 5–48.

Koster, R. D., P. A. Dirmeyer, Z. Guo, G. Bonan, E. Chan, P. Cox, C. Gordon, S. Kanae, E. Kowalczyk, D. Lawrence, et al. (2004). Regions of strong coupling between soil moisture and precipitation. *Science 305*(5687), 1138–1140.

Koteswaram, P. (1958). The easterly jet stream in the tropics. *Tellus 10*(1), 43–57.

Koutavas, A., P. B. Demenocal, G. C. Olive, and J. Lynch-Stieglitz (2006). Mid-Holocene El Niño–Southern Oscillation (ENSO) attenuation revealed by individual foraminifera in eastern tropical Pacific sediments. *Geology 34*(12), 993–996.

Lafore, J.-P., C. Flamant, V. Giraud, F. Guichard, P. Knippertz, J.-F. Mahfouf, P. Mascart, and E. Williams (2010). Introduction to the AMMA Special Issue on 'Advances in understanding atmospheric processes over West Africa through the AMMA field campaign'. *Quarterly Journal of the Royal Meteorological Society 136*(S1), 2–7.

Lambert, S. J. (1989). A divergent and rotational kinetic energy budget for January and July. *Journal of Geophysical Research: Atmospheres 94*(D8), 11137–11149.

Landsea, C. W. (1993). A climatology of intense (or major) Atlantic hurricanes. *Monthly Weather Review 121*(6), 1703–1713.

Lau, K. and S. Yang (1996). Seasonal variation, abrupt transition, and intraseasonal variability associated with the Asian summer monsoon in the GLA GCM. *Journal of Climate 9*(5), 965–985.

Lavaysse, C., C. Flamant, S. Janicot, D. Parker, J.-P. Lafore, B. Sultan, and J. Pelon (2009). Seasonal evolution of the West African heat low: a climatological perspective. *Climate Dynamics 33*(2-3), 313–330.

Lebel, T. and A. Ali (2009). Recent trends in the Central and Western Sahel rainfall regime (1990–2007). *Journal of Hydrology 375*(1), 52–64.

Lebel, T., A. Diedhiou, and H. Laurent (2003). Seasonal cycle and interannual variability of the Sahelian rainfall at hydrological scales. *Journal of Geophysical Research: Atmospheres 108*(D8).

Lee, H. (2014). Climate algorithm theoretical basis document (C-ATBD): Outgoing longwave radiation (OLR)—Daily. NOAA's Climate Data Record (CDR) Program. Technical report, CDRP-ATBD-0526.

Lemburg, A. and J. Bader (2020). The role of remote versus local forcing for the interannual to decadal variability of the Tropical Easterly Jet over West Africa. *In preparation*.

Lemburg, A., J. Bader, and M. Claussen (2019). Sahel rainfall–Tropical Easterly Jet relationship on synoptic to intraseasonal time scales. *Monthly Weather Review 147*(5), 1733–1752.

Lindzen, R. S. and A. V. Hou (1988). Hadley circulations for zonally averaged heating centered off the equator. *Journal of the Atmospheric Sciences 45*(17), 2416–2427.

Losada, T., B. Rodriguez-Fonseca, E. Mohino, J. Bader, S. Janicot, and C. Mechoso (2012). Tropical SST and Sahel rainfall: A non-stationary relationship. *Geophysical Research Letters 39*(12).

Lu, J. and T. L. Delworth (2005). Oceanic forcing of the late 20th century Sahel drought. *Geophysical Research Letters 32*(22).

Mathon, V. and H. Laurent (2001). Life cycle of Sahelian mesoscale convective cloud systems. *Quarterly Journal of the Royal Meteorological Society 127*(572), 377–406.

Mathon, V., H. Laurent, and T. Lebel (2002). Mesoscale convective system rainfall in the Sahel. *Journal of applied meteorology 41*(11), 1081–1092.

Matsuno, T. (1966). Quasi-geostrophic motions in the equatorial area. *Journal of the Meteorological Society of Japan. Ser. II 44*(1), 25–43.

Meehl, G. A. (1992). Effect of tropical topography on global climate. *Annual Review of Earth and Planetary Sciences 20*(1), 85–112.

Mekonnen, A. and C. D. Thorncroft (2016). On mechanisms that determine synoptic time scale convection over East Africa. *International Journal of Climatology 36*(12), 4045–4057.

Mekonnen, A., C. D. Thorncroft, and A. R. Aiyyer (2006). Analysis of convection and its association with African easterly waves. *Journal of Climate 19*(20), 5405–5421.

Mohino, E., S. Janicot, and J. Bader (2011). Sahel rainfall and decadal to multi-decadal sea surface temperature variability. *Climate dynamics 37*(3-4), 419–440.

Mounier, F., S. Janicot, and G. N. Kiladis (2008). The West African monsoon dynamics. Part III: The quasi-biweekly zonal dipole. *Journal of Climate 21*(9), 1911–1928.

Nicholson, S. (2000). Land surface processes and Sahel climate. *Reviews of Geophysics 38*(1), 117–139.

Nicholson, S., A. Barcilon, M. Challa, and J. Baum (2007). Wave activity on the tropical easterly jet. *Journal of the atmospheric sciences 64*(7), 2756–2763.

Nicholson, S. E. (1985). Sub-saharan rainfall 1981–84. *Journal of climate and applied meteorology 24*(12), 1388–1391.

Nicholson, S. E. (2008). The intensity, location and structure of the tropical rainbelt over west Africa as factors in interannual variability. *International Journal of Climatology 28*(13), 1775–1785.

Nicholson, S. E. (2009). On the factors modulating the intensity of the tropical rainbelt over West Africa. *International Journal of Climatology: A Journal of the Royal Meteorological Society 29*(5), 673–689.

Nicholson, S. E. (2013). The West African Sahel: A review of recent studies on the rainfall regime and its interannual variability. *ISRN Meteorology 2013*.

Nicholson, S. E., C. Funk, and A. H. Fink (2018). Rainfall over the African continent from the 19th through the 21st century. *Global and planetary change 165*, 114–127.

Nithya, K., M. Manoj, and K. Mohankumar (2017). Effect of El Niño/La Niña on tropical easterly jet stream during Asian summer monsoon season. *International Journal of Climatology*.

Okumura, Y. and S.-P. Xie (2004). Interaction of the Atlantic equatorial cold tongue and the African monsoon. *Journal of Climate 17*(18), 3589–3602.

Otto-Bliesner, B. L. (1999). El Nino/La Nina and Sahel precipitation during the middle holocene. *Geophysical Research Letters 26*(1), 87–90.

Park, J.-y., J. Bader, and D. Matei (2016). Anthropogenic Mediterranean warming essential driver for present and future Sahel rainfall. *Nature Climate Change*.

Pattanaik, D. and V. Satyan (2000). Fluctuations of Tropical Easterly Jet during contrasting monsoons over India: A GCM study. *Meteorology and Atmospheric Physics 75*(1-2), 51–60.

Plumb, R. A. and A. Y. Hou (1992). The response of a zonally symmetric atmosphere to subtropical thermal forcing: Threshold behavior. *Journal of the atmospheric sciences 49*(19), 1790–1799.

Preethi, B., T. Sabin, J. Adedoyin, and K. Ashok (2015). Impacts of the ENSO Modoki and other tropical Indo-Pacific climate-drivers on African rainfall. *Scientific reports 5*.

Ramage, C. S. (1995). Forecasters Guide to Tropical Meteorology. AWS TR 240 Updated. Technical report, AIR WEATHER SERVICE SCOTT AFB IL.

Ramel, R., H. Gallée, and C. Messager (2006). On the northward shift of the West African monsoon. *Climate Dynamics 26*(4), 429–440.

Rao, P. K. (1952). Probable regions of jet streams in the upper air over India. *Current Science 21*(3), 63–64.

Rao, S. and J. Srinivasan (2016). The impact of latent heating on the location and strength of the tropical easterly jet. *Meteorology and Atmospheric Physics 128*(2), 247–261.

Ratnam, M. V., M. R. Raman, S. K. Mehta, D. Nath, B. Krishnamurthy, M. Rajeevan, S. V. B. Rao, and D. N. Rao (2011). Sub-daily variations observed in Tropical Easterly Jet (TEJ) streams. *Journal of Atmospheric and Solar-Terrestrial Physics 73*(7-8), 731–740.

Raymond, D., Ž. Fuchs, S. Gjorgjievska, and S. Sessions (2015). Balanced dynamics and convection in the tropical troposphere. *Journal of Advances in Modeling Earth Systems 7*(3), 1093–1116.

Redelsperger, J.-L., A. Diongue, A. Diedhiou, J.-P. Ceron, M. Diop, J.-F. Gueremy, and J.-P. Lafore (2002). Multi-scale description of a Sahelian synoptic weather system representative of the West African monsoon. *Quarterly Journal of the Royal Meteorological Society: A journal of the atmospheric sciences, applied meteorology and physical oceanography 128*(582), 1229–1257.

Reed, R. J., D. C. Norquist, and E. E. Recker (1977). The structure and properties of African wave disturbances as observed during Phase III of GATE. *Monthly Weather Review 105*(3), 317–333.

Rodríguez-Fonseca, B., E. Mohino, C. R. Mechoso, C. Caminade, M. Biasutti, M. Gaetani, J. Garcia-Serrano, E. K. Vizy, K. Cook, Y. Xue, et al. (2015). Variability and predictability of West African droughts: a review on the role of sea surface temperature anomalies. *Journal of Climate 28*(10), 4034–4060.

Rowell, D. P. (2001). Teleconnections between the tropical Pacific and the Sahel. *Quarterly Journal of the Royal Meteorological Society 127*(575), 1683–1706.

Rowell, D. P., C. K. Folland, K. Maskell, and M. N. Ward (1995). Variability of summer rainfall over tropical North Africa (1906–92): Observations and modelling. *Quarterly Journal of the Royal Meteorological Society 121*(523), 669–704.

Sathiyamoorthy, V., P. Pal, and P. Joshi (2007). Intraseasonal variability of the tropical easterly jet. *Meteorology and Atmospheric Physics 96*(3-4), 305–316.

Sato, T. and F. Kimura (2007). How does the Tibetan Plateau affect the transition of Indian monsoon rainfall? *Monthly Weather Review 135*(5), 2006–2015.

Schneider, E. K. and R. S. Lindzen (1977). Axially symmetric steady-state models of the basic state for instability and climate studies. Part I. Linearized calculations. *Journal of the Atmospheric Sciences 34*(2), 263–279.

Smith, T. A. (2008). *Observational analyses and idealized numerical simulations of African wave dynamics*. ProQuest.

Stickler, A. and S. Brönnimann (2011). Significant bias of the NCEP/NCAR and twentieth-century reanalyses relative to pilot balloon observations over the West African Monsoon region (1940–1957). *Quarterly Journal of the Royal Meteorological Society 137*(659), 1400–1416.

Street-Perrott, F. and R. Perrott (1993). Holocene vegetation, lake levels and climate of Africa. *Global climates since the last glacial maximum*, 318–356.

Sultan, B. and S. Janicot (2000). Abrupt shift of the ITCZ over West Africa and intraseasonal variability. *Geophysical Research Letters 27*(20), 3353–3356.

Sultan, B., S. Janicot, and A. Diedhiou (2003). The West African monsoon dynamics. Part I: Documentation of intraseasonal variability. *Journal of Climate 16*(21), 3389–3406.

Sylla, M., A. Dell'Aquila, P. Ruti, and F. Giorgi (2010). Simulation of the intraseasonal and the interannual variability of rainfall over West Africa with RegCM3 during the monsoon period. *International Journal of Climatology 30*(12), 1865–1883.

Tanaka, M. (1982). Interannual fluctuations of the tropical easterly jet and the summer monsoon in the Asian region. *Journal of the Meteorological Society of Japan. Ser. II 60*(3), 865–875.

Taylor, C. M., E. F. Lambin, N. Stephenne, R. J. Harding, and R. L. Essery (2002). The influence of land use change on climate in the Sahel. *Journal of Climate 15*(24), 3615–3629.

Thorncroft, C. and M. Blackburn (1999). Maintenance of the African easterly jet. *Quarterly Journal of the Royal Meteorological Society 125*(555), 763–786.

Thorncroft, C. and K. Hodges (2001). African easterly wave variability and its relationship to Atlantic tropical cyclone activity. *Journal of Climate 14*(6), 1166–1179.

Thorncroft, C. D., H. Nguyen, C. Zhang, and P. Peyrillé (2011). Annual cycle of the West African monsoon: regional circulations and associated water vapour transport. *Quarterly Journal of the Royal Meteorological Society 137*(654), 129–147.

Uccellini, L. W. and D. R. Johnson (1979). The coupling of upper and lower tropospheric jet streaks and implications for the development of severe convective storms. *Monthly Weather Review 107*(6), 682–703.

Van Tuyl, A. H. and J. A. Young (1982). Numerical simulation of nonlinear jet streak adjustment. *Monthly Weather Review 110*(12), 2038–2054.

Villamayor, J. and E. Mohino (2015). Robust Sahel drought due to the Interdecadal Pacific Oscillation in CMIP5 simulations. *Geophysical Research Letters 42*(4), 1214–1222.

Webster, P. J. (1981). Monsoons. *Scientific American 245*(2), 108–119.

Wu, M.-L. C., O. Reale, S. D. Schubert, M. J. Suarez, R. D. Koster, and P. J. Pegion (2009). African easterly jet: structure and maintenance. *Journal of Climate 22*(17), 4459–4480.

Xie, P. and P. A. Arkin (1996). Analyses of global monthly precipitation using gauge observations, satellite estimates, and numerical model predictions. *Journal of climate 9*(4), 840–858.

Xue, Y. and J. Shukla (1993). The influence of land surface properties on Sahel climate. Part 1: desertification. *Journal of climate 6*(12), 2232–2245.

Yang, G.-Y., J. Methven, S. Woolnough, K. Hodges, and B. Hoskins (2018). Linking African Easterly Wave Activity with Equatorial Waves and the Influence of Rossby Waves from the Southern Hemisphere. *Journal of the Atmospheric Sciences 75*(6), 1783–1809.

Yang, W., R. Seager, and M. A. Cane (2013). Zonal momentum balance in the tropical atmospheric circulation during the global monsoon mature months. *Journal of the Atmospheric Sciences 70*(2), 583–599.

Zhai, J. and W. Boos (2015). Regime transitions of cross-equatorial Hadley circulations with zonally asymmetric thermal forcings. *Journal of the Atmospheric Sciences 72*(10), 3800–3818.

Zhang, R. and T. L. Delworth (2006). Impact of Atlantic multidecadal oscillations on India/Sahel rainfall and Atlantic hurricanes. *Geophysical Research Letters 33*(17).

Zhao, Y., P. Braconnot, S. Harrison, P. Yiou, and O. Marti (2007). Simulated changes in the relationship between tropical ocean temperatures and the western African monsoon during the mid-Holocene. *Climate Dynamics 28*(5), 533–551.

2

Sahel rainfall – Tropical Easterly Jet relationship on synoptic to intraseasonal time scales

This chapter has been published in nearly identical form regarding content as an article in the "Monthly Weather Review" under the following authorship and title:

Lemburg, A., Bader, J., Claussen, M. (2019). Sahel Rainfall – Tropical Easterly Jet Relationship on Synoptic to Intraseasonal Time Scales. Monthly Weather Review, 147(5), 1733-1752.

A. L., J. B. and M. C. developed the ideas of this paper. A. L. conducted all data analyses. A.L wrote the manuscript with input from J. B. and M. C. .

In contrast to the published version, this version already includes corrections for minor errors which unfortunately made it to the final published version. The correction leaves all main results and conclusions unchanged but leads to minor changes of numerical values in the manuscript as well as slight changes in figure 11 and nearly unnoticeable changes in figure 9, 10 and 12. A corrigendum will be submitted shortly to the "Monthly Weather Review" in order to update also the published version. In addition, this version contains some minor editorial changes in the way the sections are structured.

Abstract:
The Tropical Easterly Jet (TEJ) is a characteristic upper-level feature of the West African Monsoon (WAM) circulation. Moreover, the TEJ over West Africa is significantly correlated with summer Sahel rainfall on interannual and decadal time scales. In contrast, the relationship between Sahel rainfall and the regional TEJ on synoptic to intraseasonal time scales is unclear. Therefore, this relationship is investigated by means of multiple statistical analyses using temporally highly resolved measurement and reanalysis data. It is shown that average correlations between convective activity and regional TEJ intensity remain below 0.3 for all synoptic to intraseasonal time scales. Especially on the synoptic time scale, the TEJ significantly lags anomalies in convective activity by one or two days which indicates that convection anomalies are more likely to drive changes in the regional TEJ than vice versa. To further shed light on the role of the TEJ for rainfall over West Africa, a previously proposed effect of TEJ-induced upper-level divergence on the development of mesoscale convective systems (MCS) is examined more closely. An analysis of nearly 300 Sahelian MCSs shows that their initiation is generally not associated with significant TEJ anomalies or jet-induced upper-level divergence. Furthermore, no statistically significant evidence is found that pre-existing TEJ-related upper-level divergence anomalies affect intensity, size and lifetime of MCSs. A limiting factor of this study is the focus on TEJ-induced upper-level divergence. Therefore, a possible effect of the TEJ on Sahel rainfall via other mechanisms cannot be ruled out and should be subject to future studies.

2.1 Introduction

Rainfall in sub-Saharan West Africa is inextricably linked to the West African Monsoon (WAM) which is characterized by a pronounced seasonal wind shift initiated by thermodynamic contrasts between land and ocean. A prominent feature of the summertime WAM circulation is the Tropical Easterly Jet (TEJ), an upper-tropospheric (100-200 hPa) easterly current between 5°N and 20°N, first described by Rao (1952) and Koteswaram (1958). The TEJ originates in the South Asian monsoon system over the Bay of Bengal, extends westwards to Africa and decays over the tropical Atlantic. Observations, reanalyses and model simulations have shown that anomalously wet years in the Sahel are often characterized by a regionally stronger TEJ compared to its summer (JJAS) climatology whereas dry years exhibit a weaker TEJ over West Africa (e.g., Grist and Nicholson, 2001; Sylla et al., 2010).

Figure 2.1 shows that not only decadal trends (thicker lines) are very similar, but even on a year-to-year basis changes in rainfall often coincide with changes in TEJ intensity. Years with higher Sahel precipitation are on average accompanied by a regionally enhanced TEJ south of the main rain band (Fig. 2.2). This distinct regional maximum might be mainly considered as the time-integrated response of the regional upper-level circulation to the positive diabatic heating anomaly of a wetter than normal monsoon season. Nonetheless, it would probably be mistaken to view the TEJ exclusively as a passive byproduct of the WAM circulation because the TEJ and WAM rainfall might substantially interact with each other. Moreover, Nicholson (2009) suggested that "the link between the TEJ and rainfall is a causal one with the strong TEJ enhancing rainfall by enhancing upper-level divergence". Redelsperger et al. (2002) highlighted that the dynamic configuration between convection and the TEJ over West Africa exhibits simi-

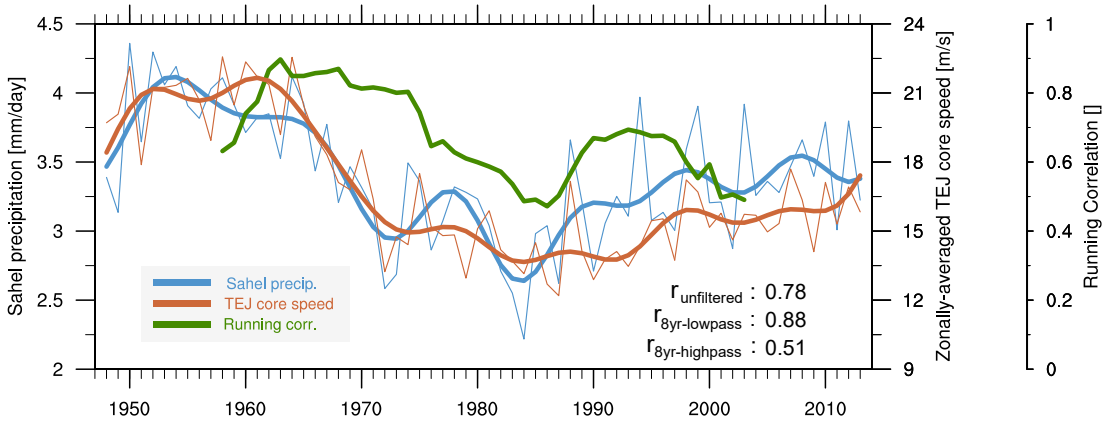

Figure 2.1: Time series from 1948 - 2013 of JJAS Sahel precipitation (from CRU TS3.22 data spatially averaged over 10°W to 10°E and 10°N to 20°N) and JJAS 200 hPa TEJ core speed (for a representative core speed measure that is insensitive to latitude changes, the average JJAS TEJ core speed was calculated from daily NCAR NCEP reanalysis fields of 200 hPa zonal wind data as follows: Within a domain between 15°W to 15°E and 5°S to 25°N, the daily maximum of easterly 200 hPa zonal wind speed is found for each longitudinal strip of grid points. The found maximum speeds of each longitude are then averaged over the whole domain to obtain an average speed of the TEJ core). Thin, light lines depict the unfiltered yearly means. Thick lines show the 10-year low pass filtered time series. The green line depicts the 21-year running correlation.

larities with that observed for mid-latitude jets and stressed the uncertainty with regard to the cause and effect relationship. Assessing a number of synoptic cases, Besson and Lemaître (2014) found that upper-level divergence in the entrance region of regional TEJ maxima (jet streaks) might play an important role by promoting development of mesoscale convective systems (MCSs).

However, previous studies cannot fully prove or explain substantial interaction between the TEJ and Sahel rainfall. Nicholson (2013) only provides a qualitative picture by suggesting two mechanisms (divergence, wave disturbances) by which the TEJ might influence rainfall. The findings of Besson and Lemaître (2014) might not be generally valid as they are only based on one in-depth and 16 brief synoptic case studies. Therefore, further research is needed to gain a more comprehensive view of the possible role of the TEJ in modulating WAM rainfall.

In the first part, this study quantifies the covariability and the lead-lag relationship between the TEJ and Sahel rainfall over a range of synoptic to intraseasonal time scales. For this, spectral analysis, lead-lag correlations and regression analysis are applied to a 32-year long record of daily outgoing longwave radiation as proxy for rainfall and daily output from multiple reanalyses. The second part of this study challenges the ideas of Besson and Lemaître (2014) who suggested that TEJ streaks aid MCS development, mainly by inducing significant upper-level divergence. Theoretical considerations, that follow in the next section, render a pivotal role of the TEJ on MCS initiation via upper-level divergence unlikely. A secondary order effect of TEJ-related divergence on convective initiation cannot be ruled out, though, and a possible impact on MCS organization is still an open question. We therefore extend the work of Besson and Lemaître (2014) and provide a more complete statistical investigation of upper-level winds before the initiation of Sahelian MCSs, also testing whether changes in MCS lifetime, size or intensity are associated with TEJ-induced divergence. In contrast to Besson and Lemaître

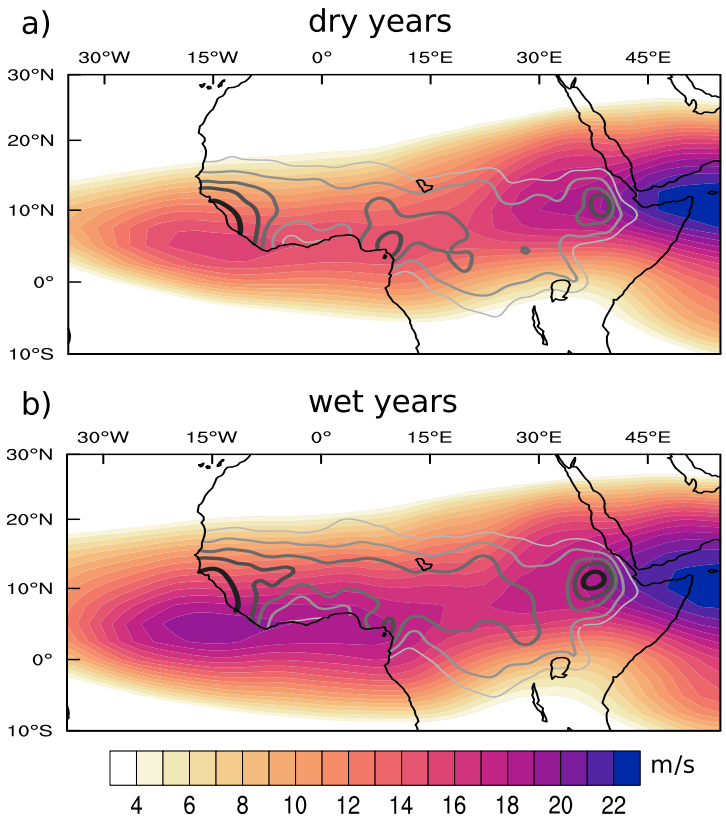

Figure 2.2: Composite comparison of August easterly 200 hPa zonal wind from NCEP-NCAR1 for interannually-measured dry (a) and wet (b) Sahel years. For the composite, the eight driest and wettest years of the 15 year high-pass filtered CRU precipitation data set since 1948 were chosen. The grey contour lines depict CRU August precipitation in form of the 2,4,7,10 and 15 mm/d isohyet.

(2014), our analysis is not limited to a few individual MCS events, but involves roughly 300 MCS initiation cases in the period 2007-2015 allowing us to assess statistical significance.

2.2 Theoretical Background

The subseasonal variability of WAM precipitation can be broken up into three time scales: 2–8 day (referred to as synoptic-scale variability hereafter), 10–25 day, and 30–90 day variability. Synoptic-scale variability dominates on smaller regional scales (∼1000 km) and is strongly linked to westward propagating wave disturbances, so-called African Easterly Waves (AEWs), with typical wavelengths between 2000 and 5000 km and periods of mostly 2–7 days (Carlson, 1969; Burpee, 1972; Kiladis et al., 2006; Mekonnen et al., 2006). At larger spatial scales (≫1000 km), synoptic-scale variability is not as important and rainfall variability is increasingly confined to time scales longer than 10 days. On the 10–25 day time scale two dominant modes of variability exist: the quasi-biweekly zonal dipole mode (QBZD) (Mounier et al., 2008) which only affects the southern parts of the Sahel and the so-called Sahel mode (Sultan et al., 2003; Janicot et al., 2010). The QBDZ is characterized by a quasi-stationary zonal dipole of convection and a corresponding Walker-type circulation between the Guinean coast

and the western part of the equatorial Atlantic which changes sign about every 7 days. The Sahel mode is associated with a first northward and then westward propagating signal of enhanced convective activity starting over Central Africa, travelling through the Sahel region and dissipating over the equatorial Atlantic. Variability on the lower frequency band (30–90 days) is mainly associated with the Madden-Julian Oscillation (MJO) (Maloney and Shaman, 2008; Alaka Jr and Maloney, 2012). In contrast to WAM precipitation, subseasonal variability of the West African TEJ has been much less studied and it is not clear whether it is linked to any of the above-mentioned modes. The first part of this study aims to close this gap.

From a more phenomenological than statistical point of view, Sahel rainfall is mainly linked to the number of mesoscale convective systems (MCS) (Lebel et al., 2003; Lebel and Ali, 2009). Of particular importance are large and well-organized MCSs which move westward with speeds between 10 and 15 $\mathrm{m\,s^{-1}}$ and often persist for more than 24 hours. Although such MCSs represent only 12% of all convective systems in the Sahel, they are responsible for up to 90% of all rainfall over that region (Mathon et al., 2002).

For any kind of deep, moist convection to occur, three necessary ingredients have to be in place at the same time (Doswell III et al., 1996): Besides the presence of 1) sufficiently moist air and 2) a conditionally unstable stratification, 3) a lifting mechanism is needed to lift a parcel to its level of free convection (LFC). In the Sahel, convective inhibition is often high and therefore vigorous lift is required to raise a parcel to its LFC. Sufficient lift can be produced by orography, cold pools or mesoscale circulations arising from surface inhomogeneities (Lafore et al., 2017). While such mesoscale scale processes are pivotal for the initiation of deep convection, synoptic-scale atmospheric dynamics might also play an important role in the formation and in particular organization of deep, moist convection. Over 60% of organized squall lines in summer are associated with AEWs (Fink and Reiner, 2003) suggesting that synoptic-scale dynamics might be a crucial factor for well-organized Sahelian MCSs. Whereas convective clouds can be found in each sector of AEWs, most organized convective systems tend to occur at or ahead of the trough (Diedhiou et al., 1999; Duvel, 1990; Fink and Reiner, 2003). One of the main reasons is the increased lower-level shear between a southwesterly monsoon flow and northerly flow at the AEJ level (600 hPa).

Recently, Besson and Lemaître (2014) suggested that not only the mid-troposheric AEJ and associated AEWs but also the upper-tropospheric TEJ might affect MCSs, mainly via its impact on upper-level divergence. As shown in figure 2.2b, the TEJ can exhibit a distinct regional maximum over the coastal region of West-Africa – even in the seasonal mean. On synoptic time scales, this maximum can be much more pronounced (Fig. 2.3a), giving it a similar appearance to jet streaks found at mid-latitude jets.

According to quasi-geostrophic theory, jet streaks are associated with substantial ageostrophic flows in their entrance and exit regions. In the idealized case of a straight jet streak in a flow with a Rossby number small in comparison to unity, theory predicts a symmetric four cell divergence-convergence pattern with upper-level divergence at the anticyclonic-shear side (poleward in case of an easterly jet) entry and cyclonic-shear side (equatorward) exit of a jet stream (e.g., Uccellini and Johnson, 1979). The conditions for the development of a symmetric four cell pattern (shown in idealized form

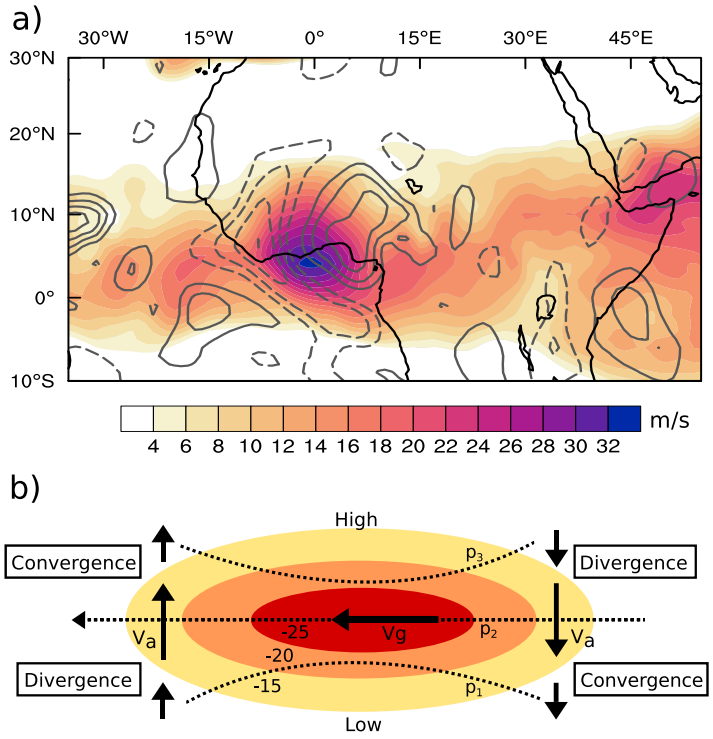

Figure 2.3: Divergence pattern possibly associated with regional TEJ maxima. **a)** 12-hour averaged 200 hPa zonal wind field from ERA-Interim on August 28th 2009. Contours show anomalous divergence (solid) and convergence (dashed) with an interval of $5 \cdot 10^{-6}\,\mathrm{s}^{-1}$. **b)** Sketch of the idealized situation at a straight easterly jet streak with the typical upper-level divergence at the right entry/left exit. Dashed lines depict isobars and the contours show isotaches.

in Fig. 2.3b) are stringent and numerous factors including curvature of the jet axis and latent heat release strongly modulate the patterns of divergence and convergence. The four cell pattern changes more towards a two-cell pattern if the Rossby number surpasses 0.5 (Van Tuyl and Young, 1982). Given that the mean position of the TEJ ($\sim 6°\mathrm{N}$) results in typical Rossby numbers around 0.7 (see calculation in Besson and Lemaître, 2014), a simple two-cell pattern might be the most realistic depiction. Substantial divergence can therefore only be expected at jet entrance regions. Besson and Lemaître (2014) linked divergence values of up to $3 \cdot 10^{-5}\,\mathrm{s}^{-1}$ to the entrance region of a pronounced TEJ streak. By integrating the continuity equation from the top (100 hPa) downward to 200 hPa, they then estimated maximal TEJ-related upward motion at about 10 cm s^{-1} in 200 hPa. For this computation, the aforementioned divergence value of $3 \cdot 10^{-5}\,\mathrm{s}^{-1}$ was assumed to be constant and the vertical velocity was set to zero at the tropopause.

It is, however, questionable whether possible jet streak-related upper-level divergence can be of any significance for convection over the Sahel. Most studies investigating the impact of jet streaks on convection focus on highly baroclinic jet configurations in mid-latitude regions; There, the ageostrophic flow in the entrance region is often accompanied by a thermally direct, transverse circulation which is characterized by deep synoptic-scale ascent along sloped isentropes (e.g., Uccellini and Johnson, 1979). Literature on jet streaks in tropical regions is sparse, however, likely because synoptic-scale dry ascent is assumed to be weak there due to the smallness of the Coriolis parameter

(Charney, 1963; Raymond et al., 2015). Therefore, it is unclear whether jet streaks at the TEJ also enable synoptic-scale ascent throughout the whole troposphere or whether the divergence-related mass deficit is compensated by convergence in layers directly below. In their in-depth case study, Besson and Lemaître (2014) described TEJ-forced ascending motions and associated adiabatic cooling reaching down as far as 4 km above ground level. Even if some TEJ-related uplift at the order of cm s^{-1} extends down to the boundary layer, it is certainly too weak to lift a potentially buoyant parcel to its LFC (Doswell III, 1987). Nonetheless, even weak synoptic-scale rising motion can be pivotal for convection in some cases. If it persists for at least some hours, synoptic-scale ascent pre-conditions the atmosphere through adiabatic cooling which increases CAPE and lowers CIN. Couvreux et al. (2012) have shown with idealized LES simulations that prescribed anomalies in large-scale mid-tropospheric ascent of only 2 cm s^{-1} can be a deciding factor for the initiation of convection in the semi-arid Sahel region. Such cases might be rare, though, and the initiation of deep convection should mainly be controlled by thermodynamic factors and mesoscale dynamic forcing. In line with this thought, Besson and Lemaître (2014) ascribe TEJ streaks a subordinate role in convective initiation. They argue, however, that jet streak-related divergence may strongly benefit the organization and in particular the persistence of MCSs. Hence, a possible influence of the TEJ and embedded jet streaks on MCSs is still in debate which motivates our more statistical analysis which will follow in the second part of this paper.

2.3 Data and Methods

2.3.1 Statistical analysis of synoptic to intraseasonal covariability

All statistical analyses described below are applied to a 32-year long (1979–2012, 1982 and 1985 are left out because of too many missing values) daily record of Outgoing Longwave Radiation (OLR) measurements from NOAA (Lee, 2014) and diurnally-averaged reanalysis output from ERA-Interim (Dee et al., 2011), NCEP-NCAR1 (Kalnay et al., 1996), MERRA-2 (Gelaro et al., 2017) and JRA-55 (Kobayashi et al., 2015) for the same time period. OLR is chosen as a suitable proxy for rainfall which is generally deemed to be valid in tropical regions where rainfall associated with deep convection predominates. All analyses are limited to the WAM season comprising June, July, August and September (JJAS).

First, power spectra for local and regional scales are calculated to identify typical time scales associated with most variation in OLR and wind speeds at the TEJ level (200 hPa). For this and the following analysis, regional averages for OLR are calculated from 15°W – 15°E over 8°N – 16°N which represents the typical latitudinal extent of the WAM rain belt. For the TEJ, an averaging domain of the same size is used but shifted 6° to the south to account for the typical mean position of the TEJ core (6°N). To remove the signal of the annual cycle, daily-averaged data of each year are prepared by subtracting the first three harmonics of the respective annual cycle and an additional detrending. JJAS power spectra are then calculated for each year separately and averaged afterwards. The spectral analysis is carried out using the NCL function specx_anal. 10% of the time series is tapered and some smoothing is applied by averaging three periodogram estimates. To check statistical significance of spectral peaks

of the averaged spectra we calculate the best-fitting Markov spectrum and its lower 5% and upper 95% confidence bounds via the NCL function specx_ci. The Markov spectrum refers to a univariate lag-1 autoregressive process and can therefore represent white or red noise spectra. Spectral peaks that lie outside of the confidence bounds are considered to be significant because they differ from white or red noise.

Bandpass-filtering is applied to the deseasonalized daily-averaged data to investigate the relationship between the TEJ and Sahel rainfall separately for three typical rainfall variability time scales: synoptic variability (2–8 days), submonthly variability (10–25 days) and MJO time scale variability (30–90 days). The bandpass filter used for all analyses in this study is a standard top hat spectral filter as implemented in the Climate Data Operators package. For each time scale, the JJAS lead-lag correlations between regionally averaged OLR and 200 hPa zonal wind are calculated individually for each year and averaged afterwards. Before calculating the 10–25 day and the 30–90 day correlations, time series are smoothed by a 3-day running mean.

Spatial patterns of anomalous upper-level flow linked to Sahel convection anomalies on synoptic and submonthly time scales are explored via linear regression, similar to Kiladis and Weickmann (1997). Bandpass-filtered, spatially-averaged OLR in a selected Sahel base region is regressed separately against the filtered zonal and meridional components of the 200 hPa wind and OLR itself for each grid point at different time lags. The linear dependence of circulation and OLR anomalies is then mapped by evaluating the respective regression equations for each grid point using one negative standard deviation in OLR at the base region as the independent variable. Statistical significance of the linear relationships is tested via a student t-test that takes into account the reduction in the degrees of freedom due to autocorrelation.

2.3.2 Relationship between TEJ and MCSs

The possible relationship between the TEJ and initiation and further development of MCSs is explored by analyzing a large number of MCS initiations and associated upper-tropospheric dynamics. The focus is laid on large and organized MCSs because they are responsible for the bulk of rainfall and are more likely to interact with large-scale atmospheric dynamics than smaller, unorganized convection.

An objective MCS tracking algorithm developed by Huang (2017), based on the conventional area overlapping method combined with a Kalman filter, is applied to the Gridsat-B1 brightness temperature data set (Knapp and Wilkins, 2017). We use the traditional 233 K threshold to identify deep convective cells and demand that the 233 K isotherm encloses a minimum of 30 000 km^2 (cloud shield radius $\gtrapprox$ 100 km) and that the system has a lifetime of at least nine hours. This choice of minimum size and lifetime is justified for our purposes because MCS with radii $\geq$ 100 km explain more than 80% of the MCS-associated integrated cloud cover according to Mathon and Laurent (2001). The same is true for systems with lifetimes $\geq$ 9 hours. To prevent that a possible effect of the TEJ is overshadowed by precedent or adjacent MCS, each tracked MCS should represent a more or less isolated system that is neither the product of an MCS split nor directly triggered by systems nearby. For that, only those MCSs are selected for which no grid point with brightness temperature below 233 K is found three hours before initiation in a box of 5° longitudinal and 2° latitudinal extent east of the genesis

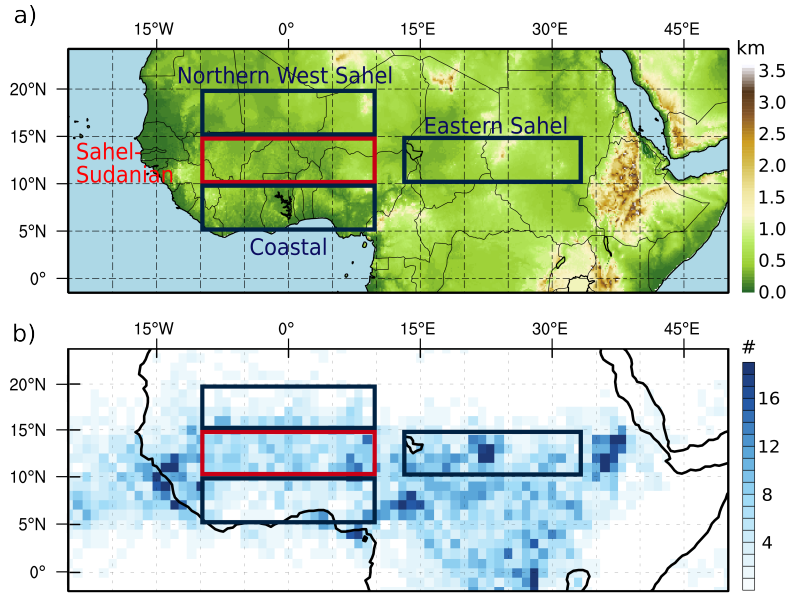

Figure 2.4: a) Topographic map of our study areas. The boxes show the chosen spatial composite regions. We lay the focus of our investigations on the mixed Sahel/Sudanian region which is defined as a latitudinal band from 10°N to 15°N spanning from 10°W to 10°E. **b)** Initiations of large (maximum size $\geq$ 30 000 km^2) and long-lived (lifetime $\geq$ 9 hours) Sahelian-type MCS per $1^\circ \cdot 1^\circ$ grid boxes summed over 9 JJAS seasons (2007–2015).

area. In addition, each found event is required to be temporally separated by at least 24 hours. As a consequence of these further selection criteria we exclude about 60% of all large Sahelian-type MCS initiations from our analysis which is a large but necessary trade-off to eliminate most effects from possible earlier or adjacent MCSs. Gradually relaxing these selection criteria and therefore increasing the number of examined MCS initiations leaves our results more blurred but mostly unchanged in their key aspects which is why we are confident that the selection of MCSs does not compromise the general validity of our study. The MCS tracking algorithm is applied for 9 monsoon seasons (JJAS) between 2007–2015 (limited to the availability period of the Eumetsat divergence data set which is described later) and found MCS genesis cases are binned into $1^\circ \cdot 1^\circ$ grid boxes (Fig. 2.4b).

Assuming that surface characteristics and atmospheric dynamics do not differ fundamentally within a Sahel-Sudanian band between 10°W to 10°E and 10°N to 15°N, we create a temporal and spatial composite of all MCSs initiated within this band in 9 years, such that all developing MCSs are now centred at the origin of a MCS genesis relative coordinate system. Because of the comparably high number of Sahelian-type MCSs and their large contribution to total rainfall there, we focus on the Sahel-Sudanian region in our study but also examine MCS-related upper-tropospheric conditions in three other areas as depicted in figure 2.4a.

The resulting large MCS ensemble (289 MCS initiations in the Sahel-Sudanian region) enables a statistically robust investigation of mean synoptic conditions before, during and after initiation of MCSs and allows further to assess the range of conditions under which MCSs form. For the analysis of the atmospheric state, the output of the three reanalyses ERA-Interim, JRA-55 and MERRA-2 is used and compared among

each other. In the case of ERA-Interim and JRA-55, 6-hourly output is interpolated to 3 hours to match the temporal resolution of the MCS tracking. In the results section, most in-depth analysis is shown for ERA-Interim as it seems to resolve MCSs and their imprint on the synoptic-scale dynamics better than other reanalyses. OLR fields are displayed using the CERES SYN1deg OLR data set (Rutan et al., 2015). Upper-level divergence is a crucial quantity for which we do not want to rely solely on reanalyses, as was the case in previous studies. Therefore we use the Eumetsat divergence product (EUMETSAT, 2005) which is derived from satellite-derived atmospheric motion vectors (AMVs) and represents average divergence between 400 hPa and 100 hPa. The calculation of AMVs in this product is based on the tracking of upper-level moisture features using successive satellite images of the water vapour channel (6.2 μm) of Meteosat-8 at a 15 minute interval. As a result, the derivation of AMVs and the subsequent calculation of upper-level divergence is not reliant on the presence of any clouds. The Eumetsat divergence product is available at spatial resolution of 1° and temporal resolution of 3 hours for the years 2007–2015. Although we consider the data set to be sufficiently representative of the divergence at the TEJ level (200 hPa), we will designate it as 100–400 hPa divergence throughout the paper.

Anomalies analysed in this part of the study are calculated as deviations from 12-day low-pass filtered values calculated separately for each 3-hourly time step of the day. This method provides a time of day dependent reference state which removes the signals of the diurnal cycle for the respective anomalies. The filtering cut-off period – 12 days – is sufficiently above the time scales associated with MCS passages and synoptic-scale phenomena such as AEW (2–7 days) but short enough to exclude any effects from the seasonal cycle or the MJO. Statistical significance is assessed via a bootstrapping method of sampling with replacement using 5000 iterations.

2.4 Statistical analysis of synoptic to intraseasonal covariability

2.4.1 Spectral variability

If the TEJ and Sahel rainfall are assumed to interact on synoptic to intraseasonal time scales, similar distributions of spectral power would be expected. However, their respective 32-year averaged power density spectra exhibit substantial differences across all time scales. OLR displays highest spectral power in a period range between 3 and 7 days which is certainly associated with AEWs (Fig. 2.5a). Strongly apparent is the much higher local- than regional-scale variability (red vs. blue lines) on synoptic time scales, likely due to the rather small-scale nature of convection. Beyond the synoptic time scale, the OLR spectrum shows – on average – no significant peaks in the 10–25 day band. For some years, however, a significant peak can be observed (see light shadings) which is likely associated with the QBZD and Sahel mode. A broader peak exists at the 30–90 day time scale which is hypothesized to be attributable to the MJO.

Compared to convection (OLR), the TEJ appears to be much more spatially homogeneous with typically larger spatial scales and longer time scales. The power spectrum of zonal wind speed at 200 hPa resembles a red noise spectrum with no distinctive

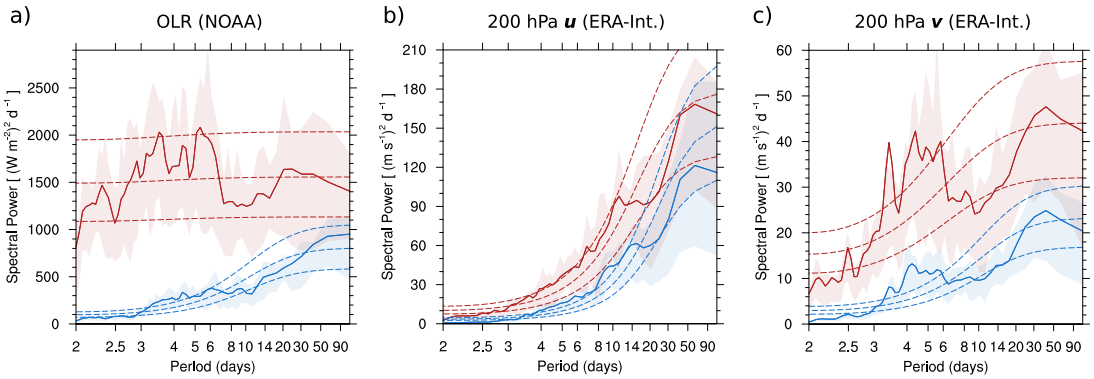

Figure 2.5: Subseasonal power spectra for OLR, zonal and meridional 200 hPa wind in the Sahel region. Thick lines show the averaged power spectra of 32 individual monsoon seasons for Outgoing Longwave Radiation (OLR), 200 hPa zonal wind and 200 hPa meridional wind. Analysis is based on JJAS daily means of NOAA-OLR from 1979–2012 and JJAS daily means of ERA-Interim 200 hPa wind from 1979–2012. Blue lines depict the regional variability as evaluated by a field mean (15°W – 15°E, 8°N – 16°N for OLR, 15°W – 15°E, 2°N – 10°N for zonal and meridional wind), red lines depict the local variability (at 0°E, 12°N for OLR, 0°E, 6°N for zonal and meridional wind). The light shading represents the respective interquartile range. As an indicator for significance, dashed lines show a theoretical Markov red noise spectrum with its 5 and 95% percentile. x-axis is logarithmic.

spectral peaks on shorter time scales (Fig. 2.5b). By far the strongest, albeit insignificant variability can be observed at periods around 50 days. Contrary to the OLR power spectrum, the local scale variability is very similar to regional scale variability – even on very short time scales. Although highest spectral power is found on the MJO time scale, a broader significant signal exists between 4 and 15 days with some marked peaks at 9 and 14 days. A similar significant concentration of spectral power for such periods was found for symmetric OLR spectra as shown in Wheeler and Kiladis (1999, their Fig. 3), hinting at the substantial impact of equatorial waves (in particular Kelvin waves) on the TEJ variability.

In contrast to the zonal component of the TEJ, the power spectrum of the meridional wind in 200 hPa looks much more similar to the OLR spectrum with a strong peak at about 3.5 days and a broader maximum between 4 and 6 days (Fig. 2.5c). The broad maximum is consistent with the findings of Nicholson et al. (2007) who have shown that planetary waves with periods of 5-6 days are observed in the upper-tropospheric flow over West Africa. Furthermore, the aforementioned equatorial waves might explain a considerable portion of the variability of the 200 hPa meridional wind field.

2.4.2 Correlations on synoptic to intraseasonal time scales

We calculate – individually for each year – the lead-lag correlation between daily Sahel region averages of OLR (averaged from 15°W to 15°E and 8°N to 16°N) and 200 hPa zonal wind (averaged from 15°W to 15°E and 2°N to 10°N). A positive correlation coefficient means that increased convection (negative OLR anomaly) goes along with an increased TEJ speed (negative zonal wind anomaly). When a maximal positive correlation is observed at positive time lags, it indicates that phases of an intensified TEJ lag phases of stronger convective activity.

For synoptic time scales, by far the highest 32-year averaged correlation of 0.28 is ob-

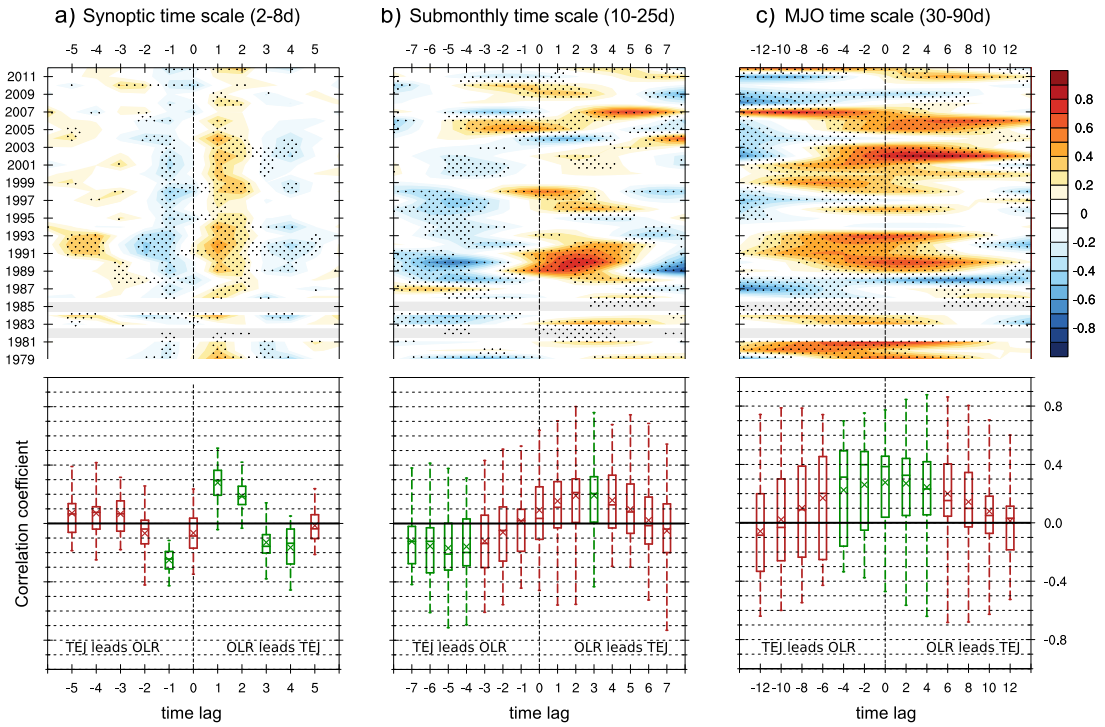

Figure 2.6: Relationship between regional TEJ intensity and convective activity in the Sahel over a range of synoptic to intraseasonal time scales. Top: Lead-lag correlations between OLR and 200 hPa zonal wind throughout 32 years. A positive correlation coefficient means that increased convection (negative OLR anomaly) goes along with increased TEJ speed (negative zonal wind anomaly) or vice versa. Positive correlations observed at positive time lags indicate that phases of an intensified TEJ lag phases of stronger convective activity. The correlations are calculated separately for each year from daily bandpass-filtered JJAS data of regionally averaged OLR (15°W to 15°E and 8°N to 16°N OLR and 200 hPa zonal wind (averaged from 15°W to 15°E and 2°N to 10°N). Stippling indicates statistical significance at the 5% level determined by a bootstrapping test with 5000 iterations. Bottom: Box and Whisker plot for the corresponding minima, maxima, the 25%, 50% and 75% quartiles and the average (crosses) of the correlation coefficients. Positive lag means that changes in OLR lead changes in 200 hPa zonal wind. The green color of the boxes denote time lags for that the average correlation is statistically significant at the 5% level (determined by a bootstrapping test with 5000 iterations).

served when OLR anomalies lead TEJ anomalies by one or two days (Fig. 2.6a), meaning that an intensified TEJ is mostly observed after a period of increased convective activity and not vice versa. On time scales between 10 and 90 days, the lead-lag correlations remain below 0.3 – without pronounced peak values – and therefore do not surpass the distinct maximum value found for synoptic time scales. The relationship on the MJO time scale is characterized by a broad interval of significant correlations of up to 0.28 from -4 to +4 days (Fig. 2.6c). On the submonthly time scale, the only barely significant positive correlation of 0.2 is observed at a time lag of +3 (Fig. 2.6b). Significant westerly anomalies at 200 hPa and therefore a weakening of the TEJ are observed 1 day before maximum convection on synoptic and some 5 days prior on submonthly time scales. While it is clear for synoptic time scales, the significance of the found lead-lag relationships is doubtful for the submonthly and MJO time scale. In particular on the MJO time scale, there are no distinct peaks in the which could indicate a clear lead-lag relationship. Moreover, the OLR - TEJ relationship on both time scales between 10 and 90 days exhibits a strong interannual and decadal variability such that in about

20-25% of all years the correlation becomes negative at time lags from +1 to +3 (bar plots at bottom of Fig. 2.6b and c).

The main findings regarding maximum correlations and corresponding time lags are consistent among all reanalyses (table 2.4.1). We further test the sensitivity of the lead-lag relationships against the area and position of the region over which the spatial averages are calculated. There are no major contradictions to the results presented: smaller averaging boxes, small latitudinal shifts or a change of the latitudinal shift between the boxes result in lower correlations but the most important result, which is that the TEJ generally lags convection anomalies, is unchanged (not shown).

For a better understanding of the lead-lag relationships, the next two subsections present upper-tropospheric circulation patterns associated with Sahel convection anomalies on synoptic and submonthly time scales. The MJO time scale will not be discussed because the OLR regression pattern on the selected Sahel base region OLR is nearly identical to the MJO in phase 1 as depicted in Alaka Jr and Maloney (2012, their Fig. 6). During this phase, increased convective activity over West Africa co-occurs with increased upper-level easterlies about the equator which can be understood as an equatorial Rossby wave response to anomalous heating over the equatorial Indian ocean. Although the strength of the anomalous easterlies decreases exponentially from the equator, some significant anomalies extend northward to about 10°N. These remotely induced anomalies that co-occur with increased convection over the Sahel may explain the significant correlations on the MJO time scale at time steps -4 to +4.

Table 2.4.1: Maximal 32-year averaged lead-lag correlations and corresponding time lags (in days) between OLR (NOAA) and 200 hPa zonal wind on synoptic to intraseasonal time scales for all reanalyses. Positive time lag means that changes in OLR lead changes in 200 hPa zonal wind.

	2d-8d		10d-25d		30d-90d	
ERA-Interim	0.28	+1	0.19	+3	0.28	+0
NCAR NCEP	0.24	+1	0.15	+3	0.23	-1
MERRA-2	0.28	+1	0.22	+2	0.26	+0
JRA-55	0.27	+1	0.18	+2	0.27	+1

2.4.3 Spatio-temporal relationship on synoptic time scales

The spatio-temporal analysis of the Sahel rainfall – TEJ relationship on the synoptic time scale (2–8 days) shows – in agreement to the previously found lead-lag relationship – that periods with a stronger TEJ (i.e., negative 200 hPa zonal wind anomalies) seem to lag periods of increased convection. These results are obtained by regressing OLR and 200 hPa circulation anomalies on the 2–8 days bandpass-filtered OLR values in the selected Sahel base region (red box in Fig. 2.7). Without any imposed time lag (at day 0), the OLR regression pattern shows a negative OLR anomaly of up to 30 W m^{-2} (Fig. 2.7a). The negative OLR signal appears to be embedded in an AEW-like structure as it is associated with a significant lower- and mid-tropospheric wind anomaly pattern

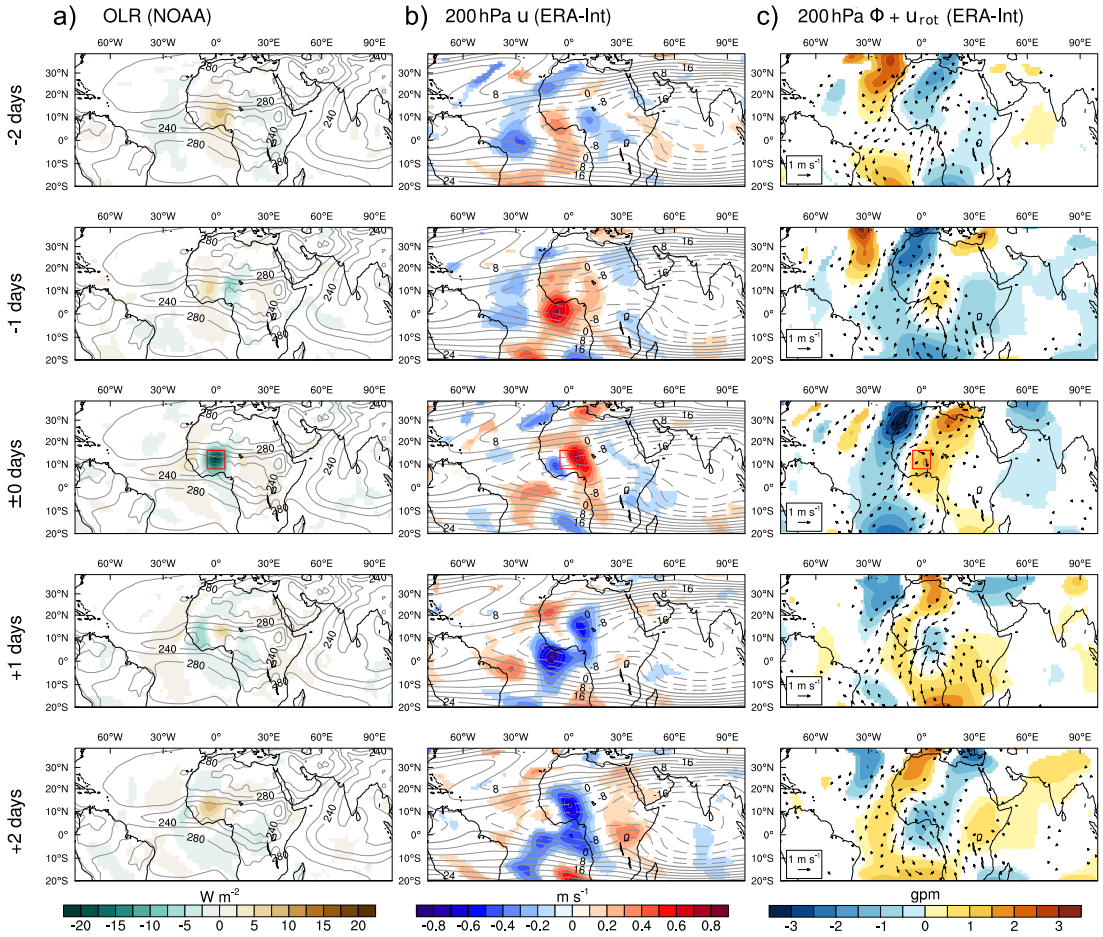

Figure 2.7: OLR and 200 hPa circulation features associated with synoptic-scale anomalies of Sahel convection. Left column: 2–8 days bandpass-filtered OLR anomalies predicted by linear regression using one negative standard deviation in 2–8 days bandpass-filtered OLR at the base region (red box) as independent variable. Middle column: Corresponding 2–8 days filtered anomalies of 200 hPa zonal wind (u). Right column: Corresponding 2–8 days filtered anomalies of bandpass-filtered 200 hPa geopotential (Φ) and non-divergent wind ($\vec{u}_{\mathrm{rot}}$) anomalies. Each row has a designated time lag, going from -2 days to +2 days. All anomalies shown (including wind vectors) are statistically significant at the 5% level determined by bootstrapping method with 1000 iterations.

akin to AEW composites as presented in Kiladis et al. (2006, their Fig. 3) (not shown). Upper-tropospheric wind anomalies (here we show ERA-Interim) at day 0 can be identified as mostly divergent outflow with westerly anomalies behind and easterly anomalies ahead of the OLR signal (Fig. 2.7b). One day later the OLR signal moves westward by about 5°, accompanied by a significant decrease of its amplitude to less than - 10 W m^{-2}. During this time, a significant 200 hPa easterly anomaly of about 0.5 m s^{-1} evolves near the selected Sahel base region where the OLR signal reached its maximum amplitude two days earlier. In addition, a zonally elongated easterly anomaly of up to 0.8 m s^{-1} appears near the equator. After two days, the OLR anomaly dissipates but the easterly anomalies at the TEJ level still persist.

Before the appearance of the negative OLR anomaly, the TEJ does not show any striking features besides a weakening near the Guinean coast. A jet streak-like pattern is neither observed in the mean state nor in the anomalies. The anomalous 200 hPa geopo-

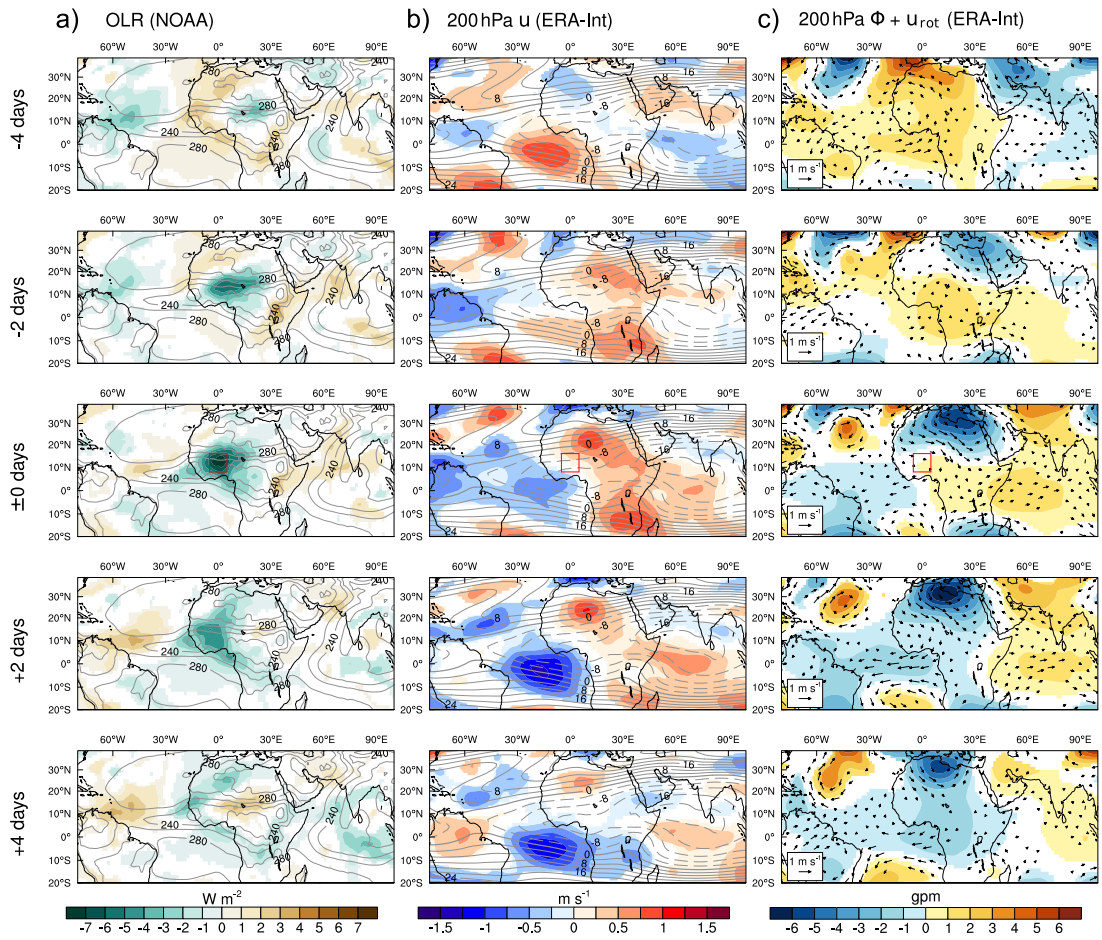

Figure 2.8: OLR and 200 hPa circulation features associated with anomalies of Sahel convection on the submonthly time scale. Left column: 10–25 days bandpass-filtered OLR anomalies predicted by linear regression using one negative standard deviation in 10–25 days bandpass-filtered OLR at the base region (red box) as independent variable. Middle column: Corresponding 10–25 days filtered anomalies of 200 hPa zonal wind (u). Right column: Corresponding 10–25 days filtered anomalies of bandpass-filtered 200 hPa geopotential (Φ) and non-divergent wind ($\vec{u}_{\mathrm{rot}}$) anomalies. Each row has a designated time lag, going from -2 days to +2 days. All anomalies shown (including wind vectors) are statistically significant at the 5% level determined by bootstrapping method with 1000 iterations.

tential field is characterized by a westward-propagating wave-like pattern (Fig. 2.7c). At a time lag of -1 day, widespread cross-equatorial southerlies are observed in relation to that wave structure. Given an approximate frequency of five days, a wavelength of about 6000 km and the typical cross-equatorial flow associated with geopotential anomalies roughly asymmetrical about the equator, the observed wave pattern appears to be related to a mixed Rossby gravity wave (e.g., Matsuno, 1966; Yang et al., 2007; Kiladis et al., 2009).

2.4.4 Spatio-temporal relationship on submonthly time scales

On the submonthly time scale (10–25 days) the OLR field regressed on OLR in the Sahel base region shows a pattern that might be interpreted as the weighted superposition of the Sahel mode (Sultan et al., 2003) and the QBZD (Mounier et al., 2008). For the selected Sahel base region which represents the average extent of the main mon-

soon rainbelt, the Sahel Mode is more strongly present than the QBDZ. At day 0, a large region spanning from Africa's west coast to about 20°E and from the Gulf of Guinea up to the northern Sahel is covered by OLR anomalies of up to -8 W m^{-2} (Fig. 2.8a). Four days prior to the OLR minimum over the Sahel, the first significant negative OLR anomaly appears over the central and eastern Sahel. This convective signal travels westward while strengthening until reaching maximum amplitude over the Sahel region.

Upper-tropospheric circulation changes associated with one negative standard deviation of OLR are mostly constrained to the coastal region and the Northern Sahel region (Fig. 2.8b). The TEJ remains mostly unchanged. At a time lag of -2 days, an easterly anomaly first appears over northeastern Brazil. This signal moves eastwards and reaches maximum amplitude of about -1.5 m s^{-1} over the equatorial Atlantic at a time lag of +2 days. Although this signal does not reach further northwards than 10°N, it might explain the low, albeit significant positive lag-correlation between 200 hPa zonal wind and OLR in the Sahel region on this time scale. Two days later, the eastward movement seems to come to a halt and the amplitude weakens. The described equatorial and eastward-travelling 200 hPa easterly anomaly is likely associated with the QBDZ although this mode of biweekly convection is much less visible in the OLR field. When the OLR base region is shifted further to the south, the regressed OLR pattern resembles more and more the QBDZ as described in Mounier et al. (2008). The corresponding upper-level circulation features are then mostly confined to the equator and are identifiable as the eastward-propagating Kelvin wave-like anomalies related to the Walker-type circulation across the Atlantic.

In synopsis, the statistical analysis of the spatio-temporal relationship between Sahel convection and TEJ intensity for synoptic and submonthly time scales yields a clear result: Consistent among all reanalysis models, there is no indication that phases of increased convective activity are preceded by an anomalously strong TEJ or a jet streak pattern. Upper-level easterlies are increased south of increased convection after one or two days which is in accordance with the maximum lag correlation found in the previous section. These findings are in good agreement with one key result of Kiladis and Weickmann (1997) who explored the relationship between upper-tropospheric circulation and convective activity in tropical regions on the 6–30 day time scale: In regions with persistent upper-level easterlies, which includes the Sahel region, upper-tropospheric circulation anomalies are induced by anomalous convective activity – and not vice versa.

2.5 Interaction between TEJ and MCS

2.5.1 Atmospheric conditions before MCS genesis

Initiation of deep convection is complex and demands the simultaneous presence of many ingredients. The primary aim of this section, however, is not to unravel the complex interplay of all involved processes but to analyse upper-level winds before MCS initiation within a more complete statistical approach than Besson and Lemaître (2014). Following this investigation, a brief analysis of the most important mid- and lower-tropospheric processes will be presented.

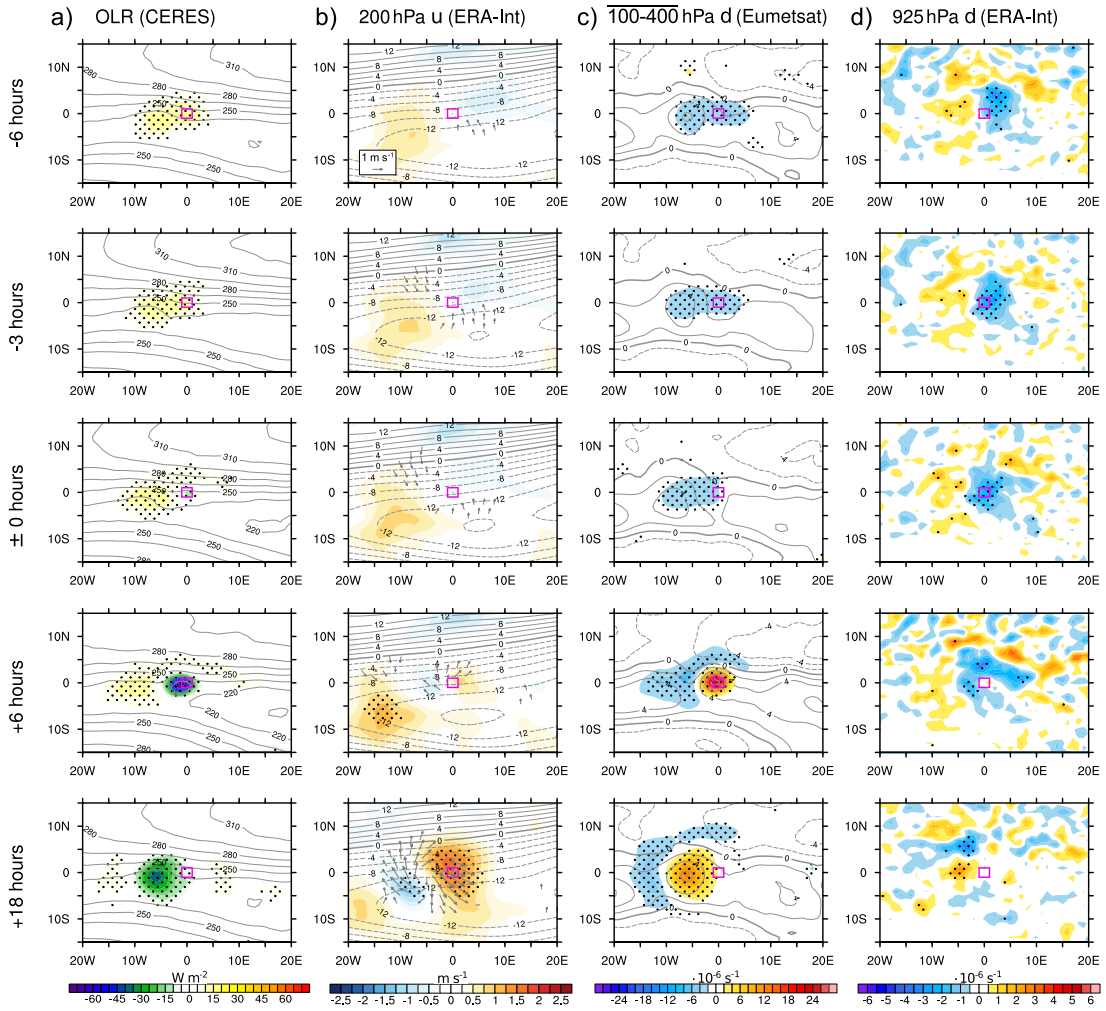

Figure 2.9: MCS initiation centred relative latitude – longitude maps of composite mean anomalies (average over 289 MCS initiation cases in the Sahel-Sudanian region) of OLR (CERES), 200 hPa zonal wind u (shaded) and significant 200 hPa wind vectors (both ERA-Interim), upper-tropospheric $\overline{100\text{–}400\,\text{hPa}}$ divergence d (Eumetsat), and 925 hPa divergence d (ERA-Interim). Anomalies are calculated against the time of day reference state obtained by 12-day low-pass filtering (shown with contour lines). Rows designate different time lag/lead relative to the time of MCS genesis. The small magenta box is a visual aid depicting the MCS genesis area. Dots indicate statistical significance at the 5% level tested by bootstrapping with 5000 iterations.

Figure 2.9 shows the composite-averaged OLR (CERES SYN1deg) anomaly of 289 newly-forming MCSs and associated anomalies of dynamical quantities (ERA-Interim) in form of lat-lon maps centred on a common, initiation-relative grid over the course of 24 hours – beginning with the situation 6 hours before initiation (top row) and ending with the dissipation stage (bottom row). Maximal negative OLR anomalies of about 70 W m^{-2} are observed 3 or 6 hours after initiation which is consistent with the widespread and vigorous deep convection in the early mature MCS stage (Fig. 2.9a). The TEJ, depicted by anomalous 200 hPa ERA-Interim zonal winds, shows on average no distinct features in the 6 hours before MCS initiation (Fig. 2.9b). Only a westerly wind anomaly of up to 1m s^{-1}, which later becomes significant, is found slightly south-west of the future MCS genesis region. A weak but significant southerly anomaly of 0.5m s^{-1} is observed at 200 hPa east of the formation region shortly before MCS initi-

ation (Figs. 2.9b and 2.10k). Although the signals in the composite means are weak, the high variability of upper-level wind anomalies among all 289 composite members should be stressed. In a $2° \cdot 2°$ box around the MCS initiation area, the 200 hPa easterly wind anomaly before initiation ranges from roughly -10 to +10 m s^{-1} (Fig. 2.10h, blue line; please note the scaling factor applied to the 10–90 percentile range).

Consistent with the composite-averaged anomalous wind field in the ERA-Interim reanalysis, the Eumetsat divergence product shows a small but significant upper-tropospheric convergence anomaly in the MCS initiation area (Fig. 2.9c). This anomalous convergence is observed over 24 hours before MCS formation – in both, the Eumetsat and ERA-Interim data sets (Figs. 2.10b,c). Ensemble-wide evaluation of absolute Eumetsat divergence averaged over 6 hours before MCS genesis and spatially averaged within a $2° \cdot 2°$ box centred at the MCS genesis location yields: Only 21% of all 289 MCSs are initiated under large-scale upper-level divergence exceeding the climatological summer mean of that area. Substantial divergence values larger than $5 \cdot 10^{-6}$ s^{-1} only appear in 15% of all cases, values above 10^{-5} s^{-1} exist in only 2% of all cases. Divergence as high as $3 \cdot 10^{-5}$ s^{-1} is not observed before MCS genesis. Besson and Lemaître (2014) reported such a value as solely induced by a TEJ streak. In our analysis based on satellite-derived divergence, such high values are only observed after MCS initiation as a result of the MCS' convective outflow. The analysis in Besson and Lemaître (2014) relied exclusively on reanalyses and the higher divergence values could therefore have been a consequence of spurious convection.

Albeit less pronounced in the upper-level divergence (Fig. 2.10d), the aforementioned variability in the upper-level winds before MCS genesis motivates a deeper analysis of the entire MCS ensemble. A non-negligible number of cases could exist in which an anomalous TEJ and/or a distinct jet streak might exert an effect on the organization of MCSs. This hypothesis is tested by plotting key parameters (size, lifetime, intensity, speed) of each of the 289 MCSs against the large-scale Eumetsat divergence anomaly averaged over the 6 hours before MCS initiation in a box slightly upstream (-1° – 3°E, -2° – 2°N) of the future MCS genesis location. Pre-existing upper-level divergence seems to have no substantial effect on organization of MCSs. All scatter plots strongly resemble random distributions with no apparent clusters (Fig. 2.11a-d). The correlations between preceding anomalous upper-level divergence and all MCS parameters are low and statistically insignificant ($p > 0.05$). To gain further insight, the noise of the anomalous $\overline{100–400\,\text{hPa}}$ divergence field is filtered out by only considering substantial deviations from the median. For this, only those data points are selected that lie either below the first or above the second tertile with respect to both the anomalous divergence and the respective MCS parameter (shaded outer quadrants in Fig. 2.11a-d). It is then counted how often distinctly above or below median MCS parameters values co-occur with substantially increased or decreased preceding upper-level divergence. This procedure is repeated for 5000 times after resampling the data each time. According to this method, above-median MCS lifetime, size, intensity or movement speed are not significantly more frequent in situations with pre-existing anomalous divergence at the TEJ level.

The same scatter plot analysis is carried out for a jet streak measure to guarantee that possible jet-induced divergence is not overshadowed by other effects. Inspired by

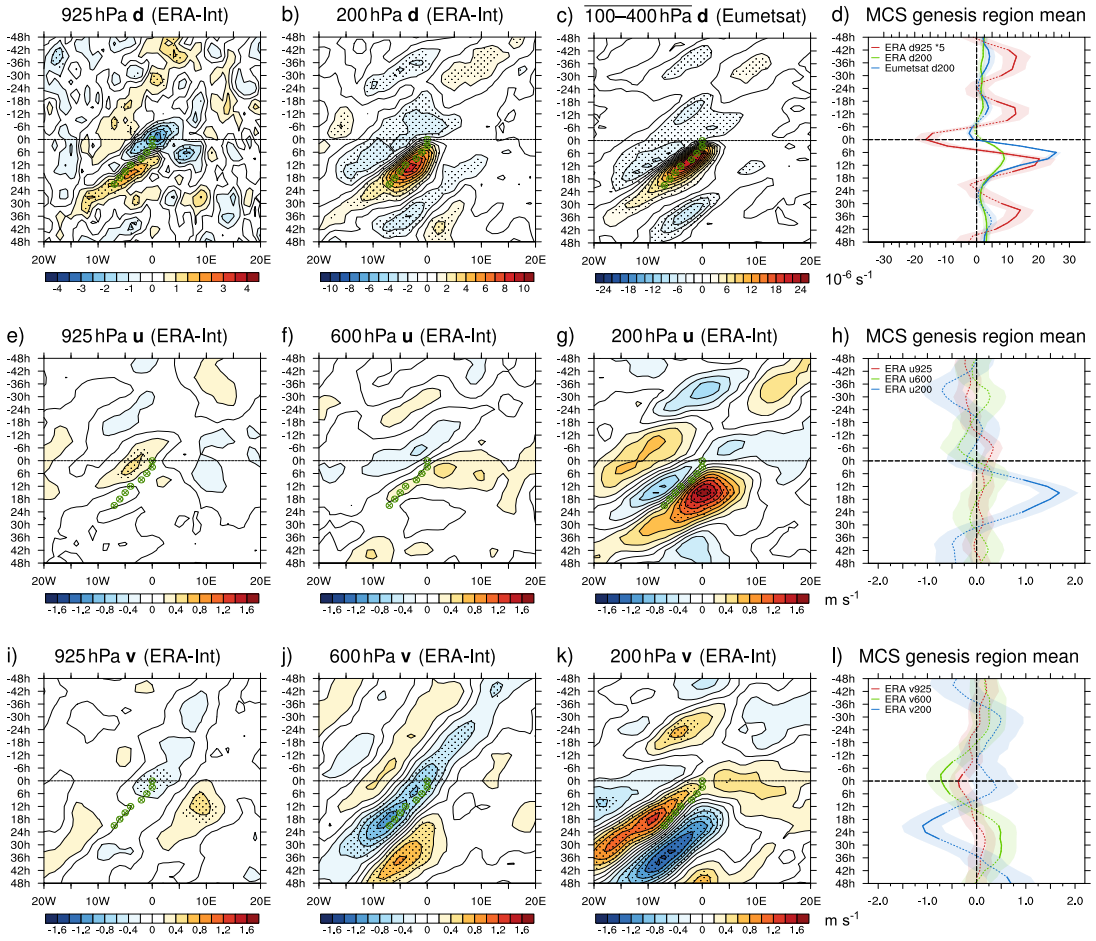

Figure 2.10: Hovmoeller plots of several composite mean anomalies (average over 289 MCS initiation cases in the Sahel-Sudanian region). Dots indicate statistical significance at the 5% level tested by bootstrapping with 5000 iterations. Crosses depict the path of the composite MCS. The right column shows the course in time for the initiation location field mean (2° · 2° box) of the three quantities within each row. The 925 hPa divergence from ERA-Interim has been scaled up by a factor of 5 for better visibility. The shaded areas around the lines depict the 10% and 90% percentile scaled by a factor of 0.1. Solid line parts denote statistical significance at the 5% level.

the conceptual jet streak picture depicted in Besson and Lemaître (2014, their Fig. 7a), we define the jet streak measure as the spatially averaged 200 hPa zonal wind anomaly in a region slightly ahead and south (-10° – 0°E, -4° – 2°N) of the MCS genesis location from which the average zonal wind anomaly in a larger area (-15° – 15°E, -5° – 5°N) is subtracted. In a further test, the relationship between the local TEJ intensity and MCS parameters is investigated for a possible effect of upper-level wind shear on MCS organization. As was the case before with upper-level divergence, no significant statistical connection is found between any MCS parameter and these two TEJ-related measures (not shown). This result further indicates that the TEJ plays no major role for MCS organization, at least not by affecting upper-level shear or divergence.

Beyond the scope of upper-tropospheric dynamics, there is mostly agreement with earlier studies: The composite-averaged MCS forms within a significant pre-existing wave-like pattern at 600 hPa which moves westwards at a speed of approximately 6.5 m s^{-1} and might be associated with an AEW (Fig. 2.10j). Average initiation within

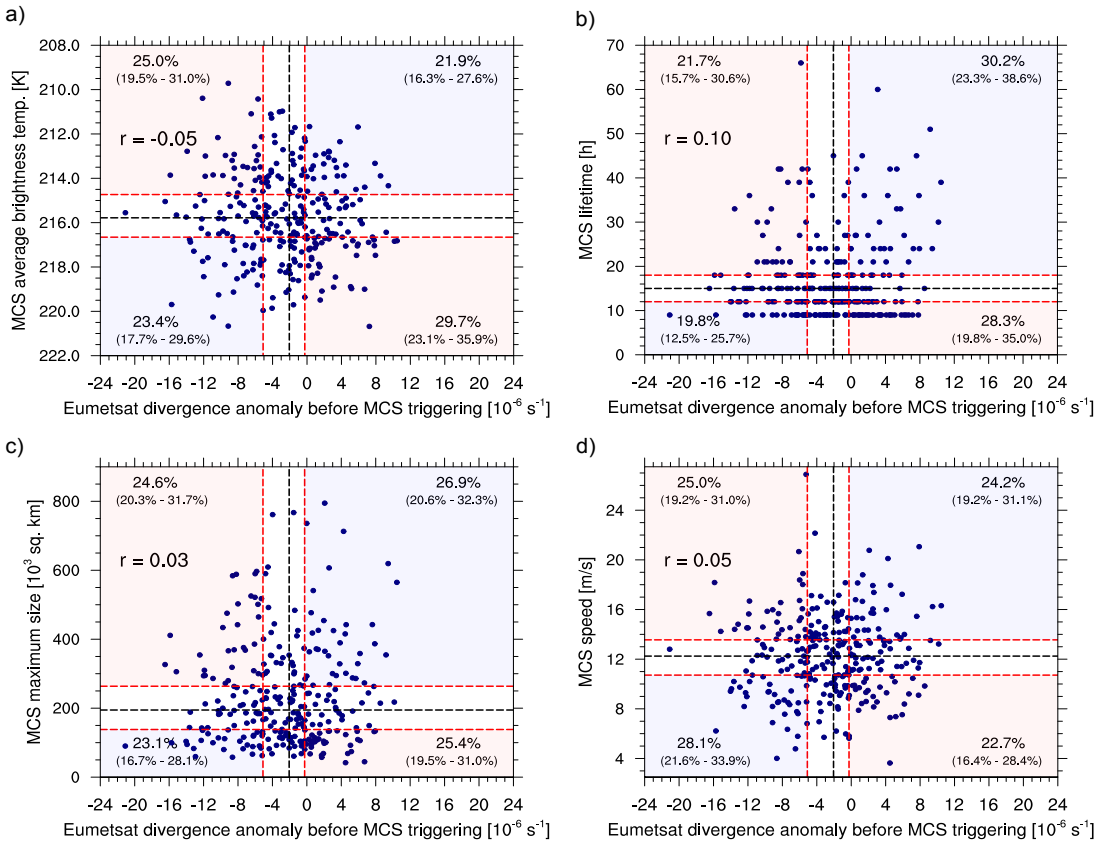

Figure 2.11: Relationship between pre-existing large-scale divergence and several MCS parameters characterizing its degree of organization for the ensemble of 289 MCSs in the Sahel-Sudanian region. Scatter plots showing the a) MCS intensity (average brightness temperature), b) MCS lifetime, c) MCS maximal size and d) MCS travel speed as a function of anomalous large-scale divergence 6 hours prior to MCS genesis. The horizontal black line shows the median value of the respective MCS quantity, the black vertical line represents the median for the preceding divergence anomaly. Red lines depict the respective tertiles for the MCS quantity and preceding divergence. The percentage values express the relative frequency of MCS for each of the four outer quadrants which are bounded by the horizontal and vertical red lines (and marked by the light shading). The percentages in parentheses denote the 2.5% and 97.5% confidence bound determined by a bootstrapping routine with 5000 iterations. If 25% is not within this span, we assume that above/below median MCS parameter values are significantly more/less often observed in the respective quadrant.

the northerly wind anomaly ahead of the AEW trough would be in agreement with previous studies that found that West-Sahelian MCSs are most frequent in this wave sector (Diedhiou et al., 1999; Duvel, 1990; Fink and Reiner, 2003). Because MCSs can also be initiated in each other sector of an AEW or without the presence of AEWs, the composite mean does not show a coherent AEW-like circulation structure (not shown). Prior to initiation, AEJ speed is on average increased by nearly $1\,\mathrm{m\,s^{-1}}$ ahead and slightly south of the future genesis area (Fig. 2.10f; anomaly is less pronounced in the Hovmoeller plot). This observation, although just missing the 5% significance level, stands in contrast with the favourable dynamical configuration between the AEJ and well-organized MCSs as proposed in Besson and Lemaître (2014). Even though many typical mesoscale convergence lines are not resolved, all reanalyses show a significant increase of large-scale low-level convergence some hours before MCS initiation (Figs. 2.9d and 2.10a). This increase in low-level convergence might be a spurious artifact of the reanalysis assimilation scheme but could also be associated with a shal-

low convection phase preceding deep convection. Consistent with the convergent low-level flow, ERA-Interim shows an anomalously cyclonic near-surface circulation with slightly albeit significantly increased monsoon flow to the west, increased northerly flow at and stronger southerly flow behind the MCS genesis region (Fig. 2.10e,i). Associated with that cyclonic circulation is a noticeable, albeit non-significant decrease in 925 hPa geopotential height. Significantly higher CAPE values and a significant mainly temperature related increase of moist static energy in lower levels are present before the MCS forms (not shown). Orography is another crucial forcing, since according to Mathon and Laurent (2001), 55% of MCSs develop in regions above 400 m. Although the selected Sahel-Sudanian region is rather flat and not crossed by prominent mountain ranges, slightly more MCS initiations are detected at or near elevated terrain. Roughly 30% of MCS are initiated in regions above 400 m (topography data at 0.25° resolution) but these regions take up only 22% of the study area (not shown).

In summary, the investigation of nearly 300 Sahelian MCSs shows that the initiation is generally not associated with jet streak-like configurations or any striking anomalies in the upper-troposheric wind field. Substantial upper-tropospheric divergence exceeding climatological mean values is only present in 26% of all examined MCS initiations. There is further no significant relationship between pre-existing TEJ-related divergence and intensity, size or longevity of MCSs. A brief analysis beyond the scope of upper-tropospheric dynamics confirms the important role of orography, favourable local-scale thermodynamic conditions and low- to mid-level dynamical forcing. What cannot be excluded within the scope of this analysis are possible interactions between the TEJ and some of the above-mentioned forcings.

2.5.2 Modification of the TEJ by MCSs

Some hours after initiation, the MCS develops a typical upper-level outflow anticyclone. North of the MCS, where the Coriolis force is higher, we observe a stronger westerly anomaly in the northeastern sector of the MCS compared to a weaker easterly anomaly in the southwestern sector. Weak southerly anomalies are found in the northwestern sector and stronger northerly anomalies exist in the southeastern sector (Figs. 2.9b and 2.10g,k). Albeit significant, the modification of the TEJ is rather weak in the composite mean because averaging of a high number of different MCS cases acts as rather heavy spatial smoothing. For some single cases, though, a strong easterly anomaly of up to $5\,\mathrm{m\,s^{-1}}$ is found in the southwest sector of the MCS (not shown), which is in good agreement with the results of numerical simulations in Diongue et al. (2002). They found that an MCS' vigorous equatorward outflow deflected to the right by the Coriolis force can result in a significant intensification of the TEJ of about $15\,\mathrm{m\,s^{-1}}$ over scales of hundreds of kilometres. This regional intensification might lead to a marked jet streak-like appearance in the regional 200 hPa zonal wind field.

2.5.3 Comparison between different regions and reanalyses

Composite-averaged upper-tropospheric winds before MCS initiation are similar for all other examined African regions. As in the main study area, the Sahel-Sudanian zone, no significant anomalies in upper-level zonal wind speed are found near the MCS gene-

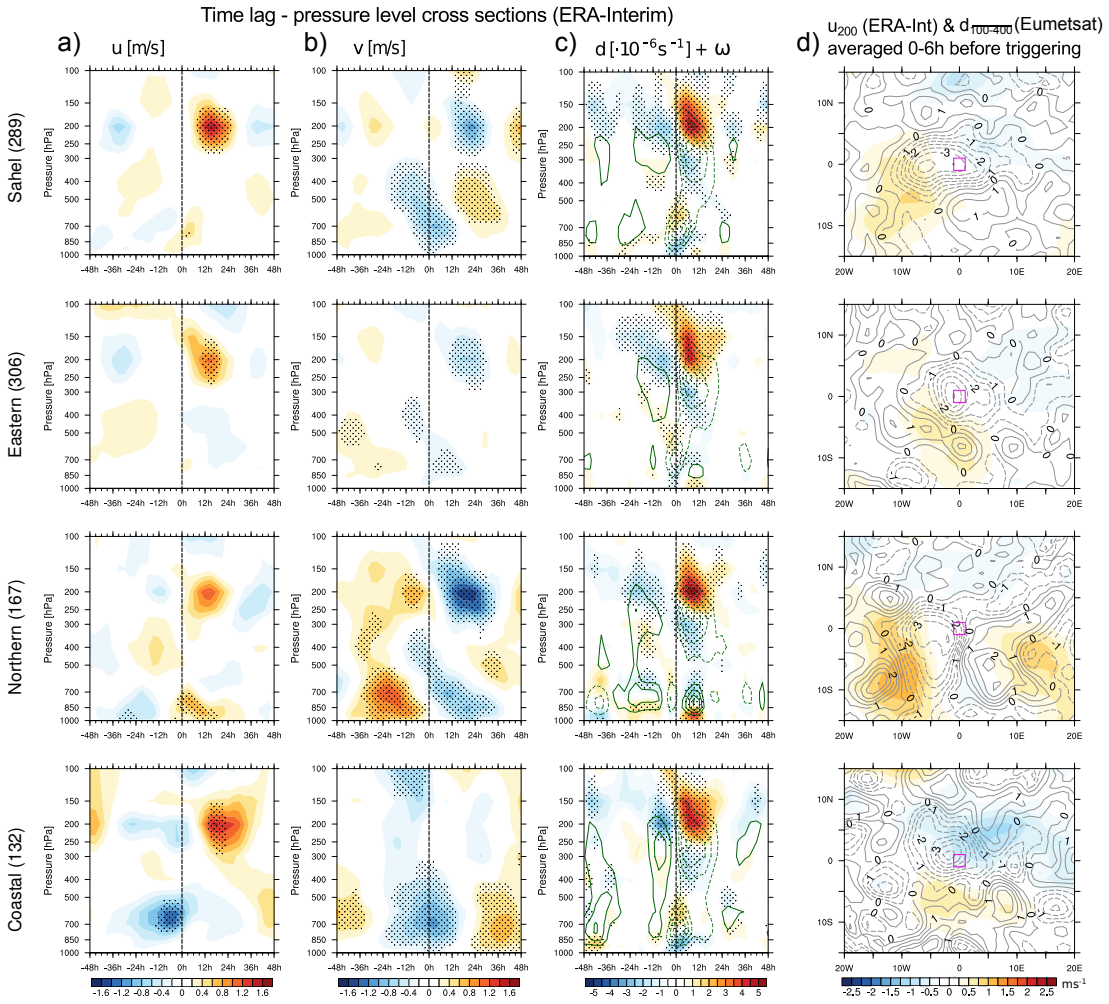

Figure 2.12: Comparison of atmospheric conditions before MCS genesis between different regions. First three columns from the left show time lag – pressure level plots of composite mean anomalies for the $2^\circ \cdot 2^\circ$ area mean around the MCS initiation location for the quantities (from left to right): zonal wind u, meridional wind v, divergence d (shaded) + vertical motion ω (contour interval: 0.01 Pa/s, dashed contours depict ascent) from the ERA-Interim data set. The rightmost column depicts lon-lat plots of ERA-Interim 200 hPa zonal wind anomalies (shaded) and Eumetsat $\overline{100\text{–}400\,\text{hPa}}$ divergence anomalies (contours every $0.5 \cdot 10^{-6}\,\text{s}^{-1}$, divergence solid, convergence dashed) averaged over the 6 hours before MCS initiation. For all columns, the rows show results for the different regions as introduced in figure 2.4. The number of MCS initiations (the composite size) is given in the parentheses. Shown are always the anomalies against an time of day reference state obtained by 12-day low-pass filtering. Dots indicate statistical significance at the 5% level tested by bootstrapping with 5000 iterations.

sis area on average (Fig. 2.12a,d). Significant upper-level convergence and descending motion is apparent in all regions some 12–24 hours before MCS initiation (Fig. 2.12c,d). Moreover, no statistical evidence is found that preceding jet anomalies and associated upper-level divergence affects MCS intensity, lifetime or maximum size in any of the selected regions (not shown). With the exception of the Northern Sahel, no significant meridional wind anomalies are present in the upper troposphere before MCS initiation. The main difference between the four regions is the involvement of AEWs. In the Eastern Sahel region many AEWs are weaker, have not formed yet or might be initiated later by strong MCSs (Fig. 2.12b).

The consistency of our findings is further tested by comparing MCS-associated mean atmospheric fields of ERA-Interim to those of MERRA-2 and JRA-55 for the Sahel-Sudanian region (not shown). High agreement among all three reanalyses is found for the atmospheric conditions before MCS genesis. None of the reanalyses show significant zonal wind anomalies or any significant divergence at the TEJ level. In synopsis, the comparison between different regions and different reanalyses provides further strong evidence that MCS initiation and organization are not associated with significant TEJ anomalies.

2.6 Summary and concluding discussion

Previous studies found a significant positive correlation between the strength of the TEJ over West Africa and Sahel rainfall on decadal and interannual time scales. A causal relationship was suggested but it has been unclear whether substantial interaction exists on much shorter time scales. In the first part of this study, we therefore investigate the relationship between the West African TEJ and Sahel rainfall (using OLR as proxy) over a range of synoptic to intraseasonal time scales. Using a variety of statistical analyses, we find:

- The statistical relationship between the intensity of the West African TEJ and convective activity in the Sahel is much weaker on synoptic to intraseasonal (correlations below 0.3) than on interannual and decadal time scales (correlations between 0.5 and 0.9)
- On synoptic time scales, phases of anomalous convective activity significantly lead changes in the regional TEJ intensity by one or two days, suggesting that convection anomalies are more likely to cause changes in the regional TEJ than vice versa

A weaker statistical connection on shorter time scales is expected because high-frequent noise is not filtered out, as is the case for correlations calculated on longer multi-year time scales. Therefore, a strong relationship between the TEJ and Sahel rainfall might only be reflected in seasonal averages; one could assume a mainly one-way interaction in which the seasonally integrated effect of excess rainfall results in a stronger than normal TEJ over West Africa. However, the question arises as to whether the strong statistical correlation on longer time scales is mainly explained by such a direct relationship or whether a "third variable" considerably controls both the TEJ and Sahel rainfall simultaneously. Large-scale SST anomalies and their effect on the planetary-scale tropical circulation are a potential candidate, since they are not only linked to Sahel rainfall changes on interannual and (multi-)decadal time scales (Folland et al., 1986; Janicot et al., 1996; Giannini et al., 2003; Bader and Latif, 2003), but also affect the TEJ intensity over India (Abish et al., 2013; Chen and van Loon, 1987; Nithya et al., 2017) and over West Africa (Preethi et al., 2015). In ongoing idealized model experiments, we seem to be able to confirm the role of global SST anomalies as said "third variable". By inducing changes in the planetary-scale tropical circulation through anomalous diabatic heating, large-scale SST anomalies influence both Sahel precipitation and the TEJ largely independently, but in a way that years of higher precipitation are usually accompanied by

a stronger TEJ. Thereby, a high statistical connection between the regional TEJ and Sahel rainfall on interannual to multi-decadal time scales is possible without any strong underlying interaction.

The second part of this study revisits the role of TEJ-induced upper-level divergence in promoting convection over the Sahel. By analyzing only 17 MCS initiation cases, Besson and Lemaître (2014) concluded that TEJ streaks and associated anomalous upper-level divergence might be favourable for the development of well-organized and persistent MCSs. In contrast, we use a statistical approach with a larger sample size (289 MCS initiation cases) to investigate the synoptic upper-level wind conditions under which MCSs form and find:

- In the majority of cases, MCS initiation is not associated with TEJ streaks or any other significant anomalies of the upper-tropospheric wind field
- TEJ streak-related upper-level divergence and/or anomalous TEJ intensity are not correlated with size, lifetime, intensity or movement speed of MCSs

Our analysis does not rule out that there are individual cases in which a pronounced TEJ streak could significantly aid MCS development. Thus, the presented results do not necessarily contradict those of Besson and Lemaître (2014). Because of the much larger sample size, however, it becomes clear that jet streaks on the TEJ do not occur in conjunction with MCSs in most cases – that is prior to their initiation. Only after an MCS has already formed, may its anticyclonic divergent outflow alter upper-level winds such that the zonal wind field resembles a classic jet streak configuration. Our results therefore cast doubt on the validity of a jet-streak based conceptual framework at very low latitudes and, more generally, question the relevance of synoptic-scale ascent for promoting tropical convection. Thus, our findings are consistent with previous theoretical work which emphasized that balanced dry ascent is weak in the tropics (e.g., Charney, 1963; Raymond et al., 2015) and that synoptic-scale vertical motions are typically too weak to play a primary role for convection (e.g., Doswell and Bosart, 2001).

In summary, this study challenges the previously proposed hypothesis that the TEJ might play an important role for Sahel rainfall via its control on upper-level divergence. Our multiple statistical analyses show that the regional TEJ intensity over West Africa is only weakly correlated with Sahel rainfall on synoptic to intraseasonal time scales. More importantly, anomalies in convective activity appear to cause changes in the regional TEJ and not the other way around, which suggests a rather passive role for the TEJ. This result is further confirmed by the in-depth analysis of nearly 300 MCSs for which neither their initiation nor their degree of organization is significantly associated with TEJ-induced upper-level divergence or anomalous TEJ intensity.

Some questions, however, remain open due to the limitations of our study. First, by confining our analysis to the satellite era (after 1979) we cannot cover the wet WAM period of the 1950s and 1960s which was characterized by a stronger statistical relationship between rainfall and the TEJ (Fig. 1). Therefore it cannot be ruled out that the more intense TEJ over West Africa might have played a more active role for Sahel rainfall in that period. Another limitation is the use of OLR as a proxy for rainfall. The

advantage of using OLR, namely its availability for about four decades in almost gapless, spatially homogeneous data sets, could be partly offset by the disadvantage that the correlation between OLR and rainfall might decrease on sub-synoptic spatial and daily or sub-daily time scales. For instance, the lowest OLR values associated with an MCS do not necessarily indicate its convective core region, which can lead to several inaccuracies. An additional problem is the coarse temporal (3 hours) and spatial resolution (1°), not only of the OLR data set, but also of the reanalyses. Because the TEJ and possible embedded streaks are mainly synoptic-scale features, we are nonetheless confident that they are reasonably well represented by reanalyses. Therefore, one of our study's focuses, the analysis of the upper-tropospheric flow prior to the formation of MCSs, should not be limited too severely by low resolution. However, it is not possible for us to investigate a potential interaction between the mesoscale flow of an already developed MCS and the synoptic-scale upper-level flow due to the mainly resolution-related limitations of reanalyses.

Moreover, and most importantly, the TEJ could still have an influence on Sahel rainfall via other mechanisms than through affecting upper-level divergence. For instance, the role of the observed planetary-scale waves at the TEJ and their possible interaction with AEWs and synoptic-scale convection was stressed in Nicholson et al. (2007) and Mekonnen and Thorncroft (2016). A further important question is whether not only fluctuations but rather the background mean state of the TEJ influences Sahel rainfall. Yang et al. (2018) showed that AEW activity depends on the background mean flow in the equatorial upper troposphere. A stronger and wider TEJ is associated with favourable equatorial Rossby wave propagation characteristics which promotes AEW activity. Therefore, further study is needed to understand what determines the TEJ mean state, how it is affected by remote influences and, in particular, how it interacts with Sahel rainfall.

Acknowledgments

We thank Dr. Cathy Hohenegger for a thorough internal review and many suggestions for improvement. Further thanks go to Dr. Thomas Riddick for proofreading. We are grateful for the numerous valuable comments by the reviewers and the editor that greatly helped to improve the structure and clarity of the paper. We also thank Huang (2017) for developing the MCS tracking algorithm and making it available. This work was supported by the International Max Planck Research School on Earth System Modelling (IMPRS-ESM) and the Max Planck Society (MPG). The computational resources were provided by the Deutsches Klimarechenzentrum (DKRZ). All data used in this study are freely available on the web. A detailed description of how the data was obtained and processed as well as scripts used in the analysis and other supplementary information that may be useful in reproducing the author's work are archived by the Max Planck Institute for Meteorology and can be obtained by contacting publications@mpimet.mpg.de

Bibliography

Abish, B., P. Joseph, and O. M. Johannessen (2013). Weakening trend of the tropical easterly jet stream of the boreal summer monsoon season 1950–2009. *Journal of Climate 26*(23), 9408–9414.

Alaka Jr, G. J. and E. D. Maloney (2012). The influence of the MJO on upstream precursors to African easterly waves. *Journal of Climate 25*(9), 3219–3236.

Bader, J. and M. Latif (2003). The impact of decadal-scale Indian Ocean sea surface temperature anomalies on Sahelian rainfall and the North Atlantic Oscillation. *Geophysical Research Letters 30*(22).

Besson, L. and Y. Lemaître (2014). Mesoscale convective systems in relation to African and tropical easterly jets. *Monthly Weather Review 142*(9), 3224–3242.

Burpee, R. W. (1972). The origin and structure of easterly waves in the lower troposphere of North Africa. *Journal of the Atmospheric Sciences 29*(1), 77–90.

Carlson, T. N. (1969). Synoptic histories of three African disturbances that developed into Atlantic hurricanes. *Monthly Weather Review 97*(3), 256–276.

Charney, J. G. (1963). A note on large-scale motions in the tropics. *Journal of the Atmospheric Sciences 20*(6), 607–609.

Chen, T.-C. and H. van Loon (1987). Interannual variation of the tropical easterly jet. *Monthly Weather Review 115*(8), 1739–1759.

Couvreux, F., C. Rio, F. Guichard, M. Lothon, G. Canut, D. Bouniol, and A. Gounou (2012). Initiation of daytime local convection in a semi-arid region analysed with high-resolution simulations and AMMA observations. *Quarterly Journal of the Royal Meteorological Society 138*(662), 56–71.

Dee, D., S. Uppala, A. Simmons, P. Berrisford, P. Poli, S. Kobayashi, U. Andrae, M. Balmaseda, G. Balsamo, P. Bauer, et al. (2011). The ERA-Interim reanalysis: Configuration and performance of the data assimilation system. *Quarterly Journal of the royal meteorological society 137*(656), 553–597.

Diedhiou, A., S. Janicot, A. Viltard, P. De Felice, and H. Laurent (1999). Easterly wave regimes and associated convection over West Africa and tropical Atlantic: results from the NCEP/NCAR and ECMWF reanalyses. *Climate Dynamics 15*(11), 795–822.

Diongue, A., J.-P. LaFore, J.-L. Redelsperger, and R. Roca (2002). Numerical study of a Sahelian synoptic weather system: Initiation and mature stages of convection and its interactions with the large-scale dynamics. *Quarterly Journal of the Royal Meteorological Society 128*(584), 1899–1927.

Doswell, C. A. and L. F. Bosart (2001). Extratropical synoptic-scale processes and severe convection. In *Severe Convective Storms*, pp. 27–69. Springer.

Doswell III, C. A. (1987). The distinction between large-scale and mesoscale contribution to severe convection: A case study example. *Weather and Forecasting 2*(1), 3–16.

Doswell III, C. A., H. E. Brooks, and R. A. Maddox (1996). Flash flood forecasting: An ingredients-based methodology. *Weather and Forecasting 11*(4), 560–581.

Duvel, J. P. (1990). Convection over tropical Africa and the Atlantic Ocean during northern summer. Part II: Modulation by easterly waves. *Monthly Weather Review 118*(9), 1855–1868.

EUMETSAT (2005). Upper level Divergence Product Algorithm Description. Technical report, EUM/MET/REP/05/0163.

Fink, A. H. and A. Reiner (2003). Spatiotemporal variability of the relation between African easterly waves and West African squall lines in 1998 and 1999. *Journal of Geophysical Research: Atmospheres 108*(D11).

Folland, C., T. Palmer, and D. Parker (1986). Sahel rainfall and worldwide sea temperatures, 1901–85. *Nature 320*(6063), 602–607.

Gelaro, R., W. McCarty, M. J. Suárez, R. Todling, A. Molod, L. Takacs, C. Randles, A. Darmenov, M. G. Bosilovich, R. Reichle, et al. (2017). The Modern-Era Retrospective Analysis for Research and Applications, Version 2 (MERRA-2). *Journal of Climate* (2017).

Giannini, A., R. Saravanan, and P. Chang (2003). Oceanic forcing of Sahel rainfall on interannual to interdecadal time scales. *Science 302*(5647), 1027–1030.

Grist, J. P. and S. E. Nicholson (2001). A study of the dynamic factors influencing the rainfall variability in the West African Sahel. *Journal of climate 14*(7), 1337–1359.

Huang, X. (2017). A comprehensive Mesoscale Convective System (MSC) dataset, links to files in MatLab and plain text format.

Janicot, S., V. Moron, and B. Fontaine (1996). Sahel droughts and ENSO dynamics. *Geophysical Research Letters 23*(5), 515–518.

Janicot, S., F. Mounier, S. Gervois, B. Sultan, and G. N. Kiladis (2010). The dynamics of the West African monsoon. Part V: The detection and role of the dominant modes of convectively coupled equatorial Rossby waves. *Journal of Climate 23*(14), 4005–4024.

Kalnay, E., M. Kanamitsu, R. Kistler, W. Collins, D. Deaven, L. Gandin, M. Iredell, S. Saha, G. White, J. Woollen, et al. (1996). The NCEP/NCAR 40-year reanalysis project. *Bulletin of the American meteorological Society 77*(3), 437–471.

Kiladis, G. N., C. D. Thorncroft, and N. M. Hall (2006). Three-dimensional structure and dynamics of African easterly waves. Part I: Observations. *Journal of the Atmospheric Sciences 63*(9), 2212–2230.

Kiladis, G. N. and K. M. Weickmann (1997). Horizontal structure and seasonality of large-scale circulations associated with submonthly tropical convection. *Monthly weather review 125*(9), 1997–2013.

Kiladis, G. N., M. C. Wheeler, P. T. Haertel, K. H. Straub, and P. E. Roundy (2009). Convectively coupled equatorial waves. *Reviews of Geophysics 47*(2).

Knapp, K. R. and S. Wilkins (in prep., 2017). Gridded Satellite (GridSat) GOES and CONUS data. *Earth systems Science Data*.

Kobayashi, S., Y. Ota, Y. Harada, A. Ebita, M. Moriya, H. Onoda, K. Onogi, H. Kamahori, C. Kobayashi, H. Endo, et al. (2015). The JRA-55 reanalysis: General specifications and basic characteristics. *Journal of the Meteorological Society of Japan. Ser. II 93*(1), 5–48.

Koteswaram, P. (1958). The easterly jet stream in the tropics. *Tellus 10*(1), 43–57.

Lafore, J. P., N. Chapelon, M. Diop, B. Gueye, Y. Largeron, S. Lepape, O. Ndiaye, D. J. Parker, E. Poan, R. Roca, et al. (2017). Deep convection. *Meteorology of Tropical West Africa: The Forecasters' Handbook*, 90–129.

Lebel, T. and A. Ali (2009). Recent trends in the Central and Western Sahel rainfall regime (1990–2007). *Journal of Hydrology 375*(1), 52–64.

Lebel, T., A. Diedhiou, and H. Laurent (2003). Seasonal cycle and interannual variability of the Sahelian rainfall at hydrological scales. *Journal of Geophysical Research: Atmospheres 108*(D8).

Lee, H. (2014). Climate algorithm theoretical basis document (C-ATBD): Outgoing longwave radiation (OLR)—Daily. NOAA's Climate Data Record (CDR) Program. Technical report, CDRP-ATBD-0526.

Maloney, E. D. and J. Shaman (2008). Intraseasonal variability of the West African monsoon and Atlantic ITCZ. *Journal of Climate 21*(12), 2898–2918.

Mathon, V. and H. Laurent (2001). Life cycle of Sahelian mesoscale convective cloud systems. *Quarterly Journal of the Royal Meteorological Society 127*(572), 377–406.

Mathon, V., H. Laurent, and T. Lebel (2002). Mesoscale convective system rainfall in the Sahel. *Journal of applied meteorology 41*(11), 1081–1092.

Matsuno, T. (1966). Quasi-geostrophic motions in the equatorial area. *Journal of the Meteorological Society of Japan. Ser. II 44*(1), 25–43.

Mekonnen, A. and C. D. Thorncroft (2016). On mechanisms that determine synoptic time scale convection over East Africa. *International Journal of Climatology 36*(12), 4045–4057.

Mekonnen, A., C. D. Thorncroft, and A. R. Aiyyer (2006). Analysis of convection and its association with African easterly waves. *Journal of Climate 19*(20), 5405–5421.

Mounier, F., S. Janicot, and G. N. Kiladis (2008). The West African monsoon dynamics. Part III: The quasi-biweekly zonal dipole. *Journal of Climate 21*(9), 1911–1928.

Nicholson, S., A. Barcilon, M. Challa, and J. Baum (2007). Wave activity on the tropical easterly jet. *Journal of the atmospheric sciences 64*(7), 2756–2763.

Nicholson, S. E. (2009). On the factors modulating the intensity of the tropical rainbelt over West Africa. *International Journal of Climatology: A Journal of the Royal Meteorological Society 29*(5), 673–689.

Nicholson, S. E. (2013). The West African Sahel: A review of recent studies on the rainfall regime and its interannual variability. *ISRN Meteorology 2013*.

Nithya, K., M. Manoj, and K. Mohankumar (2017). Effect of El Niño/La Niña on tropical easterly jet stream during Asian summer monsoon season. *International Journal of Climatology*.

Preethi, B., T. Sabin, J. Adedoyin, and K. Ashok (2015). Impacts of the ENSO Modoki and other tropical Indo-Pacific climate-drivers on African rainfall. *Scientific reports 5*.

Rao, P. K. (1952). Probable regions of jet streams in the upper air over India. *Current Science 21*(3), 63–64.

Raymond, D., Ž. Fuchs, S. Gjorgjievska, and S. Sessions (2015). Balanced dynamics and convection in the tropical troposphere. *Journal of Advances in Modeling Earth Systems 7*(3), 1093–1116.

Redelsperger, J.-L., A. Diongue, A. Diedhiou, J.-P. Ceron, M. Diop, J.-F. Gueremy, and J.-P. Lafore (2002). Multi-scale description of a Sahelian synoptic weather system representative of the West African monsoon. *Quarterly Journal of the Royal Meteorological Society: A journal of the atmospheric sciences, applied meteorology and physical oceanography 128*(582), 1229–1257.

Rutan, D. A., S. Kato, D. R. Doelling, F. G. Rose, L. T. Nguyen, T. E. Caldwell, and N. G. Loeb (2015). CERES synoptic product: Methodology and validation of surface radiant flux. *Journal of Atmospheric and Oceanic Technology 32*(6), 1121–1143.

Sultan, B., S. Janicot, and A. Diedhiou (2003). The West African monsoon dynamics. Part I: Documentation of intraseasonal variability. *Journal of Climate 16*(21), 3389–3406.

Sylla, M., A. Dell'Aquila, P. Ruti, and F. Giorgi (2010). Simulation of the intraseasonal and the interannual variability of rainfall over West Africa with RegCM3 during the monsoon period. *International Journal of Climatology 30*(12), 1865–1883.

Uccellini, L. W. and D. R. Johnson (1979). The coupling of upper and lower tropospheric jet streaks and implications for the development of severe convective storms. *Monthly Weather Review 107*(6), 682–703.

Van Tuyl, A. H. and J. A. Young (1982). Numerical simulation of nonlinear jet streak adjustment. *Monthly Weather Review 110*(12), 2038–2054.

Wheeler, M. and G. N. Kiladis (1999). Convectively coupled equatorial waves: Analysis of clouds and temperature in the wavenumber–frequency domain. *Journal of the Atmospheric Sciences 56*(3), 374–399.

Yang, G.-Y., B. Hoskins, and J. Slingo (2007). Convectively coupled equatorial waves. Part I: Horizontal and vertical structures. *Journal of the Atmospheric Sciences 64*(10), 3406–3423.

Yang, G.-Y., J. Methven, S. Woolnough, K. Hodges, and B. Hoskins (2018). Linking African Easterly Wave Activity with Equatorial Waves and the Influence of Rossby Waves from the Southern Hemisphere. *Journal of the Atmospheric Sciences 75*(6), 1783–1809.

3

Role of remote versus local diabatic forcing for the interannual to decadal variability of the Tropical Easterly Jet over West Africa

This chapter is currently prepared for submission as a research article in the "Journal of Climate" under the following authorship and title:

Lemburg, A. and Bader, J. (2020). Role of remote versus local diabatic forcing for the interannual to decadal variability of the Tropical Easterly Jet over West Africa

A. L. developed the original ideas for this paper. A. L. adapted the PUMA model for this study, conducted all numerical simulations and performed all analyses. A.L wrote the manuscript with input from J. B.

Abstract:

The upper-tropospheric Tropical Easterly Jet over West Africa (WA-TEJ), an integral part of the West African Monsoon (WAM) circulation, is strongly correlated with Sahel rainfall changes on interannual and decadal time scales. To better understand the covariability between the WA-TEJ and Sahel rainfall, this study investigates whether the variability of the summer mean WA-TEJ intensity is mainly forced by local WAM rainfall changes or whether the WA-TEJ variability is caused by variations in the remote diabatic forcing which in turn might also drive Sahel rainfall variability. For this purpose, PUMA, a simple AGCM based on dry dynamics, is driven with summer mean 3D diabatic heating (Q) fields derived from reanalyses and rainfall observations. The focus is set on simulating the decadal and in particular the interannual variability of the WA-TEJ due to the limited temporal availability of reliable forcing data (satellite era, 1979-2017). To disentangle the effects of remote versus local Q anomalies, the global Q field is geographically split up into an African part (local forcing) and rest of the globe (remote forcing) such that Q in one part can vary from year to year while Q in the other part is set constant to climatological values. The PUMA simulations replicate 66% of the ERA-Interim observed WA-TEJ variability when driven with the full Q variability, meaning that both the local and remote Q vary from year to year. With respect to this total forcing simulation, the remote forcing simulations explain 91% of the simulated variability (58% with respect to ERA-Interim). Anomalies of the remote Q are therefore the dominant driver of WA-TEJ variability, at least in the analyzed period 1979-2017. Local Q anomalies associated with WAM rainfall anomalies only explain a smaller, albeit significant share of 35% of the the WA-TEJ variability on interannual to decadal time scales (33% with respect to ERA-Interim). While the isolated local forcing-induced WA-TEJ anomalies are strongly correlated to Sahel rainfall, they are too weak, though, to be on par with the much stronger anomalies caused by the remote forcing. With the help of idealized experiments in which Q anomalies are restricted to certain regions, ENSO-related Q anomalies in the tropical Pacific are identified as the dominant forcing. La Niña strengthens the WA-TEJ whereas El Niño weakens it by about 20%. Q anomalies associated with Indian monsoon rainfall variability do not significantly affect the WA-TEJ intensity. As an interpretation of our results, we propose that the variability of the diabatic heating over the tropical Pacific is an important driver of today's observed Sahel rainfall – WA-TEJ covariability.

3.1 Introduction

Abundant rainfall in sub-Saharan West Africa occurs only some months per year in connection with the West African Monsoon (WAM) which is the denomination for the marked seasonal wind reversal between summer and winter in this region – first described as early as 1686 by Halley. Nowadays, the term WAM further designates a complex circulation system which can in good approximation be thought of as regional cross-equatorial Hadley-type circulation whose initiation and maintenance mechanisms are however not fully understood yet. The WAM is characterized by multiple pronounced and sustained dynamical features: a westerly monsoon flow in the lower troposphere, the mid-tropospheric African Easterly Jet and the upper-level Tropical Easterly Jet (TEJ). The TEJ was first described by Rao (1952) and Koteswaram (1958) by means of radiosonde measurements over India. This jet originates over the South Asian monsoon system where it is also most pronounced. The TEJ is close to geostrophic

balance most of the time and is therefore associated with an upper-level thermal contrast between relatively cooler deep tropics and the strongly heated subtropics (with a possible enhancing role of the elevated heating over the Tibetan plateau). Although substantially weaker, it is still visible over Western Africa and only begins to decay over the tropical Atlantic.

By analyzing observations and reanalyses or using numerical modelling it was shown that wet years in the Sahel region are often accompanied by a more intense TEJ over West Africa whereas dry years tend to exhibit a weaker TEJ (e.g., Grist and Nicholson, 2001; Sylla et al., 2010). Although the TEJ is often viewed as a mainly passive feature, some researchers proposed the idea that the TEJ might play an active role by its possible control on upper-level divergence. For instance, Nicholson (2009) considered the "link between the TEJ and rainfall to be a causal one with a strong TEJ enhancing rainfall by enhancing upper-level divergence and sustaining a strong Hadley-type overturning over West Africa". Besson and Lemaître (2014) suggested that regional maxima of the TEJ, so called jet streaks, might promote the development of mesoscale convective systems. Motivated by this previous work, Lemburg et al. (2019) conducted an in-depth statistical investigation of the TEJ – Sahel rainfall relationship for synoptic to intraseasonal time scales. They found that TEJ-induced upper-level divergence plays no robust statistical role for convection and suggested that fluctuations of the TEJ on this time scale are mainly a consequence of anomalies in convective activity – and not vice versa.

Besides the role of high-frequent fluctuations, the relevance of the summer mean background state of the TEJ has also been investigated. Yang et al. (2018) showed that the activity of African Easterly Waves (AEW) depends on the background mean flow in the equatorial upper troposphere. A stronger and wider TEJ is associated with favourable equatorial Rossby wave propagation characteristics which promotes AEW activity. Moreover, Bordoni and Schneider (2008) discussed the role of the TEJ (or in more general terms, upper-level easterlies) in modifying the monsoon circulation by shielding the lower-level cross-equatorial monsoonal flow from the effects of extratropical eddies. Therefore, the width and intensity of the summer mean TEJ over West Africa might be an important factor for the WAM circulation and may possibly contribute to the interannual to decadal variability of rainfall over the Sahel. That poses the question: What are the most important forcings that control the interannual to decadal variability of the summer mean TEJ?

Early observational studies by Kobayashi (1974) and Kanamitsu and Krishnamurti (1978) reported a link between monsoonal rainfall over India and the strength of the regional TEJ. With idealized numerical simulations, Rao and Srinivasan (2016) could show for the Indian monsoon system that the latent heat release associated with deep convection is an important factor for determining the location, structure and strength of the TEJ over India and the adjacent ocean. Analogue to the Indian monsoon system, the latent heating associated with the WAM might be an important driver of the West African branch of the TEJ (WA-TEJ). The question arises whether the heat release of the WAM controls most of the WA-TEJ variability or whether changes in the remote latent heating (e.g., Indian monsoon, ENSO) also play an important role. The high correlation between Sahel rainfall and WA-TEJ intensity might suggest that the former is true such

that WAM seasons with excess rainfall might lead to a regionally stronger than normal WA-TEJ. But as there are years with anomalously high Sahel rainfall but an average or slightly weaker than average WA-TEJ (e.g., 1994), increased WAM convection and the associated circulation anomalies alone cannot be the sole reason for a substantially more intense WA-TEJ.

Chen and Yen (1993) found that the interannual variability of the TEJ at least over South Asia is primarily explained by the interannual variability of summer time stationary eddies over the Indian monsoon region. The position and amplitude of those eddies is closely linked to the strength of the planetary-scale divergent circulation which is, in turn, associated with the interannual variation of tropical diabatic heating. This is why the TEJ over India is not only governed by the regional monsoon circulation but is also modulated by remote forcings. Transferred to the WAM region, we therefore assume that the WA-TEJ might also be substantially modulated by remote anomalies of the tropical diabatic heating. The remote tropical diabatic heating, in turn, and particularly its interannual to decadal variability is mainly governed by global-scale SST anomalies which play a key role in modulating the planetary-scale distribution of tropical rainfall. The dominant mode of interannual SST variability is ENSO. Multiple studies have highlighted the impact of ENSO on the Indian branch of the TEJ (Abish et al., 2013; Chen and van Loon, 1987; Nithya et al., 2017) – with La Niña tending to increase and widen the TEJ and El Niño to weaken and narrow the TEJ. A possible role of ENSO in modulating the intensity of the TEJ over Africa was also discussed by Preethi et al. (2015). However, their analysis could not shed light on whether the changes in WA-TEJ intensity are directly induced by ENSO or whether they are caused indirectly by changes in regional rainfall.

In contrast to a possible impact on the TEJ, much more studies have investigated how large-scale SST anomalies in various basins affect WAM rainfall on interannual and decadal time scales (Folland et al., 1986; Janicot et al., 1996; Giannini et al., 2003; Bader and Latif, 2003). Some regional-scale SST anomalies which are known to substantially increase Sahel rainfall, for instance a warming of the eastern Mediterranean Sea (Park et al., 2016), are in our opinion unlikely to affect the planetary-scale tropical circulation. However, large-scale tropical SST anomalies as the aforementioned ENSO might do so – and might thereby represent a common forcing governing both, WAM rainfall and the intensity of the WA-TEJ. As an example, one could consider the following scenario: A marked La Niña-like SST anomaly leads to increased Sahel rainfall via a teleconnection mechanism. Concurrently, the summer mean WA-TEJ is also stronger than normal. In this case, the intensified WA-TEJ might not be a mere consequence of intensified WAM circulation but might also be subject to remotely-induced planetary-scale changes in the upper-level circulation which project onto the WA-TEJ. Formulated as a more general question one might ask: How much of the interannual to decadal WA-TEJ variability is explained by remote forcing (planetary-scale circulation changes induced by anomalous tropical diabatic heating) in comparison to the local forcing (due to WAM convection)? In this paper, we will put an emphasis on addressing this particular question. Answering it will help to better understand the reasons for the observed high correlation between the WA-TEJ intensity and Sahel rainfall. By means of multiple semi-realistic sensitivity experiments, we will further try to identify

the regions of the globe in which the observed variability of diabatic heating is key for modulating the WA-TEJ. The paper is organized as follows:

In the first part, we use observational and reanalysis data to quantify the decadal and in particular the interannual variability of the WA-TEJ and its covariability with WAM rainfall and SST anomalies. For this, we employ linear regression and correlation analysis to map the linear relationships between an WA-TEJ intensity index and global rainfall as well as SST anomalies. In a second part, we employ an AGCM based on dry dynamics which will be driven with diabatic heating fields derived from reanalyses and measurements. We conduct simulations in which we either just vary the local or the remote diabatic forcing. This allows us to quantify how much of the interannual to decadal TEJ variability is the consequence of planetary-scale circulation changes induced by remote diabatic heating changes and how much is caused directly by changes in the local monsoon circulation. We will further conduct some more idealized simulations in which we diagnose how strongly the WA-TEJ is affected by changes of diabatic heating in certain regions of the globe.

3.2 Data and Methods

3.2.1 Analysis of observed TEJ variability – Data sets

We primarily use the ERA-Interim reanalysis (Dee et al., 2011) to characterize the summer mean intensity of the TEJ over West Africa. For a brief comparison, we also include the reanalysis data of NCEP-NCAR1 (Kalnay et al., 1996) and ERA-40 (Uppala et al., 2005) which have the advantage of covering the wet period of the WAM in the 1950s and 1960s (albeit limited by increased uncertainty). We further utilise the GPCP monthly global precipitation data set (Adler et al., 2003) to investigate the relationship between the WA-TEJ and global rainfall. The dependence of WAM rainfall and the WA-TEJ on global SST anomalies is explored with the help of the monthly SST data set from ERSSTv5 (Huang et al., 2017).

3.2.2 Analysis of observed TEJ variability – Statistical methods

Because the core of the WA-TEJ shifts latitudinally within the season, simply calculating the spatial average of the seasonally-averaged 200 hPa zonal wind over a certain area in West Africa would likely not be an accurate representation of the JJAS mean WA-TEJ intensity. We therefore employ a more sophisticated method to characterise the summer mean intensity, latitude and width of the WA-TEJ: we use daily-averaged reanalysis data of easterly 200 hPa zonal wind and search for the maximum easterly wind speed at each longitudinal strip over the whole of West Africa (from 15°S to 30°N). Then we zonally average the found maxima over 15°W to 15°E. Afterwards, the zonally-averaged jet core speed, latitude and width are temporally averaged over the monsoon season which we define as comprising of June, July, August and September (JJAS). In addition to the WA-TEJ intensity, its width or in our case more generally the width of the upper-level easterlies are also of interest. Using again daily averages of the 200 hPa zonal wind speed, we determine for each longitudinal strip the latitudinal span over which winds are easterly. Then, we take again the zonal mean between 15°W to 15°E and average

over the monsoon season afterwards.

Global JJAS mean precipitation and SST anomalies are regressed onto the JJAS mean WA-TEJ intensity thus obtained. This regression analysis is performed for two time scales. The interannual time scale is defined as the 8-year highpass-filtered signal, whereas the decadal to multi-decadal time scale is the 10-year lowpass-filtered time series. For comparison to the relationships with regard to WA-TEJ intensity, we further produce correlation maps between SST anomalies and area-averaged Sahel rainfall anomalies (averaged over 10°W to 10°E and 10°N to 20°N). Statistical significance of the linear relationships is tested by means of a student t-test that takes into account the reduction in the degrees of freedom due to autocorrelation as in Zwiers and Von Storch (1995).

3.2.3 PUMA: model description, setup & study-specific adaptations

A number of numerical experiments are conducted with the Portable University Model of the Atmosphere (PUMA), a spectral atmospheric circulation model consisting of a dynamical core based on the Primitive Equations with simple parametrizations for friction and diabatic heating (Fraedrich et al., 1998). In the classic case, a model with dry dynamics is only forced by the permanent nudging towards a zonally-uniform relaxation temperature field with a specific time constant τ. For this study, we include a 3D diabatic heating field as additional forcing and further make a few adaptions which are briefly outlined in this section and described in detail in the appendix.

For all simulations within this study, the PUMA model is run with 31 vertical levels in a T63 resolution which translates to a resolution of 1.85° (≈200 km). The vertical coordinate is a terrain-following sigma coordinate with equally-spaced sigma levels from 0.984 to the model top at 0.016. All simulations are run with the inclusion of realistic orography. For the purpose of this study – to realistically simulate the effect of tropical diabatic heating anomalies on the WA-TEJ – the original simple Newtonian cooling scheme is extended by an additional time-constant but spatially and vertically varying diabatic heating rate Q (unit: K/s):

$$\frac{\Delta T}{\Delta t} = -\frac{T - T_{eq}}{\tau} + Q$$

In this formula, which represents a simplified discrete difference with a time step of $\Delta\, t$, T denotes the actual temperature whereas T_{eq} denotes a fictive temperature towards which the actual temperature is relaxed with the time constant τ. Even though we drive the model with realistic 3D fields of diabatic heating, we cannot do without Newtonian cooling. A nudging towards a baroclinically unstable zonally-uniform relaxation temperature profile T_{eq} is necessary to enforce a realistic global circulation (including realistic extratropical jets and baroclinic eddies). With the diabatic forcing Q alone, the model would also not be able to run into an equilibrium state because the diagnosed JJAS mean diabatic heating would slowly lead to an unrealistic drift in global temperature and latitudinal temperature gradient. To obtain a relaxation temperature profile that works well in combination with the imposed diabatic heating, we conduct an iterative tuning of T_{eq}. The final zonally-uniform T_{eq} profile is depicted in figure 3.1. In-depth information on the tuning process is given at the beginning of section

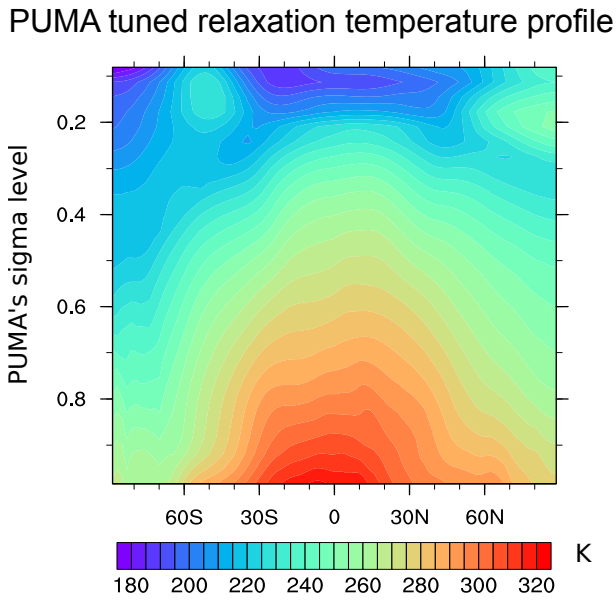

Figure 3.1: Latitude – height cross section of the zonally-symmetric relaxation temperature used for all PUMA simulations. The relaxation temperature field is the result of a multiple-step iteration process that started from a classic Held-Suarez temperature profile.

3.A.1 in the appendix. τ is assigned a globally-uniform value of 30 days for the whole troposphere.

To adequately represent the tropical circulation, the effect of convective momentum transport (CMT) has to be considered. On larger scales, CMT generally acts as a kind of vertical diffusion (Gregory et al., 1997; Lin et al., 2008). We therefore rewrite the original simple vertical diffusion scheme in order to calculate the diffusion in grid point space. This allows the use of a 3-d varying parameter of diffusion of momentum K_m. To mimic CMT, we introduce a convective diffusion parameter K_c which is approximated as a simple function of rainfall and multiple fixed parameters (based on a parametrization used in GFDL; Anderson et al., 2004). The resulting year-to-year varying 3D field of K_c is added on top of a climatological 3D background diffusivity field K_t that mainly represents the turbulent exchange of momentum within the boundary layer. Figure 3.A1 (in the appendix) shows an overview of the final tuned version of K_m in form of a zonal-mean vertical cross section and two maps showing K_m near the surface and in the mid troposphere. All in all, the inclusion of this simple vertical diffusion scheme generally increases our model's capability to realistically reproduce the tropical circulation as it dampens the otherwise too high speeds of the TEJ, improves the TEJ core latitude and eliminates unrealistic westerlies in the tropical middle troposphere. The main findings of our study do not depend on whether this vertical diffusion scheme is turned on or off. Minor effects on some of the results will be discussed later.

As a last modulation of the default PUMA model, we extend the formulation of the simple, globally-uniform Rayleigh friction scheme to include a land-sea mask. This modulation allows for realistic differential friction between land and ocean which rectifies the otherwise too weak trade winds over oceans and the too strong monsoon flow over land.

3.2.4 PUMA input data sets

We use the ERA-Interim reanalysis (Dee et al., 2011) to derive the JJAS climatological mean diabatic heating for our simulations. The diabatic heating rates can be retrieved via two methods. At first, we considered the diabatic heating to be equivalent to the so-called apparent heating Q_1. Using 6-hourly three-dimensional temperature data, on pressure levels, we calculated Q_1 as a residual of the temperature tendency equation

$$Q_1 = c_\mathrm{p}\left[\frac{\partial T}{\partial t} + v\cdot\nabla T + \omega\frac{\partial \Theta}{\partial p}\left(\frac{p}{p_0}\right)^\kappa\right]$$

where T is the temperature, v denotes the horizontal wind vector and ω denotes the vertical component of the wind in pressure coordinates. p stands for the pressure whereas p_0 stands for the reference pressure of 1000 hPa. c_p is the specific heat at constant pressure and κ designates the isentropic exponent.

As a second method, diabatic heating rates are retrieved directly from the model output, if available. In the case of ERA-Interim, we consider the variable *ttpha*, which is the temperature tendency due to model physics, to be equivalent to the diabatic heating. This is confirmed by a comparison against the calculated Q_1 to which only little differences exist. Because we face less interpolation errors and nearly no computational expense, we use the direct model output as diabatic heating in the case of ERA-Interim. The diabatic heating fields, whether they are explicitly provided in the output data or calculated from 6-hourly data as residual of the temperature tendency equation, show distinct differences among the available reanalyses. Not only do spatial distributions differ but also the vertical structure displays very different characteristics. Therefore, we set up multiple test simulations forced by the respective diabatic heating rates from multiple reanalysis data sets – either diagnosed from temperature increments or directly taken from model output. We find that simulations driven with ERA-Interim diabatic heating provide by far the most realistic results.

A striking problem of all used reanalysis data sets is the substantial misrepresentation of rainfall variability over West Africa, in particular on (multi-)decadal but also on interannual time scales. Unfortunately, this problem is also apparent in our preferred data set ERA-Interim. Therefore, a realistic local diabatic forcing over West Africa is not available through reanalyses. We circumvent this major problem by estimating the respective JJAS diabatic heating rate anomalies from measured rainfall. With the help of TRMM rainfall and latent heating data (TRMM, 2006), we find the best-fitting vertical latent heating profile for each specific location in the tropics via linear regression. Afterwards, the resulting 3D latent heating field is vertically integrated for each grid point. By multiplication with the latent heat of condensation we convert the vertically integrated field back to a precipitation anomaly. For each grid point, the vertical profile of LH is then scaled with a grid point specific factor such that the precipitation anomaly matches the actual GPCP precipitation anomaly. In a last step, the heating anomalies thus obtained are upscaled by 10% which proved to generate more realistic results. We then use the scaled 3D latent heating anomalies and add them to the climatological ERA-Interim-derived 3D diabatic heating data set. The climatological diabatic forcing at a level typical for maximal latent heating (PUMA sigma level 0.468) is shown in form as a global map plot at the top of figure 3.A2. The bottom of figure 3.A2 features multi-

ple time series of spatially averaged diabatic heating in selected tropical regions of the globe. Here, the thin, dashed lines show the original ERA-Interim output whereas the thicker, solid lines depict the GPCP-derived variability of the diabatic heating.

3.2.5 Model experiments

In the main experiment suite, we attempt to realistically model the interannual to decadal variability of the WA-TEJ over the last four decades. To robustly unravel the effects of local and remote diabatic forcing, we aim to isolate the steady-state response to any given heating, or in other words, to maximize the signal-to-noise ratio. We therefore do not conduct transient simulations but simulate the year-to-year WA-TEJ variability in individual time slice experiments. For each individual monsoon season from 1979-2017, we run the PUMA model to a quasi-equilibrium, forced by the time-constant respective JJAS mean diabatic heating. Each run is integrated for 11 simulated years during which a quasi-equilibrium state is generally reached after some 150 - 200 days. Therefore, we consider the first year as model spin-up and only calculate averages over the last 10 integration years.

To disentangle the effects of the local diabatic heating (the latent heating due to WAM rainfall) from the effects of remote diabatic forcing, we geographically split the global diabatic heating field into a local African and an remote (rest of world except African monsoon region) part. The local African region is described by a box spanning longitudinally from 15°W to 52°E and latitudinally from 10°S to 25°N. Therefore, the rainfall (and diabatic forcing) variability in association with the WAM and slightly beyond will be within this box. Everything that lays outside this box is considered to belong to the remote forcing. The results are quite sensitive to the exact choice of the box width with regard to its westward border, as then parts of the Atlantic ITCZ (and quite strong associated forcing variability) are somewhat more or less included. We will discuss the implications of this choice later in the results section.

In our so-called remote forcing simulations (PUMA-RF), the remote forcing patterns are let to vary from year to year while the local forcing over the West African monsoon region is held constant at climatological values. Local forcing simulations (PUMA-LF) are set up vice versa, such that the remote forcing is held constant and only the WAM-related diabatic heating over Africa changes from year to year. To avoid any sharp gradients, some smoothing is applied at the edges between the African and remote part. An exemplary depiction of the diabatic heating fields arising from this method is given in figure 3.2.

In a second set of experiments we test the influence of heating anomalies in different regions of the globe in a more idealized way. The aim of these experiments is to identify the regions of the globe which diabatic heating variability is key for modulating the WA-TEJ. These experiments further allow to disentangle the relative importance of the numerous heating anomalies which co-occur in a lot of regions in conjunction with the dominant planetary-scale forcing, namely ENSO. For this, we set up a number of sensitivity experiments in which we impose semi-realistic heating anomalies in certain "hot spot" regions on top of the ERA-Interim climatology. Semi-realistic means that we use realistic rainfall anomaly patterns which resemble the observed variability in terms of amplitude and spatial distribution. Therefore we are able to distinguish between La

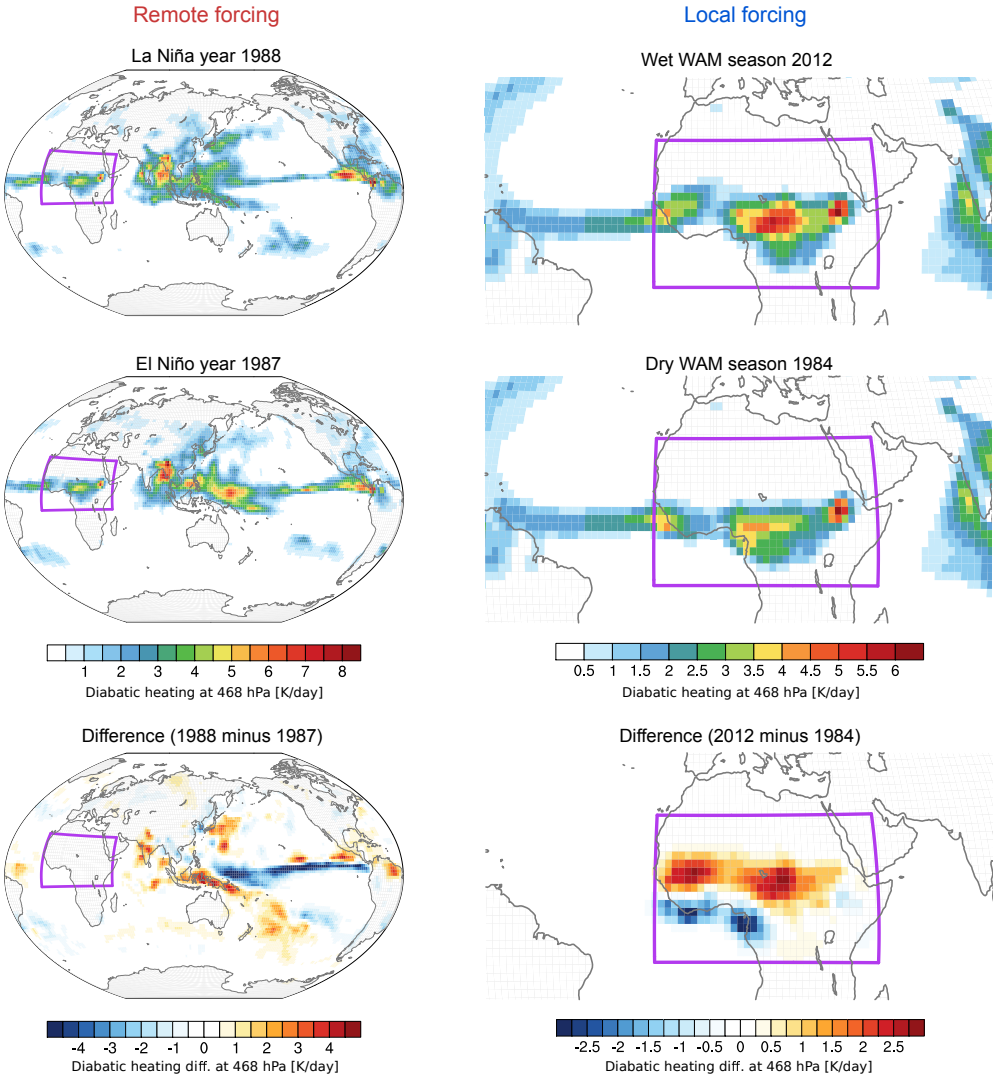

Figure 3.2: Illustration of the geographical split-up of diabatic heating fields into remote and local forcing experiments. The climatological diabatic heating field is based on ERA-Interim climatology whereas the year-to-year variability is derived from observed GPCP rainfall. The right column shows two exemplary years for the local forcing experiment in which the variability of the diabatic heating is restricted to parts of Africa (heating kept constant at climatological values outside of the magenta box). The left column depicts the remote forcing experiment for which the diabatic forcing is held at climatological values over parts of Africa (inside the magenta box) whereas it retains its year-to-year variability over the rest of the globe.

Niña and El Niño, for example, and do not implement unrealistically negative heating rates by imposing too strong of a negative anomaly. However, for the sake of simplicity, we always assume the same idealized heating profile and neglect any modulations of the total diabatic heating profile via concurrent changes in radiative heating/cooling.

The semi-realistic heating anomalies are technically implemented by first performing a regional EOF analysis on 8-year highpass-filtered observed rainfall (GPCP) in the region of interest (e.g., Maritime Continent or tropical Pacific). The principal component time series of the dominant and in some cases the second most important mode are then used to construct an anomaly composite which represents a typical positive (all years in which the EOF anomaly is greater than one standard deviation) or negative

event (all years in which the EOF anomaly is lower than one negative standard deviation). In a next step, the obtained anomaly patterns are simplified by removing weaker anomalies far outside of the focus region. To achieve this, we subjectively constrain the anomalies to one or multiple ellipses with a certain lon/lat pair as centre and a certain longitudinal/latitudinal span as semi-major/semi-minor axis. Finally, the rainfall anomaly pattern is translated into a latent heating anomaly by assigning an idealized profile typical for deep convection: In the vertical, the anomaly is characterized by a idealized profile typical for deep convection:

$$Q = C \cdot \sin\left(\frac{p - 100\,\mathrm{hPa}}{p_{\mathrm{surf}} - 100\,\mathrm{hPa}} \cdot \pi\right) \cdot \exp\left(-1 \cdot \frac{p - 100\,\mathrm{hPa}}{p_{\mathrm{surf}} - 100\,\mathrm{hPa}}\right)$$

The parameter C (=1.5687..) is used to normalize this function such that the maximum heating at a pressure level near 500 hPa becomes 1 K/d. Where the function returns negative values (above a pressure level of 100 hPa), the diabatic heating is set to zero. The representation of Q on pressure levels as described by the formula above is then transferred to the sigma levels of PUMA, taking into account the model orography. To avoid a large net heating of the tropical atmosphere for more monopole-like heating cases, we always compensate the global mean net heating by imposing a spatially-uniform cooling over the (sub-)tropical regions from 30°S to 30°N (which then linearly declines until 40°S/N). The selected regions and the ellipse parameters are presented in table 3.A2. Depending on their relevance, some anomalous diabatic heating fields might further be depicted in form of lat-lon plots alongside the results.

3.3 Statistical analysis of WA-TEJ variability

3.3.1 Time series of WA-TEJ – Sahel rainfall relationship

Figure 3.3 shows the statistical relationship between observed JJAS mean Sahel rainfall and reanalysis-derived JJAS mean WA-TEJ intensity over the last six decades. Each individual plot shows the same rainfall data set (CRU TS3.22, see blue lines), but different values for the WA-TEJ intensity (red lines) as derived from three different reanalysis data sets: the preferred reanalysis ERA-Interim and two additional reanalyses (NCAR-NCEP1, ERA-40) which have the advantage to span both, the wet phase of the WAM in the 1950s and 1960s and the dry period in the 1970s and 1980s.

Summer mean WA-TEJ intensity and Sahel rainfall are closely linked on interannual and decadal time scales. Especially after 1978, with the beginning of the satellite era, all depicted reanalyses generally agree well with each other regarding the summer mean WA-TEJ intensity and its correlation with Sahel rainfall (r=0.67-0.73). Statistical tests with a bootstrapping method underline the robustness of the positive linear relationship between rainfall and WA-TEJ intensity (see table 3.A1 in the appendix).

For the time before 1978, however, some remarkable differences are found between NCAR-NCEP1 and ERA-40. The longest available data set, NCAR-NCEP1, displays a very strong WA-TEJ – Sahel rainfall relationship over the complete covered period 1948-2013, especially on (multi-)decadal time scales (r=0.88 for the 8-year lowpass-filtered time series). For instance, the decline in summer mean TEJ intensity beginning in the

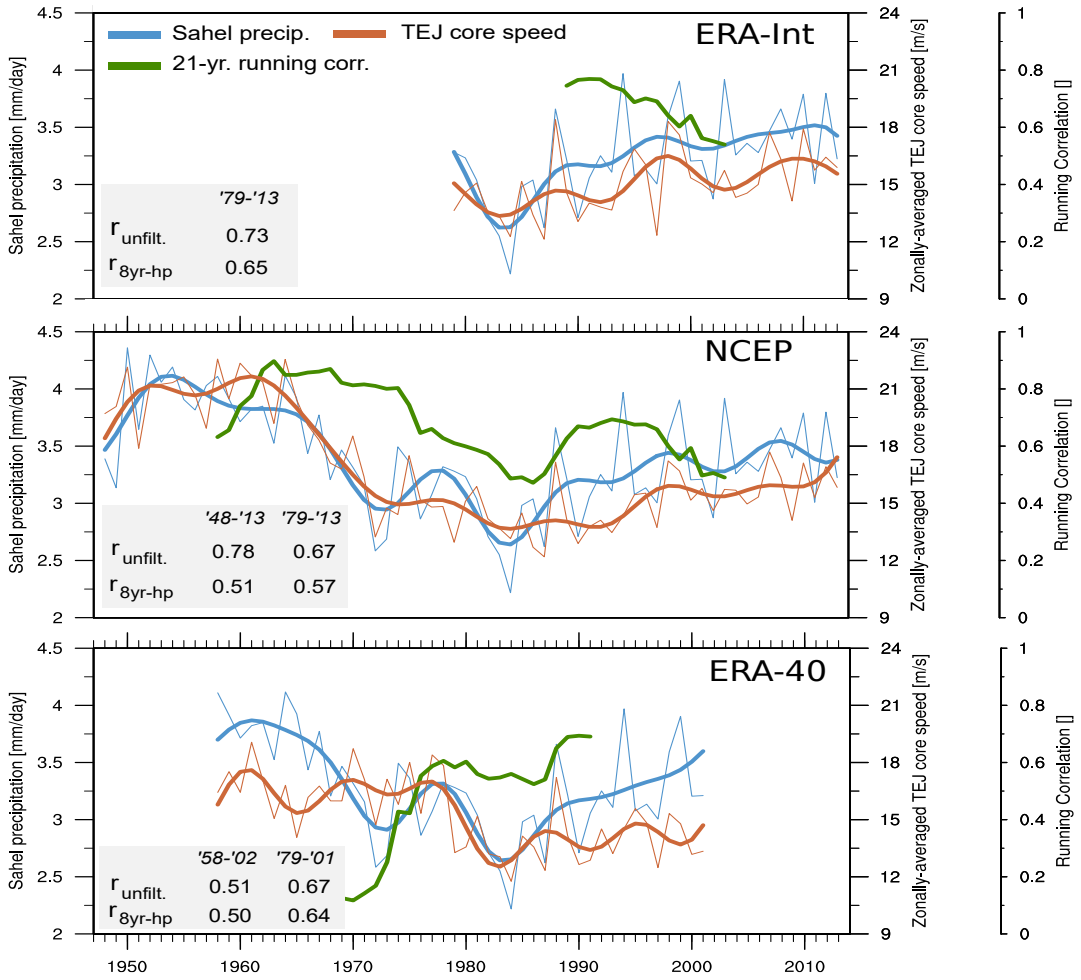

Figure 3.3: Time series from 1948 - 2013 of JJAS mean Sahel precipitation (from CRU TS3.22 data spatially averaged over 10°W to 10°E and 10°N to 20°N) and JJAS mean 200 hPa WA-TEJ intensity derived from three different reanalyses (for a representative WA-TEJ intensity measure that is insensitive to latitude changes, the average JJAS WA-TEJ core speed was calculated from daily ERA-Interim/NCEP-NCAR1/ERA-40 reanalysis fields of 200 hPa zonal wind data as follows: Within a domain between 15°W to 15°E and 5°S to 25°N, the daily maximum of easterly 200 hPa zonal wind speed is found for each longitudinal strip of grid points. The found maximum speeds of each longitude are then averaged over the whole domain to obtain an average speed of the TEJ core). Thin, light lines depict the unfiltered yearly means. Thick lines show the 10-year low pass filtered time series. The green line depicts the 21-year running correlation. The 95% confidence intervals of the depicted correlation coefficients as well as additional correlations coefficients are provided in table 3.A1 in the appendix.

early 1960s is perfectly in line with the observed drop in precipitation. The same is true for the recovery period after the dry period of the 1980s. In stark contrast to NCAR-NCEP1, ERA-40 shows a much lower correlation on (multi-)decadal time scales and opposing trends in rainfall and TEJ intensity around the end of the wet period (late 1960s). The contrasting behaviour between these reanalyses becomes further evident when comparing the running 21-year correlations (green lines). In general, the running correlations between the local TEJ intensity over West Africa and rainfall in the Sahel show a decadal to (multi-)decadal variability in both ERA-40 and NCAR-NCEP1. NCAR-NCEP1 shows particularly high correlations in the wet period of the WAM of the 1950s whereas ERA-40 displays nearly no significant correlation in this period. This

is an indicator that caution should be applied when interpreting the reanalysis-derived WA-TEJ intensity before 1979. Before the satellite era, the WA-TEJ intensity is not sufficiently constrained because of the scarceness of upper troposphere measurements (Stickler and Brönnimann, 2011). Therefore the WA-TEJ intensity could be much more strongly coupled to the modelled rainfall which is also rather poorly constrained and strongly dependent on model physics.

On the interannual time scale, the discrepancy between the different reanalyses vanishes, in particular since the begin of the satellite period. From 1979-2013 (1979-2001 in case of ERA-40), the correlations on interannual time scales range from 0.57 to 0.65 among the selected reanalyses, with ERA-Interim exhibiting the highest value. Interestingly, the interannual correlation strength does not stay constant when all years with strong ENSO are removed from the time series. Averaged over all three reanalysis (averaging with the method of Olkin et al., 1958), the interannual correlation drops from 0.63 to 0.40. Due to the rather low sample size, the robustness of this decline in correlation strength is questionable, however.

3.3.2 WA-TEJ variability: Relation to global rainfall and SST anomalies

In this section we investigate how the variability of WA-TEJ intensity is connected to tropical rainfall anomalies – either in a local or remote sense. To better understand the drivers of the WA-TEJ, we further explore the statistical linear relationship between WA-TEJ intensity and SST anomalies and compare it with the one obtained between Sahel rainfall and SSTs. For these analyses, we concentrate exclusively on the interannual time scale as no statistically robust results can be obtained for the decadal to multi-decadal time scale. The reason for this is the very low number of effective degrees of freedom due to the high autocorrelation and the too short sampling period (1979-2016).

Figure 3.4 depicts the linear relationship between the summer mean TEJ intensity (as derived from ERA-Interim) over West Africa and global rainfall (GPCP) in form of point-wise correlation and point-wise linear regression plots. The interannual variability of the WA-TEJ over the last 38 years (1979-2016) is strongly connected to globe-spanning tropical rainfall anomalies which strongly resemble the typical anomaly patterns associated with ENSO (Fig. 3.4a,b). A stronger TEJ over West Africa goes along with substantially lowered precipitation over the central and eastern Pacific and increased rainfall over large parts of the Maritime Continent and parts of India. The WA-TEJ variability is, however, not only linked to changes in rather remote regions. An equally strong correlation also exists to WAM rainfall, particularly in the Sahel region. Since ENSO appears to be a dominant signal, the regression analysis was carried out again for years without strong ENSO events (Fig. 3.4c,d). Interestingly, the large-scale correlation patterns do not substantially change. WA-TEJ anomalies are still strongly linked to rainfall anomalies in most of the aforementioned key regions with the exception of the West Indian coast.

From the correlation and linear regression analysis alone, it cannot be decided which are the regions in which rainfall anomalies are the main drivers of WA-TEJ changes and which are the regions where changes simply co-occur but play no important role. However, some more insight into the main drivers of WA-TEJ variability can be gained from the analysis of the respective relationships to observed global SST. We now plot point-

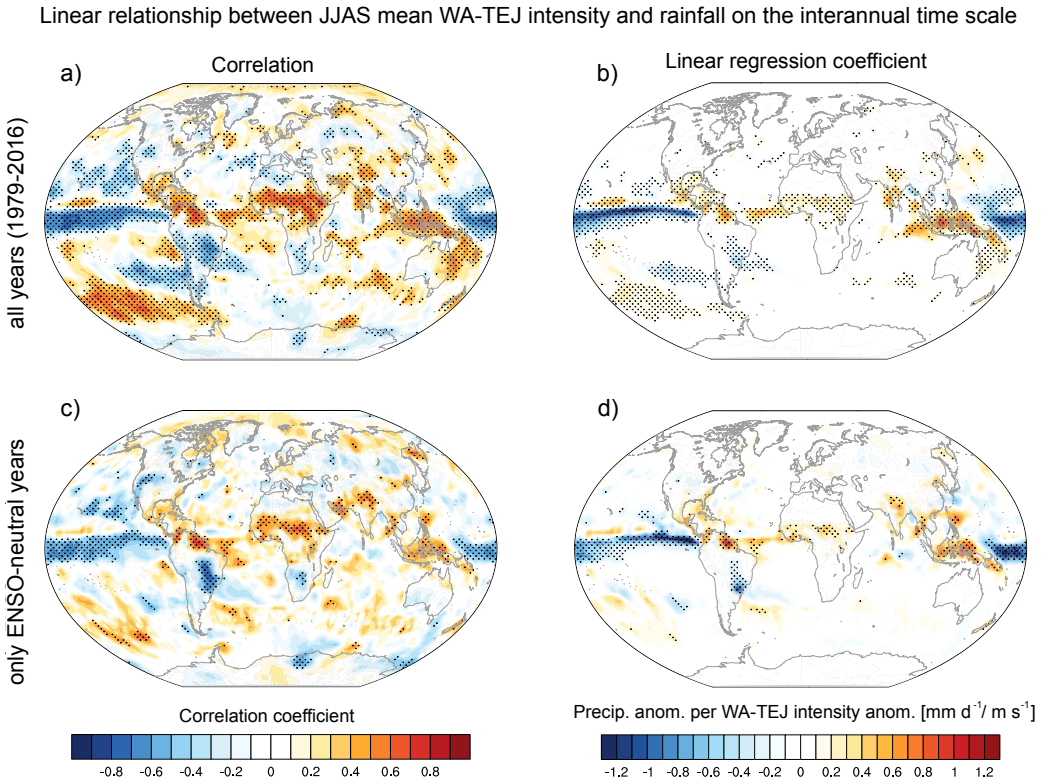

Figure 3.4: Linear point-wise relationship between the WA-TEJ intensity and global observed precipitation. The left column depicts the Pearson correlation coefficient between 8-year high-pass filtered values of the WA-TEJ intensity index (derived from ERA-Interim) and global observed precipitation (GPCP). The WA-TEJ intensity is derived from ERA-Interim via the method explained in the Methods section. The right column depicts the linear regression coefficient determined via least-squares method. For the top row, all years from 1979-2016 are used to calculate the correlations/regression coefficients. In the bottom row, years with strong ENSO events are omitted from the analysis (1982, 1986, 1987, 1988, 1991, 1997, 1998, 1999, 2000, 2003, 2007, 2008, 2010, 2011, 2012 and 2015 are left out).

wise correlations coefficients between the WA-TEJ intensity and SST anomalies all over the globe – again for all years and only for years without strong ENSO signal (Fig. 3.5a,c). The same statistical analysis is also conducted for a Sahel rainfall index (spatial average from 15°W to 15°E and 10°N to 20°N) to check whether differences exist in the drivers of Sahel rainfall and WA-TEJ variability (Fig. 3.5b,d). Comparing the left column with the right column of the upper row in figure 3.5, a marked difference immediately jumps to the eye: The interannual variability of the WA-TEJ is much stronger correlated with tropical SST anomalies whereas Sahel rainfall is in comparison more correlated with extratropical SST anomalies, in particular those in the eastern Mediterranean Sea. Even more clear differences exist in years without strong ENSO signal: In such years, Sahel rainfall is almost exclusively significantly linked to extratropical SST anomalies. However, the intensity of the WA-TEJ is still substantially correlated with tropical SST anomalies, in particular to those in the eastern Pacific region.

The highlighted differences might imply that the interannual WA-TEJ variability is only weakly influenced by changes in WAM rainfall. The fact that considerable correlations exist even on this time scale can probably be attributed to the simultaneous effect of a third variable, namely remote SST anomalies in the tropics. In years, in which

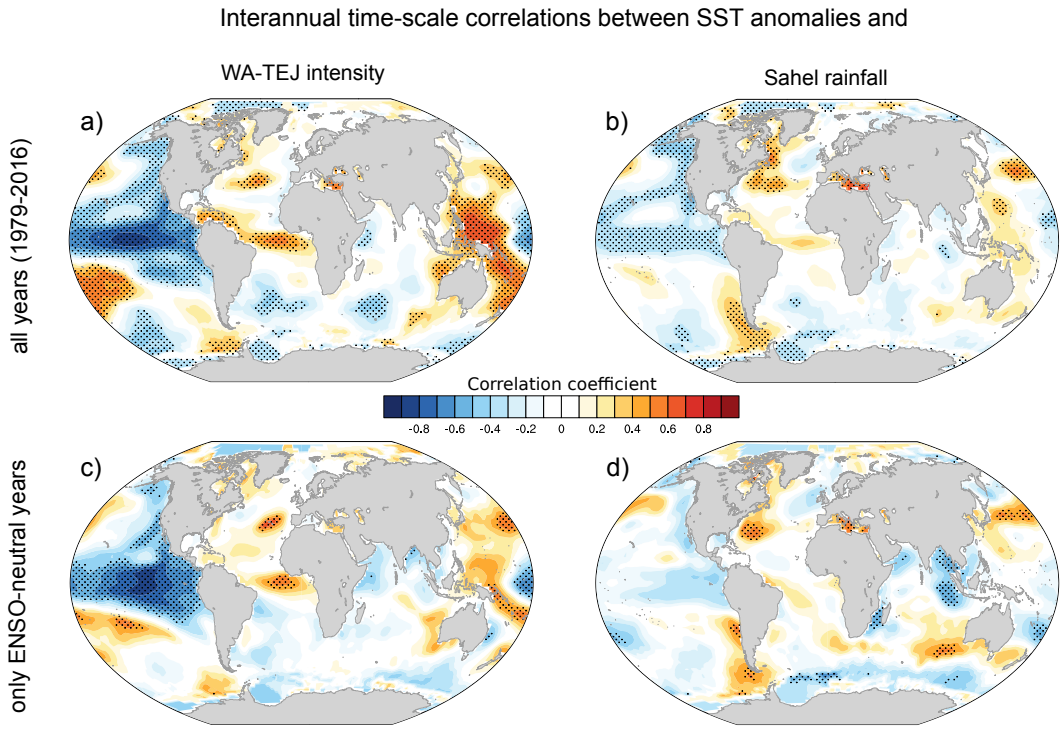

Figure 3.5: Linear point-wise correlations between observed SST anomalies and WA-TEJ intensity (left column) and Sahel rainfall (right column). The WA-TEJ intensity is derived from ERA-Interim via the method explained in the Methods section. Sahel rainfall is represented by a field mean in a box over 15°W to 15°E and 10°N to 20°N). For the top row, all years from 1979-2016 are used to calculate the correlations/regression coefficients. In the bottom row, years with strong ENSO events are omitted from the analysis (1982, 1986, 1987, 1988, 1991, 1997, 1998, 1999, 2000, 2003, 2007, 2008, 2010, 2011, 2012 and 2015 are left out).

a strong remote tropical forcing exists (in particular years with El Niño or La Niña conditions), this forcing may impact both, WAM rainfall and the WA-TEJ intensity simultaneously. This hypothesis will be tested by the numerical experiments that follow in the second part of this paper.

3.4 WA-TEJ variability simulated in PUMA

3.4.1 Model performance

Figure 3.6 reviews the model's capacity to accurately capture the large-scale features of the upper-level global circulation with an emphasis on the tropical divergent circulation represented by the 200 hPa velocity potential (right column of Fig. 3.6, in colours). Compared to the ERA-Interim climatology, PUMA performs reasonably well at representing most of the large-scale features of the global circulation, including both the position and intensity of the mid-latitude jets (left column of Fig. 3.6, contours) and the spatial extent and strength of the upper-level easterlies in the tropics (right column, streamlines). Some differences are found for the position and strength of the Tibetan anticyclone. The tropical divergent circulation is well captured in its spatial features but is about 10% too intense.

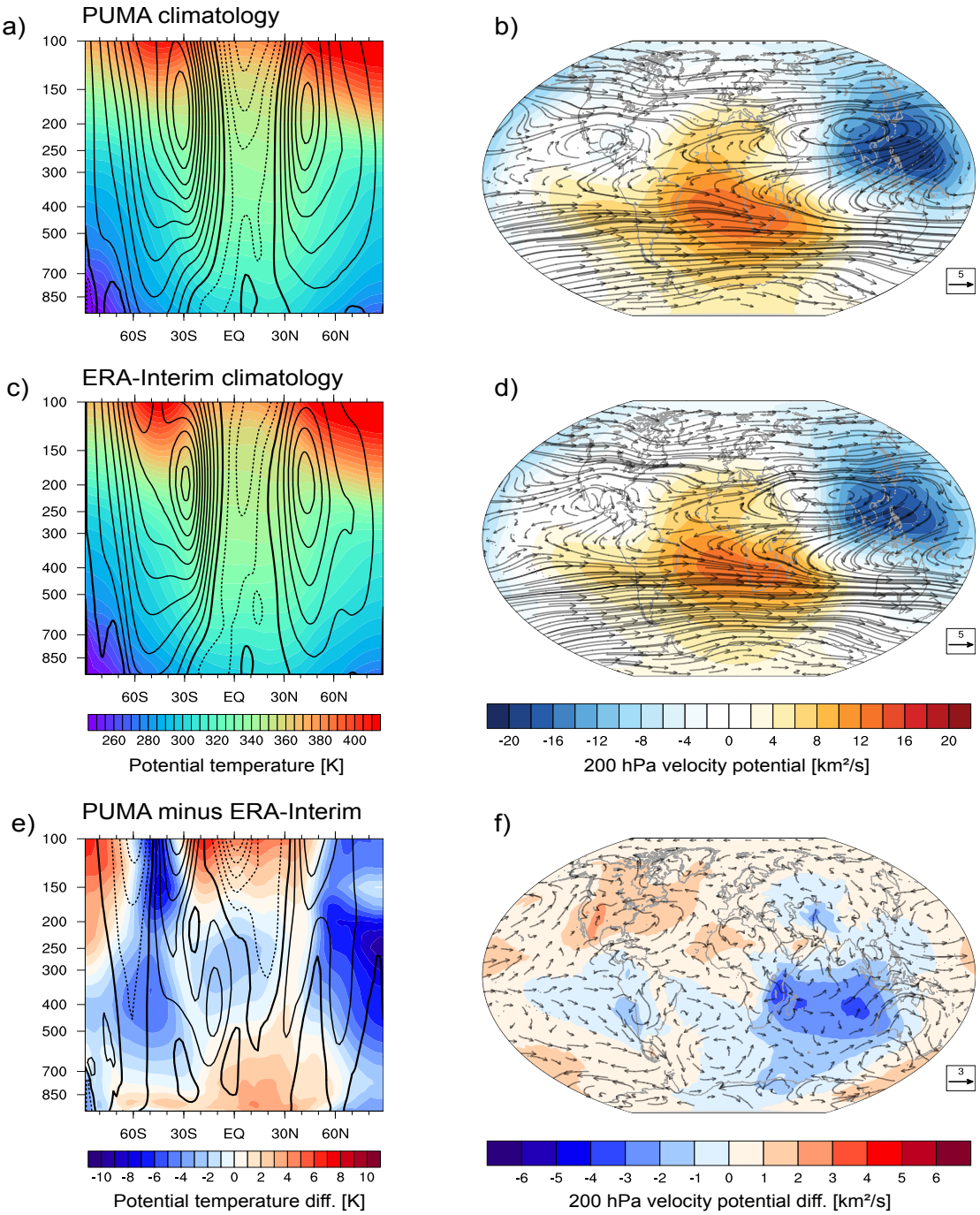

Figure 3.6: Comparison of the main climatological features of the global circulation in PUMA simulations against ERA-Interim climatology. The left column shows a latitude – height cross section of zonal winds (contours from -48 to 48 m s^{-1} with an interval of 4 m s^{-1}, westerlies as solid lines) and potential temperature (shadings). The right column depicts the circulation at 200 hPa in form of streamlines. The planetary-scale centres of upper-level convergence and divergence, which characterize the tropical overturning circulation, are shown with the help of the velocity potential (shadings).

The PUMA simulations also perform reasonably well at reproducing the main dynamical features of the local monsoon circulation over West Africa. The comparison against ERA-Interim in form of a latitude - pressure level cross section shows that our simulations capture the depth and northward extent of the near-surface western mon-

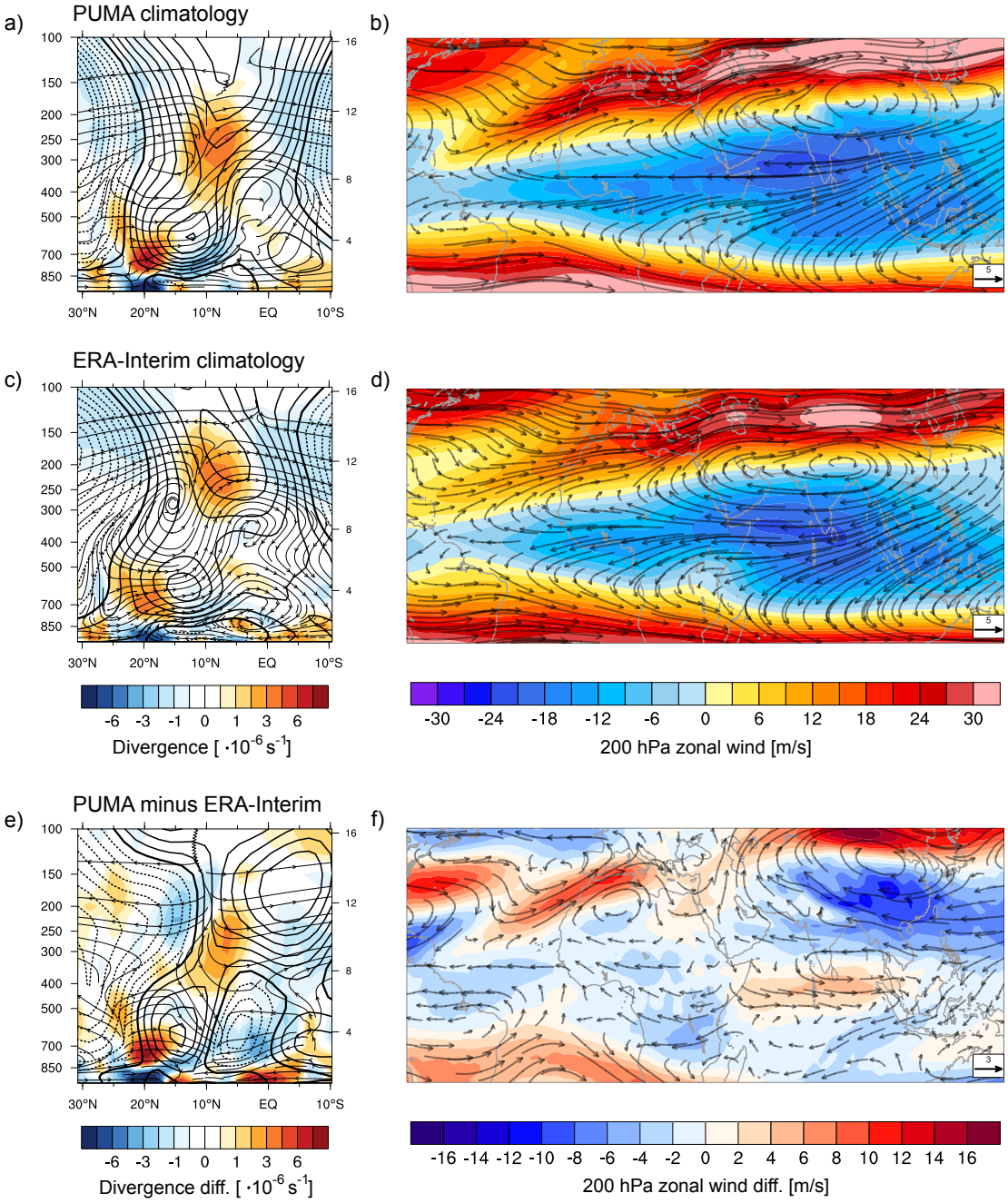

Figure 3.7: Comparison of the climatological WAM circulation and the TEJ spatial structure and intensity between PUMA simulations and the ERA-Interim climatology. The left column depicts a regional latitude – height cross section for West Africa with zonal mean values averaged over 15°W to 15°E. Shown is the divergence in shadings, the zonal wind in contours (interval 2 m s^{-1}, easterlies as solid lines) and the meridional-vertical circulation is depicted with streamlines (vertical velocity is multiplied by 100 to make the overturning circulation visible). The right column depicts the zonal wind speed at 200 hPa in shadings and the total circulation with streamlines.

soon flow well (Fig. 3.7, left column). The position of the near surface ITCZ at around 20°N is accurately simulated as well as the latitudinal position of the main branch of deep ascent between around 8°N and 12°N. The AEJ is well-represented as a distinct circulation feature close to the observed latitudinal position, although slightly too in-

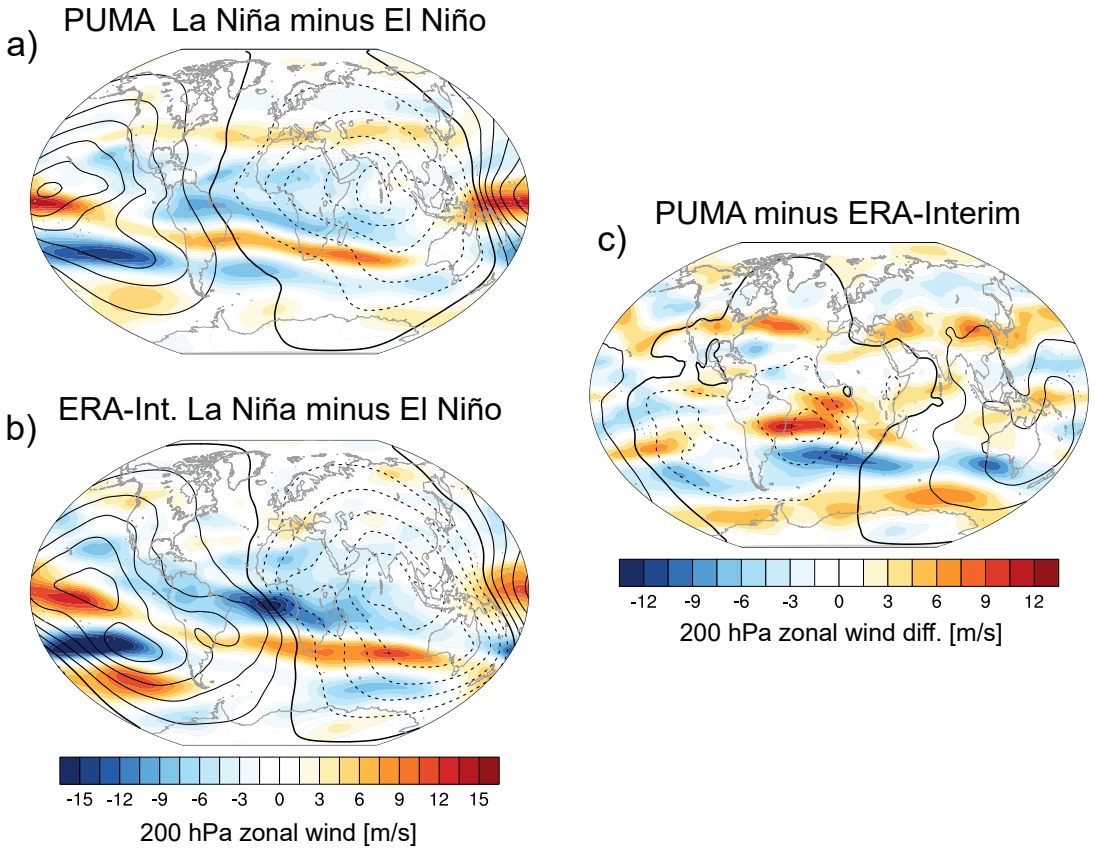

Figure 3.8: Comparison between composite mean response to ENSO forcing (JJAS mean La Niña minus El Niño composite). 200 hPa zonal wind speed (shaded) and 200 hPa velocity potential difference (contour interval 1.5 $km^2\,s^{-1}$, dashed lines denote anomalous divergence) between La Niña and El Niño for, a) PUMA, b) ERA-Interim and, c) the difference between PUMA and ERA-Interim. Selected El Niño years are 1982, 1987 and 1997. La Niña years are 1988, 1998 and 2007.

tense. Discrepancies to the reanalysis exist at the tropopause and in the stratosphere where the easterlies are too strong and too symmetric about the equator.

The spatial structure and intensity of the TEJ is well captured by PUMA. Some minor differences exist over the Indian monsoon system where PUMA tends to display a double jet structure with one jet core over India at roughly 20°N and a second one near the equator (Fig. 3.7, right column). Over West Africa, the climatological TEJ is well represented in terms of its width and the jet core latitude, but it is slightly too intense and the rapid deceleration over the Atlantic is less pronounced.

As a last test of the model's performance we show how the model reacts to ENSO which is a considerable large planetary-scale forcing. We calculate the composite mean from three simulations of the La Niña years 1988, 1998, 2007 and subtract the composite mean of the three El Niño years 1982, 1987 and 1997. The response to the ENSO-related remote changes in the JJAS mean diabatic heating seems to be well simulated in general (Fig. 3.8). Marked differences exist for instance some 15° south of the West African coast where ERA-Interim does show a nearly double as strong easterly anomaly. A closer investigation reveals that PUMA does not display a strong barotropic signal there compared to ERA-Interim. However, most of the more baroclinic responses in the tropics are generally well simulated in terms of spatial distribution and amplitude.

3.4.2 Role of local vs. remote diabatic forcing

In this section we discuss the experiment suite in which we aim to realistically simulate the variability of the WA-TEJ over the last four decades, and, more importantly, try to answer the question whether its interannual to decadal variability is more governed by the local forcing through WAM rainfall variability or the remote forcing through anomalies of the diabatic heating outside of Africa.

Figure 3.9 shows a time series of the simulated and observed summer-mean WA-TEJ intensities for 1979-2017. Solid lines depict the simulated WA-TEJ variability as a concatenation of the 39 individual quasi-equilibrium integrations of the PUMA model driven with the respective JJAS mean diabatic heating of each respective year. As a reference, the black dashed line shows the "observed" WA-TEJ intensity as provided by the ERA-Interim reanalysis. The climatological mean WA-TEJ intensity over West Africa is well represented (PUMA-TF mean 1979-2017: 14.6 $\mathrm{m\,s^{-1}}$; ERA-Interim mean: 15.1 $\mathrm{m\,s^{-1}}$). The interannual to decadal variability is also captured in good approximation. For PUMA-TF (green line), one obtains for the unfiltered WA-TEJ time series a standard deviation of 1.75 $\mathrm{m\,s^{-1}}$ compared to 1.63 $\mathrm{m\,s^{-1}}$ in ERA-Interim. Similarly close together are the standard deviations for the interannual time scale (8-year highpass-filtered): 1.49 $\mathrm{m\,s^{-1}}$ in PUMA-TF versus 1.38 $\mathrm{m\,s^{-1}}$ in ERA-Interim. The root mean square error (RMSE) of the PUMA-TF-simulated WA-TEJ intensity with regard to ERA-Interim amounts to 1.16 $\mathrm{m\,s^{-1}}$.

The conducted PUMA-LF and PUMA-RF simulations suggest that the remote forcing is the dominant driver of the WA-TEJ variability on interannual to decadal time scales. The local forcing through WAM rainfall variability plays a minor role. We obtain this result by comparing the WA-TEJ variability in PUMA-RF and PUMA-LF to both PUMA-TF (as an evaluation within the "model space") and the ERA-Interim reanalysis. Due to inherent model biases and experiment design-dependent limitations, we focus on evaluating statistical relationships within the PUMA model space. Henceforth, we therefore express the role of the local versus remote forcing by means of correlations (Pearson's r), explained variances (r^2) and RMSE calculated with respect to PUMA-TF. A multivariate regression analysis is not performed because the local forcing is substantially forced by the remote diabatic heating and is therefore not an independent predictor. This is why the explained variances do not add up to 100%. Statistical relationships between PUMA simulations and ERA-Interim may sometimes be added and can be further looked up in table 3.A3.

The dominance of the remote forcing becomes immediately apparent by comparing the typical amplitudes of interannual WA-TEJ variations in PUMA-RF to PUMA-LF. With 1.54 $\mathrm{m\,s^{-1}}$, the standard deviation of the WA-TEJ intensity in PUMA-RF is close to the one in PUMA-TF whereas it only amounts to 0.5 $\mathrm{m\,s^{-1}}$ in PUMA-LF. Moreover, the correlation to PUMA-TF is very high with 0.95 which translates to an explained variance of 91% (58% with respect to ERA-Interim). A bootstrapping method (a repeated recalculation of correlations after resampling the time series with 5000 iterations) gives a 95% confidence interval of 84.4-95.2% which highlights the robustness of this result. Furthermore, the outstanding importance of the remote forcing is irrespective of the considered time scale (see table 3.A3). What also becomes evident from figure 3.9 is the substantial effect of ENSO. In accordance to ERA-Interim, the largest simulated

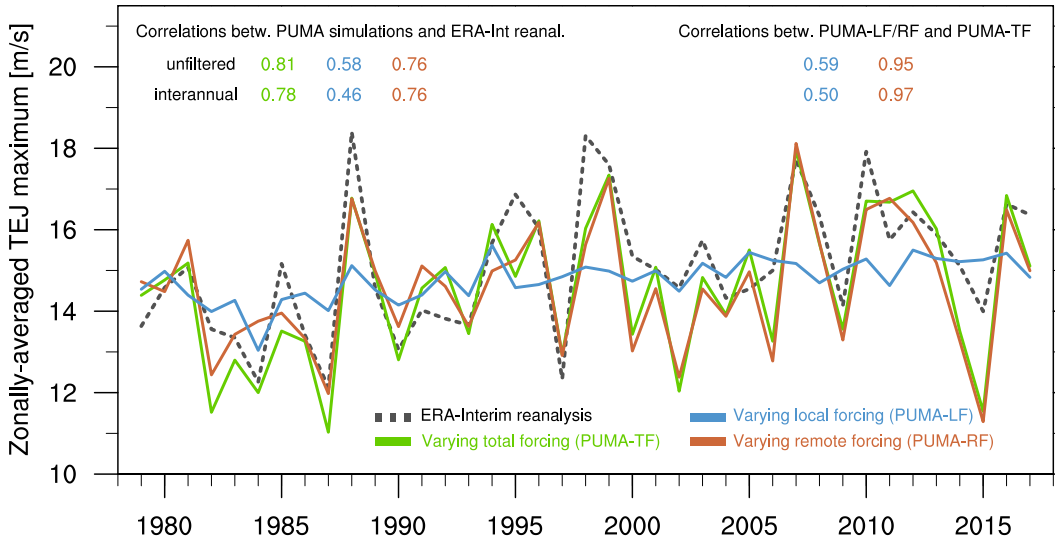

Figure 3.9: The conducted PUMA simulations suggest that the remote forcing is the dominant driver of the interannual to decadal variability of the West African TEJ intensity. The dashed black line depicts the TEJ intensity as given by the ERA-Interim reanalysis. The blue lines show the simulated TEJ intensity of the **PUMA-LF** (local forcing) simulations in which the year-to-year variability of the JJAS mean diabatic heating fields is restricted to the African region, meaning that outside of Africa, the diabatic heating is kept constant to climatological values. The red lines depict the simulated TEJ intensity of the **PUMA-RF** (remote forcing) simulations in which the diabatic heating is kept constant over Africa but is allowed to vary in the rest of the globe. The green line shows the results of simulations driven with the **PUMA-TF** (total forcing), in which the total (local and remote) variability of the diabatic heating is retained. All simulations were run with the same PUMA model setup with a tuned zonally-uniform relaxation temperature field in order to enforce a realistic extratropical circulation, and a simple, subjectively tuned vertical diffusion scheme that mimics the convective momentum transport. All depicted correlations coefficients (Pearson's r) are significant at the 5% level tested via bootstrapping with 5000 iterations.

WA-TEJ intensity deviations from the climatological mean mainly occur in years with strong ENSO events (e.g., 1983, 1988, 1998, 2007), but only in PUMA-RF. This is consistent with the previously conducted model performance test where PUMA was shown to accurately represent the impact of ENSO-induced changes of the tropical diabatic heating. A closer look at the special role of ENSO and other possibly important remote forcings will follow in the next section.

The simulation in which only the sole effect of the local forcing is considered – PUMA-LF – displays a correlation of 0.59 to PUMA-TF (95% confidence interval: 0.33-0.77). Therefore, the WAM rainfall-related variability of the local diabatic heating explains only 34.5% (10.6-59.3%) of the simulated WA-TEJ variability. In addition, the RMSE of PUMA-LF is with 1.53 $\mathrm{m\,s^{-1}}$ substantially larger than the one of PUMA-RF (0.55 $\mathrm{m\,s^{-1}}$). The role of the local forcing may become more important on (multi-) decadal time scales. After lowpass-filtering the WA-TEJ intensity time series with a cut-off at 8 years, the explained variance in PUMA-LF increases to 57.4% (28.5-76.3%). This result is mainly attributable to a linear trend that is observed in both WAM rainfall (rainfall recovery since the 1980s) and in the WA-TEJ intensity. Due to the strongly reduced number of degrees of freedom, this result has to be met with caution, though (reflected in the wide bootstrap confidence interval).

Interestingly, the role of the local forcing is not stationary over the simulated four recent decades. During the 1980s and the first half of the 1990s, the local forcing is

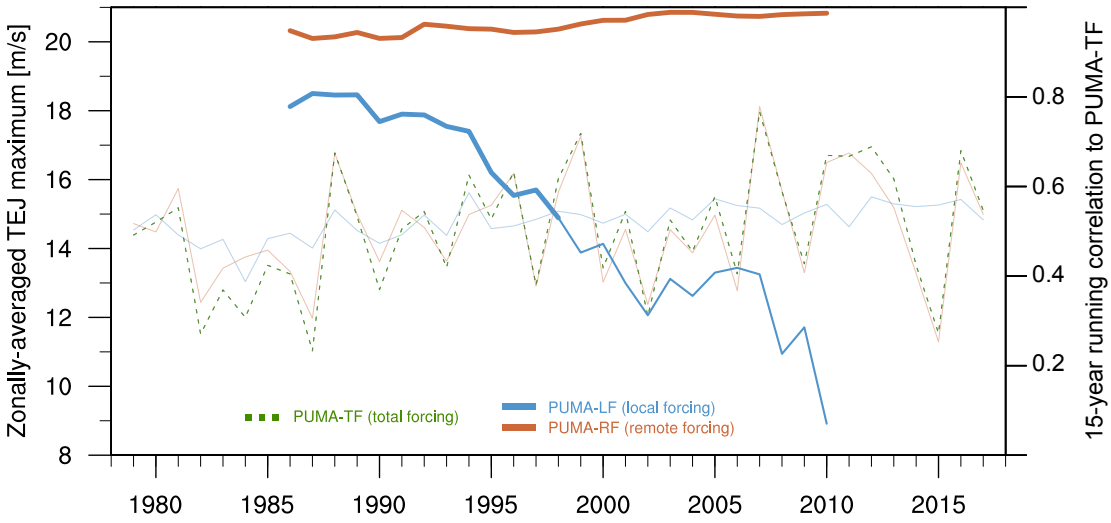

Figure 3.10: The share of variability of the PUMA-simulated WA-TEJ intensity explained by the local forcing alone decreases substantially over the last 40 years whereas the dominance of the remote forcing remains constant. The blue line shows the 15-year running correlation calculated between the **PUMA-LF**-simulated and the **PUMA-TF**-simulated WA-TEJ intensity. Similarly, the red lines depicts also the 15-year running correlation with respect to PUMA-TF, but calculated for the **PUMA-RF** simulation. Significant running correlation coefficients (tested via bootstrapping with 5000 iterations) are denoted by an increased line thickness. In the background, the thin lines depict, as an orientation, the simulated WA-TEJ intensity for PUMA-TF (green, dashed line), PUMA-LF (blue line) and PUMA-RF (red line).

comparably important. A 15-year running correlation between the WA-TEJ intensity in PUMA-LF and PUMA-TF yields significant correlations of up to 0.8 for the period 1979-1994 (Fig. 3.10). Shortly after, the role of the local forcing becomes insignificant, though. A combination of two factors explains this substantial decrease. First, one has to recall that the remotely induced WA-TEJ anomalies are in many cases substantially stronger than the ones induced solely by local forcing. The explained variance due to the local forcing therefore depends on whether the remote forcing cancels the effects of the local forcing or whether it induces same-sign anomalies. This "degree of synchronization" can be expressed via the correlation between PUMA-LF and PUMA-RF. Whereas in the period 1979-1994 this correlation amounts to 0.56, it drops to 0.11 in the period 1995-2017. Hence, a decoupling between remote and local forcing emerged in the 1990s, meaning that above-average Sahel rainfall and the associated locally-induced intensification of the WA-TEJ occurs more often simultaneously to a remotely induced weakening of the WA-TEJ. A second explanation for the diminishing of the role of the local forcing can be found in the changed characteristics of typical year-to-year anomalies of WAM rainfall. Figure 3.11 shows the results of a regional EOF analysis applied to JJAS mean WAM rainfall based on GPCP. In the period of 1979-1994, the dominant mode of rainfall variability was a dipole (explained variance 30%). In its positive phase, this dipole mode represents an off-equatorial heating which is likely to induce a Gill-type increase of easterlies to its southwest. The Gill-type response does in fact cause a robust intensification of the WA-TEJ that is reflected in a high correlation of 0.91 between the PUMA-LF simulated WA-TEJ intensity and Sahel rainfall (averaged over 15°W to 15°E and 10°N to 20°N). After 1995, the dipole mode becomes less pronounced and is no longer the dominant mode of variability (explained variance

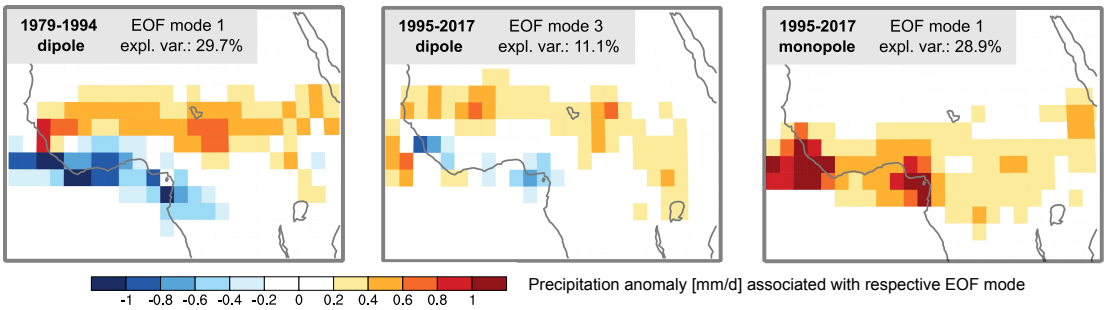

Figure 3.11: During the 1990s, the dominant mode of WAM rainfall variability changes from a dipole pattern towards a monopole pattern. The left plot shows the dominant rainfall anomaly pattern derived from a regional EOF analysis applied to JJAS mean GPCP rainfall over the period 1979-1994. The plot in the middle and the one on the right show the results for the period 1995-2017. Note that for this period, the dipole pattern depicted in the middle is not the dominant mode any longer and makes way for a monopole mode as shown in the right plot.

11%). It makes way for a monopole mode that is no longer able to substantially alter the TEJ intensity over West Africa. As a consequence, the correlation between PUMA-LF simulated WA-TEJ intensity and Sahel rainfall drops to 0.57.

On first sight, our main result – the dominance of the remote forcing and the minor role of the local forcing – stands in contrast to WAM-focused dynamical-core simulations conducted by Chadwick et al. (2017). The authors noted that the "strengths of both jet cores (AEJ and TEJ) appear to be connected to regional West African heating, as would be expected from thermal wind balance." However, Chadwick et al. (2017) refer to the climatological mean state of the TEJ over West Africa in absence of any remote forcing. As a test, we performed a simulation in which we completely set any diabatic heating outside of our selected African region to zero. In such a simulation we obtain results similar to Chadwick et al. (2017) confirming that the African heating alone might be able to generate dynamical features which are to first order comparable to the observed TEJ, AEJ and monsoon flow. However, the **variability** of the WA-TEJ seems to be strongly linked to remote influences.

In addition to the JJAS mean WA-TEJ intensity, the latitudinal width of the WA-TEJ or more generally the width of the upper-level easterlies is also of interest. The easterlies shield the WAM circulation from any extratropical influences (Bordoni and Schneider, 2008) and further play a role for equatorial Rossby wave propagation characteristics which may, in turn, promote AEW activity and therefore convection over the Sahel (Yang et al., 2018). The width of upper-level easterlies is strongly correlated with the WA-TEJ intensity in both the ERA-Interim reanalysis (r=0.87) but also in the PUMA-TF simulation (r=0.93) and the PUMA-RF simulation. Interestingly, PUMA-LF displays a weak anti-correlation meaning that a local forcing-induced intensification of the WA-TEJ core goes along with a tightening of the upper-level easterlies. However, the variations in width due to the local forcing are rather small and possibly not robust with regard to the applied rather simple measure. Due to the high correlation between WA-TEJ intensity and WA-TEJ width in PUMA-RF, it is expected that the remote forcing explains a considerable amount of the width of the upper-level easterlies over Africa. As evident from figure 3.A3 (in the appendix), PUMA-RF explains in fact 56% of the observed variability of the width of the upper-level easterlies. Within the model space,

96% of the width variation is attributable to the sole effect of the remote forcing.

The robustness of our main findings is examined by checking how sensitive our results are to the geographic split-up of the diabatic heating fields, to changes in the selection of the years (omitting ENSO), and to the switch-off the vertical diffusion scheme. We concentrate on the respective shares of WA-TEJ intensity variability explained by the local and remote forcing with respect to PUMA-TF. The results of these sensitivity experiment are summed up in figure 3.12.

The amount of WA-TEJ variability explained by the local forcing alone depends strongly on the exact definition of the local forcing. In our default experiment, we selected a box spanning from 15°W to 52°E and thereby confined the local forcing to the continental WAM rainfall. However, when the box is extended westwards towards the Atlantic ITCZ, the explained variance by the local forcing changes substantially. An extension of the local forcing box to 35°W results in a decline in explained variance to a non-significant 3%. However, a corresponding westward shift of the eastern boundary of where the diabatic heating field is considered to be part of the remote forcing does only slightly change the explained variance by the remote forcing. Therefore, the dominance of the remote diabatic heating is insensitive to the selection of the geographical split between local and remote regions.

As mentioned before, ENSO marks a particularly intense forcing that possibly explains the dominance of the remote forcing. If we omit all years with ENSO conditions from our analysis (1982, 1986, 1987, 1988, 1991, 1997, 1998, 1999, 2000, 2003, 2007, 2008, 2010, 2011, 2012, 2015), our results do change. With respect to the ERA-Interim observed TEJ variability, the role of the remote forcing dwindles strongly whereas the share of explained variance attributable to the local forcing rises slightly. However, measured within the PUMA model space, the remote forcing remains the dominant one (80% explained by the sole effect of the remote forcing compared to 40% explained by the local forcing alone), underlining the robustness of this result.

As a last test of the robustness of our main results we discuss the role of vertical diffusion. Re-running our suite of experiments with turned-off vertical diffusion has no significant effect on the dominant role of the remote forcing. However, the effect of the local forcing on the WA-TEJ variability vanishes. We suppose that a combination of both, a too northward position of the WA-TEJ core and the modulation of the upper-level (Gill-type) response due to an unrealistically high vertical wind shear may explain this observation of a diminished role of the local forcing.

In summary, the PUMA simulations have shown that the interannual to decadal variability is to large parts governed by the effects of remote diabatic heating variability, especially on the interannual time scale on which ENSO is dominant. Multiple sensitivity tests have underlined the robustness of this finding. In contrast, the role of the local forcing in explaining the WA-TEJ variability is more uncertain. First of all, the importance of the local forcing has apparently substantially decreased over the last four decades. Moreover, the role of the local forcing depends much more strongly on the actual definition of "local" and is further sensitive to the inclusion of a vertical diffusion scheme that mimics convective momentum transport. Because the remote forcing has come out as the most important, the next section will focus on identifying the regions of the globe in which typical heating anomalies have the largest impact on WA-TEJ

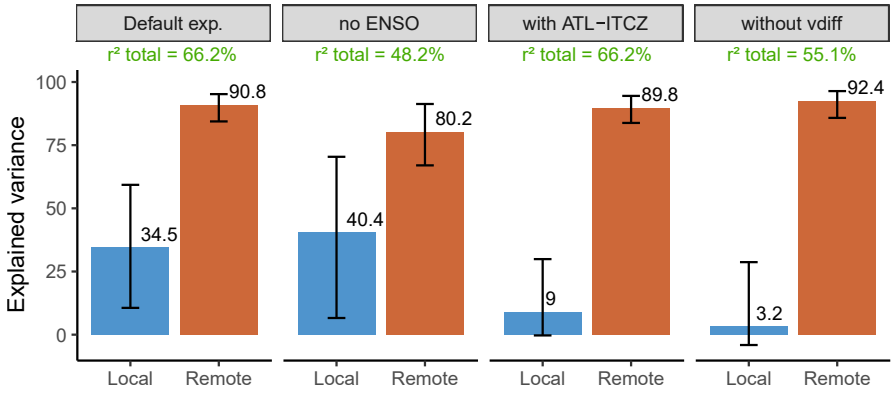

Figure 3.12: Whereas the dominance of the remote forcing is a robust result, the role of the local forcing is more uncertain. Results of three sensitivity studies compared to the default experiment: the blue bars denote the explained WA-TEJ variability due to the local forcing (PUMA-LF) while the red bars denote the explained WA-TEJ variability due to the remote forcing (PUMA-RF). Error bars show the 95% confidence interval as determined by a bootstrapping procedure with 5000 iterations. "no ENSO" is no new additional experiment, but designates the result of the default experiment, when all ENSO years are removed from the 39-year time series. "with ATL-ITCZ" labels an experiment where the local forcing box is extended by 20° to the West such that parts of the Atlantic ITCZ rainbelt are included in the local African forcing. "without vdiff" denotes a repetition of the default experiment for which vertical diffusion is completely turned off (as is the default case in the PUMA model). The green numbers printed above the bars denote the explained variance of the respective PUMA-TF simulation with respect to the ERA-Interim observed WA-TEJ variability.

variability. We will also briefly discuss the physical mechanism by which remote heating anomalies induce circulation anomalies over West Africa, focusing on the question: Why is the TEJ over West Africa so strongly affected by ENSO?

3.4.3 Understanding the role of the remote forcing

We conduct a number of experiments that assess the isolated effect of diabatic heating anomalies in certain remote regions on the WA-TEJ intensity. The amplitude of the respective heating anomalies is chosen to be representative of the observed variability (composite mean of all years where the respective principal component time series of a regional EOF analysis surpasses one standard deviation). The selected regions of the globe represent those regions for which we observe a substantial linear relationship between the respective regional rainfall and the WA-TEJ intensity. Here we will only discuss in-depth those simulations for which a *substantial* effect on the WA-TEJ intensity is found. We define *substantial* anomalies as follows: The WA-TEJ intensity has to surpass the ERA-Interim-derived interannual WA-TEJ intensity variability without ENSO in the period 1979-2017. This variability, as measured by the standard deviation of the 8-year-highpass-filtered WA-TEJ intensity time series in which all ENSO years are omitted, amounts to 1.14 $\mathrm{m\,s^{-1}}$. For the width of the upper-level easterlies, the same measure yields a typical (ENSO-excluded) variability of 1.6°.

Our experiments show that the observed substantial modulations of the summer mean WA-TEJ intensity are to large extent exclusively attributable to anomalous diabatic heating over the Pacific. In most other regions, the amplitudes of the typically observed diabatic heating variations are generally too small to produce any robust steady-state responses in the tropical upper troposphere. The dominance of ENSO is depicted exemplarily by figure 3.13 which displays the upper-level circulation response to im-

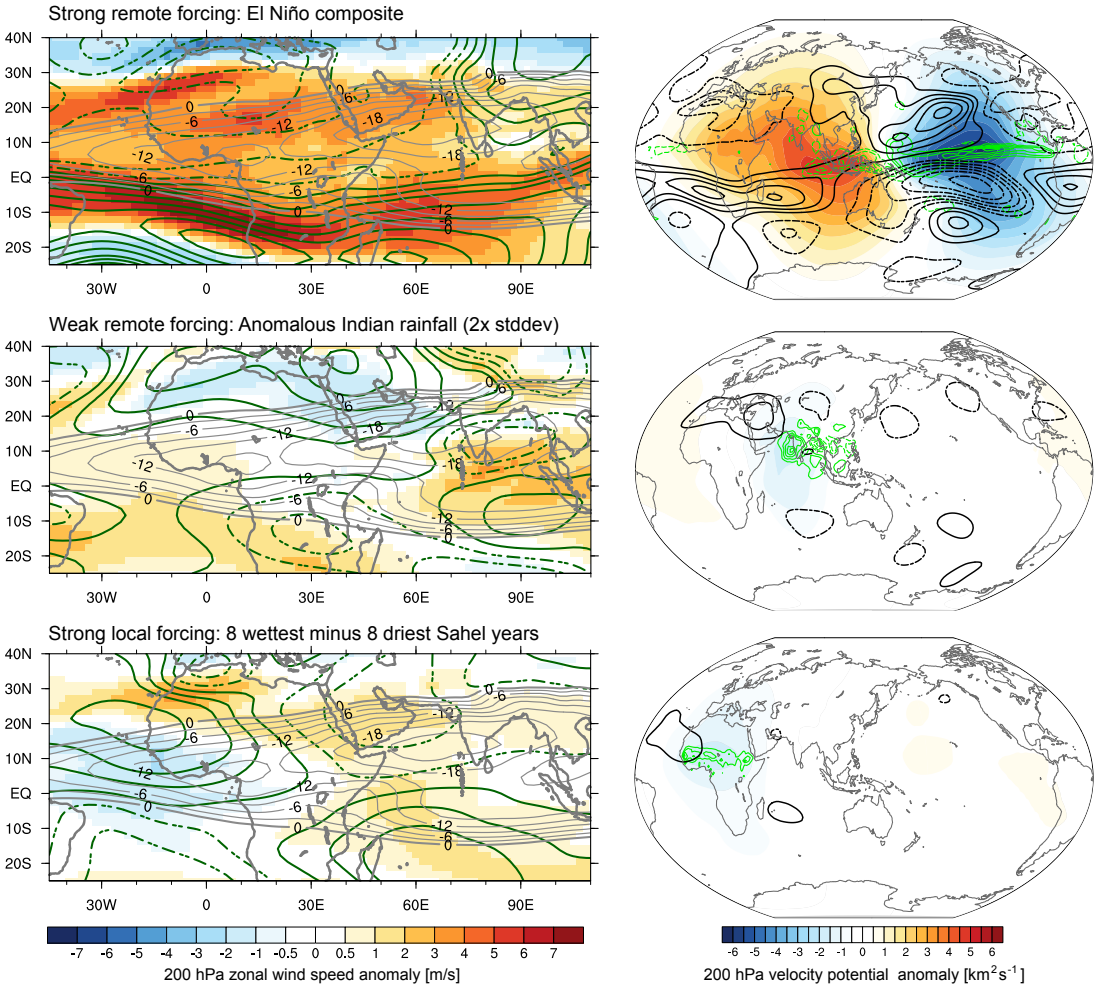

Figure 3.13: ENSO dominates the effect of any local and any remote forcing outside of the tropical Pacific. Zoomed-in and global overview of upper-level circulation responses to top) an El Niño-type composite anomalous diabatic heating (ENSO-COMPLETE_mode0_pos, see table 3.A2), middle) anomalous heating related to a composite of strong Indian monsoon seasons with rainfall two times above standard deviation (INDIA-ALL_mode0_pos_fac2) and bottom) anomalous heating related to a composite of the eight wettest minus the eight driest years in the Sahel (SAHEL_8wettest-8driest_pos). On the left hand side, the grey contours depict the PUMA-simulated climatological mean TEJ. Coloured shadings depict the 200 hPa zonal wind anomaly with respect to the climatology. The thicker green contours indicate the anomalous eddy streamfunction (interval 0.5 $km^2\,s^{-1}$, solid lines denote positive values). On the right hand side, the green contours depict the imposed anomalous diabatic heating in around 500 hPa (solid lines denote heating, interval 0.5 $K\,d^{-1}$). The anomalies of the tropical overturning circulation are shown with the help of the 200 hPa velocity potential (coloured shadings, blue means anomalous divergence). Black contour lines depict the stationary eddy streamfunction at 200 hPa (interval 1 $km^2\,s^{-1}$, solid lines denote positive values).

posed anomalous heating in three different regions. The full El Niño type composite heating induces a reduction of the WA-TEJ intensity by 3.1 $m\,s^{-1}$ which translates to a weakening of about 20% with respect to the climatological JJAS mean (experiment ENSO-COMPLETE_mode0_pos, see table 3.A2). Interestingly, anomalies in Indian rainfall do not pose a substantial forcing for the WA-TEJ intensity. For better comparability to the vigorous ENSO-type forcing, the middle of figure 3.13 shows results of an experiment where the typically observed interannual heating deviations over India are multiplied by a factor of 2. This off-equatorial heating over India does not induce

any robust stationary wave response and has no substantial influence on the WA-TEJ intensity. Possible causes may be the rather limited spatial extent of the heating signal or modulating effects of the complex basic state. An additional experiment with a more idealized, broader heating anomaly with stronger amplitude displays a more robust response. However, the intensification of upper-level easterlies due to anomalous heating over India stays confined to the subtropical regions over North Africa. The WA-TEJ intensity remains unaffected (not shown). To compare the effects of the strongest possible local and remote forcings, we also simulate the response to a strong local diabatic forcing over Africa. The imposed heating anomaly is derived from the precipitation difference of the eight wettest and the eight driest years in the Sahel (bottom plot in Fig. 3.13). This forcing does cause a substantial intensification of the WA-TEJ. However, compared to the effect of ENSO the effect of the local forcing remains minor.

To better understand the substantial effect of ENSO on the WA-TEJ, we briefly assess the underlying dynamical mechanisms (for the case of the full El Niño forcing simulation as shown in Fig. 3.13). The substantial modulation of the WA-TEJ intensity by ENSO-type anomalous heating is attributable to a planetary-scale response that induces anomalous westerlies in the upper troposphere over a broad region of the Tropics. The spatial pattern with regard to the stationary eddies looks remarkably similar to the familiar quadrupoles of the Gill model (Gill, 1980). Therefore, the modulation of the WA-TEJ by ENSO may in good approximation be understood in terms of a linear first baroclinic mode response to equatorial heating. As a test of this hypothesis we conduct an additional simulation in which we aim to reproduce the linear Gill-type response to our imposed El Niño-type heating. To do so, we introduce a resting background state and scale down the heating amplitude by a factor of 10. Finally, we only average the response over the days 6-12 where the linear response should be akin to the analytical solution to the Gill model. Averaging over days 6 to 12 is necessary since our model still includes transient eddies that are, however, not yet important at this time (Lin et al., 2007). Figure 3.14 shows that the thus obtained more or less linear response does not differ too strongly from the fully non-linear response, in particular over the African region at the climatological latitude of the WA-TEJ. We therefore deduce that the deceleration of the WA-TEJ due to El Niño is mainly attributable to the Kelvin wave response towards the east of the anomalous heating over the Pacific. Of course, some differences are evident with regard to the anticyclonic Rossby gyres which are shifted to the west. This is consistent with existing literature which notes that the non-linear interaction with the background state generally shifts the anticyclones closer to the heating (Hendon, 1986). Furthermore, the circulation response in the non-linear case with a realistic basic state is much less confined to the equatorial region.

At the end of this section, we want to stress that in some of the conducted experiments, the imposed anomalous tropical heating substantially alters the zonal mean circulation. In most cases, a general tendency to weakened upper-level easterlies over the tropics is found. This may not be unexpected as anomalous westerlies (or even equatorial superrotation) are a common observation when idealized general circulation models are driven with a zonally varying, steady tropical heating (Showman and Polvani, 2010). Held (1999) suggested that the equatorial superrotation observed in simplified AGCMs is attributable to the poleward propagation of Rossby waves forced

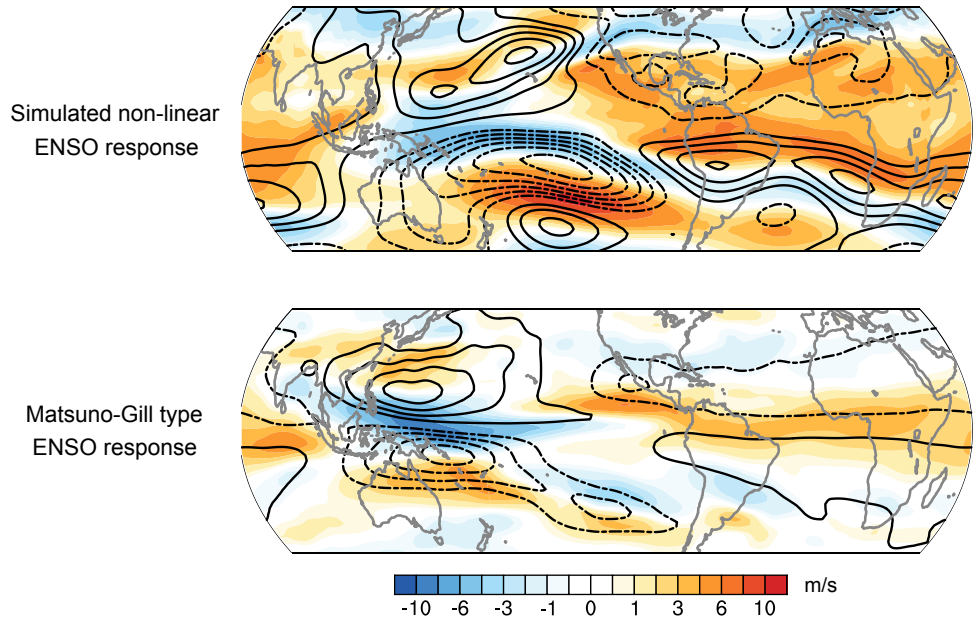

Figure 3.14: Within the WA-TEJ region, the PUMA-simulated non-linear response to a realistic composite ENSO heating bears similarity to the linear Matsuno-Gill type response. The upper plot shows the PUMA-simulated steady-state response to the full ENSO-composite anomalous diabatic heating. This solution represents a complex response that is subject to a realistic basic state and non-linear interactions. The bottom plot shows the PUMA-simulated approximate Matsuno-Gill-type linear response to the same anomalous heating. For this simulation, a resting basic state is used and the heating is scaled down by a factor of 10. To exclude the effect of transients (which still exist in this model setup), we average the response over the simulated days 6 to 12. For comparability, all anomalies in the bottom plot are scaled up again by a factor of 10. Contours show the anomalous eddy streamfunction (interval 1.5 $km^2\,s^{-1}$, solid lines denote positive values). 200 hPa wind anomalies are shown by coloured shadings.

by the imposed tropical heating. The dissipation or breaking of these waves at higher latitudes accelerates the mean flow in the source region, i.e., in the tropics. In the scope of this paper, we cannot finally clarify whether the tendency to anomalous equatorial westerlies is realistic or whether it is an erroneous feature related to the model's simple physics. Possibly related to the aforementioned problem is the finding that the response to La Niña is unexpectedly sensitive against the imposed heating pattern and amplitude. For instance, the default anomalous heating composite, based on a composite of all events with anomalous cooling below one standard deviation (ENSO-COMPLETE_mode0_neg, see table 3.A2), does not produce a substantial response over West Africa (not shown). However, by multiplying the El Niño composite heating (ENSO-COMPLETE_mode0_pos) by -1, the response becomes closer to an inverted El Niño response (WA-TEJ intensity increased by about 2.1 $m\,s^{-1}$).

In summary, the results of these additional experiments are consistent with the correlation maps shown earlier that highlighted the very high connection between WA-TEJ intensity and Pacific SSTs. The additional information of the conducted experiments is that only the diabatic heating anomalies over the Pacific are strong enough to have a robust impact on the WA-TEJ. In all other regions with high correlations, the increase in precipitation often co-occurs with ENSO, but there is no additional robust influence on the TEJ. Some of our results with regard to weaker forcings (e.g., anomalous Indian

rainfall) may be met with caution as they might be compromised by the tendency of PUMA to simulate possibly unrealistic deposition of westerly momentum in the tropical upper troposphere. Nevertheless, we are confident that the observed pronounced interannual modulations of the WA-TEJ can to large extent be understood in terms of a linear Gill-type response to strong anomalous heating over the Pacific.

3.5 Discussion

In this section we will first discuss the limitations of our study especially with regard to the numerical experiments conducted with PUMA. The second part of this section puts our results in a larger context and discusses the possible implications for the interpretation of the observed relationship between Sahel rainfall and WA-TEJ intensity.

As the first limitation, we note that the conducted PUMA simulations only reproduce 66% of the observed WA-TEJ variability when driven with the total variability of the global diabatic forcing. The most likely explanation is the chosen modelling strategy where each monsoon season is simulated as a time slice in order to isolate the steady-state response to the given diabatic forcing. Averaging over the 10-year integration time eliminates any atmospheric noise due to transient disturbances. Differences to the real-world observed state are therefore to expect, particularly in years where the anomalous diabatic forcing and therefore the signal-to-noise ratio is weak. By using a time-constant JJAS heating anomaly for each season, it is further assumed that the steady-state response to a constant anomalous heating is equivalent to the time-averaged response to a more realistic transient heating. We are nonetheless confident that the chosen modelling strategy is justified as the removal of atmospheric noise should vastly improve the distinction between the effects of local and remote diabatic forcing. Further explanations are the simplified physics of the model and any systematic errors of the model input fields as for instance the relaxation temperature or the diabatic heating fields. In this context, one can directly refer to the concluding remark of Sardeshmukh and Hoskins (1985): "To model the atmosphere's response to a given distribution of anomalous SST correctly, it is then not only necessary to take the non-linear nature of the vorticity dynamics into account, but also vitally important to model the intensity and the horizontal and vertical structure of the associated atmospheric heating with precision." Since all reanalyses do not adequately reflect the interannual to decadal precipitation variability over West Africa, the diabatic heating anomalies to the ERA-Interim-derived climatology are derived from observed GPCP rainfall. Therefore, the anomalous heating is only representative of the latent heating which is why the vertical profile of the anomalous diabatic heating fields may contain systematic errors, particularly near the surface and in the upper troposphere where the diabatic heating is not dominated by the latent heating. Nevertheless, the derivation of the heating variability from observed rainfall anomalies is overall justified because the spatial distribution of vertically-integrated diabatic heating and in particularly the role of the local forcing is represented much more accurately.

Further possible sources of error are short-comings of the model in accurately simulating the background circulation. Although possibly more important for the barotropic responses outside the tropics, the simulated basic state, i.e., the horizontal and verti-

cal wind shear might also affect the response of the tropical circulation to an imposed heating (Robertson and Frankignoul, 1990). Moreover, the vertical momentum transport associated with deep convection is not explicitly modelled and the effect is only parametrized in a simplified way by means of an additional vertical diffusion. In this context, it should generally be stressed that a model with simple physics as the one employed in this study is mainly suitable to realistically capture the effects of large-scale heating anomalies. However, changes in diabatic heating intensity and distribution are rather small over West Africa compared to the substantial large-scale changes associated with, for instance, ENSO. Therefore, certain details of the circulation that might be associated with sub-scale features (e.g., convective momentum transport by MCSs) may be missing or be underrepresented in our model.

Despite their limitations, what do the results of this study tell us about the observed TEJ – Sahel rainfall relationship on interannual to (multi-)decadal time scales? If the variability of the WA-TEJ intensity would not be influenced by remote diabatic forcing or any atmospheric noise, but strictly be forced by WAM rainfall variability alone, the statistical connection would probably even be higher. This becomes evident when one calculates the correlations between Sahel rainfall and the WA-TEJ intensity in the local forcing simulations (r=0.82). However, the WA-TEJ anomalies induced exclusively by the anomalous heating in association with WAM rainfall variability, are rather small. In reality, the summer mean WA-TEJ intensity of each individual monsoon season is likely affected by various transient disturbances. The effects of this "atmospheric noise" may not get filtered out over the some 100 days of a monsoon season – in contrast to the conducted PUMA simulations which represent the steady-state response without any noise. Therefore, only the remote forcing induces substantial variability that may stand out against a background noise level. How this then affects the TEJ – Sahel rainfall relationship depends on whether the remote diabatic forcing tends to simultaneously induce same-sign changes in Sahel rainfall.

To answer this question, one may focus on the tropical Pacific region where we generally find the dominant variability of the remote diabatic heating (within a planetary-scale perspective). The variability of the diabatic heating there is closely related to the interannual SST variability, especially to ENSO. Correlation maps presented in this study (Fig. 3.5) highlight that both the WA-TEJ intensity and Sahel rainfall show a similar in-phase relationship to SST variability in the tropical Pacific. This statistical observation of significant correlations between Sahel rainfall and Pacific SSTs is consistent with the literature highlighting the importance of interannual Pacific SST variability for Sahel rainfall by means of model experiments (Janicot et al., 1996; Rowell, 2001). The suppression of rainfall by El Niño, for instance, is mainly explained by the increase in static stability due to upper-level warming which is induced by the Gill-type Kelvin wave response to the east of the ENSO region. An opposite mechanism favours anomalously high Sahel precipitation during La Niña (Lintner and Chiang, 2007). However, Sahel rainfall is influenced by numerous other factors which is why the effect of ENSO on rainfall is not as robust as the effect on the WA-TEJ intensity (see in-depth discussion in Nicholson, 2013). This is in line with the correlations maps presented in figure 3.5 where the Pacific SST – Sahel rainfall relationships are comparably weak and become insignificant when years with pronounced ENSO signal are omitted from the analy-

sis. Nonetheless, especially in the recent decades, the remote diabatic heating can be considered an important forcing that not only governs the WA-TEJ variability but often induces same-sign changes in rainfall. We therefore suggest that the variability of the remote diabatic heating – especially over the tropical Pacific – can be understood as a third quantity that is ultimately one of the most important drivers of the Sahel rainfall – TEJ relationship over the recent decades. This hypothesis might be supported by the substantial, albeit not statistically robust, drop in correlations when only years without strong ENSO conditions are considered (from $r = 0.62$ to $r = 0.40$, see subsection 3.3.1).

We want to stress that the scope of our study is limited to the time period for which reliable forcing data is available (satellite era). Therefore we cannot make any predictions about the WA-TEJ variability on decadal to multi-decadal time scales. The above-mentioned interpretation with regard to the dominance of the remote diabatic heating is therefore only valid for the last four decades, and in particular for interannual time scales. On decadal to multi-decadal time scales, the strong "noise" of the interannual variability would be filtered out. Therefore, long-term trends in WAM rainfall as for instance the transition from the wet 1950s and 1960s to the drought of the 1970s and 1980s or the recent recovery in Sahel rainfall – albeit representing a rather small diabatic forcing – may become more important in explaining the variability of the WA-TEJ on longer, decadal to multi-decadal time scales.

3.6 Summary and conclusions

Sahel rainfall and the intensity of the TEJ over West Africa (WA-TEJ) are strongly correlated on interannual to multi-decadal time scales. It is unclear whether the high correlation can be explained by a causal link. Many studies investigated what causes changes in WAM and particularly Sahel rainfall on these time scales. What has been missing so far is an in-depth analysis of the variability of the WA-TEJ. In this paper we therefore explore the dominant tropical drivers of the interannual to decadal variability of the WA-TEJ with a clear focus on the interannual time scale due to the limited time period of robust data (satellite period since 1979). We primarily aim to answer the question whether the observed WA-TEJ variability is mainly directly linked to WAM rainfall changes or whether remote influences – anomalies in the tropical diabatic heating far away from Africa – play an important role.

In the first part, we use linear regression and correlation analysis to discover the linear relationships between the reanalysis-derived WA-TEJ intensity and observed rainfall and their respective connections to global SST anomaly patterns. It is shown that the interannual variability of the WA-TEJ is strongly correlated with changes in WAM rainfall, but also with remote changes in rainfall over India, the Maritime Continent and the Pacific. For a better understanding, we further examine how both, WA-TEJ and WAM rainfall are connected to SST anomalies. When comparing the global correlation maps between WA-TEJ intensity and SST anomalies to those between WAM rainfall and SSTs, some distinct differences stand out immediately. The interannual variability of the WA-TEJ appears to be significantly stronger linked to remote tropical SST anomalies, especially ENSO-like ones in the Pacific whereas WAM rainfall is generally less influenced by Pacific SST anomalies but more associated with extratropical

SST anomalies.

For more clarity, we employ PUMA, an AGCM based on dry dynamics with very simple physics, and force it with 3D time-constant diabatic heating patterns. The TEJ variability over the years 1979-2017 is simulated via 39 individual time-slice experiments that isolate the steady-state response to the given diabatic heating. The climatology of the 3D diabatic heating fields is based on ERA-Interim whereas the year-to-year variability is derived from GPCP rainfall. An additional nudging towards a previously-tuned zonally-uniform relaxation temperature is set in a way that it enforces a quite realistic global circulation (extratropical jets, baroclinic eddies) while simultaneously allowing an as free as possible response to diabatic forcing anomalies. We design three experiments: In the control experiment, we simulate the interannual to decadal variability of the TEJ as realistically as possible by letting the total global summer mean diabatic heating field vary from year to year. In the other two experiments, we disentangle the respective contributions from the local WAM-related forcing and the remote forcing. To do so, we perform on the one hand side so-called local forcing experiments where the year-to-year diabatic heating variability is restricted to the African monsoon region (with diabatic heating kept constant at climatological values everywhere else). By contrast, in the so-called remote forcing experiments, the diabatic heating fields are held constant over Africa, while retaining their variability everywhere else on the globe. The main results of the suite of PUMA experiments can be summed up as follows:

- Remote diabatic heating variability is the dominant driver of West African TEJ variability: in PUMA simulations, which are able to explain 66% of the observed TEJ variability from 1979-2017, 91% of the interannual to decadal variability of the TEJ intensity can be attributed towards the sole effect of the remote forcing
- The local forcing through WAM rainfall changes alone only explains 35% of the West African TEJ variability within the PUMA model space and only induces TEJ anomalies one third as strong compared to the remote forcing

In addition to the WA-TEJ intensity, the width of the upper-tropospheric easterlies is also governed almost exclusively by the variability of the remote diabatic heating (96% explained variance with the PUMA model space). Multiple sensitivity experiments demonstrate that the dominance of the remote diabatic forcing is a robust result. To better understand the role of the remote diabatic forcing, we perform additional experiments in which we discover how individual heating anomalies in certain parts of the globe affect the WA-TEJ intensity. These supplementary experiments show:

- By far the strongest forcing responsible for WA-TEJ variations are heating anomalies associated with ENSO: La Niña related changes in the tropical diabatic heating significantly increase the intensity of the WA-TEJ whereas typical El Niño type anomalies substantially weaken the WA-TEJ by about 3 $\mathrm{m\,s^{-1}}$.
- With the exception of the Pacific region, there is no region in the world in which the typically observed variability of the diabatic heating exerts a substantial influence on the WA-TEJ

The effect of ENSO on the WA-TEJ can in good approximation be understood in terms of a classic Matsuno-Gill type response to a strong equatorial heating where West Africa is

mainly affected by the stationary Kelvin wave response to the east of the Pacific heating anomaly. Changes in the Indian monsoon rainfall show no significant impact on the intensity of the WA-TEJ. More generally, nearly all diabatic heating anomalies besides those in the tropical Pacific region fail to produce any robust upper-level responses in the WAM region as long as the imposed heating anomalies stay within range of observed variability. The conducted simulations therefore suggest that the variability of the diabatic heating over the Pacific region stands out as the most important driver of WA-TEJ variability on interannual time scales.

In synopsis, our results might contribute to the understanding of the observed correlation between the WA-TEJ intensity and Sahel rainfall on interannual to decadal time scales although the interpretation is not straightforward. In the PUMA simulations, WA-TEJ anomalies that are exclusively attributable to the variability of the local WAM-confined diabatic heating are strongly correlated to Sahel rainfall. These solely local forcing-induced anomalies are comparably weak, though, and would therefore be unlikely to stand out against the internal variability of the WA-TEJ (due to non-filtered out effects of any transient disturbances). However, the dominant variability of the remote diabatic heating, which is found over the tropical Pacific, tends to induce same-sign changes in both Sahel rainfall and WA-TEJ intensity, especially in years with pronounced ENSO signal. The remote diabatic forcing may therefore be viewed as one of the most important drivers of today's observed Sahel rainfall – WA-TEJ relationship, at least on interannual time scales over the last four decades. This hypothesis would imply that the strength of the relationship may change when the importance of the remote diabatic forcing diminishes, or when the current tendency to in-phase effects on TEJ intensity and Sahel rainfall changes.

As a next step, our proposed hypothesis could be tested with a more complex model that allows simulating both the response of the WA-TEJ and Sahel rainfall to a given diabatic forcing. A disadvantage is that the use of a complex model would not allow to unravel the respective contributions of the local and remote forcing on the modulation of the WA-TEJ intensity. However, taking the results of this study into consideration, one can safely assume that especially the interannual deviations of the WA-TEJ intensity are to large extent solely attributable to the direct effect of the remote diabatic heating. Multiple SST sensitivity experiments with imposed ENSO-type anomalies could then be designed to systematically study whether the TEJ – Sahel rainfall covariability is indeed higher when a strong anomalous diabatic heating over the Pacific exists. It would further be of interest to investigate the Sahel rainfall – WA-TEJ relationship in a different climate in which the role of the remote diabatic heating variability might be attenuated. A suitable example would be the mid-Holocene during which the interannual variability of the tropical Pacific SST was likely weaker than today (Otto-Bliesner, 1999; Koutavas et al., 2006; Zhao et al., 2007).

Acknowledgments

This work was supported by the International Max Planck Research School on Earth System Modelling (IMPRS-ESM) and the Max Planck Society (MPG). The computational resources were provided by the Deutsches Klima Rechenzentrum (DKRZ).

3.7 Appendix

3.A.1 Study-specific adaptations to the PUMA model

Iterative tuning of the zonally-uniform relaxation temperature

To obtain an zonally-uniform relaxation temperature field that works well in combination with the imposed diabatic heating, some tuning of T_{eq} is necessary. Starting from a standard Held-Suarez type tropospheric T_{eq} which is combined with the stratospheric profile of Jucker et al. (2013), we tune T_{eq} in an iterative process in a very similar way as described in Jucker et al. (2013). The difference is, however, that we only tune the zonal mean temperature and not the full temperature field. This is necessary to guarantee that the model is still able to react as freely as possible to different diabatic forcings. After each model integration into quasi-equilibrium, the model's zonally and temporally averaged 3D temperature field is compared to the 1979-2017 JJAS climatology as provided by ERA-Interim on pressure levels. For the next iteration step, the relaxation temperature is adapted by adding 2/3 of the difference between the previous run's temperature field and that of the reanalysis. The factor of 2/3 follows Chang (2006) to avoid over-correction. Since we do not use a full three-dimensional relaxation temperature, the iterative tuning procedure will not yield continuous improvements of the modelled circulation and can therefore be stopped after only a few iterations. This is an acceptable trade-off in order to keep the model's capacity to react freely to imposed changes in the diabatic heating field. Our final zonally-symmetric profile of T_{eq} for our PUMA-RC setup is presented in Fig. 3.1.

Simple vertical diffusion to mimic convective momentum transport

In addition to the standard model version, we also include a more realistic representation of vertical diffusion of momentum. We rewrite the formulation of the existing spectral vertical diffusion scheme of PUMA to calculate the diffusion in grid point space which allows use of a 3-d varying parameter of diffusion of momentum $\mathrm{K_m}$. The vertical diffusion is thought of being comprised of a background eddy-diffusivity K_{t} (strongest in the planetary boundary layer) and a convection-related diffusion (cumulus friction) K_{c} which mimics the vertical momentum transport via convection which is to first order against the vertical gradient on larger spatial scales. The cumulus friction is described by the parameter of convective diffusion of momentum K_{c}. K_{c} is approximated by a simple parametrization in dependence of the convective mass flux K_{c} (used for instance in GFDL; Anderson et al., 2004):

$$K_{\mathrm{c}} = \gamma \, M_{\mathrm{c}} \, d_{\mathrm{c}} / \rho$$

Here, the three-dimensional variable M_{c} stands for the cumulus mass flux at a certain level and grid point while the two-dimensional d_{c} describes the depth of the convection at a certain grid point. ρ denotes the density of air and γ is a dimensionless tuning parameter that is given the value of 0.2.

The convective mass flux M_{c}, in turn, can be estimated in good approximation by

the following equation:

$$M_{\mathrm{c}} = \frac{1}{g} \frac{\partial p}{\partial \Theta} Q$$

In this equation, g is the Earth's gravitational acceleration, p is the pressure and Θ denotes the potential temperature. For simplicity, we calculate a vertically and globally-averaged value of $\partial p / \partial \Theta$ to obtain a fix parameter. Furthermore, we set d_{C} of the previous equation to a fixed value of 10 km. Therefore our three-dimensional K_{c} remains a simplified function of Q. For Q, we do not consider the actual diabatic heating rate but construct an idealized latent heating from observed rainfall.

We performed multiple tests for finding an appropriate formulation of the background eddy diffusivity K_{t} which mainly represents the turbulent vertical exchange of momentum in the boundary layer. Simply using climatological values derived from reanalysis models is not a sufficient solution. The reason is that the PUMA model is driven with reanalysis-derived diabatic heating rates. In this quantity, however, the effect of diffusion of heat and momentum is already implicitly included. Therefore we use the climatological spatial distribution of eddy diffusivity as provided by the MERRA-2 reanalysis (Gelaro et al., 2017), scale it by a factor of 0.1 and smooth it spatially. Multiple test simulations were performed in order to further tune the vertical diffusion field subjectively. An additional zonally-uniform zone of increased $\mathrm{K_m}$ that decreases linearly with height is included in the tropics and over the Southern hemisphere which leads to a much better representation of the winter-hemisphere jet stream. Figure 3.A1 shows an overview of the final tuned version of $\mathrm{K_m}$ in form of a zonal-mean vertical cross section and two maps showing $\mathrm{K_m}$ near the surface and in the mid troposphere.

More realistic Rayleigh friction

In the default model version, the simple linear Rayleigh friction near the surface has a globally uniform time scale which leads to unrealistically weak trade winds over oceans and too strong monsoon flow over land. Therefore, we included a simple land-sea mask based scheme such that the time scale τ_{F} of the Rayleigh friction F is shorter over land and longer over ocean. In the following formula for F, v denotes the horizontal wind vector, σ denotes the model's vertical sigma level. We select a τ_{F_O} of 2 days for the ocean and a τ_{F_O} of 0.5 days for the land.

$$F = -\frac{v}{\tau_{F_{O/L}}} \quad \text{with} \quad \tau_F = \mathrm{e}^{(10 \cdot (1-\sigma) \cdot 86400 \cdot \tau_O)}$$

3.A.2 Supplementary figures and tables

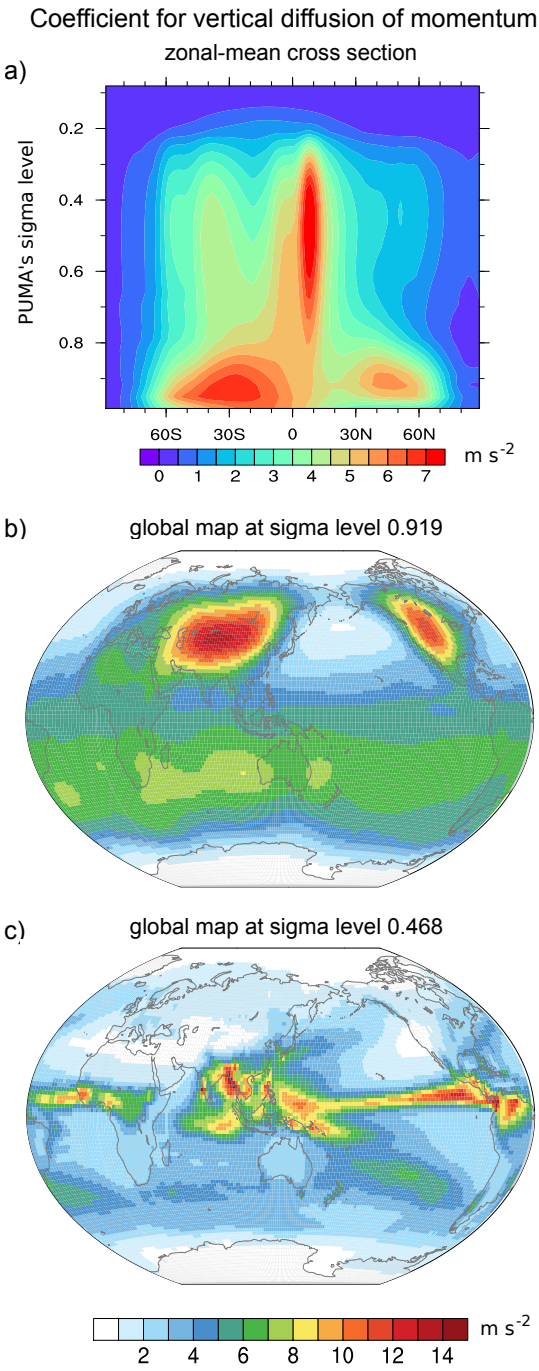

Figure 3.A1: Top: Latitude – height cross section of the coefficient for the vertical diffusion of momentum used in our PUMA simulations. Middle and bottom: Global map of the coefficient for the vertical diffusion of momentum used in our PUMA simulations at 919 and 468 hPa, respectively. All three plots depict the respective climatological mean values (1979-2017).

Table 3.A1: Pearson's r correlation coefficients and corresponding 95% confidence intervals between observed Sahel rainfall and WA-TEJ intensity for the three reanalyses ERA-Interim, NCAR-NCEP1 and ERA-40. Sahel rainfall is represented by JJAS-averaged rainfall from CRU TS3.22 precipitation data spatially averaged over 10°W to 10°E and 10°N to 20°N). The WA-TEJ intensity is derived with the following method for all three different reanalyses: Within a domain between 15°W to 15°E and 5°S to 25°N, the daily maximum of easterly 200 hPa zonal wind speed is found for each longitudinal strip of grid points. The found maximum speeds of each longitude are then averaged over the whole domain to obtain an average speed of the TEJ core. Numbers in bold denote the standard Pearson's r calculated over the stated period. Numbers in parentheses display the 95% confidence as determined by a bootstrapping with 5000 iterations.

		ERA-Interim	NCAR-NCEP1	ERA-40
1979-2013(01)	unfiltered	**0.73** (0.57-0.83)	**0.67** (0.45-0.81)	**0.67** (0.43-0.83)
	8yr-highpass	**0.65** (0.47-0.78)	**0.57** (0.33-0.74)	**0.64** (0.28-0.84)
1948-2013	unfiltered	-	**0.78** (0.66-0.86)	-
	8yr-highpass	-	**0.51** (0.33-0.67)	-
1958-2001	unfiltered	-	-	**0.51** (0.27-0.71)
	8yr-highpass	-	-	**0.50** (0.24-0.71)
1979-2013 without ENSO	unfiltered	**0.54** (-0.04-0.80)	**0.35** (-0.17-0.66)	**0.58** (-0.04-0.84)
	8yr-highpass	**0.47** (0.06-0.76)	**0.35** (0.00-0.64)	**0.38** (-0.15-0.70)

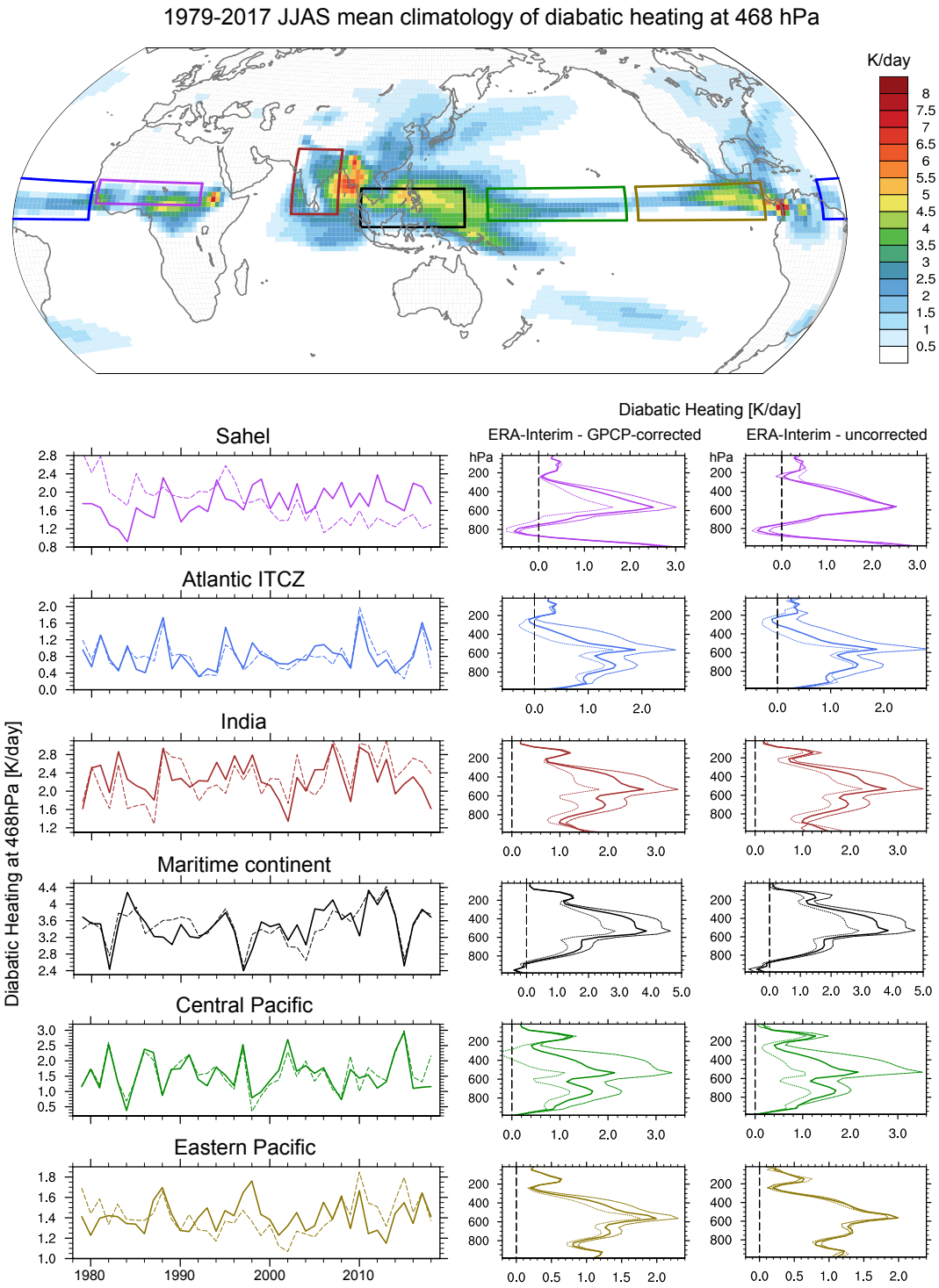

Figure 3.A2: Top: Global map of the climatological summer mean diabatic heating at 468 hPa derived from ERA-Interim output. Bottom: On the left hand side, time series of spatially averaged diabatic heating at 468 hPa are shown for the six selected tropical regions highlighted on the global map. The thin, dashed lines depict the interannual to decadal variability of the diabatic forcing as provided by ERA-Interim. The solid lines show the GPCP-corrected version used in this study. On the right hand side, vertical profiles of the diabatic heating are shown for the GPCP-corrected and original ERA-Interim derived version. The thick lines show the 40-year means, whereas the thinner lines depict the vertical profile for either the driest or the wettest year.

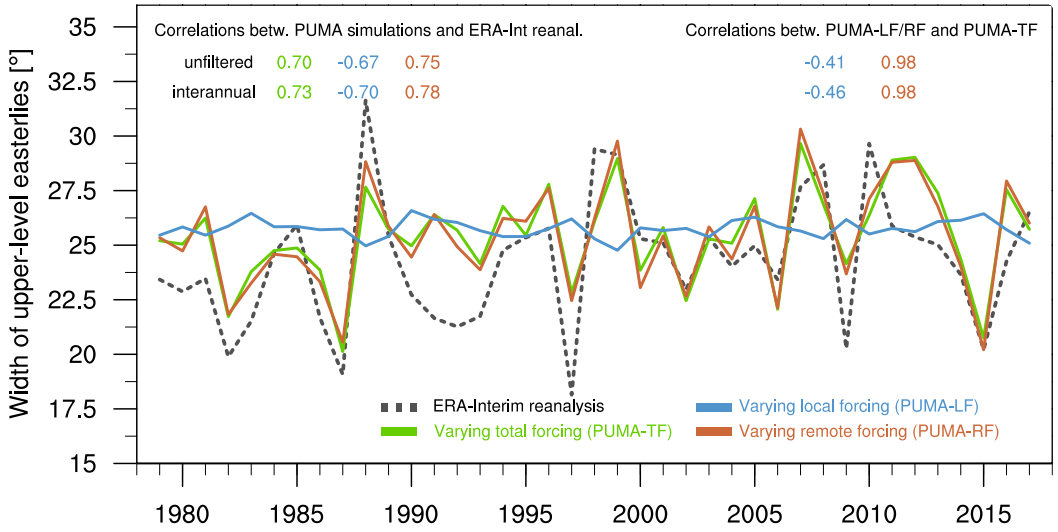

Figure 3.A3: The conducted PUMA simulations suggest that the remote forcing is the dominant driver of the interannual to decadal variability of the latitudinal width of the upper-level easterlies over West Africa. The dashed black line depicts the width of the easterlies as derived from the ERA-Interim reanalysis. The blue lines show the simulated width of the **PUMA-LF** (local forcing) simulations in which the year-to-year variability of the JJAS mean diabatic heating fields is restricted to the African region, meaning that outside of Africa, the diabatic heating is kept constant to climatological values. The red lines depict the simulated width of the **PUMA-RF** (remote forcing) simulations in which the diabatic heating is kept constant over Africa but is allowed to vary in the rest of the globe. The green line shows the results of simulations driven with the **PUMA-TF** (total forcing), in which the total (local and remote) variability of the diabatic heating is retained. All simulations were run with the same PUMA model setup with a tuned zonally-uniform relaxation temperature field in order to enforce a realistic extratropical circulation, and a simple, subjectively tuned vertical diffusion scheme that mimics the convective momentum transport. All depicted correlation coefficients (Pearson's r) are significant at the 5% level tested via bootstrapping with 5000 iterations.

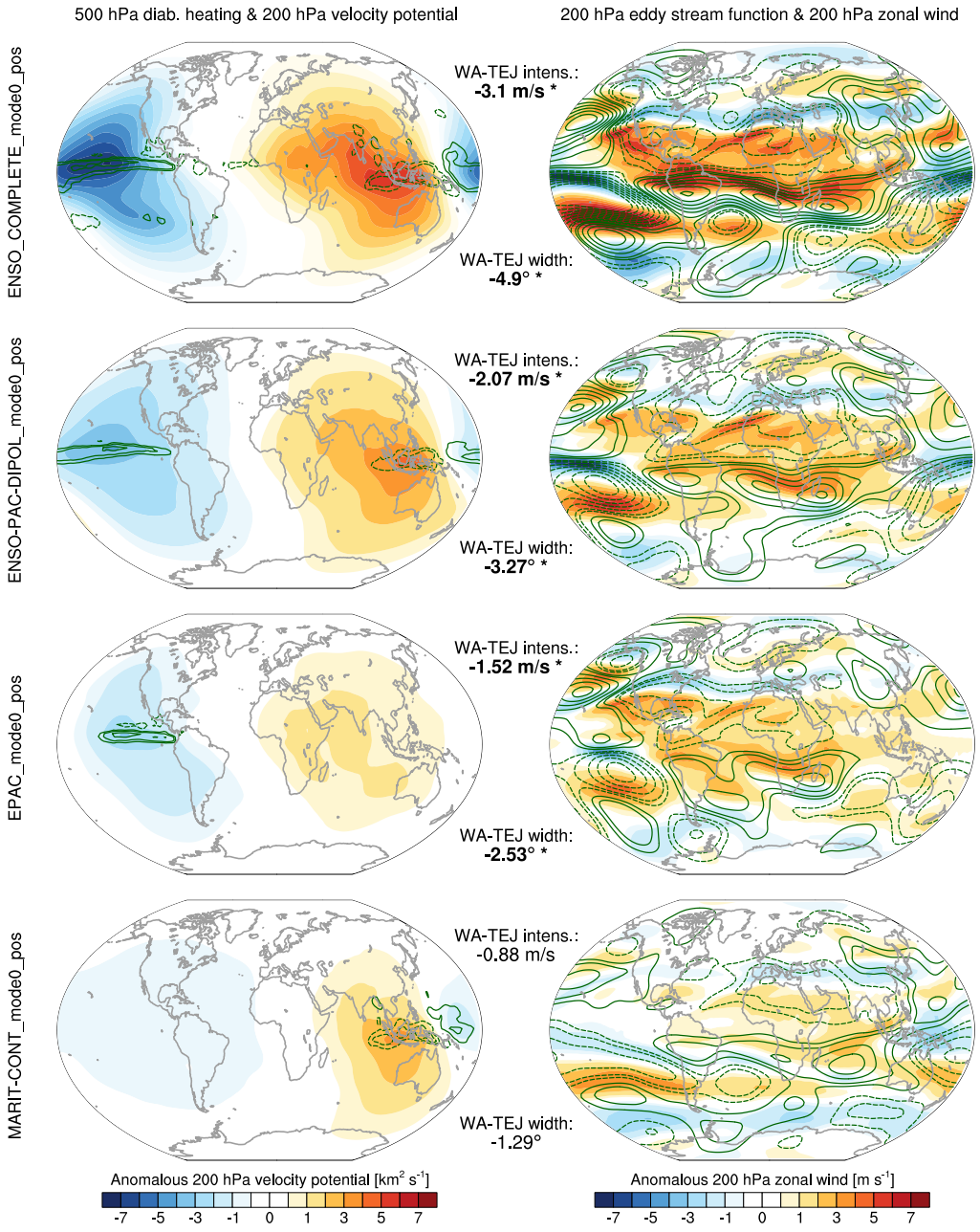

Figure 3.A4: Comparison between the full El Niño composite heating against some more regionally confined anomalous heating over the Pacific region. On the left hand side, coloured shadings show the anomalous 200 hPa velocity potential (red means anomalous convergence). Solid lines depict the imposed heating at its maximum level around 500 hPa (solid contours denote heating). On the right hand side, coloured shadings show the anomalous 200 hPa zonal wind speed. Contour lines depict the anomalies of the stationary eddy streamfunction at 200 hPa (interval 0.5 $km^2\,s^{-1}$ from -1 $km^2\,s^{-1}$ to 1 $km^2\,s^{-1}$, otherwise 1.0 $km^2\,s^{-1}$, solid lines denote positive values).

Table 3.A2: Table of all semi-idealized PUMA experiments conducted to understand the impact of different forcings on the WA-TEJ. The first part of the experiment name describes the region to which the anomalous is confined. The second part denotes the EOF mode on which the anomalies are based. The next four parameters describe the zonal/meridional centre and the semi-major and semi-minor axes of the ellipse to which the anomalies are confined. $Q_{\max}$ and $Q_{\min}$ denote the global maximum diabatic heating/cooling rate at the 0.468 model sigma level. The last column features the global integral of the absolute values of the vertically integrated heating rate which is used to measure the intensity of the heating on a global scale.

Experiment name	EOF box [°]	h_{zon} [°]	k_{mer} [°]	a [°]	b [°]	$Q_{\max}$ [K/d]	$Q_{\min}$ [K/d]	$\int \lvert \int Q\, dp \rvert\, dA$ [W]
ATLANTIC-ITCZ_mode0_pos	70W-10E; 5S-20N	40W	10N	50	20	0.48	-1.17	$5.34 \cdot 10^{19}$
ATLANTIC-ITCZ_mode0_neg	70W-10E; 5S-20N	40W	10N	50	20	0.83	-0.16	$5.36 \cdot 10^{19}$
ENSO-COMPLETE_mode0_pos	180W-180E; 30S-30N	-	-	-	-	2.77	-2.32	$4.63 \cdot 10^{20}$
ENSO-COMPLETE_mode0_neg	180W-180E; 30S-30N	-	-	-	-	2.04	-1.43	$3.31 \cdot 10^{20}$
ENSO-COMPLETE_mode1_pos	180W-180E; 30S-30N	-	-	-	-	0.98	-1.05	$2.47 \cdot 10^{20}$
ENSO-COMPLETE_mode1_neg	180W-180E; 30S-30N	-	-	-	-	1.06	-1.28	$2.61 \cdot 10^{20}$
ENSO-PAC-DIPOL_mode0_pos	65E-70W; 30S-30N	145W	5N	95	12	2.60	-2.03	$1.77 \cdot 10^{20}$
ENSO-PAC-DIPOL_mode0_neg	65E-70W; 30S-30N	145W	5N	95	12	1.39	-1.16	$1.07 \cdot 10^{20}$
MARIT-CONT_mode0_pos	90E-160E; 10S-25N	120E	5N	70	50	1.11	-1.86	$1.38 \cdot 10^{20}$
MARIT-CONT_mode0_neg	90E-160E; 10S-25N	120E	5N	70	50	1.67	-1.59	$1.48 \cdot 10^{20}$
MARIT-CONT_mode1_pos	90E-160E; 10S-25N	120E	5N	70	50	0.96	-0.95	$8.68 \cdot 10^{19}$
MARIT-CONT_mode1_neg	90E-160E; 10S-25N	120E	5N	70	50	0.64	-1.26	$1.04 \cdot 10^{20}$
EPAC_mode0_pos	140W-75W; 5S-20N	100W	7.5N	55	25	2.78	-0.78	$9.87 \cdot 10^{19}$
EPAC_mode0_neg	140W-75W; 5S-20N	100W	7.5N	55	20	0.71	-1.6	$5.68 \cdot 10^{19}$
INDIA-ALL_mode0_pos	60E-100E; 0N-35N	85E	20N	55	30	1.48	-1.21	$6.69 \cdot 10^{19}$
INDIA-ALL_mode0_neg	60E-100E; 0N-35N	85E	20N	55	30	0.87	-0.83	$4.12 \cdot 10^{19}$
SAHEL_mode0_pos	20W-45E; 5S-25N	17.5E	12.5N	55	40	0.53	-0.17	$3.05 \cdot 10^{19}$
SAHEL_mode0_neg	20W-45E; 5S-25N	17.5E	12.5N	55	40	0.11	-0.66	$3.17 \cdot 10^{19}$
SAHEL_mode1_pos	20W-45E; 5S-25N	17.5E	12.5N	55	40	0.41	-0.30	$2.02 \cdot 10^{19}$
SAHEL_mode1_neg	20W-45E; 5S-25N	17.5E	12.5N	55	40	0.62	-0.35	$1.78 \cdot 10^{19}$
SAHEL_8wettest-8driest_pos	-	-	-	-	-	2.32	-0.81	$6.02 \cdot 10^{19}$
SAHEL_8wettest-8driest_pos	-	-	-	-	-	0.81	-2.32	$6.02 \cdot 10^{19}$

Table 3.A3: Statistical relationships between PUMA-simulated WA-TEJ variability with respect to PUMA-TF and ERA-Interim. This table shows the correlations coefficients (Pearson's r), explained variance and RMSE with respective 95% confidence intervals determined by a bootstrapping method with 5000 iterations. "Unfiltered" means that the correlations, explained variances and RMSE are calculated over the unfiltered 39-year-long time series. For the interannual measure, the time series are filtered prior with a highpass-filter with a cut-off at 8 years. The term (multi-)decadal denotes a prior lowpass-filtering with a cut-off at 8 years. The abbreviation "(mul.)dec. - detr" stands for prior lowpass-filtering in combination with an additional detrending.

	PUMA-TF			ERA-Interim		
	r [ ]	$\mathrm{Var}_{\mathrm{expl}}$ [%]	RMSE [$\mathrm{m\,s^{-1}}$]	r [ ]	$\mathrm{Var}_{\mathrm{expl}}$ [%]	RMSE [$\mathrm{m\,s^{-1}}$]
PUMA-TF						
unfiltered				**0.81** (0.71-0.88)	**66.2%** (51.0-77.9%)	**1.16** (0.90-1.39)
interannual				**0.78** (0.65-0.86)	**61.2%** (42.4-74.8%)	**0.95** (0.81-1.10)
(multi-)decadal				**0.89** (0.81-0.94)	**78.6%** (64.8-87.6%)	**0.69** (0.56-0.81)
(mul.)dec. - detr.				**0.83** (0.73-0.91)	**69.3%** (53.7-82.0%)	**0.45** (0.38-0.52)
PUMA-LF						
unfiltered	**0.59** (0.33-0.77)	**34.5%** (10.6-59.3%)	**1.53** (1.22-1.83)	**0.58** (0.36-0.72)	**33.3%** (13.2-52.5%)	**1.43** (1.10-1.72)
interannual	**0.50** (0.31-0.68)	**24.7%** (9.7-45.7%)	**1.35** (1.06-1.62)	**0.46** (0.23-0.68)	**21.5%** (5.2-45.8%)	**1.26** (0.89-1.60)
(multi-)decadal	**0.76** (0.53-0.87)	**57.4%** (28.5-76.3%)	**0.77** (0.61-0.92)	**0.78** (0.62-0.87)	**60.7%** (38.4-75.5%)	**0.72** (0.55-0.86)
(mul.)dec. - detr.	**0.65** (0.37-0.82)	**41.7%** (13.3-67.6%)	**0.70** (0.59-0.81)	**0.53** (0.25-0.73)	**28.5%** (6.5-53.4%)	**0.59** (0.50-0.67)
PUMA-RF						
unfiltered	**0.95** (0.92-0.98)	**90.8%** (84.4-95.2%)	**0.55** (0.40-0.70)	**0.76** (0.63-0.85)	**57.8%** (40.1-72.6%)	**1.21** (0.94-1.45)
interannual	**0.97** (0.93-0.98)	**93.2%** (87.1-96.5%)	**0.39** (0.30-0.48)	**0.76** (0.62-0.84)	**58.1%** (38.2-71.3%)	**0.95** (0.81-1.10)
(multi-)decadal	**0.94** (0.89-0.97)	**87.9%** (79.1-93.2%)	**0.38** (0.30-0.46)	**0.77** (0.61-0.87)	**59.2%** (37.2-75.3%)	**0.77** (0.63-0.89)
(multi-)decadal	**0.97** (0.96-0.98)	**93.7%** (91.4-95.7%)	**0.22** (0.17-0.27)	**0.80** (0.69-0.88)	**63.3%** (48.0-76.7%)	**0.44** (0.37-0.51)

Bibliography

Abish, B., P. Joseph, and O. M. Johannessen (2013). Weakening trend of the tropical easterly jet stream of the boreal summer monsoon season 1950–2009. *Journal of Climate 26*(23), 9408–9414.

Adler, R. F., G. J. Huffman, A. Chang, R. Ferraro, P.-P. Xie, J. Janowiak, B. Rudolf, U. Schneider, S. Curtis, D. Bolvin, et al. (2003). The version-2 global precipitation climatology project (GPCP) monthly precipitation analysis (1979–present). *Journal of hydrometeorology 4*(6), 1147–1167.

Anderson, J. L., V. Balaji, A. J. Broccoli, W. F. Cooke, T. L. Delworth, K. W. Dixon, L. J. Donner, K. A. Dunne, S. M. Freidenreich, et al. (2004). The new GFDL global atmosphere and land model AM2–LM2: Evaluation with prescribed SST simulations. *Journal of Climate 17*(24), 4641–4673.

Bader, J. and M. Latif (2003). The impact of decadal-scale Indian Ocean sea surface temperature anomalies on Sahelian rainfall and the North Atlantic Oscillation. *Geophysical Research Letters 30*(22).

Besson, L. and Y. Lemaître (2014). Mesoscale convective systems in relation to African and tropical easterly jets. *Monthly Weather Review 142*(9), 3224–3242.

Bordoni, S. and T. Schneider (2008). Monsoons as eddy-mediated regime transitions of the tropical overturning circulation. *Nature Geoscience 1*(8), 515.

Chadwick, R., G. Martin, D. Copsey, G. Bellon, M. Caian, F. Codron, C. Rio, and R. Roehrig (2017). Examining the West African Monsoon circulation response to atmospheric heating in a GCM dynamical core. *Journal of Advances in Modeling Earth Systems 9*(1), 149–167.

Chang, E. K. (2006). An idealized nonlinear model of the Northern Hemisphere winter storm tracks. *Journal of the atmospheric sciences 63*(7), 1818–1839.

Chen, T.-C. and H. van Loon (1987). Interannual variation of the tropical easterly jet. *Monthly Weather Review 115*(8), 1739–1759.

Chen, T.-C. and M.-C. Yen (1993). The effect of planetary-scale divergent circulation on the interannual variation of the summertime stationary eddies: the tropical easterly jet. *Tellus A 45*(1), 15–27.

Dee, D., S. Uppala, A. Simmons, P. Berrisford, P. Poli, S. Kobayashi, U. Andrae, M. Balmaseda, G. Balsamo, P. Bauer, et al. (2011). The ERA-Interim reanalysis: Configuration and performance of the data assimilation system. *Quarterly Journal of the royal meteorological society 137*(656), 553–597.

Folland, C., T. Palmer, and D. Parker (1986). Sahel rainfall and worldwide sea temperatures, 1901–85. *Nature 320*(6063), 602–607.

Fraedrich, K., E. Kirk, and F. Lunkeit (1998). Portable university model of the atmosphere. *DKRZ Rep 16*.

Gelaro, R., W. McCarty, M. J. Suárez, R. Todling, A. Molod, L. Takacs, C. Randles, A. Darmenov, M. G. Bosilovich, R. Reichle, et al. (2017). The Modern-Era Retrospective Analysis for Research and Applications, Version 2 (MERRA-2). *Journal of Climate* (2017).

Giannini, A., R. Saravanan, and P. Chang (2003). Oceanic forcing of Sahel rainfall on interannual to interdecadal time scales. *Science 302*(5647), 1027–1030.

Gill, A. (1980). Some simple solutions for heat-induced tropical circulation. *Quarterly Journal of the Royal Meteorological Society 106*(449), 447–462.

Gregory, D., R. Kershaw, and P. Inness (1997). Parametrization of momentum transport by convection. II: Tests in single-column and general circulation models. *Quarterly Journal of the Royal Meteorological Society 123*(541), 1153–1183.

Grist, J. P. and S. E. Nicholson (2001). A study of the dynamic factors influencing the rainfall variability in the West African Sahel. *Journal of climate 14*(7), 1337–1359.

Held, I. M. (1999). Equatorial superrotation in Earth-like atmospheric models. *Proc. Bernhard Haurwitz Memorial Lecture*, 1–24.

Hendon, H. H. (1986). The time-mean flow and variability in a nonlinear model of the atmosphere with tropical diabatic forcing. *Journal of the atmospheric sciences 43*(1), 72–89.

Huang, B., P. W. Thorne, V. F. Banzon, T. Boyer, G. Chepurin, J. H. Lawrimore, M. J. Menne, T. M. Smith, R. S. Vose, and H.-M. Zhang (2017). Extended reconstructed sea surface temperature, version 5 (ERSSTv5): upgrades, validations, and intercomparisons. *Journal of Climate 30*(20), 8179–8205.

Janicot, S., V. Moron, and B. Fontaine (1996). Sahel droughts and ENSO dynamics. *Geophysical Research Letters 23*(5), 515–518.

Jucker, M., S. Fueglistaler, and G. Vallis (2013). Maintenance of the stratospheric structure in an idealized general circulation model. *Journal of the Atmospheric Sciences 70*(11), 3341–3358.

Kalnay, E., M. Kanamitsu, R. Kistler, W. Collins, D. Deaven, L. Gandin, M. Iredell, S. Saha, G. White, J. Woollen, et al. (1996). The NCEP/NCAR 40-year reanalysis project. *Bulletin of the American meteorological Society 77*(3), 437–471.

Kanamitsu, M. and T. Krishnamurti (1978). Northern summer tropical circulations during drought and normal rainfall months. *Monthly Weather Review 106*(3), 331–347.

Kobayashi, N. (1974). Interannual variations of tropical easterly jet stream and rainfall in South Asia. *Geophys. Mag 37*, 123–134.

Koteswaram, P. (1958). The easterly jet stream in the tropics. *Tellus 10*(1), 43–57.

Koutavas, A., P. B. Demenocal, G. C. Olive, and J. Lynch-Stieglitz (2006). Mid-Holocene El Niño–Southern Oscillation (ENSO) attenuation revealed by individual foraminifera in eastern tropical Pacific sediments. *Geology 34*(12), 993–996.

Lemburg, A., J. Bader, and M. Claussen (2019). Sahel rainfall–Tropical Easterly Jet relationship on synoptic to intraseasonal time scales. *Monthly Weather Review 147*(5), 1733–1752.

Lin, H., J. Derome, and G. Brunet (2007). The nonlinear transient atmospheric response to tropical forcing. *Journal of Climate 20*(22), 5642–5665.

Lin, J.-L., B. E. Mapes, and W. Han (2008). What are the sources of mechanical damping in Matsuno–Gill-type models? *Journal of Climate 21*(2), 165–179.

Lintner, B. R. and J. C. Chiang (2007). Adjustment of the remote tropical climate to El Niño conditions. *Journal of climate 20*(11), 2544–2557.

Nicholson, S. E. (2009). On the factors modulating the intensity of the tropical rainbelt over West Africa. *International Journal of Climatology: A Journal of the Royal Meteorological Society 29*(5), 673–689.

Nicholson, S. E. (2013). The West African Sahel: A review of recent studies on the rainfall regime and its interannual variability. *ISRN Meteorology 2013*.

Nithya, K., M. Manoj, and K. Mohankumar (2017). Effect of El Niño/La Niña on tropical easterly jet stream during Asian summer monsoon season. *International Journal of Climatology*.

Olkin, I., J. W. Pratt, et al. (1958). Unbiased estimation of certain correlation coefficients. *The Annals of Mathematical Statistics 29*(1), 201–211.

Otto-Bliesner, B. L. (1999). El Nino/La Nina and Sahel precipitation during the middle holocene. *Geophysical Research Letters 26*(1), 87–90.

Park, J.-y., J. Bader, and D. Matei (2016). Anthropogenic Mediterranean warming essential driver for present and future Sahel rainfall. *Nature Climate Change*.

Preethi, B., T. Sabin, J. Adedoyin, and K. Ashok (2015). Impacts of the ENSO Modoki and other tropical Indo-Pacific climate-drivers on African rainfall. *Scientific reports 5*.

Rao, P. K. (1952). Probable regions of jet streams in the upper air over India. *Current Science 21*(3), 63–64.

Rao, S. and J. Srinivasan (2016). The impact of latent heating on the location and strength of the tropical easterly jet. *Meteorology and Atmospheric Physics 128*(2), 247–261.

Robertson, A. W. and C. Frankignoul (1990). The tropical circulation: Simple model versus general circulation model. *Quarterly Journal of the Royal Meteorological Society 116*(491), 69–87.

Rowell, D. P. (2001). Teleconnections between the tropical Pacific and the Sahel. *Quarterly Journal of the Royal Meteorological Society 127*(575), 1683–1706.

Sardeshmukh, P. D. and B. J. Hoskins (1985). Vorticity balances in the tropics during the 1982-83 El Niñio-Southern oscillation event. *Quarterly Journal of the Royal Meteorological Society 111*(468), 261–278.

Showman, A. P. and L. M. Polvani (2010). The Matsuno-Gill model and equatorial superrotation. *Geophysical Research Letters 37*(18).

Stickler, A. and S. Brönnimann (2011). Significant bias of the NCEP/NCAR and twentieth-century reanalyses relative to pilot balloon observations over the West African Monsoon region (1940–1957). *Quarterly Journal of the Royal Meteorological Society 137*(659), 1400–1416.

Sylla, M., A. Dell'Aquila, P. Ruti, and F. Giorgi (2010). Simulation of the intraseasonal and the interannual variability of rainfall over West Africa with RegCM3 during the monsoon period. *International Journal of Climatology 30*(12), 1865–1883.

TRMM (2006). Tropical Rainfall Measuring Mission. Convective and Stratiform Heating L3 1 month 0.5 degree x 0.5 degree V6, Greenbelt, MD, USA, Goddard Earth Sciences Data and Information Services Center (GES DISC).

Uppala, S. M., P. Kållberg, A. Simmons, U. Andrae, V. D. C. Bechtold, M. Fiorino, J. Gibson, J. Haseler, A. Hernandez, G. Kelly, et al. (2005). The ERA-40 re-analysis. *Quarterly Journal of the Royal Meteorological Society: A journal of the atmospheric sciences, applied meteorology and physical oceanography 131*(612), 2961–3012.

Yang, G.-Y., J. Methven, S. Woolnough, K. Hodges, and B. Hoskins (2018). Linking African Easterly Wave Activity with Equatorial Waves and the Influence of Rossby Waves from the Southern Hemisphere. *Journal of the Atmospheric Sciences 75*(6), 1783–1809.

Zhao, Y., P. Braconnot, S. Harrison, P. Yiou, and O. Marti (2007). Simulated changes in the relationship between tropical ocean temperatures and the western African monsoon during the mid-Holocene. *Climate Dynamics 28*(5), 533–551.

Zwiers, F. W. and H. Von Storch (1995). Taking serial correlation into account in tests of the mean. *Journal of Climate 8*(2), 336–351.

4

West African Monsoon rainfall – Tropical Easterly Jet relationship during the mid-Holocene

This chapter presents ongoing work which may be intended for publication in the near future. Some of the results of this chapter may be considered preliminary and the scope of the analysis may change or be extended upon in the future.

Alexander Lemburg developed the original ideas for this paper. A. L. adapted the PUMA model for this study, conducted all numerical simulations and performed all analyses. A.L wrote the manuscript with input from Jürgen Bader.

Abstract:
During the mid-Holocene, the West African Monsoon (WAM) circulation was much more intense and extended substantially farther north than today. Moreover, model studies suggest that the TEJ, an integral upper-tropospheric feature of the WAM circulation, was much more pronounced over West Africa than today. In present-day climate, one observes a high covariability between the West African TEJ (WA-TEJ) intensity and WAM rainfall on interannual to multi-decadal time scales. However, much less is known about the relationship between the WA-TEJ and WAM rainfall during the mid-Holocene. In this study, we therefore shed light onto the mid-Holocene WA-TEJ – WAM rainfall relationship, focusing on interannual to decadal time scales. We analyse simulations conducted with the complex coupled Earth system model MPI-ESM and further employ PUMA, a much simpler AGCM based on dry dynamics, to understand the tropical drivers of WA-TEJ variability. In contrast to the pre-industrial control climate, MPI-ESM simulates for the mid-Holocene a weaker covariability between the WA-TEJ intensity and WAM rainfall, in particular in the western Sahel region. Furthermore, both the simulated variability of WA-TEJ intensity and particularly that of mid-Holocene WAM rainfall are much less linked to tropical SST anomalies than under present-day conditions. To understand the weakened WA-TEJ – WAM rainfall correlation, we explore what drives the interannual to decadal variability of the WA-TEJ under mid-Holocene conditions. For this, we force PUMA with JJAS mean diabatic heating fields taken from the previously conducted MPI-ESM simulations. For the pre-industrial control climate, the simulated WA-TEJ variability is nearly exclusively explained by the variability of the remote heating associated with tropical SST variability, particularly in the Pacific. Under mid-Holocene conditions, however, the WA-TEJ variability is no longer dominated by the remote diabatic heating but is affected in equal parts by the local heating associated with WAM precipitation. This different behaviour compared to today appears to be mainly caused by the substantially diminished importance of the remote diabatic forcing, whose amplitude and effect on West Africa is lowered mainly due to the overall reduction and changed characteristics of the interannual variability of SSTs in the tropical Pacific. We propose that the diminished importance of the remote diabatic forcing also mainly explains the simulated decrease in WA-TEJ – WAM rainfall covariability during the mid-Holocene.

4.1 Introduction

About 12 000 years ago, the last glacial period finally came to an end and heralded the beginning of the current geological and climatic epoch – the Holocene. During the mid of the epoch, some 8000 to 6000 years ago, the climate of the earth was quite alike today's conditions on a first sight. However, in this period commonly called the mid-Holocene, some remarkable climatic distinctions to the present state existed. A mixture of an increased Earth's axis tilt (obliquity) and an altered eccentricity led to a more pronounced seasonality in climate compared to today. Between 15 000 and 5000 years before present, northern hemispheric summer insolation at 20°N was elevated by about 4-8% (Berger and Loutre, 1991). This orbital climate forcing is seen as the main driver of seasonal climate changes that occurred during the mid-Holocene (Kutzbach and Guetter, 1986). One of the hot spots regarding regional climate changes was the West African Monsoon (WAM) region. Evidence in form of pollen or other proxy data suggests that WAM-related rainfall was substantially more intense and extended some 10°

farther northwards than today (Street-Perrott and Perrott, 1993; Claussen and Gayler, 1997; Jolly et al., 1998). The intensification and northward migration of monsoonal precipitation was likely amplified by feedback mechanisms involving the local vegetation and its impact on multiple surface characteristics (Claussen and Gayler, 1997). Interestingly, the so-called African Humid period (AHP) came to a rather abrupt end some 5500 years before present (Demenocal et al., 2000; Renssen et al., 2006). The southward retreat of monsoon precipitation happened at a pace that was much faster than the rather slow and nearly linear decline in orbital forcing – stressing again the likely involvement of positive feedback mechanisms. Collins et al. (2017) suggested that the Tropical Easterly Jet (TEJ) might have played a role in explaining the rapid end of the AHP.

In today's climate the TEJ is considered an integral part of the WAM circulation. The TEJ is observed in boreal summer as a distinct upper-tropospheric easterly current spanning from the Indian monsoon system towards the Atlantic. Observations and model studies show that the intensity of the TEJ over West Africa (WA-TEJ) is strongly correlated with monsoonal rainfall over West Africa, in particular with that over the Sahel (Grist and Nicholson, 2001; Sylla et al., 2010). Recent studies have investigated the possible causes and also tackled the important question of cause and effect. Some scholars have attributed the TEJ an active role for rainfall through its control on the large-scale upper-level divergence (Nicholson, 2009; Besson and Lemaître, 2014). Lemburg et al. (2019) have shown, however, that the WA-TEJ – Sahel rainfall relationship is much weaker on subseasonal time scales. More importantly, increased convective activity was shown to lead changes in the WA-TEJ, not vice versa, and neither the initiation nor the organization of mesoscale convective systems are significantly affected by WA-TEJ-induced anomalous divergence. In a follow-up study, Lemburg and Bader (2020, in prep., see chapter 3 of this thesis) aimed to understand the causes of the high WA-TEJ – Sahel rainfall relationship observed over the last 40 years by investigating the tropical drivers of the WA-TEJ variability. They found that the variability of the WA-TEJ intensity is mainly explained by remote influences, i.e., changes of the planetary-scale tropical circulation induced by anomalies of the remote diabatic heating. This complicates the interpretation of the WA-TEJ – Sahel rainfall relationship. Even though there are apparently still gaps in our understanding for the present-day climate, much less is known about the role of the WA-TEJ during the mid-Holocene.

Coming back to the possible contribution of the WA-TEJ in causing the abrupt end of the AHP, we think it would be valuable to first ask some basic questions about the relationship between the WA-TEJ and WAM rainfall during the mid-Holocene. Is the spatio-temporal relationship between WA-TEJ intensity and WAM rainfall on interannual to decadal time scales similar to the present-day climate? What is the role of remote influences? Some compelling evidence from climate proxies and coupled model results suggest that the WAM was generally less affected by teleconnections as a consequence of attenuated tropical SST variability (Otto-Bliesner, 1999; Koutavas et al., 2006; Zhao et al., 2007). This may then also have affected the variability of both WAM rainfall and the WA-TEJ as well as the correlation between both quantities. We therefore think it is of interest to characterize the WA-TEJ – WAM rainfall relationship during the mid-Holocene to further our understanding and explore possible differences to the

present-day state. To our best knowledge, there has been no extensive study yet of the WA-TEJ and its connection to WAM rainfall during the mid-Holocene.

In this study, we therefore use the state-of-the-art coupled Earth system model MPI-ESM to investigate the WA-TEJ – WAM rainfall relationship during the mid-Holocene. Using 60-year long simulations of the mid-Holocene and pre-industrial climate, we characterize the interannual to decadal variability of the WA-TEJ and its connection to monsoonal rainfall under mid-Holocene conditions and draw a comparison to the simulated present-day climate. Moreover, we explore how both the WA-TEJ and WAM rainfall are connected to global SST anomalies under mid-Holocene conditions and whether marked differences to today's climate exist. In a second part of this study we concentrate on what are the tropical drivers that explain the interannual to decadal variability of the WA-TEJ. Is the remote diabatic heating still a dominant forcing as in today's climate or does the local forcing associated with WAM rainfall become more important during the mid-Holocene? To answer this question we conduct in addition simulations with PUMA, an AGCM based on dry dynamics and very simple physics. In these simulations we use the diabatic heating fields derived from the previously conducted MPI-ESM simulations and split them up geographically into an African and rest of globe part. By restricting the year-to-year variability of the diabatic heating only to either the local or remote part, we are able to disentangle the main drivers of WA-TEJ variability.

4.2 Methods

4.2.1 MPI-ESM fully coupled simulations

For this study, we use daily output of 60-year long excerpts of existing fully coupled mid-Holocene and pre-industrial control simulations conducted with the complex earth system model MPI-ESM 1.2 (Giorgetta et al., 2013) in LR mode. In this mode (LR = low resolution), the atmospheric module ECHAM is characterized by 47 vertical levels and the spectral resolution T63 which translates to a spatial resolution of about 2° in grid point space. The ocean is represented by MPIOM (Jungclaus et al., 2013) in GR15 resolution (corresponding to 1.5°) and land surface processes are handled by JSBACH (Raddatz et al., 2007; Reick et al., 2013).

For the mid-Holocene simulation (henceforth abbreviated as MPIESM-MH), multiple orbital parameters and atmospheric gas concentrations were prescribed to values which best represent mid-Holocene conditions according to multiple reconstructions. The simulation features a quasi-equilibrium mid-Holocene vegetation distribution that has fully adapted to the changes in climate. In addition, the impact of corresponding soil carbon changes on albedo is modelled with an interactive background albedo scheme (Vamborg et al., 2011). The ocean component has been sufficiently spun-up such that the climate state can be considered to represent a quasi-equilibrium climate state at 8000 years before present. More details for the setup of the model are available in Brovkin et al. (2019, see setup of the simulation 8KAF).

As a control simulation representing today's climate, we use a pre-industrial control simulation in which most model parameters are equal to the CMIP5 protocol. In

contrast to the CMIP5 model version, the model's land hydrology in JSBACH has been updated and the aforementioned dynamic soil carbon scheme is included to be consistent with the mid-Holocene simulation. For this study, the pre-industrial control simulation will be referred to with the acronym MPIESM-PI.

4.2.2 Dedicated PUMA simulations

In addition to the complex, fully-coupled ESM simulations with MPI-ESM, we conduct numerical experiments with PUMA, a spectral AGCM based on dry dynamics with very simple physics (Fraedrich et al., 1998). The aim of these simulations is to understand the dominant tropical drivers of the WA-TEJ variability on interannual to decadal time scales. We want to understand whether the TEJ variability is mainly driven by the local forcing due to the WAM-related anomalous heating or more by remote forcing due to any anomalies in the large-scale tropical diabatic heating outside of Africa.

The PUMA model is set up in the same way as in Lemburg and Bader (2020, in prep., see chapter 3 of this thesis): PUMA is run in a spectral T63 resolution (1.85°, ≈200 km) with 31 vertical levels. The vertical coordinate is a terrain-following sigma coordinate with equally spaced sigma levels from 0.984 to the model top at 0.016. The model is forced by time-constant 3D diabatic heating fields. An additional Newtonian cooling towards a previously tuned zonally-uniform relaxation temperature field with a globally-uniform time scale of 30 days ensures a realistic "background circulation" in the extratropics (including mid-latitude jets and baroclinic eddies). The only difference to the setup described in Lemburg and Bader (2020, in prep., see section 3.2 of this thesis) is an altered zonally-uniform relaxation temperature which was tuned in multiple iterative steps for both the simulated mid-Holocene and the simulated pre-industrial control climate starting from a standard Held-Suarez profile (see Fig. 4.A1). Moreover, the 3D vertical diffusion field is slightly different due to changes in rainfall. The 3D diabatic heating used as a forcing is directly derived from model output of the previously conducted MPI-ESM simulations. For each of the 60 simulated monsoon seasons, we first calculate a JJAS mean diabatic heating by summing up and temporally averaging all temperature tendency terms from the extended MPI-ESM diagnostics output. In a final step, the JJAS mean heating fields are vertically interpolated from MPI-ESM's 47 hybrid levels to PUMA's 31 sigma levels. The obtained 3D heating fields of each respective monsoon season are then read into the PUMA model as a constant thermal forcing which is applied at each time step.

To unravel the tropical drivers of WA-TEJ variability, we conduct a suite of experiments that is virtually identical to one of the main experiment suites in Lemburg and Bader (2020). Three experiments are designed as follows: In the first control experiment, so-called PUMA-TF, the interannual to decadal variability of the TEJ is simulated as realistically as possible by letting the total global JJAS mean diabatic heating field vary from year to year. In the other two experiments, we restrict the variability of the diabatic heating to either the local (African) or remote (rest of world) part. This allows us to disentangle the interannual to decadal TEJ variability into a locally-driven and remotely-driven part. To do this, we geographically split the global diabatic heating field into a local and remote part. In our so-called remote forcing simulations (PUMA-RF), the remote forcing patterns are let to vary from year to year while the local forcing

over West Africa is held constant at climatological values. Local forcing simulations (PUMA-LF) are set up vice versa, such that the remote forcing is held constant and only the WAM-related diabatic heating over Africa changes from year to year. An exemplary depiction of the diabatic heating fields arising from this method is given in Lemburg and Bader (2020, see chapter 3, Fig. 3.2). These experiments are conducted for both the mid-Holocene and for pre-industrial period such that we end up with 6 experiments each encompassing 60 individually simulated monsoon seasons. The naming convention is as follows: The abbreviation of the climate period, either MH or PI, will be inserted between PUMA and the handling of the diabatic forcing. PUMA-MH-LF, for instance, refers to the PUMA experiment in which the variability of the mid-Holocene diabatic heating is restricted to the local African region.

For each experiment and each simulated monsoon season thereof, the model is run for 6 simulated years to obtain robust estimates of the quasi-equilibrium response to the fixed diabatic forcing. A more or less steady state is generally reached after some 150 - 200 days. Therefore, we consider the first year as model spin-up and only calculate averages over the last 5 integration years.

4.2.3 Statistical analyses

Measuring summer mean TEJ intensity

We measure the summer mean intensity of the WA-TEJ by calculating a temporal and zonal average of the core velocity of the TEJ. Simply calculating the spatial average of the seasonally-averaged 200 hPa zonal wind over a certain area in West Africa would not be fully sufficient to capture the WA-TEJ intensity because the TEJ core latitude tends to shift over the course of a season. We therefore use a more sophisticated method to characterize the summer mean intensity of the WA-TEJ: we use daily-averaged model output of easterly 200 hPa zonal wind and search for the maximum easterly wind speed at each longitudinal strip over the whole of West Africa. Then we zonally average the found jet core velocities from 15°W to 15°E. Afterwards, the zonally-averaged WA-TEJ intensity is temporally averaged over the monsoon season which we define as comprising of June, July, August and September (JJAS) for both the mid-Holocene and the present-day climate. The described method is applied identically to both MPI-ESM and PUMA output.

Correlation analysis

The linear relationship between the summer mean (JJAS) WA-TEJ intensity thus obtained and global precipitation is explored by means of the standard Pearson's correlation. In addition, correlations maps with respect to global SST anomalies are presented for both, WA-TEJ intensity and Sahel rainfall. The focus for this analysis is set on the interannual time scale which is defined as the 8-year highpass-filtered signal. Statistical significance of the linear relationships is tested via a student t-test that takes into account the reduction in the degrees of freedom due to autocorrelation (Zwiers and Von Storch, 1995).

4.3 Simulated mid-Holocene TEJ and WAM rainfall climatology

In this section we briefly describe the MPI-ESM-simulated climatology of the mid-Holocene and compare it with the pre-industrial control simulations. The focus is set on highlighting the main differences in the planetary-scale upper-level circulation of the tropics and changes in WAM rainfall and WA-TEJ intensity and position.

Figure 4.1 characterizes the simulated climatological planetary-scale upper-level circulation for both the mid-Holocene and the pre-industrial period by depicting the JJAS mean velocity potential, eddy streamfunction and total wind vectors at 200 hPa. The velocity potential outlines the large-scale centres of upper-level divergence and convergence whereas the eddy streamfunction provides useful information about the position and intensity of stationary eddies. Two main differences become evident when comparing MPIESM-MH to MPIESM-PI: First, in MPIESM-MH the planetary-scale centre of upper-level divergence moves westwards by some degrees. A divergent branch extends all the way to West Africa which signals the much stronger WAM over West Africa during the mid-Holocene. Second, the WAM in MPIESM-MH is characterized by a distinct monsoon anticyclone that nearly reaches the strength of the Asian monsoon anticyclone over the Tibetan plateau. The distinct changes in the upper-tropopsheric tropical circulation – the shift of the divergent centres and the emergence of a pronounced WAM anticyclone – are further accompanied by changes in the extratropics. Due to the warming of the Northern Hemisphere, the summer mean extratropical jet in the northern hemisphere is shifted polewards by some 2° and slightly weakened by some 1 $m\,s^{-1}$ on zonal average. A very similar poleward shift and a comparable slight weakening is also present on the southern-hemispheric winter-time jet (not shown).

Figure 4.2 zooms in on the simulated climatological WAM precipitation as well as the latitudinal position and intensity of the TEJ core. As expected, MPIESM-MH simulates a northwards extension and a general intensification of WAM rainfall over large parts of North Africa. Whereas the 3 $mm\,d^{-1}$ isohyet does not surpass 16°N in MPIESM-PI, it reaches up to 23°N in the Western Sahel and 18°N at the Red Sea coast in MPIESM-MH. Compared to proxy data, the northward extent might be underestimated, though – a problem that is common among most complex earth system models (Braconnot et al., 2007; Harrison et al., 2014). To characterize the rainfall intensity changes, we calculate spatial rainfall averages for two regions: first, an often used box in the western Sahel that is spanning the longitudes 15°W to 15°E and the latitudes 10°N to 20°N. A second box is tailored to capture the distinct extension of rainfall to the northeast. We characterize northeastern Sahel rainfall by averaging over a box spanning from 0°E to 30°E and 12°N to 25°N. In the western Sahel, JJAS mean rainfall amounts to 8.35 $mm\,d^{-1}$ in MPIESM-MH which is nearly a tripling compared to the value obtained for MPIESM-PI (2.96 $mm\,d^{-1}$). The ratio becomes even higher for the northeastern Sahel where MPIESM-MH simulates 3.52 $mm\,d^{-1}$ and MPIESM-PI only 1.0 $mm\,d^{-1}$. It has to be stressed that the fully-coupled MPI-ESM in T63 resolution is plagued by a bias in maritime precipitation that is particularly pronounced in MPIESM-PI. The overestimation of rainfall off the coast of West Africa is related to warm biases in the regional SSTs which may be ultimately attributable in large parts to the rather

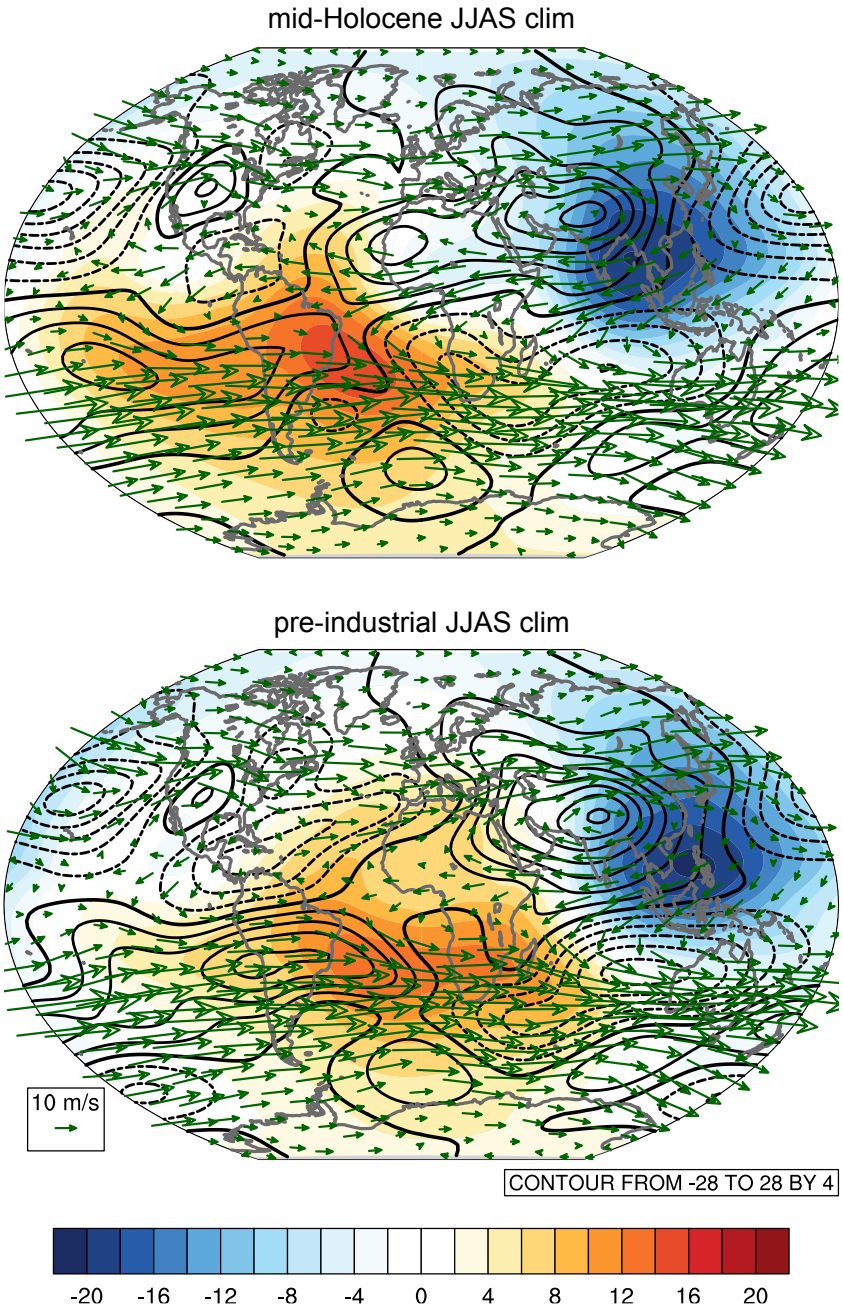

Figure 4.1: Comparison of the MPI-ESM-simulated planetary-scale upper-level circulation between mid-Holocene and present-day climate. The planetary-scale centres of upper-level convergence and divergence, which characterize the tropical overturning circulation, are shown with the help of the 200 hPa velocity potential (coloured shadings, unit $km^2\,s^{-1}$, blue denotes divergence). Contour lines depict the stationary eddy streamfunction at 200 hPa (interval 4 $km^2\,s^{-1}$, solid lines denote positive values). Dark green vectors represent the total circulation at 200 hPa.

coarse model resolution (Milinski et al., 2016; Müller et al., 2018). The too high precipitation over the ocean between 0°N and 5°N might also exert a braking effect on the TEJ via an increase of convective momentum transport which tends to act as vertical diffusion on large scales (Gregory et al., 1997; Lin et al., 2008). The simulated climatological WA-TEJ intensity in MPIESM-PI is in fact smaller compared to what reanalyses show

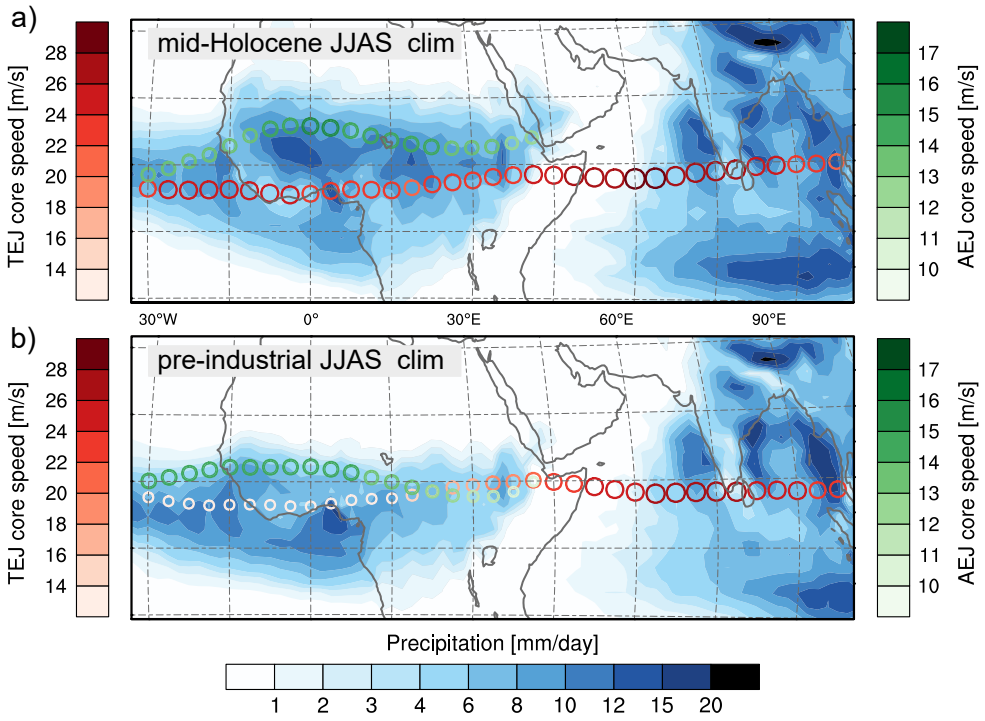

Figure 4.2: 60-year JJAS mean rainfall and TEJ climatology in a fully coupled MPI-ESM mid-Holocene control (a) and pre-industrial control (b) simulation. The climatological position and intensity of the TEJ (depicted by reddish circles) was derived by finding the daily jet core maximum for each longitudinal strip on the basis of daily model output of zonal wind at 200 hPa. The same method was applied to zonal wind at 600 hPa to find the climatological position and intensity of the AEJ which is depicted by greenish circles.

for the recent four decades. Whereas MPIESM-PI simulates a climatological intensity of 12.9 m s^{-1}, ERA-Interim climatology from 1979-2017 gives 15.1 m s^{-1}. For the mid-Holocene, MPIESM-MH simulates a WA-TEJ intensity of 24.1 m s^{-1} which is nearly a doubling compared to MPIESM-PI. As evident from figure 4.2, the pronounced TEJ intensification is mainly restricted to the African branch of the TEJ and not found over the Indian monsoon system. The climatological latitudinal position of the WA-TEJ core remains nearly unchanged with only a slight southwards shift in MPIESM-MH compared to MPIESM-PI (from 6.7°N to 6.0°N).

4.4 TEJ intensity – WAM rainfall relationship in MPI-ESM simulations

Figure 4.3 depicts the interannual to (multi-)decadal variability of the WA-TEJ intensity (red lines) and Sahel rainfall (blue lines) for the simulated mid-Holocene climate (Fig. 4.3a,b) and the pre-industrial control climate (Fig. 4.3c). The statistical relationship between both quantities is quantified by a 21-year running correlation (green lines). For the pre-industrial climate, MPIESM-PI simulates a very high and statistically significant correlation between western Sahel rainfall and WA-TEJ intensity which is irrespective of the time scale and the selected region over which rainfall is spatially averaged. Over the total 60 simulated years, the unfiltered correlation amounts to 0.77. A bootstrapping procedure with 5000 iterations yields a 95% confidence interval ranging from 0.64

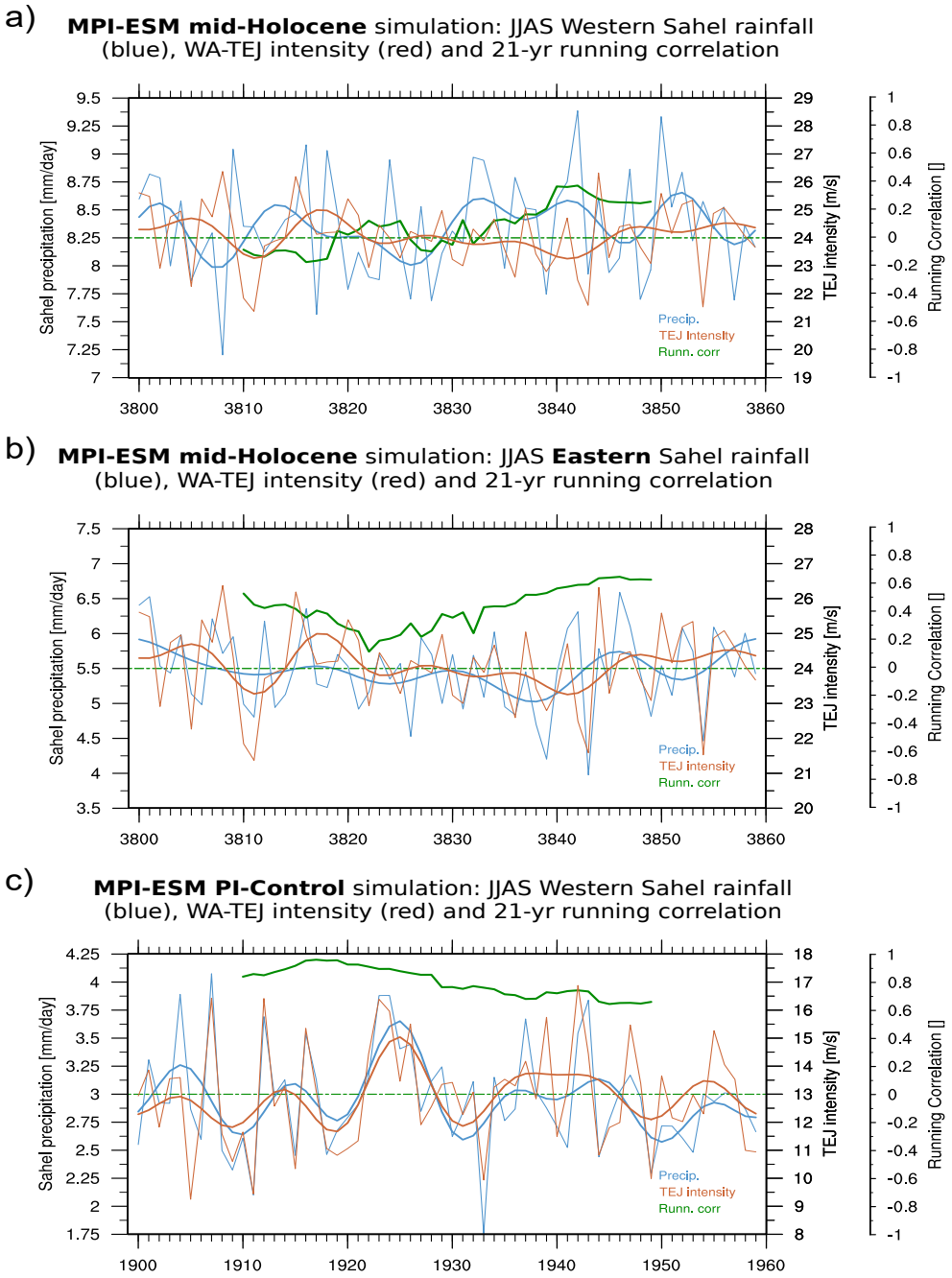

Figure 4.3: 60-year time series of simulated JJAS mean Sahel precipitation and WA-TEJ intensity, and running correlations between both quantities for the mid-Holocene (a,b) and the pre-industrial control climate (c). The difference between a) and b) is the region over which Sahel rainfall is averaged: for a) the western Sahel, rainfall is averaged over 15°W to 15°E and 10°N to 20°N whereas for b) the eastern Sahel, rainfall is averaged over 0°E to 30°E and 12°N to 25°N. For a representative WA-TEJ intensity measure that is insensitive to latitude changes, the average JJAS TEJ core speed was calculated from daily output of 200 hPa zonal wind data as follows: Within a domain between 15°W to 15°E, the daily maximum of easterly 200 hPa zonal wind speed is found for each longitudinal strip of grid points. The found maximum speeds of each longitude are then averaged over the whole domain to obtain an average speed of the TEJ core). Thin, light lines depict the unfiltered yearly means. Thick lines show the 10-year low pass filtered time series. The green lines depict the 21-year running correlations. Please note that the years displayed on the x-axis represent an arbitrary selection with no relation to the real calendar years and therefore only serve as orientation.

to 0.86. After highpass-filtering the time series with a cut-off at eight years, we obtain a very similar correlation for the interannual time scale (0.76). When precipitation is averaged over the northeastern Sahel region, both unfiltered and the interannual correlation remains high at 0.75 and 0.76, respectively.

A fundamentally different picture emerges for the simulated statistical relationship during the mid-Holocene. If the same averaging box for western Sahel rainfall is used, the correlation between WA-TEJ intensity and rainfall drops to an insignificant value of 0.06 in MPIESM-MH (0.1 on the interannual time scale). However, if we shift the spatial averaging box to the northeastern Sahel, the correlation rises to 0.54 and becomes statistically significant again (95% confidence interval: 0.33-0.71). The strength of the WA-TEJ – rainfall relationship remains nonetheless substantially below what is simulated for the modern climate, though.

Another important observation to gather from figure 4.3 is the unexpectedly low interannual to decadal variability simulated in MPIESM-MH for both Sahel rainfall and the WA-TEJ intensity. The standard deviation of JJAS mean rainfall in the western Sahel is the same in MPIESM-MH as in MPIESM-PI although the climatological rainfall amount is nearly threefold. For the WA-TEJ intensity, MPIESM-MH even simulates a drop in the standard deviation, from 1.82 m s^{-1} in MPIESM-PI to 1.15 m s^{-1}. It should be kept in mind, however, that we have just discussed the variability of area-averaged rainfall. When one first calculates the temporal variability grid point-wise and take the spatial average afterwards, the result changes. The thus obtained alternative measure of rainfall variability would be substantially higher during the mid-Holocene than today (see next section).

To better understand the simulated attenuation of the TEJ – WAM rainfall relationship during the mid-Holocene, we investigate first how the correlation between the WA-TEJ intensity and global precipitation changes compared to today's climate. In a further step, we examine how both Sahel rainfall and the WA-TEJ intensity are connected to SST anomalies, respectively. For these analyses, we focus exclusively on the interannual time scale because of the low decadal variability within the 60 simulated years. Figure 4.4a depicts point-wise linear correlation coefficients between the WA-TEJ intensity and the global precipitation field for MPIESM-MH and MPIESM-PI. What immediately catches the eye is the reduction in correlations all over the globe that is simulated for the mid-Holocene. In MPIESM-PI, the WA-TEJ intensity is strongly correlated ($r > 0.75$) with the local WAM rainfall, but also with rainfall over parts of the Indian monsoon region and over the tropical Pacific. In the simulated mid-Holocene climate, however, correlations do not surpass 0.6 anywhere. Particularly strong reductions in correlation strength are found over India and the tropical Pacific. Another distinct change is evident over West Africa. Whereas in MPIESM-PI, the correlation between WA-TEJ intensity and rainfall is high over all parts of the Sahel region, it drops to zero over parts of the westernmost Sahel in MPIESM-MH. Negative correlations that exist only near the Guinean coast in the present-day climate spread northwards reaching parts of the western Sahel. This observation supports what already has become evident in the time series analysis where the correlation depends on the choice of the spatial averaging: in the simulated mid-Holocene climate, the "centre of action" in the spatio-temporal TEJ – rainfall relationship (the region over which rainfall is highly cor-

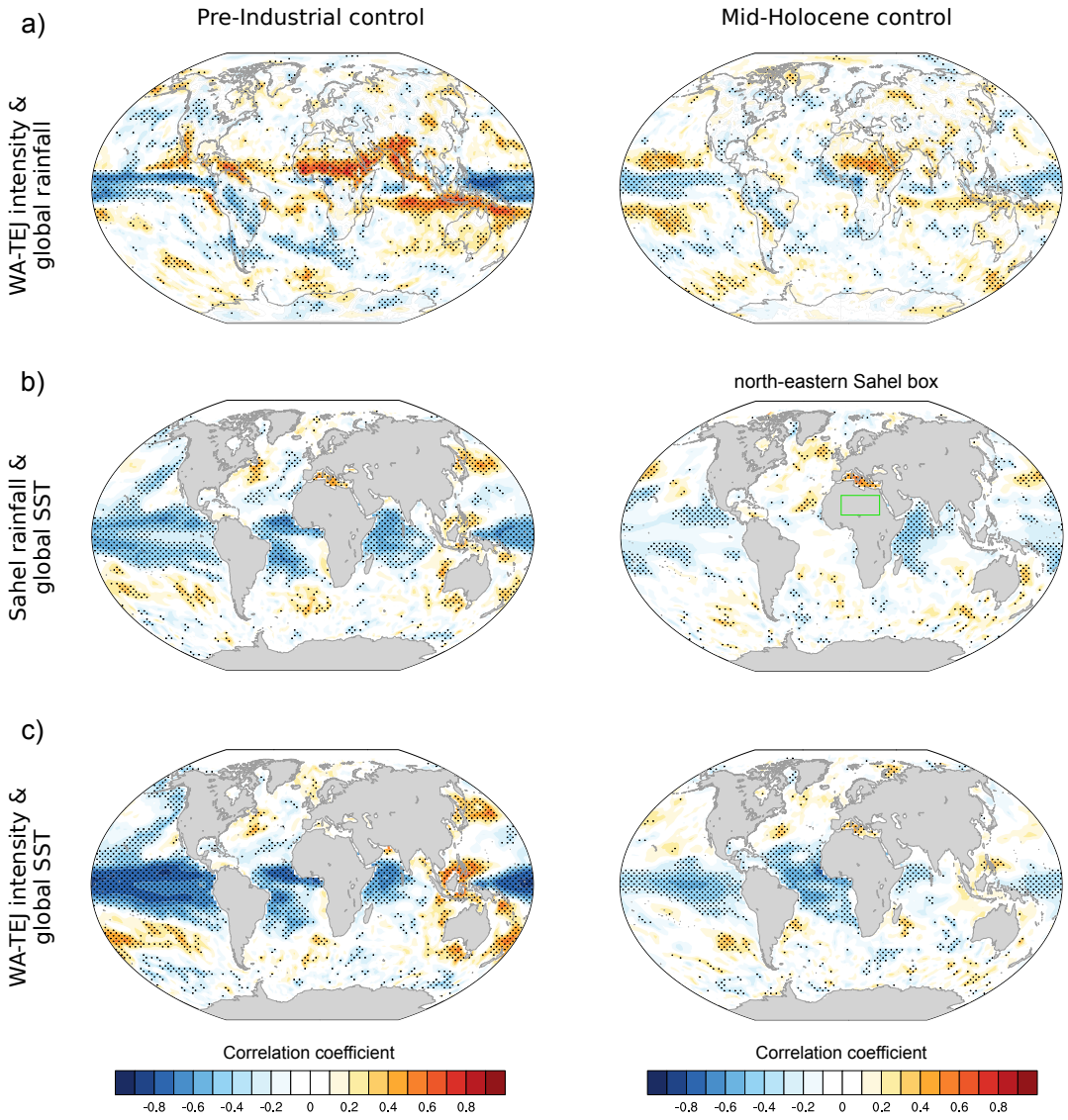

Figure 4.4: a) Linear point-wise correlations between the WA-TEJ intensity and global rainfall on interannual time scales in MPIESM-PI (left) and MPIESM-MH (right). b) Linear point-wise correlations between Sahel rainfall and global SST anomalies. For MPIESM-PI, Sahel rainfall is represented by a field mean in a box over 15°W to 15°E and 10°N to 20°N whereas for MPIESM-MH, Sahel rainfall is averaged over 0°E to 30°E and 12°N to 25°N. c) Linear point-wise correlations between WA-TEJ intensity and global SST anomalies. For both simulations, the WA-TEJ intensity represents a TEJ core mean velocity 15°W to 15°E that is derived from daily model output via the method explained in the Methods section.

related to WA-TEJ intensity) moves substantially to the northeast.

Figure 4.4b shows that WAM rainfall in MPIESM-PI is strongly associated with tropical SST anomalies in all ocean basins. Both a cooling of the tropical Pacific and a cooling of the Indian Ocean go along with increased Sahel rainfall. During the mid-Holocene, however, Sahel rainfall seems to be more or less decoupled from tropical SST anomalies. For the northeastern Sahel, some significant correlation is still found to SSTs in the western Indian Ocean. Similarly, western Sahel rainfall is also affected much less by tropical SST anomalies. In contrast to MPIESM-PI, positive correlations appear in parts

of the northern tropical Atlantic and the gulf of Guinea (not shown). The only clear common feature between MPIESM-PI and MPIESM-MH is the simulated substantial positive correlation between Sahel rainfall and SSTs in the Mediterranean Sea.

In contrast to the Sahel rainfall – SST relationship, less marked differences exist in the statistical connection between the WA-TEJ intensity and remote SSTs (Fig. 4.4c). Both the pre-industrial and the mid-Holocene state are characterized by substantial negative correlations between WA-TEJ intensity and tropical SSTs. The strength of the statistical relationship, however, is overall substantially lower in the simulated mid-Holocene climate, particularly in the tropical Pacific.

In summary, the conducted analyses stress that both the WA-TEJ intensity and in particular WAM rainfall are less associated with remote SST anomalies in the simulated mid-Holocene climate. We suppose that there are two possible hypotheses why teleconnections may had been less important in the mid-Holocene than today. First, one could assume that the much stronger WAM was generally less affected by remote influences, likely through changes in the background circulation or the increased importance of more locally confined forcings. Another likely reason is the overall attenuation of the remote forcing compared to today which might be a direct consequence of an altered tropical SST variability. In the next section, we therefore take a closer look at the changes in tropical SST variability that are simulated for the mid-Holocene in comparison to the present-day climate.

4.4.1 The role of tropical SST variability

Previous studies, either based on the analysis of climate proxies or complex earth system models, suggested that the SST variability of the tropical Pacific was attenuated during the mid-Holocene (Otto-Bliesner, 1999; Zhao et al., 2007). In particular today's dominant mode of interannual SST variability – ENSO – was likely weaker during the mid-Holocene (McGregor and Gagan, 2004; Koutavas and Joanides, 2012; Karamperidou et al., 2015). The conducted MPI-ESM simulations confirm this hypothesis. Figure 4.5 depicts the interannual to multi-decadal variability of tropical SST in form of the standard deviation calculated over the unfiltered 60 years of the conducted simulations. Whereas MPIESM-PI depicts a clear local maximum in the typical El Niño/La Niña region, MPIESM-MH simulates a much weaker SST variability for large parts of the tropical Pacific. In the western parts of the tropical Pacific, the depicted differences in SST standard deviation are statistically significant at the 5% level according to a standard f-test.

Does this significant reduction in SST variability also lead to significantly altered precipitation variability and therefore changes in the variability of the remote diabatic heating? Figure 4.6 depicts analogue to figure 4.5 the standard deviation over the 60 simulated years in MPIESM-MH and MPIESM-PI, now for tropical rainfall. Even without looking at the difference plot, it is immediately noticeable that the mid-Holocene precipitation variability is substantially suppressed over the western Pacific (Fig. 4.6a). An increase in rainfall variability, in turn, is observed over parts of the tropical Indian Ocean and especially over Northern Africa – in the northern Sahel region where the substantial rainfalls have extended to in the mid-Holocene. However, one has to be cautious when interpreting the changes in rainfall variability shown in figure 4.6c. As

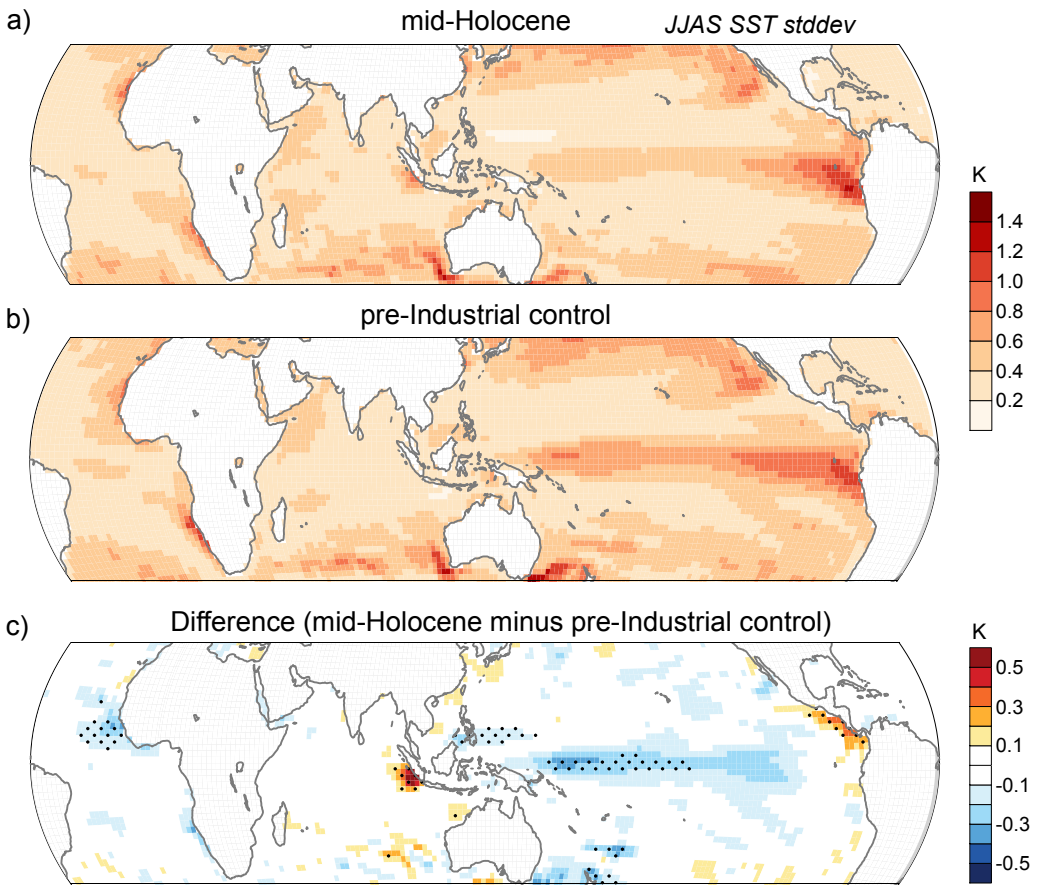

Figure 4.5: Tropical SST variability depicted in form of the JJAS mean standard deviation of 60 simulated years for a) the mid-Holocene simulation MPIESM-MH and b) the pre-industrial control simulation MPIESM-PI. The tropical SST variability difference between the mid-Holocene and the pre-industrial climate is depicted in c) where statistically significant differences in standard deviation according to a standard F-test are highlighted by dots.

mentioned in the previous section (and evident from figure 4.3), the actual *large-scale* rainfall variability over Africa is not higher during the mid-Holocene (i.e., when rainfall is averaged over a larger area prior to the calculation of the standard deviation). We therefore calculate in addition the standard deviation of area-averaged precipitation in the Western Pacific region (over 130°E–180°E and 10°S–10°N). In contrast to West Africa, one nonetheless obtains a robust change in rainfall variability also when taking the spatial average first: 0.62 mm d^{-1} for the mid-Holocene versus 1.27 mm d^{-1} for the present-day climate. Therefore, the diminishing of year-to-year rainfall variability in the western Pacific is concomitant with a spatially coherent large-scale reduction of the amplitude of the respective annual rainfall anomalies in this region. This finding might have implications for the WA-TEJ variability in the mid-Holocene. One has to keep in mind that the interannual to decadal variability of the present-day WA-TEJ is dominated by the variability of the remote diabatic forcing (Lemburg and Bader, 2020). A reduction of large-scale precipitation variability in the western Pacific is synonymous with an attenuation of the remote forcing. It is therefore conceivable that the WA-TEJ variability during the mid-Holocene is less controlled by remote forcings compared to today. In the next section, this hypothesis will be tested.

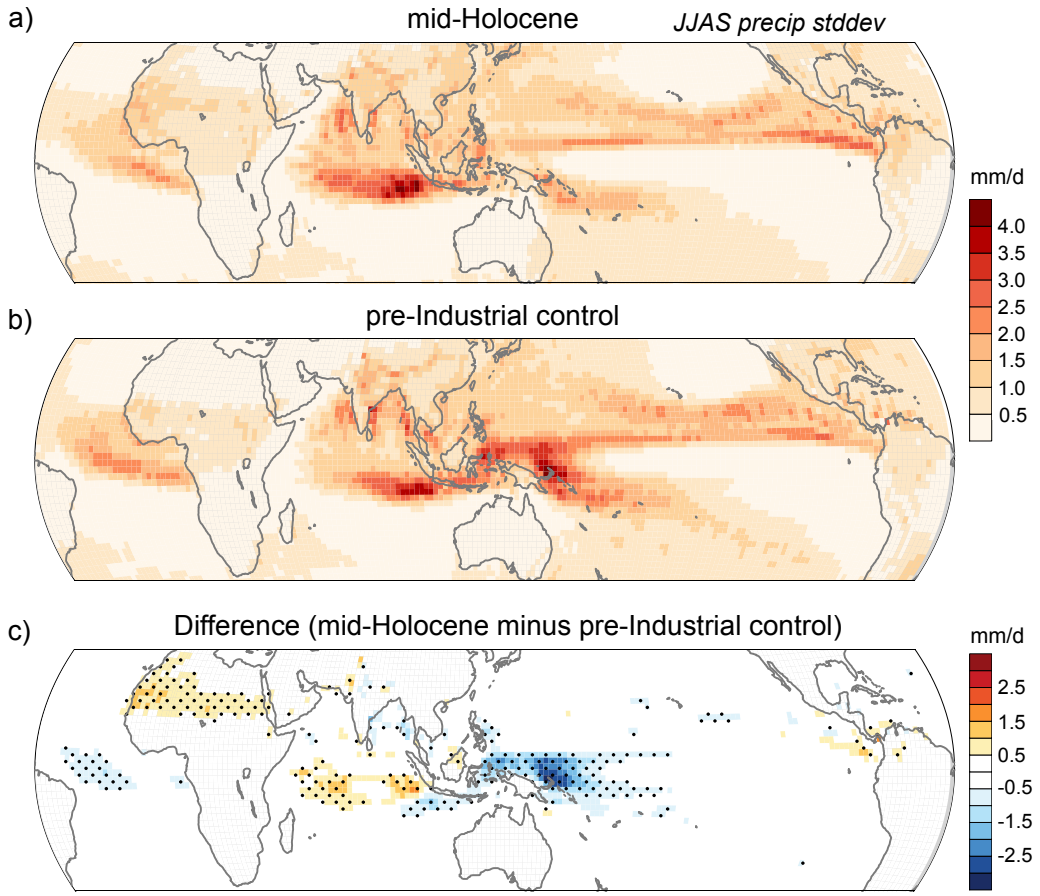

Figure 4.6: Tropical precipitation variability depicted in form of the JJAS mean standard deviation of 60 simulated years for a) the mid-Holocene simulation MPIESM-MH and b) the pre-industrial control simulation MPIESM-PI. The tropical precipitation variability difference between the mid-Holocene and the pre-industrial climate is depicted in c) where statistically significant differences in standard deviation according to a standard F-test are highlighted by dots.

4.5 Role of remote vs. local forcing for mid-Holocene TEJ variability

In this section, we present the results of simulations conducted with the simple dry-dynamics model PUMA. We designed a suite of experiments to investigate what is the dominant driver of the interannual to decadal variability of the WA-TEJ during the mid-Holocene – is it the variability of the WAM-related diabatic heating or the variability of the remote diabatic heating. Are there any substantial differences to the pre-industrial climate, and if yes, why?

4.5.1 PUMA-simulated WA-TEJ variability

We conducted three numerical experiments in which PUMA is forced by 3D diabatic heating fields derived from the output of the MPIESM-MH and MPIESM-PI simulations. The first experiment is a control run in which the JJAS mean diabatic heating fields are unaltered and therefore retain the total global year-to-year variability of the diabatic heating (PUMA-TF). In the other two experiments, the variability of the 3D

diabatic heating fields is either restricted to the African region (local forcing, PUMA-LF) or restricted to the rest of the globe excluding Africa (remote forcing, PUMA-RF). Each experiment encompasses 60 individual 6-year long integrations that represent the steady-state response to the imposed time-constant diabatic forcing of the respective monsoon season. We use daily output of the last 5 years of the individual simulations to derive the summer mean WA-TEJ intensity for each simulated monsoon season (as described in the Methods section).

The results of the PUMA experiments are depicted in form of a time series in figure 4.7. Solid, coloured lines show the PUMA-simulated summer mean WA-TEJ intensity for the 60 individually simulated monsoon seasons. The dashed black line displays, as a comparison, the WA-TEJ intensity derived from the transient and much more complex MPIESM simulations. For the pre-industrial control climate, PUMA appears to adequately reproduce the climatological intensity and variability of the WA-TEJ (Fig. 4.7b). Driven with the total forcing (PUMA-TF), PUMA displays a near-zero bias in mean WA-TEJ intensity ($+0.01\ \mathrm{m\,s^{-1}}$) and is further able to explain 59% of the interannual to decadal variability ($r = 0.77$). A less optimal result is obtained for the mid-Holocene where PUMA underestimates the climatological WA-TEJ intensity by $1\ \mathrm{m\,s^{-1}}$ and is only able to explain 46% of its variability (Fig. 4.7a). The reasons for this behaviour and possible implications will be discussed in the next section.

Keeping its limited capability in mind, what can the PUMA simulations nonetheless tell us about the role of the local versus the remote forcing for the TEJ variability during the mid-Holocene? The most striking result is the strongly reduced importance of the remote forcing compared to the present-day state. As a consequence, the mid-Holocene WA-TEJ variability is no longer dominated by the remote forcing but is equally driven by the local WAM-related forcing and remote influences.

In the pre-industrial control simulation, the interannual to decadal variability of the TEJ over West Africa is explained to a large extent by the variability of the remote diabatic heating (Fig. 4.7b, red line). PUMA-PI-RF displays a correlation of 0.94 to PUMA-PI-TF on both the (8-year highpass-filtered) interannual and the (unfiltered) interannual to (multi-)decadal time scale. A bootstrapping method, in this case a repeated recalculation of correlations after resampling the time series with 5000 iterations, yields a narrow 95% confidence interval of 0.90 to 0.96, underlining the robustness of this result. Expressed in terms of r^2, the remote forcing therefore explains 87.5% (80.7-92.2%) of the interannual to decadal TEJ variability in the simulated pre-industrial climate. With respect to the MPIESM-PI simulation one obtains a value of 64%. The isolated local forcing associated with WAM rainfall anomalies explains a substantially smaller, albeit also significant portion of the TEJ variability in the simulated pre-industrial climate. With respect to PUMA-PI-TF, PUMA-PI-LF shows a correlation of 0.49 (95% confidence interval: 0.25-0.66), which translates to an explained variance fraction of 24.3% (6.1-44.2%). These results for the pre-industrial control climate are very similar to the findings of Lemburg and Bader (2020). In this study, where ERA-Interim reanalysis and rainfall observations were used as input for PUMA to understand the WA-TEJ variability over the last 4 decades (1979-2017), the remote forcing was also the dominant driver of TEJ variability (91% explained variance within the PUMA model space compared to 35% explained variance by the local forcing).

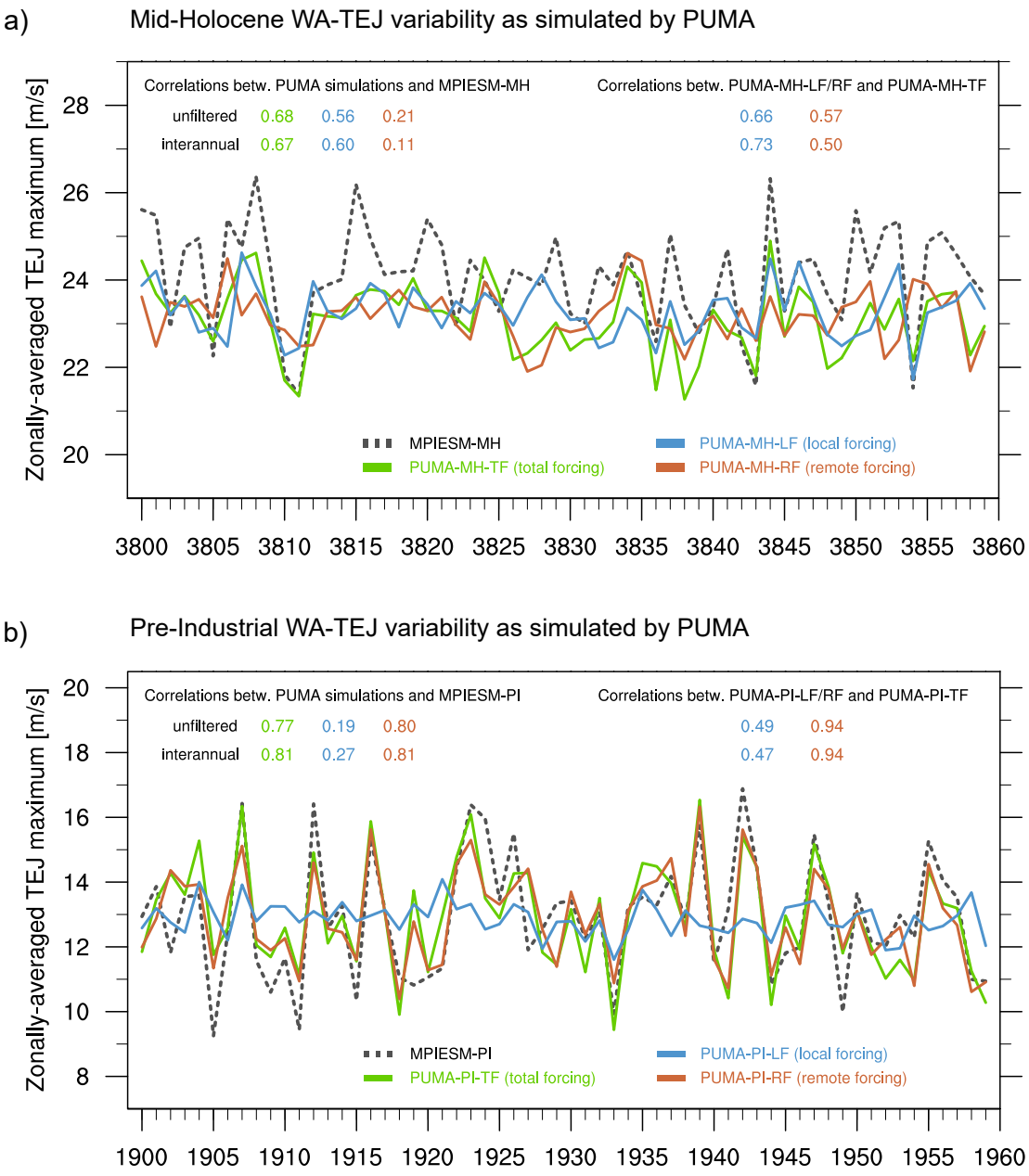

Figure 4.7: PUMA simulations driven with diabatic heating derived from the previously conducted MPI-ESM mid-Holocene (MPIESM-MH) and pre-industrial simulations (MPIESM-PI). The dashed black lines depict the WA-TEJ intensity calculated from the MPIESM-MH/PI output. The blue lines show the PUMA-simulated TEJ intensity of the **Local Forcing** simulations in which only the regional WAM rainfall-related diabatic forcing over Africa varies from year to year (diabatic heating is held constant to climatological values in the rest of the globe). The red lines depict the simulated WA-TEJ intensity of the **Remote Forcing** simulations in which the regional diabatic forcing over Africa is kept constant whereas its year-to-year variability is preserved in the rest of the globe. The green line shows the results of simulations driven with the **Total Forcing**, in which both the local and the remote forcing variability is retained. Please note that the years displayed on the x-axis represent an arbitrary selection with no relation to the real calendar years and therefore only serve as orientation.

A contrasting behaviour is simulated for the mid-Holocene experiments: The share of explained WA-TEJ variance attributable to the remote forcing drops substantially compared to the pre-industrial simulations. The correlation coefficient between PUMA-

MH-RF and PUMA-MH-TF amounts to 0.57 (95% confidence interval: 0.42-0.71) which corresponds to 32.9% (17.4-49.7%) explained variance (Fig. 4.7a). Evaluated with respect to the MPIESM-MH simulation, the influence of the remote forcing even becomes insignificant as the 5% tail of the bootstrap correlation distribution contains negative values. The local forcing becomes much more important under mid-Holocene conditions. PUMA-MH-LF explains 43.9% (24.7-61.8%) of the interannual to decadal WA-TEJ variability (31.3% with respect to MPIESM-MH). On the interannual time scale, the differences between the role of the local and remote forcing become amplified, with PUMA-MH-LF explaining 53% of the WA-TEJ variability whereas PUMA-MH-RF only explains 25%. However, a bootstrapping test reveals that no forcing can be considered dominant when one demands a typical probability of 95% for this hypothesis being true.

In summary, the PUMA simulations suggest that it is particularly the role of the remote forcing which fundamentally changes. Under mid-Holocene conditions, the variability of the WA-TEJ intensity is not governed by remote influences as in the present-day state, but is to equal parts driven by the local WAM-related heating and remote forcing. This result is, however, compromised by the comparatively low capability of the model to reproduce the TEJ variability for the mid-Holocene.

4.5.2 The diminished role of the remote diabatic forcing

Why is the mid-Holocene WAM characterized by such a pronounced shift from a remote forcing-dominated to a much more local forcing-driven WA-TEJ variability? A possible explanation is the simulated attenuation of the tropical rainfall variability over the western Pacific. This rainfall variability reduction, which is mainly confined to the interannual time scale, translates to a lowered variability of the remote diabatic heating in this region. How does this affect the TEJ over West Africa? As shown by Lemburg and Bader (2020), the intensity of the WA-TEJ is strongly influenced by large-scale anomalies of the diabatic heating over the tropical Pacific. If the anomalous heating is close to the equator – which is most often the case – it excites an atmospheric response which is similar to the classic Matsuno-Gill quadrupole (Gill, 1980). To the east of the heating, a stationary Kelvin wave induces anomalous westerly flow in the upper troposphere. As Kelvin waves propagate approximately three times as fast as equatorial Rossby waves, the steady-state Kelvin wave response embraces much larger parts of the tropical belt than the Rossby wave response to the west. A reduction in the interannual variability of rainfall over the tropical Pacific is tantamount to a weakened forcing amplitude. Thereby, the remote influence on the TEJ becomes less pronounced leading to an overall reduction of the remotely-induced interannual to decadal WA-TEJ variability.

Not only is the overall reduced variability of the tropical diabatic heating important, but also the way how the dominant patterns of variability change in terms of spatial distribution and amplitude. To investigate this, we apply a standard EOF analysis to the tropical part of the global diabatic heating field. In MPIESM-PI, the first EOF mode stands out as clearly dominant (explained variance: 27%) and further bears strong resemblance to a classic ENSO pattern as observed in today's climate. This mode is indeed strongly associated with El Niño-like SST anomalies in the tropical Pacific.

MPIESM-MH does not feature a clearly dominant mode of interannual diabatic heating variability. Instead, two modes with nearly same share of explained variance exist. The breakdown of one clearly dominant mode into two less distinct modes is possibly a direct consequence of the changes in the interannual Pacific SST variability, but may also be related to changes in the background circulation. On a first sight, the first mode in MPIESM-MH also appears as an ENSO-like mode but it features some substantial changes in the details. For instance, the heating anomalies over the Pacific are less pronounced and the dipole heating/cooling pattern over the Maritime Continent is less pronounced and shifted farther to the west.

We analyse how the tropical circulation in both the complex MPI-ESM and the much simpler PUMA model react to the respective dominant mode of interannual tropical rainfall variability. Here we show the results of PUMA because it is seemingly able to reproduce many features of the atmospheric response and has the advantage that we are able to rule out that any changes on the WA-TEJ are also due to a change in the local WAM-related forcing. The corresponding results for the MPIESM simulations are shown in the appendix (Fig. 4.A2).

As a comparison between PUMA-MH-RF and PUMA-PI-RF, figure 4.8 illustrates the main features of the circulation response to the positive phase (anomalous heating over the tropical Pacific) of the respective dominant mode of interannual diabatic heating variability. For the pre-industrial control climate, the anomalous velocity potential shows a dipole with its divergent centre over the central Pacific and its convergent centre over the western Indian Ocean. A similar but substantially weaker dipole is simulated for the mid-Holocene which is consistent with the overall lower amplitude of the anomalous diabatic heating especially over the western and central Pacific (Fig. 4.8a/c). The slight differences in the anomalous tropical divergent circulation become much more pronounced in the anomalies of the rotational wind field which is depicted in form of the eddy streamfunction (Fig. 4.8b/d). The typical Matsuno-Gill type pattern with its Rossby anticyclone pair slightly west to the heating and the extended Kelvin wave response to the east is strongly pronounced in PUMA-PI-RF. In contrast, PUMA-MH-RF displays a much weaker quadrupole pattern and the influence of the stationary Kelvin wave does not reach West Africa. Hence, the mid-Holocene WA-TEJ barely feels the influence of the dominant mode of remote heating variability under mid-Holocene conditions. It has to be stressed that not only the difference in the remote heating but also the change of the background circulation likely plays a role as it modulates the response to an imposed tropical heating (via changes in the vertical and horizontal wind shear).

4.6 Discussion

In this section, we first elaborate on the possible limitations of our study, in particular with regard to the simulations conducted with the PUMA model. Thereafter, we will discuss the main findings within a larger context, trying to unravel the reasons for the weakened Sahel rainfall – TEJ relationship that is simulated for the mid-Holocene WAM.

A general limitation of this study, that concerns both the MPI-ESM and PUMA sim-

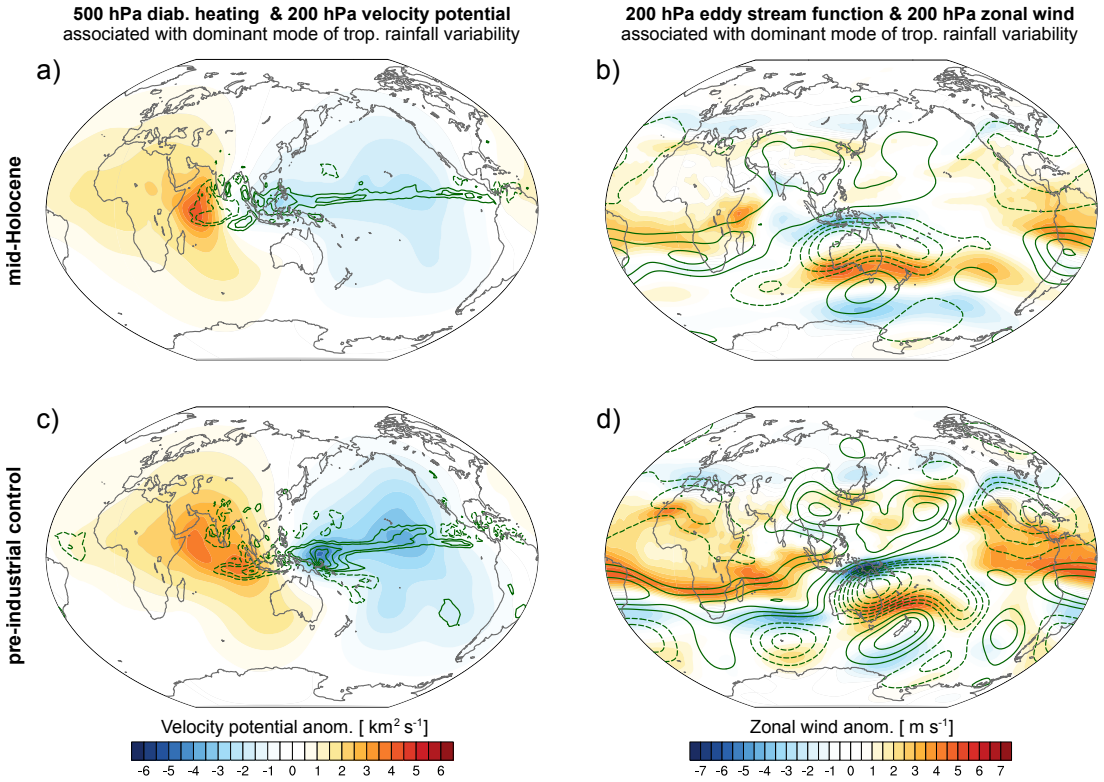

Figure 4.8: Comparison of the PUMA-simulated planetary-scale circulation responses to the respective dominant (ENSO-like) modes of interannual variability between the simulated mid-Holocene and the simulated pre-industrial climate. The top row shows results for PUMA-MH-RF while the bottom row displays the corresponding results for PUMA-PI-RF. On the left hand side, the contour lines indicate diabatic heating anomalies at around 500 hPa (solid lines depict positive values). The planetary-scale centres of upper-level convergence and divergence, which characterize the tropical overturning circulation, are shown with the help of the 200 hPa velocity potential (coloured shadings, red denotes anomalous convergence). On the right hand side, contour lines depict the stationary eddy streamfunction at 200 hPa (interval 1 $km^2\,s^{-1}$, solid lines denote positive values). Anomalies in 200 hPa zonal wind are shown via coloured shadings.

ulations, is the rather short simulation length of 60 years. As evident from the running correlations depicted in figure 4.3, the WA-TEJ – Sahel rainfall relationship is subject to decadal to multi-decadal variability, especially in the mid-Holocene simulation. Therefore, the 60 simulated years are likely not fully sufficient for exploring the contrast between the mid-Holocene and the present-day climate.

A problem specific to the conducted PUMA simulations has been already mentioned within the results section: the simulations for the mid-Holocene have problems to reproduce the WA-TEJ intensity and its variability. What are the possible causes of the decreased ability of our model to correctly simulate the climatological intensity and variability of the WA-TEJ under mid-Holocene conditions? A likely answer can be found by looking into the simulations of the complex MPI-ESM model. In the mid-Holocene simulation MPIESM-MH, the absolute variability of the WA-TEJ intensity is simulated to be weaker than in the pre-industrial simulation MPIESM-PI although the climatological mean intensity is about twofold compared to today. This diminished variability may hint at a decreased signal to noise ratio, assuming the background noise is the same for the mid-Holocene and the present-day climate. In this context, back-

ground noise can be interpreted as the effect of transients, especially those of extratropical origin but also tropical transient phenomena as for instance the MJO. Because of the long integration time (5 simulated years $\hat{=}$ 15 monsoon seasons), the time-averaged PUMA output only represents the steady-state circulation response to a fixed diabatic forcing. Therefore, any background noise due to transients is by design filtered out in the PUMA experiments. In other words, a change in the importance of transients would be a possible hypothesis for explaining the decreased ability of the PUMA model to simulate the interannual to decadal TEJ variability. Checking this hypothesis would need a more in-depth investigation of the role of extratropical influences which could follow as an extension to this study.

Further possible causes for the reduced explained variability in the PUMA simulations could be systematic errors in the simulated background circulation. In general, the response of the tropical circulation to an imposed heating is quite sensitive to the basic state, i.e., the horizontal and vertical wind shear (Robertson and Frankignoul, 1990). Therefore even small deviations in the background circulation can severely impact the capability of the model to accurately simulate the response to an imposed anomalous heating. Moreover, the physics of PUMA are very simple which means that for instance the complex effects of convective momentum transport (CMT) on the tropical circulation cannot be accurately simulated; only the overall diffusive effect was included in our model setup by means of a simple parametrization (see details in Lemburg and Bader, 2020, in prep.; section 3.2 of this thesis).

Taking the possible shortcomings of the PUMA experiments aside, how can the results be interpreted in terms of the changing WA-TEJ – Sahel rainfall relationship? As a reminder, the analysis of the MPIESM simulations has shown that the covariability between Sahel rainfall and the WA-TEJ intensity on interannual to decadal time scales is substantially lower for the mid-Holocene than for the present-day climate. One would expect that a stronger role of the local diabatic forcing should strengthen the simulated WA-TEJ – Sahel rainfall relationship. This is not the case, however. We suppose that one main reason is directly related to the aforementioned difficulties of the PUMA simulations to reproduce the mid-Holocene WA-TEJ variability. This problem can be interpreted as a model-related issue but can also reflect a diminished role of tropical diabatic heating as the main driver of WA-TEJ variability. Therefore, the importance of other drivers such as extratropical forcings may increase. As we exclusively focus on the role of tropical diabatic heating, any such drivers can therefore be interpreted as an increase of atmospheric noise. A second, directly related explanation is the attenuated role of the remote diabatic forcing due to the changed characteristics of the tropical SST variability. In the present-day climate, anomalous remote diabatic heating, particularly over the Pacific, not only induces substantial WA-TEJ anomalies, but in many cases also leads to same-sign changes in Sahel rainfall (see discussion in Lemburg and Bader, 2020, in prep.; section 3.5 of this thesis). In the simulated mid-Holocene, however, the remote diabatic heating does no longer exert a strong control on the WA-TEJ intensity which makes it much more prone to atmospheric noise. Therefore we suggest that this reduced signal-to-noise ratio may ultimately be the reason of the simulated decline of WA-TEJ – Sahel rainfall covariability.

4.7 Summary and conclusions

During the mid-Holocene, the West African Monsoon (WAM) circulation and associated Sahel rainfall were more intense and extended substantially farther northwards. Little is known, however, about the role of the West African Tropical Easterly Jet (WA-TEJ) and its relationship to rainfall during the mid-Holocene. In this study, we therefore elucidate the WA-TEJ – Sahel rainfall relationship on interannual to decadal time scales as simulated by a state-of-the-art earth system model. We use existing fully-coupled and sufficiently spun-up climate simulations conducted with the MPI-ESM 1.2 in LR resolution: a mid-Holocene control run with orbital parameters and CO2 levels prescribed to the level of 8000 years before present. A fully-coupled pre-industrial simulation with modern-day orbital parameters and greenhouse gases prescribed to pre-industrial levels serves as a control simulation. By means of standard correlation analysis applied to the respective simulated time series of WA-TEJ intensity and Sahel rainfall as well as through the additional analysis of spatial correlation maps we find two pronounced contrasts to the present-day:

- The relationship between the summer mean WA-TEJ intensity over West Africa and Sahel rainfall is simulated to be substantially weaker under mid-Holocene conditions than today
- The "centre of action" in the spatio-temporal WA-TEJ – Sahel rainfall relationship moves substantially to the northeast (correlations close to zero when evaluating western Sahel rainfall; significant correlations around 0.6, which are closer to today's observed values, only occur with respect to eastern Sahel rainfall)

As a likely explanation for the weaker WA-TEJ – Sahel rainfall relationship we propose the diminished role of teleconnections. In the present-day climate, tropical SST anomalies in remote regions (e.g., the Pacific) and the associated changes in the diabatic heating represent a strong remote forcing which affects especially the WA-TEJ intensity but also modulates Sahel rainfall. Previous studies have shown that the tropical SST variability was attenuated during the mid-Holocene, especially over the equatorial Pacific. Therefore, the role of the remote forcing in both driving Sahel rainfall and the WA-TEJ intensity may have been less pronounced in the mid-Holocene. This hypothesis is supported by our complex model as both the WA-TEJ intensity and Sahel rainfall are substantially weaker correlated to tropical SST anomalies as in today's climate.

For further confirmation, we unravel the tropical drivers that affect the mid-Holocene variability of the WA-TEJ. We ask whether the remote diabatic heating is dominant as in today's climate or whether the local forcing associated with WAM rainfall becomes more important in the simulated mid-Holocene climate? To answer this question we conduct time-slice simulations with PUMA, an AGCM based on dry dynamics. For each monsoon season over a 60-year period, we conduct long enough integrations to obtain the steady-state response to a given diabatic forcing. As a forcing, we use the respective summer mean 3D diabatic heating fields which are derived from the previously conducted MPI-ESM simulations. Experiments with a geographically split-up heating field, where the year-to-year variability of the heating is either restricted to the local African or to the remote rest of world part, produce the following results:

- In contrast to the present-day climate, the interannual to decadal variability of the TEJ is not dominated by remote diabatic forcing, but is in equal parts driven by the remote forcing and the local forcing associated with WAM rainfall anomalies
- This "regime shift" from a remotely-driven to a more locally-driven TEJ variability is likely explained by the changed character and the overall attenuation of the interannual SST variability in the tropical Pacific

In summary, this ongoing research highlights some interesting changes in the WA-TEJ – WAM rainfall relationship under mid-Holocene conditions. Compared to the present-day climate, the statistical relationship is simulated to be generally weaker on interannual to decadal time scales, particularly in the western Sahel where the correlation between the summer mean WA-TEJ intensity and rainfall becomes insignificant. As the main cause of the dwindling WA-TEJ – WAM rainfall relationship we suggest the overall diminished role of teleconnections. In contrast to today, both the WA-TEJ intensity and especially Sahel rainfall are simulated to be substantially less influenced by remote SST anomalies. The attenuated effect of the remote diabatic forcing reduces the signal-to-noise ratio, making the WA-TEJ variability more subject to other not investigated influences (e.g., seasonally-integrated effect of transient disturbances). The local diabatic forcing, although more important during the mid-Holocene, is not strong enough to induce anomalies that stand out against that "noise" in the tropical upper-level wind field.

As a next step towards a better understanding of the role of the WA-TEJ during the mid-Holocene, the focus should be shifted on shorter time scales. An in-depth investigation of the subseasonal relationship between the WA-TEJ and WAM rainfall could answer whether the WA-TEJ might had played a more active role for Sahel rainfall than today. However, such an analysis might be compromised by the rather low model resolution that does not allow an accurate representation of MCSs and their interaction with the mean flow. First analyses of the MPIESM-simulated present-day climate have shown that the simulated spatio-temporal relationship between TEJ anomalies and anomalous convective activity on synoptic time scales differs considerably from what observations show. The analysis of recently conducted high resolution simulations with explicit convection might be the way forward to tackle this problem.

Acknowledgments

This work was supported by the International Max Planck Research School on Earth System Modelling (IMPRS-ESM) and the Max Planck Society (MPG). The computational resources were provided by the Deutsches Klima Rechenzentrum (DKRZ).

4.8 Supplementary figures

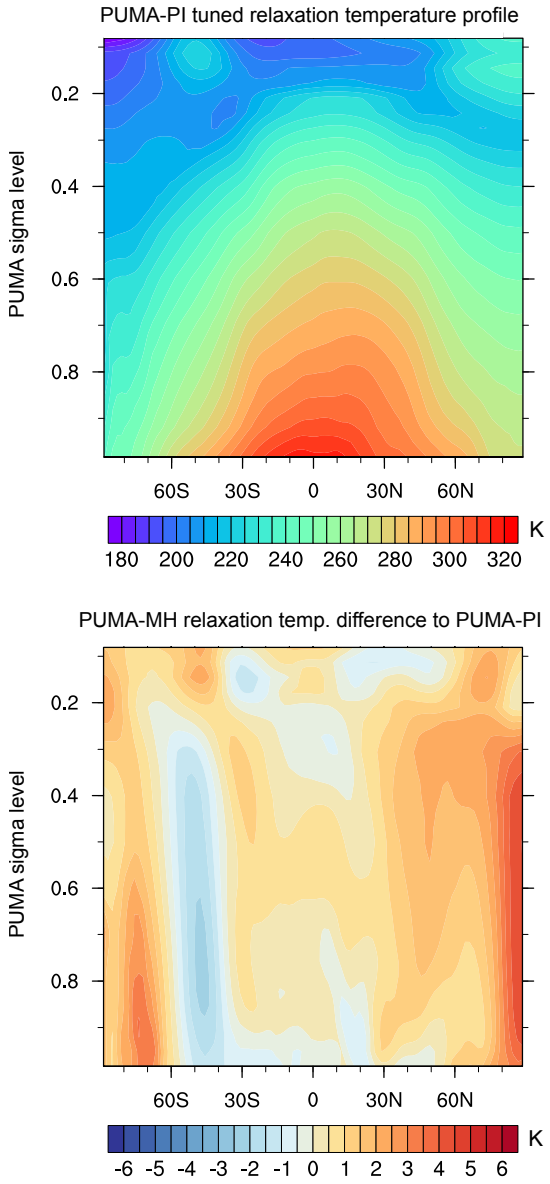

Figure 4.A1: Top) Latitude – height cross section of the zonally-symmetric relaxation temperature used in the PUMA-PI simulations. Bottom) Latitude – height cross section of the difference of zonally-symmetric relaxation temperature between PUMA-MH and PUMA-PI. The relaxation temperature field is the result of a multiple-step iteration process that started from a classic Held-Suarez temperature profile.

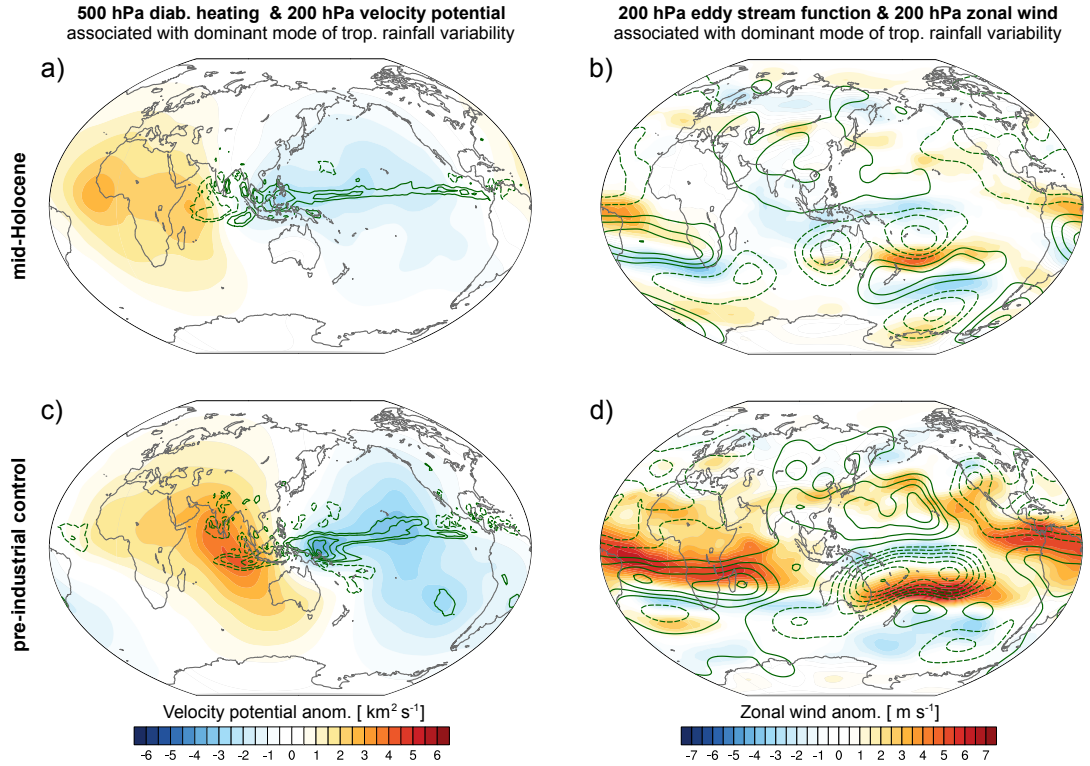

Figure 4.A2: Comparison of the MPIESM-simulated planetary-scale circulation responses to the respective dominant (ENSO-like) modes of interannual variability between the simulated mid-Holocene and the simulated pre-industrial climate. The top row shows results for MPIESM-MH while the bottom row displays the corresponding results for MPIESM-PI. On the left hand side, the contour lines indicate diabatic heating anomalies at around 500 hPa (solid lines depict positive values). The planetary-scale centres of upper-level convergence and divergence, which characterize the tropical overturning circulation, are shown with the help of the 200 hPa velocity potential (coloured shadings). On the right hand side, contour lines depict the stationary eddy streamfunction at 200 hPa (interval 1 $km^2\,s^{-1}$, solid lines denote positive values). Anomalies in 200 hPa zonal wind are shown via coloured shadings.

Bibliography

Berger, A. and M.-F. Loutre (1991). Insolation values for the climate of the last 10 million years. *Quaternary Science Reviews 10*(4), 297–317.

Besson, L. and Y. Lemaître (2014). Mesoscale convective systems in relation to African and tropical easterly jets. *Monthly Weather Review 142*(9), 3224–3242.

Braconnot, P., B. Otto-Bliesner, S. Harrison, S. Joussaume, J.-Y. Peterchmitt, A. Abe-Ouchi, M. Crucifix, E. Driesschaert, T. Fichefet, C. Hewitt, et al. (2007). Results of PMIP2 coupled simulations of the Mid-Holocene and Last Glacial Maximum–Part 1: experiments and large-scale features. *Climate of the Past 3*(2), 261–277.

Brovkin, V., S. Lorenz, T. Raddatz, T. Ilyina, M. Heinze, I. Stemmler, M. Toohey, and M. Claussen (2019). What was the source of the atmospheric CO2 increase during Holocene? *Biogeosciences 16*, 2543–2555.

Claussen, M. and V. Gayler (1997). The greening of the Sahara during the mid-Holocene: results of an interactive atmosphere-biome model. *Global Ecology and Biogeography Letters*, 369–377.

Collins, J. A., M. Prange, T. Caley, L. Gimeno, B. Beckmann, S. Mulitza, C. Skonieczny, D. Roche, and E. Schefuß (2017). Rapid termination of the African humid period triggered by northern high-latitude cooling. *Nature Communications 8*(1), 1372.

Demenocal, P., J. Ortiz, T. Guilderson, J. Adkins, M. Sarnthein, L. Baker, and M. Yarusinsky (2000). Abrupt onset and termination of the African Humid Period:: rapid climate responses to gradual insolation forcing. *Quaternary science reviews 19*(1-5), 347–361.

Fraedrich, K., E. Kirk, and F. Lunkeit (1998). Portable university model of the atmosphere. *DKRZ Rep 16*.

Gill, A. (1980). Some simple solutions for heat-induced tropical circulation. *Quarterly Journal of the Royal Meteorological Society 106*(449), 447–462.

Giorgetta, M. A., J. Jungclaus, C. H. Reick, S. Legutke, J. Bader, M. Böttinger, V. Brovkin, T. Crueger, M. Esch, K. Fieg, et al. (2013). Climate and carbon cycle changes from 1850 to 2100 in MPI-ESM simulations for the Coupled Model Intercomparison Project phase 5. *Journal of Advances in Modeling Earth Systems 5*(3), 572–597.

Gregory, D., R. Kershaw, and P. Inness (1997). Parametrization of momentum transport by convection. II: Tests in single-column and general circulation models. *Quarterly Journal of the Royal Meteorological Society 123*(541), 1153–1183.

Grist, J. P. and S. E. Nicholson (2001). A study of the dynamic factors influencing the rainfall variability in the West African Sahel. *Journal of climate 14*(7), 1337–1359.

Harrison, S., P. Bartlein, S. Brewer, I. Prentice, M. Boyd, I. Hessler, K. Holmgren, K. Izumi, and K. Willis (2014). Climate model benchmarking with glacial and mid-Holocene climates. *Climate Dynamics 43*(3-4), 671–688.

Jolly, D., I. C. Prentice, R. Bonnefille, A. Ballouche, M. Bengo, P. Brenac, G. Buchet, D. Burney, J.-P. Cazet, R. Cheddadi, et al. (1998). Biome reconstruction from pollen and plant macrofossil data for Africa and the Arabian peninsula at 0 and 6000 years. *Journal of Biogeography 25*(6), 1007–1027.

Jungclaus, J., N. Fischer, H. Haak, K. Lohmann, J. Marotzke, D. Matei, U. Mikolajewicz, D. Notz, and J. Von Storch (2013). Characteristics of the ocean simulations in the Max Planck Institute Ocean Model (MPIOM) the ocean component of the MPI-Earth system model. *Journal of Advances in Modeling Earth Systems 5*(2), 422–446.

Karamperidou, C., P. N. Di Nezio, A. Timmermann, F.-F. Jin, and K. M. Cobb (2015). The response of ENSO flavors to mid-Holocene climate: implications for proxy interpretation. *Paleoceanography 30*(5), 527–547.

Koutavas, A., P. B. Demenocal, G. C. Olive, and J. Lynch-Stieglitz (2006). Mid-Holocene El Niño–Southern Oscillation (ENSO) attenuation revealed by individual foraminifera in eastern tropical Pacific sediments. *Geology 34*(12), 993–996.

Koutavas, A. and S. Joanides (2012). El Niño–Southern oscillation extrema in the holocene and last glacial maximum. *Paleoceanography 27*(4).

Kutzbach, J. E. and P. J. Guetter (1986). The influence of changing orbital parameters and surface boundary conditions on climate simulations for the past 18 000 years. *Journal of the Atmospheric Sciences 43*(16), 1726–1759.

Lemburg, A. and J. Bader (2020). The role of remote versus local forcing for the interannual to decadal variability of the Tropical Easterly Jet over West Africa. *In preparation*.

Lemburg, A., J. Bader, and M. Claussen (2019). Sahel rainfall–Tropical Easterly Jet relationship on synoptic to intraseasonal time scales. *Monthly Weather Review 147*(5), 1733–1752.

Lin, J.-L., B. E. Mapes, and W. Han (2008). What are the sources of mechanical damping in Matsuno–Gill-type models? *Journal of Climate 21*(2), 165–179.

McGregor, H. V. and M. K. Gagan (2004). Western Pacific coral δ18O records of anomalous Holocene variability in the El Niño–Southern Oscillation. *Geophysical Research Letters 31*(11).

Milinski, S., J. Bader, H. Haak, A. C. Siongco, and J. H. Jungclaus (2016). High atmospheric horizontal resolution eliminates the wind-driven coastal warm bias in the southeastern tropical Atlantic. *Geophysical Research Letters 43*(19), 10–455.

Müller, W. A., J. H. Jungclaus, T. Mauritsen, J. Baehr, M. Bittner, R. Budich, F. Bunzel, M. Esch, R. Ghosh, H. Haak, et al. (2018). A Higher-resolution Version of the Max Planck Institute Earth System Model (MPI-ESM1. 2-HR). *Journal of Advances in Modeling Earth Systems 10*(7), 1383–1413.

Nicholson, S. E. (2009). On the factors modulating the intensity of the tropical rainbelt over West Africa. *International Journal of Climatology: A Journal of the Royal Meteorological Society 29*(5), 673–689.

Otto-Bliesner, B. L. (1999). El Nino/La Nina and Sahel precipitation during the middle holocene. *Geophysical Research Letters 26*(1), 87–90.

Raddatz, T., C. Reick, W. Knorr, J. Kattge, E. Roeckner, R. Schnur, K.-G. Schnitzler, P. Wetzel, and J. Jungclaus (2007). Will the tropical land biosphere dominate the climate–carbon cycle feedback during the twenty-first century? *Climate Dynamics 29*(6), 565–574.

Reick, C., T. Raddatz, V. Brovkin, and V. Gayler (2013). Representation of natural and anthropogenic land cover change in MPI-ESM. *Journal of Advances in Modeling Earth Systems 5*(3), 459–482.

Renssen, H., V. Brovkin, T. Fichefet, and H. Goosse (2006). Simulation of the Holocene climate evolution in Northern Africa: The termination of the African Humid Period. *Quaternary International 150*(1), 95–102.

Robertson, A. W. and C. Frankignoul (1990). The tropical circulation: Simple model versus general circulation model. *Quarterly Journal of the Royal Meteorological Society 116*(491), 69–87.

Street-Perrott, F. and R. Perrott (1993). Holocene vegetation, lake levels and climate of Africa. *Global climates since the last glacial maximum*, 318–356.

Sylla, M., A. Dell'Aquila, P. Ruti, and F. Giorgi (2010). Simulation of the intraseasonal and the interannual variability of rainfall over West Africa with RegCM3 during the monsoon period. *International Journal of Climatology 30*(12), 1865–1883.

Vamborg, F., V. Brovkin, and M. Claussen (2011). The effect of dynamic background albedo scheme on Sahel/Sahara precipitation during the Mid-Holocene. *Climate of the Past 7*, 117–131.

Zhao, Y., P. Braconnot, S. Harrison, P. Yiou, and O. Marti (2007). Simulated changes in the relationship between tropical ocean temperatures and the western African monsoon during the mid-Holocene. *Climate Dynamics 28*(5), 533–551.

Zwiers, F. W. and H. Von Storch (1995). Taking serial correlation into account in tests of the mean. *Journal of Climate 8*(2), 336–351.

List of Figures

List of Tables

Acknowledgments

First of all I would like to express my sincere gratitude towards everyone involved in the IMPRS, first and foremost the IMPRS office. Without you, Antje Weitz, Cornelia Kampmann and Michaela Born, life as a PhD student would have been much less comfortable. Your support greatly alleviated all the stress that comes with a PhD, not only in terms of all the administrative stuff.

Next I have to thank my "Doktorvater" Jürgen Bader for his great supervision that always hold the right balance between regular guidance and a more Laissez-faire approach. In most cases he let me do what I thought was the right thing to pursue and only intervened when it was really necessary. Thereby he greatly contributed to my development towards an independent, free-thinking scientist.

The same applies to my second supervisor Martin Claußen. But I do not only appreciate his Laissez-faire-type supervision. I am further very grateful that he guided me through my very first steps of my academic career (supervision of my bachelor's and master's thesis) and that he convinced me to pursue a PhD.

Further thanks go to the research group of Prof. Dr. Andreas Fink and Prof. Dr. Peter Knippertz at the KIT in Karlsruhe. The meetings throughout my PhD time have really helped to further motivate my work and resulted in some fresh ideas.

Away from my direct academic environment, I would like to first and foremost very much thank my parents Ulrike and Thomas and especially my grandparents Vera and Peter, who always supported me and enabled me to find my way into an academic career.

I thank Nora Specht and Alexander Winkler for proofreading parts of my thesis and providing valuable comments. I would also like to thank Nora Specht and Ludwig Lierhammer for the regular lunch breaks and keeping me away from my work again and again ;). Creating election posters, playing Hangman and other intellectually challenging pastimes were great fun.

In addition, I would also like to thank my old meteorology colleagues, Marvin Heidkamp, Janosch Michaelis and Thomas Möller. It was great to have you around during lunch breaks or other occasions. Special thanks go to Thomas Möller who contributed greatly to my understanding of aerodynamics.

Last but not least, I have to mention with great gratitude that I have been part of an inspiring and friendly work environment here at the MPI-M Hamburg. In this context, I have to especially thank Victor Brovkin who employed me as a student assistant in early 2014. At that time, I found my way into the Land department, where I was surrounded by all around great and helpful people. I especially appreciate the fact that, during the later stages of my PhD, I was invited to join the ranks of the legendary "coffee round" of Andreas Chlond and Heinz-Dieter Hollweg ;).

Versicherung an Eides statt

Declaration of oath

Hiermit versichere ich an Eides statt, dass ich die vorliegende Dissertation mit dem Titel: „On the relationship between the Tropical Easterly Jet over West Africa and Sahel rainfall across various time scales“ selbstständig verfasst und keine anderen als die angegebenen Hilfsmittel – insbesondere keine im Quellenverzeichnis nicht benannten Internet-Quellen – benutzt habe. Alle Stellen, die wörtlich oder sinngemäß aus Veröffentlichungen entnommen wurden, sind als solche kenntlich gemacht. Ich versichere weiterhin, dass ich die Dissertation oder Teile davon vorher weder im In- noch im Ausland in einem anderen Prüfungsverfahren eingereicht habe und die eingereichte schriftliche Fassung der auf dem elektronischen Speichermedium entspricht.

Hamburg, 12.11.19 .....

Alexander Lemburg

Hinweis / Reference

Die gesamten Veröffentlichungen in der Publikationsreihe des MPI-M
„Berichte zur Erdsystemforschung / Reports on Earth System Science“,
ISSN 1614-1199

sind über die Internetseiten des Max-Planck-Instituts für Meteorologie erhältlich:
http://www.mpimet.mpg.de/wissenschaft/publikationen.html

All the publications in the series of the MPI -M
„Berichte zur Erdsystemforschung / Reports on Earth System Science“,
ISSN 1614-1199

are available on the website of the Max Planck Institute for Meteorology:
http://www.mpimet.mpg.de/wissenschaft/publikationen.html